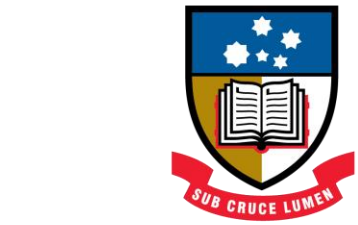

THE UNIVERSITY of ADELAIDE

Ambient Vibration Energy Harvesting

Yimin Fan

A thesis submitted in fulfilment of the requirement for the degree of

Doctor of Philosophy

School of Mechanical Engineering

The University of Adelaide

Australia

May 2022

Abstract

The recent rapid development of smart electronic devices, including wearable electronic devices, Internet of Things (IoT) devices, implantable medical devices and remote smart monitors, has raised great research interests on optimising battery power consumption in small-scaled and remotely operational electronic components. For the past ten years, there has been many research works in vibration-based energy harvesting, i.e., converting ambient vibration sources into electrical energy via different transduction methods.

In dealing with environmental vibration sources, the most pressing issue for vibration-based energy harvesters (VEHs) from mechanical and structural perspectives is whether the device can efficiently output an optimised power level under realistic (i.e., non-stationary, time-dependent, distributed in frequency spectrum, etc.) excitation sources. Additionally, the performance of VEHs is also restricted in size, complexity of design, and power density issues. Under such design criteria, introducing nonlinearities into VEHs attracted wide attention. This research work aims to investigate the bandwidth performance of vibration-based energy harvesting by subjecting nonlinear phenomena/techniques with internal and externally induced dynamic behaviours into the systems, hence broadening the operational bandwidth and optimising the power level under a wide range of frequencies. The outcomes of this research work yield five peer-reviewed journal papers and several international conference papers. The five journal papers are presented in five chapters (Chapter 3 to Chapter 7) as the main contributions of this thesis.

Paper 1 presents a magnetic VEH using combined primary and parametric resonances. In order to merge the resonant regions of fundamental primary resonance and parametric resonance as one continuously operational bandwidth, the motion limiter is utilised to induce external hardening effects that aim to eliminate the off-resonance regime between the two resonances. Theoretical investigations, including the finite element method (FEM) using ANSYS and an averaging perturbation technique, are performed to explain the experimental results. System parameter studies are also conducted to highlight the limiter gap distance, type and orientation angle effects. The paper has been published in Energy

Conversion and Management (Q1; Impact Factor =9.7; journal rank: 2 out of 135 in Mechanics).

Paper 2 aims to investigate the effects of the motion limiter on directly and parametrically excited energy harvesters based on our first paper. An array-type energy harvester is presented with piezoelectric transducers and three configurations of motion limiters. The bandwidth performance of the device under direct and parametric excitation directions is tested, and the results imply an enhanced power level and a continuous operational bandwidth. The results also demonstrate that the optimised performance is achieved by a duo-type motion limiter configuration. The effects of piezoelectric layers and nonlinear cubic stiffness terms in the governing equations are also studied and validated with experimental results. This paper has been accepted for publication in International Journal of Non-Linear Mechanics.

Paper 3, further investigates the feasibility of parametrically excited devices and focuses on reducing the level of the potential barrier and initial threshold amplitude in bistable and parametrically excited devices, respectively. From our first two papers, the results imply that triggering the parametric resonance needs a certain excitation level. By considering the joint restraint between bistable and parametrically excited energy harvesters, we propose a broadband magnetically coupled bistable VEH via parametric excitation, to reduce both the initiation threshold amplitude and the potential barrier for large-amplitude oscillations. The mathematical expression of magnetic coupling effects is presented to predict the dynamics of the system and verify the experimental results. The paper has been published in Energy Conversion and Management (Q1; Impact Factor =9.7; journal rank: 2 out of 135 in Mechanics).

Paper 4 is inspired by our previous studies on parametric resonance. The principal parametric resonance locates at twice the fundamental primary resonance (in general, the first transverse mode). A system can also possess a two-to-one internal resonance if the natural frequencies are commensurable or nearly commensurable (i.e., 1:2 frequency ratio between the first two natural frequencies). This paper presents theoretical modelling and experimental validation of a U-shaped piezoelectric energy harvester. The double-jump phenomena extend the resonance regime in a certain range, and the energy exchanges between the two transverse modes enable the motions of all segments (i.e., three cantilever beams) for high-efficient energy harvesting.

Paper 5 provides an insight into coupling bending and torsional modes on an L-shaped energy harvester. An internal resonance phenomenon between bending and torsional modes is achieved. In paper 4, we study a two-to-one internal resonance between the first two transverse modes. To optimise the strain rate-voltage transduction efficiency, we consider the out-of-plane motions in the internal resonance phenomena in this paper. In the presence of modal interactions, the power level can be greatly improved as the strain changes in both bending and torsional directions can be harvested under the same excitation frequency.

Table of Contents

Declaration

I, Yimin Fan, certify that this work contains no material which has been accepted for the award of any other degree or diploma in my name, in any university or other tertiary institution and, to the best of my knowledge and belief, contains no material previously published or written by another person, except where due reference has been made in the text. In addition, I certify that no part of this work will, in the future, be used in a submission in my name, for any other degree or diploma in any university or other tertiary institution without the prior approval of the University of Adelaide and where applicable, any partner institution responsible for the joint-award of this degree.

I acknowledge that copyright of published works contained within this thesis resides with the copyright holder(s) of those works.

I also give permission for the digital version of my thesis to be made available on the web, via the University's digital research repository, the Library Search and also through web search engines, unless permission has been granted by the University to restrict access for a period of time.

I acknowledge the support I have received for my research through the provision of an Australian Government Research Training Program Scholarship.

Yimin Fan

Date: 25/01/2022

Acknowledgements

I would like to thank my supervisors, Dr Tien-Fu Lu and Dr Mergen Ghayesh; without their help, this project would have been impossible. Tien-Fu's timely support and mentoring, both professionally and personally, to me, is the mark of a wise and trusted academic. I am deeply indebted to Mergen's valuable support and detailed technical comments, more importantly, leading me to the field of nonlinear vibration -- it could not be more interesting to study and utilise nonlinear vibration phenomena experimentally. I am privileged to have their guidance and assistance and feel very fortunate to have met such an outstanding supervisory team to guide and support me throughout my PhD journey.

I have spent more than one thousand hours in Chapman Laboratory. I truly appreciate the assistance I received from the Civil/Electrical/Mechanical workshop staff, especially from Simon Golding for software development, Lydia Zhang for fabricating test devices, and Jon Ayoub for managing and extending my Lab access hours. I also sincerely thank A/Prof. Alex Ng for sharing the experimental equipment.

Finally, but foremost, I would like to thank my wonderful parents, for giving me this life, love, endless patience and unconditional support. There is no way to express my utmost gratitude, I honestly know that without their optimism affecting me, I could not finish my degree on time. I would like to thank my partner, Yuxuan Zhang, for her constant love, support and understanding during all times. I also would like to acknowledge my cat, Rika, I can always feel deep calmness and at peace, when I look at this little treasure.

List of Publications

Journal Articles

1. **Fan, Y**., M.H. Ghayesh, and T.-F. Lu, *Enhanced nonlinear energy harvesting using combined primary and parametric resonances: Experiments with theoretical verifications.* Energy Conversion and Management, 2020. **221**: p. 113061.

2. **Fan, Y**., M.H. Ghayesh, T.-F. Lu, and M. Amabili, *Design, development, and theoretical and experimental tests of a nonlinear energy harvester via piezoelectric arrays and motion limiters*. International Journal of Non-Linear Mechanics, 2022. 142: p. 103974.

3. **Fan, Y**., M.H. Ghayesh, and T.-F. Lu, *A broadband magnetically coupled bistable energy harvester via parametric excitation.* Energy Conversion and Management, 2021. **244**: p. 114505.

4. **Fan, Y**., M.H. Ghayesh, and T.-F. Lu, *High-efficient internal resonance energy harvesting: Modelling and experimental study.* Submitted to: Mechanical Systems and Signal processing.

5. **Fan, Y**., M.H. Ghayesh and T.-F. Lu, *A proof-of-concept study on an internal-resonance based piezoelectric energy harvester with coupled three-dimensional bending-torsion motions.* Submitted to: ASME Journal of Vibration and Acoustics.

Conference Proceedings

The following conference papers have arisen from this research but are not included as main chapters of the thesis.

1. **Fan, Y**., M.H. Ghayesh, and T.-F. Lu, *Enhanced vibration energy harvesting using mechanical stoppers and parametric resonances*. in *Vibration Engineering for a Sustainable Future*. 2021. Cham: Springer International Publishing.

2. **Fan, Y**., M.H. Ghayesh, and T.-F. Lu, *Two-to-one internal resonance in bending-torsion modes of an L-shaped cantilever structure*. 10th Australasian Congress on Applied Mechanics, 2021.

Chapter 1

Introduction

1.1 Overview

As the general trend of modern electronic devices progressively becomes wireless, miniaturised, low-power consumption, and requires long-term usage, it is doubtful whether conventional electrochemical batteries are still promising in such low-power consumption devices. The competitiveness and dominance of batteries lie in their ability to provide efficient and stable power output for traditional electronic appliances. Yet, the concerns with batteries are the expense and regular operations of charging and replacement. Likewise, the performance of small-scale electronic devices such as wireless sensors, wearable devices, and medical implants are vastly dependent on working volume/size and power density, which are limited by traditional batteries.

Fortunately, the required power levels of these devices have been significantly reduced to milliwatt and even microwatt with rapid development in microsystems [1]. Such that, energy harvesting technologies, which aim to convert ambient energy sources into electrical form, are feasible to provide continuous power supplies for these compact electronic devices. With environmentally friendly energy sources, such as thermal [2], solar [3], and kinetic energy to obtain sustainable and green energy conversions, the energy harvesting technologies have received great potential for providing a new concept of compensating energy for consumable power supplies.

Kinetic energy forms mainly include ambient environmental vibration, ocean wave [4, 5] and flow-induced vibration (i.e., wind) [6, 7]. Although some industrial and commercial

applications based on the ocean wave and flow-induced energy harvesting techniques have already been established, the practicality of these devices, due to topography, construction cost, and volume/size, is restricted to use in everyday life. By contrast, ambient vibrations, as a ubiquitous form of energy, are the most reachable sources for energy conversion. Depending on the vibration sources, the applications of vibration-based energy harvesting (VEH) techniques have been applied to different fields. For moving vehicle-related applications, VEHs are employed as structural health monitors due to vibrations from engines [8], suspension systems [9], roadways and bridges [10, 11], and railways [12]. Human motions are also rich in kinetic energy for VEHs to power up wireless sensors and wearable electronic devices, such as walking [13-15] and heartbeats [16, 17]. The Internet of Things (IoT) applications have recently attracted immense attention in designing smart home and working place. However, one of the main concerns is the power consumption of wireless sensor networks [18, 19]. Unlike solar receivers or wind energy harvesters, the performance of VEHs in buildings is equally effective as in outdoor environments. Vibration sources such as periodic vibrations from operating appliances, pressure/strain changes can all be adopted by VEHs with suitable transduction methods (i.e., electromagnetic, electrostatic, piezoelectric, etc.).

Upon the above investigations, vibration-based energy harvesting is the most promising and reliable approach to conduct energy conversion between mechanical and electrical forms in ambient environment working conditions. Such that, research works based on VEHs have been carried out intensively from material, electrical circuit, and storage perspectives during the last two decades. Initially, to optimise the harvested power/voltage, the basic concept of VEHs is operating within the linear resonance region, which is only applicable with stationary vibration sources.

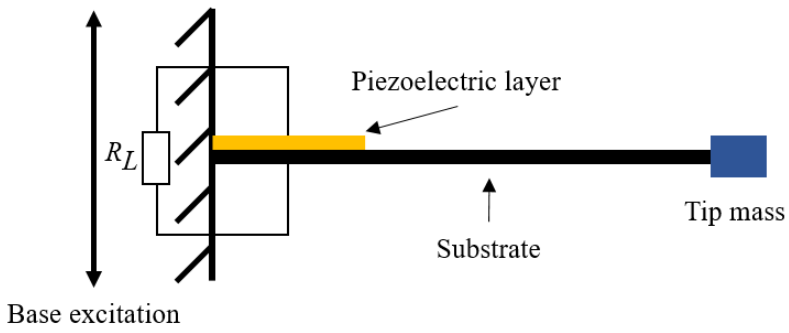

Figure 1-1. Schematic of a linear energy harvester under harmonic excitations.

Figure 1-1 shows a conventional VEH under harmonic excitations. The structure consists of a clamped-free cantilever beam, a piezoelectric layer bonded onto the main structure, and a tip mass for tuning purposes. The output voltage is measured from a loading resistor R_L. The effects of adhesive layer have been neglected. The simplified governing equation of a linear piezoelectric energy harvester can be written as a second order mass-spring-damper system

$$m\ddot{x} + c\dot{x} + kx - \varphi v = -m\ddot{y}, \tag{1.1}$$

$$c_p\dot{v} + v/R_L + \varphi\dot{x} = 0, \tag{1.2}$$

where x is displacement component, m is effective mass, c is damping coefficient, k is stiffness coefficient, φ is electromechanical coupling coefficient, $\ddot{y} = Zcos(\omega t)$ is the base excitation term, c_p is capacitance, v is output voltage. For the analytical analysis, the system parameters are set to be: $m = 0.01$, $c = 0.05$, $k = 10$, $Z = 1$, $\varphi = -1 \times 10^{-4}$, $c_p = 15 \times 10^{-9}$, $R_L = 1 \times 10^5$. Figure 1-2 (a) shows a steady-state voltage response based on Eqns (1.1) and (1.2), which indicates a narrow operational bandwidth. Under a stationary harmonic vibration source, when the frequency is within the device's resonance region, an optimised power level can be obtained. However, in dealing with a varying vibration source, which randomly distributes in a wide frequency spectrum (i.e., from 2 Hz to 10 Hz), the large-amplitude oscillation cannot be activated at off-resonance regime, the power output of the device drops significantly.

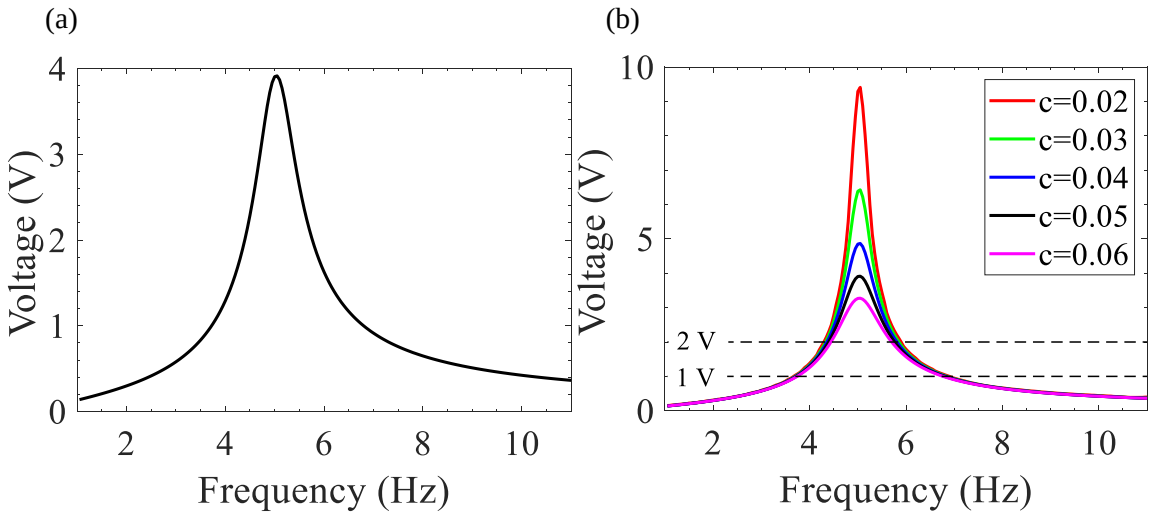

Figure 1-2. (a) Steady-state voltage response of a linear VEH; (b) Voltage responses with varying damping coefficient.

Although the power output of the device can be further increased by reducing the damping of the system through different design techniques, the operational bandwidth remains almost the same. As shown in Figure 1-2 (b), with the decreased damping coefficient, the overall output voltage of the system increases noticeably. On the other hand, with two reference voltage levels set to be 1 V and 2 V in Figure 1-2 (b), the effective bandwidth of the five cases seems to be unchanged, which implies the narrow bandwidth issue still exists even adopted with very weak damping coefficients. As the resonance region of linear VEHs naturally suffers from narrow bandwidth, the devices are capable only under stationary vibration sources.

Tuning techniques aim to settle the narrow bandwidth issue of the linear VEHs, by adjusting the resonance region of the system either passively or actively to adapt the vibration sources, for performance enhancement of VEHs. With resonance tuning, if the ambient vibration source is in the vicinity of the tuned device's resonance region, an optimised power output can be achieved. Based on the external power requirements, tuning approaches could be divided into two branches, passive tuning and active tuning. Passive tuning techniques require intermittent power input, generally use manual tuning to alter the vibrating structure's effective stiffness, then match the device's resonance with targeted excitation frequencies. To alter the system's effective stiffness, common techniques including preload approaches [20, 21] and adding magnetic attractive/repulsive forces [22, 23] have been studied intensively.

Yet, an inevitable issue for manual tuning is that the stabilised ambient frequency is infrequent in the real environment. The variation causes the device to exit from its resonance regime to off-resonance status, which can lead to a significant reduction of power output. In addition, the manual tuning approaches are not workable for real-time applications. Active tuning approaches are a primary remedy to achieve real-time applications and have the ability to adapt the ambient vibration sources automatically. On the other hand, continuous power input is required to tune the resonance of the system [24]. Compared with passive tuning, active tuning has the potential to achieve real-time applications, despite the fact that the tuneable bandwidth is still limited in specific ranges, and the required power input for tuning is contradictory to energy harvesting purposes.

As most of the vibration sources in realistic environments are distributed within certain ranges of frequency spectrums, the most pressing issue of VEHs from mechanical and

structural perspectives is whether the designed device is capable of being effectively operational with varying vibration sources.

1.2 Aims and Objectives

The thesis aims to tackle the narrow bandwidth issues in conventional VEHs by employing structural and externally induced nonlinearities into the systems, hence introducing broadband techniques to enhance the effective bandwidth as well as the power level of VEHs.

The detailed objectives of this thesis are:

1. To investigate an electromagnetic energy harvester with combined primary and parametric resonance in the presence of motion limiters.

2. To investigate a broadband piezoelectric energy harvesting array under both directly and parametrically excited conditions.

3. To optimise the performance of a bistable piezoelectric energy harvester under parametric excitation by an external oscillating source and magnetic coupling effects.

4. To investigate a U-shaped broadband energy harvester with multi-directional and multi-mode features based on a two-to-one internal resonance phenomenon.

5. To investigate an L-shaped internal-resonance-based piezoelectric energy harvester with combined in-plane and out-of-plane motions for high-efficient energy harvesting.

1.3 Preview of the thesis

Chapter 1 provides an overview of the applications of energy harvesting technologies to shed light on the significance of this work. Chapter 2 presents a detailed review of the use of internal and externally induced nonlinearities in VEHs as broadband techniques. The subsequent five chapters present five manuscripts either published or submitted as journal papers. Chapter 8 summarises the major findings of the thesis and suggests future work.

References

1. Iqbal, M., M.M. Nauman, F.U. Khan, P.E. Abas, Q. Cheok, A. Iqbal, and B. Aissa, *Vibration-based piezoelectric, electromagnetic, and hybrid energy harvesters for microsystems applications: A contributed review.* International Journal of Energy Research, 2021. **45**(1): p. 65-102.
2. Ando Junior, O.H., A.L.O. Maran, and N.C. Henao, *A review of the development and applications of thermoelectric microgenerators for energy harvesting*. Renewable and Sustainable Energy Reviews, 2018. **91**: p. 376-393.
3. Rashidi, S., M. Hossein Kashefi, and F. Hormozi, *Potential applications of inserts in solar thermal energy systems – a review to identify the gaps and frontier challenges.* Solar Energy, 2018. **171**: p. 929-952.
4. Melikoglu, M., *Current status and future of ocean energy sources: A global review.* Ocean Engineering, 2018. **148**: p. 563-573.
5. Mwasilu, F. and J.-W. Jung, *Potential for power generation from ocean wave renewable energy source: A comprehensive review on state-of-the-art technology and future prospects.* IET Renewable Power Generation, 2019. **13**(3): p. 363-375.
6. Wang, J., L. Geng, L. Ding, H. Zhu, and D. Yurchenko, *The state-of-the-art review on energy harvesting from flow-induced vibrations.* Applied Energy, 2020. **267**: p. 114902.
7. McCarthy, J.M., S. Watkins, A. Deivasigamani, and S.J. John, *Fluttering energy harvesters in the wind: A review.* Journal of Sound and Vibration, 2016. **361**: p. 355-377.
8. Beeby, S.P., L. Wang, D. Zhu, A.S. Weddell, G.V. Merrett, B. Stark, G. Szarka, and B.M. Al-Hashimi, *A comparison of power output from linear and nonlinear kinetic energy harvesters using real vibration data.* Smart Materials and Structures, 2013. **22**(7): p. 075022.
9. Abdelkareem, M.A.A., L. Xu, M.K.A. Ali, A. Elagouz, J. Mi, S. Guo, Y. Liu, and L. Zuo, *Vibration energy harvesting in automotive suspension system: A detailed review.* Applied Energy, 2018. **229**: p. 672-699.
10. Wang, H., A. Jasim, and X. Chen, *Energy harvesting technologies in roadway and bridge for different applications – a comprehensive review.* Applied Energy, 2018. **212**: p. 1083-1094.
11. Khan, F.U. and I. Ahmad, *Review of energy harvesters utilizing bridge vibrations.* Shock and Vibration, 2016. **2016**: p. 1340402.
12. Hosseinkhani, A., D. Younesian, P. Eghbali, A. Moayedizadeh, and A. Fassih, *Sound and vibration energy harvesting for railway applications: A review on linear and nonlinear techniques.* Energy Reports, 2021. **7**: p. 852-874.
13. Feenstra, J., J. Granstrom, and H. Sodano, *Energy harvesting through a backpack employing a mechanically amplified piezoelectric stack.* Mechanical Systems and Signal Processing, 2008. **22**(3): p. 721-734.
14. Xie, L. and M. Cai, *Increased energy harvesting and reduced accelerative load for backpacks via frequency tuning.* Mechanical Systems and Signal Processing, 2015. **58-59**: p. 399-415.
15. Kluger, J.M., T.P. Sapsis, and A.H. Slocum, *Robust energy harvesting from walking vibrations by means of nonlinear cantilever beams.* Journal of Sound and Vibration, 2015. **341**: p. 174-194.
16. Karami, M.A. and D.J. Inman, *Powering pacemakers from heartbeat vibrations using linear and nonlinear energy harvesters.* Applied Physics Letters, 2012. **100**(4): p. 042901.
17. Ansari, M.H. and M.A. Karami, *Modeling and experimental verification of a fan-folded vibration energy harvester for leadless pacemakers.* Journal of Applied Physics, 2016. **119**(9): p. 094506.
18. Iqbal, J., M. Khan, M. Talha, H. Farman, B. Jan, A. Muhammad, and H.A. Khattak, *A generic internet of things architecture for controlling electrical energy consumption in smart homes.* Sustainable Cities and Society, 2018. **43**: p. 443-450.

19. Shaikh, F.K. and S. Zeadally, *Energy harvesting in wireless sensor networks: A comprehensive review*. Renewable and Sustainable Energy Reviews, 2016. **55**: p. 1041-1054.
20. Leland, E.S. and P.K. Wright, *Resonance tuning of piezoelectric vibration energy scavenging generators using compressive axial preload.* Smart Materials and Structures, 2006. **15**(5): p. 1413-1420.
21. Hu, Y., H. Xue, and H. Hu, *A piezoelectric power harvester with adjustable frequency through axial preloads.* Smart Materials and Structures, 2007. **16**(5): p. 1961-1966.
22. Challa, V.R., M.G. Prasad, Y. Shi, and F.T. Fisher, *A vibration energy harvesting device with bidirectional resonance frequency tunability.* Smart Materials and Structures, 2008. **17**(1): p. 015035.
23. Challa, V., M. Prasad, and F. Fisher, *High efficiency energy harvesting device with magnetic coupling for resonance frequency tuning*. Sensors and Smart Structures Technologies for Civil, Mechanical, and Aerospace Systems. Vol. 6932. 2008: SPIE.
24. Wu, W.-J., Y.-Y. Chen, B.-S. Lee, J.-J. He, and Y.-T. Peng, *Tunable resonant frequency power harvesting devices*. Smart Structures and Materials. Vol. 6169. 2006: SPIE.

Chapter 2

Literature Review

2.1 Brief introduction

To remedy the narrow bandwidth issues in linear VEHs, nonlinearities have been introduced to enhance the effective bandwidth and overall power level of VEHs under realistic excitation sources. In this chapter, a critical review of vibration-based energy harvesting techniques is presented, which focuses on techniques/phenomena that can potentially enhance the performance in terms of bandwidth, power level, and density of VEHs by providing structural or externally induced nonlinearities.

2.2 Array-like, multi-degree-of-freedoms (MDOF) and multi-mode VEHs

As discussed in Chapter 1, the energy harvesting efficiency of passive and active tuning techniques relies on the excitation sources. In dealing with non-stationary vibration sources (environmental vibration sources are naturally varying and distributing in certain ranges of frequency spectrum), the linear resonance region limits the applicability of these techniques. Instead of tuning techniques, an alternative approach is to design broadband devices to fully cover the frequency ranges of those vibration sources. The concept of 'broadening operational frequency bandwidth' is served as the foundation, as well as the centre of interest of many nonlinear techniques for improving energy harvesting efficiency.

In early applications, researchers have utilised several linear approaches to introduce combinations of natural frequencies in one system. Figure 2-1 (a) shows a typical multi-

array energy harvester with piezoelectric transducers. By properly selecting the length, width and tip mass of each clamped-free cantilever beam, the designed system could have a wide overall bandwidth with adjacent natural frequencies under base excitations in the designed frequency ranges as shown in Fig. 2-1 (b). An array-like beam-based VEH proposed by Shahruz [1] was a typical approach based on multi-resonance accumulation. With different scaling, array-based energy harvesters can be fabricated and used for MEMS applications [2, 3]. Besides the piezoelectric transduction method, electromagnet transducers (i.e., a tip magnet on the vibrating element that interacts with designed coils can generate current flow) can also be effective in array systems. In some cases, both transduction methods were adopted to optimise the power level.

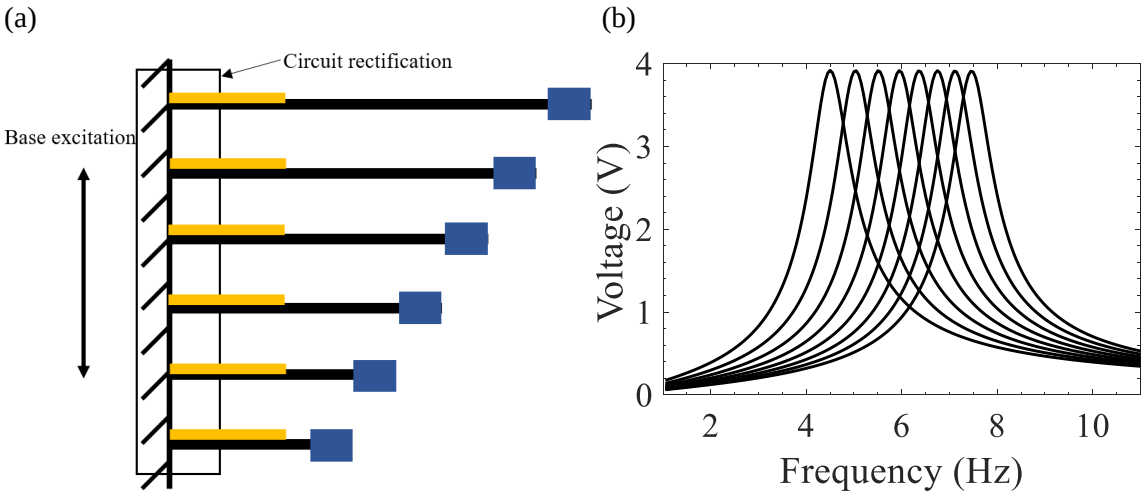

Figure 2-1. (a) A schematic of multi-array energy harvester with piezoelectric transducers. (b) Simulated frequency response of a multi-array VEH based on Eqns. (1-1) and (1-2) with different effective stiffness *k*.

Multi-mode/MDOF VEHs are counted as another type of linear broadband technique. Most of the multi-mode/MDOF VEHs utilised one main structure and additionally designed sub-structures; multiple adjacent natural frequencies could attain multiple peaks over a certain frequency range. Abdelkefi et al. [4] considered a unimorph T-shaped VEH with asymmetric tip mass blocks to undergo bending-torsion vibrations. The numerical results indicated that a broader bandwidth could be achieved by tuning the bending and torsion modes closer to each other. Li et al. [5] proposed a multi-mode VEH, a clamped-free beam as the main structure had several adjustable beams as sub-structures attached at the free end. Other recent investigations on multi-mode/MDOF VEHs can be found in [6-11]. In some cases, the overall operational bandwidth displays discontinuity in the

frequency domain and the natural frequencies of the designed device are far from each other. For these devices, researchers attempted to carry out another potential feature in multi-mode/MDOF VEHs, which is the capability of working effectively under different directional vibration sources. For instance, Zhou et al. [7] studied a piezoelectric VEH with a zigzag structure, which was capable of harvesting energy under different excitation directions. Yang et al. [12] combined multi-directional and multi-stable characteristics together on a spring-mass structure as a low-frequency VEH.

Although array-like, multi-degree-of-freedoms (MDOF) and multi-mode VEHs did have the capability to broaden the operational frequency range by accumulating multiple resonance frequencies together to create an overall wider bandwidth, as well as dealing with multi-directional vibration sources. The main concerns about these approaches are the complexity of design, as well as the sacrifice of power density. In addition, despite a 'broad' operational bandwidth that can be obtained, the overall resonance region is composed of several narrow resonance regions. In essence, the working principle of these devices is still in linear perspective. Recent investigations on MDOF and multi-mode VEHs have started to combine them with other techniques, including internal and externally induced nonlinearities, to further enhance energy harvesting efficiency.

2.3 Multi-stable VEHs

In order to achieve a broadband system, magnetic restoring force is commonly introduced by researchers to induce external nonlinearities to VEHs [13-17]. In early tunning approaches, magnetic couplings have been employed to tune the effective stiffness of the system and match the frequencies of vibration sources; however, as the magnetic couplings induce nonlinearities into the system, the governing equation of a linear piezoelectric VEH (Eqn. (1-1)) is insufficient to describe the motions of the present system. A typical design with magnetic restoring force is shown in Figure 2-2, different from linear case (Figure 1-1), a tip magnet interacts with a stationary magnet repulsively. In such conditions, the stable equilibrium state no longer stays along with the centre line position (the original position of the beam in Figure 2-2). Instead, new stable states occur at two initially curved positions and the locations/positions are dependent on the initial distance d between the two magnets and the strength of the magnetic field. This phenomenon is known as bistability; additional stable equilibrium states in the system induce different dynamic

behaviours, which can potentially be utilised in energy harvesting for optimising power level and broadening operational bandwidth.

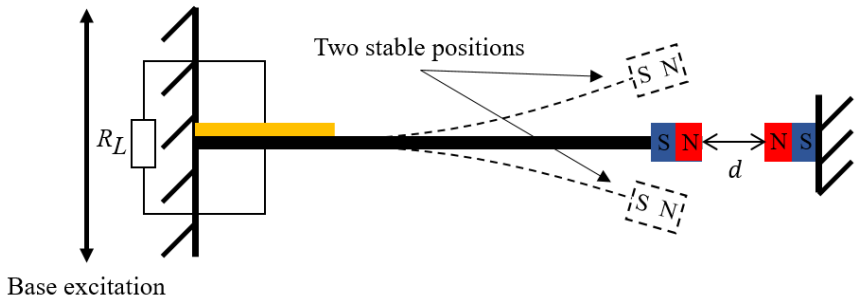

Figure 2-2. Schematic of a bistable energy harvester under a harmonic excitation.

With the magnetic coupling effects, Eqn. (1-1) has an additional magnetic restoring force term and can be expressed as

$$m\ddot{x} + c\dot{x} + kx - \varphi v + \frac{\partial U_m}{\partial x} = -m\ddot{y}, \qquad (2-1)$$

where U_m is the potential energy field caused by magnetic interactions between the two magnets. The form of the potential energy field can be expressed as [18-20]

$$U_m(x) = \frac{1}{2}k_1(1-\lambda)x^2 + \frac{1}{4}{k_3}^4, \qquad (2-2)$$

where λ is the tuning system parameter, k_1 and k_3 are the linear and nonlinear cubic stiffness terms, respectively. The magnetic restoring force can be derived from Eqn. (2-2) as

$$F_m(x) = k_1(1-\lambda)x + {k_3}^3 \qquad (2-3)$$

Figure 2-3 (a) shows the three different behaviours with varying parameters in Eqn. (2-2). The black dash plot displays two potential wells, which indicates the two equilibrium stable states. Under a sufficiently high harmonic excitation level, the system receives enough energy to overcome the potential barrier (between the two wells in Figure 2-3 (b)), it is able to move between the two stable states periodically, and the large-amplitude oscillation named periodic interwell motion can be revealed. On the contrary, under a small excitation, the device would be trapped into one potential well for periodic motion, which is named intrawell motion. By altering the distance between the two magnets, the system can display softening or hardening behaviours (i.e., the linear resonance bends to left or right), which

results in unstable regions in frequency responses and multiple solutions under different initial conditions. Generally, a system displays softening/hardening responses that has saddle-node bifurcations under harmonic base excitations. Under up sweep and down sweep harmonic excitations, the frequency response of the system has coexisting solutions, the initial conditions (i.e., displacement, velocity, acceleration) determine if it can jump to the higher branch and drop into the lower branch. Consequently, for multi-stable VEHs, the vital research interest is maintaining the device on higher-orbit branches with large-amplitude oscillations for optimised power level.

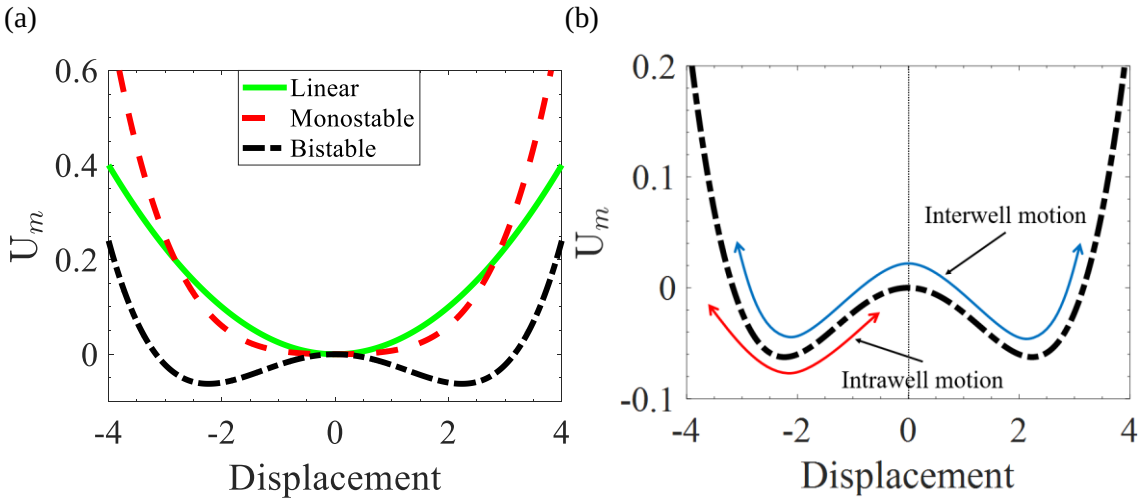

Figure 2-3. (a) Energy Potential with different parameters in Eqn. (2-2) and (b) two types of oscillations in a bistable system.

Bistable VEHs with large-amplitude oscillations from interwell motion and broader bandwidth in the presence of softening and hardening frequency responses, have attracted a great many of attention. For approaches based on the magnetic restoring force, typical modifications focused on magnetic field arrangements. By adding external stationary magnets or changing the orientations of the magnets, the system could exhibit additional stable states, such as tristable [21-23] and even quadstable states [24, 25]. Preloading and pre-shaped/pre-bent approaches are also commonly utilised to introduce bistability [26-32]. For instance, Cottone et al. [28] investigated a double-clamped beam-based piezoelectric VEH subjecting to axial compression loads. The bucked beam under base excitations showed bistable states and strong hardening responses; compared with an unbuckled case, the power level was enhanced. The properties of vibration sources (i.e., level and type) as prerequisites for measuring the effectiveness of VEHs, have been studied extensively. Cao

et al. [33] attempted to use a bistable device with a time-varying potential energy function to harvest energy from working and running. Wang et al. [34] studied an asymmetric bistable VEH subjecting to different types of excitation. The experimental results demonstrated that a certain range of bias angles was required to enhance the harvested power output from human motion.

Indeed, the large-amplitude interwell oscillations in multi-stable energy harvesters result in increased power levels and wider operational bandwidth than linear counterparts. The critical concern is whether the device is still reliable under small excitations. The high-energy orbit motions require a sufficiently high base excitation level to escape the potential barrier; otherwise, a monostable case displays more robust performance than a bistable configuration [35]. In addition, the frequency responses of most VEHs are tested under harmonic excitations, including up sweep and down sweep. Because the high-energy orbit motions can only be activated under certain initial conditions, with a suddenly changed excitation amplitude such as a random excitation source, the oscillations can possibly drop to the low-energy orbit and result in a significant power reduction.

Consequently, to improve the efficiency of multi-stable VEHs under low excitation levels, the promising approaches are either reducing the barrier between potential wells or designing shallower potential wells. Lan and Qin [36] utilised an additional stationary magnet placed at the centreline position in attractive to the tip magnet and two repulsive magnets to lower the height/depth of the potential barrier. By subjecting the device to random excitation, the power level outperformed the counterpart. Wang and Liao [37] proposed a bistable energy harvester by adding an elastic magnifier as a two-degree-of-freedom structure. The external structure aimed to magnify the base excitation level, the secondary structure as a conventional bistable VEH can be therefore easier to activate the high-energy orbit oscillations. Cao et al. [38] investigated the influence of potential well depth on a tristable energy harvester based on the potential function. Chiacchiari et al. [39] numerically investigated a bistable energy harvester coupled with a directly excited sub-structure to improve the threshold of triggering interwell oscillations under low-level impulse excitations.

Previous studies mentioned above have exploited the feasibility of employing multi-stability to VEHs. For linear and multi-stable VEHs, the latter demonstrated rich dynamics in the system, which were practically capable of enhancing the power level from intrawell

or interwell motions and broadening the effective bandwidth from softening/hardening responses. Yet, the influence of base excitation is exceedingly important on these devices for attaining the high-energy orbit. Though several investigations have studied different techniques to induce the potential function into the system, such as preloading, magnetic restoring force and gravitational potential, a more primitive question is whether the threshold of the large-amplitude interwell motion can be reduced for multi-stable VEHs to work robustly under small and realistic excitations.

2.4 Parametrically excited VEHs

Parametric resonance, sometimes also known as the Mathieu equation, has a different resonance behaviour from conventional VEHs that utilise principal primary resonances [40]. The Mathieu equation can be written as [41, 42]

$$m\frac{d^2x}{dt^2} + c\frac{dx}{dt} + (k + \epsilon Z cos\Omega t)x = 0, \qquad (2-4)$$

where x is the displacement, c is the damping, ϵ is a small parameter, k is the linear stiffness, Ω is the parametric frequency. A parametrically excited device (i.e., a cantilever beam) has a principal parametric resonance located at twice the fundamental frequency ω_n (i.e., $\Omega \cong 2\omega_n$). As shown in Eqn. (2-4), the amplitude of the system is time-dependent, which implies, under a parametric excitation, the dynamic instability leads the system to oscillate with a gradually growing amplitude.

A typical parametrically excited physical system is a moving swing (or as an inverted pendulum-mass system) with periodically increased amplitude. This interesting scientific system with rich dynamic behaviours from periodic motions to complex chaotic motions, has been actively exploited by many researchers [43-49]. One of the interests lies in the stability of the dynamic response, as shown in Figure 2-3. The simulation results of time series and phase portraits demonstrate that, the parametric resonance needs additional time to build up the amplitude but can possibly reach higher peaks than the conventional directly excited counterpart. Thus, the parametric resonance phenomenon can be utilised as a mechanical amplifier in VEHs [50, 51], if the external base excitations can satisfy certain conditions of triggering the parametric resonance. In addition, as the ambient vibration sources are naturally multi-directional, an energy harvesting device with design

mechanisms is capable of harvesting bi-directional vibration sources by its primary resonance as well as the parametric resonance as a multi-directional VEH. Unlike directly excited energy harvesters, for instance, a directly excited cantilever-based VEH has the excitation direction, which is perpendicular to the beam length (Figure 1-1). For parametric excitation, the external force direction is normally parallel to the beam length.

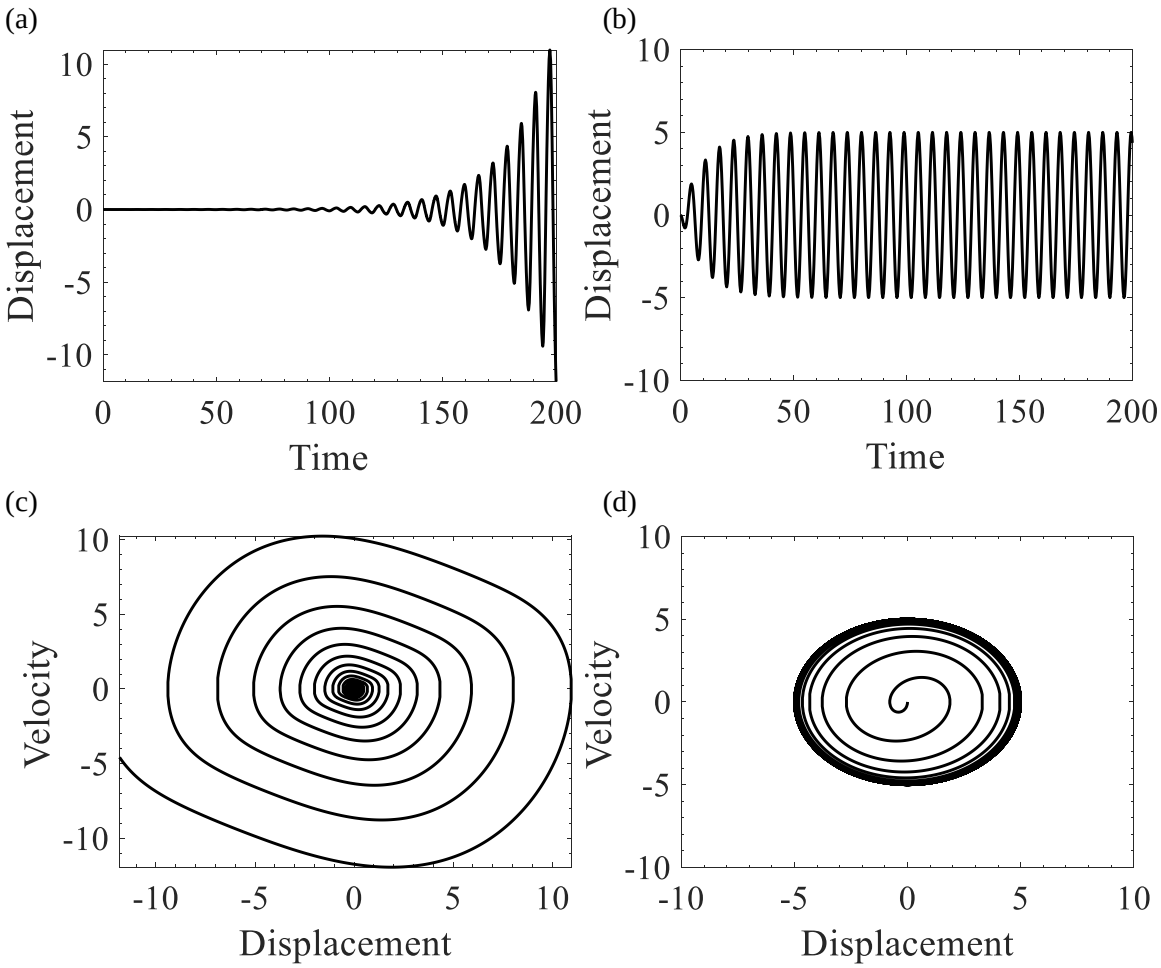

Fig 2-3. Time series and the corresponding phase portraits of a parametrically excited system based on Eqn. (2-4) ((a) and (c)) and a directly excited system without piezoelectric coupling effects based on Eqn. (1-1) ((b) and (d)). $m = 1, c = 0.2, k = 1, Z = 1, \Omega = 2; h = 0.6$.

Although the feasibility of utilising the parametric resonance for energy harvesting has been raised and theoretical investigations have been conducted, critical excitation levels (or threshold amplitudes) still exist in parametrically excited devices [50, 52]. Below the critical excitation levels, devices exhibit zero-amplitude frequency responses [40, 53]. To obtain a higher energy/power output and achieve efficient energy harvesting in the parametrically excited VEHs, the stability of the system shall be in unstable regions. As the

stability chart of parametric resonance is directly related to the damping coefficient [54], one critical design criterion of a parametrically excited VEH is lowering the mechanical and electrical damping of the system. However, piezoelectric transducers with high power density are mostly utilised in MEMS and other small-scale applications. Thus, the impacts of additional damping from piezoelectric materials further increase the initial threshold amplitude, which restricts the effectiveness of parametrically excited VEHs. To optimise the power level, fully covered unimorph or bimorph piezoelectric layers are suggested to be bonded onto the vibrating structure, but the trade-off is that activating the parametric resonance requires a much higher excitation level. To reduce the initial threshold amplitude, Jia et al. [55] experimentally utilised a pendulum-mass structure with piezoelectric transducers and a lever pivot to achieve a lower level of threshold amplitude. Yang and Towfighian [56] introduced a low threshold amplitude parametrically excited VEH by adopting magnetic coupling nonlinearity to the system.

The parametric resonance as an inherent nonlinear phenomenon indeed provides an alternative solution to increase the power level for energy harvesting. However, the narrow bandwidth issue still remains unsettled in single parametrically excited devices compared with nonlinear VEHs that utilise hardening and softening responses. In order to broaden the operational bandwidth of parametrically excited devices, externally induced nonlinearities are therefore introduced, such as a buckled beam structure subjecting to subharmonic parametric resonance [57]. By combining parametrically excited pendulum with magnetic spring forces, the strong hardening response provided the system with a broader bandwidth [58]. Internal nonlinearities such as inertial effects in a parametrically excited micro-resonator were considered by [59] for wide-range sensing purposes. Garg and Dwivedy [60] theoretically investigated a parametrically excited energy harvester with a three-to-one internal resonance and demonstrated that the proposed system had enhanced power than its conventional counterpart. To present, a number of investigations on theoretical modellings have been presented to show the effectiveness of parametrically excited VEHs [50, 52, 61]. Aghamohammadi et al. [62] presented an alternative theoretical method to predict the off-resonance responses of parametrically excited systems and Alevras et al. [63] showed that the broadband characteristics in a parametrically excited energy harvester have less dependence on the magnitude of the nonlinear cubic coefficient than Duffing type VEHs. Despite these studies theoretically validating the broadband performance of the parametric resonance and the corresponding potential applications in

energy harvesting, the practical implementations of parametrically excited VEHs are still limited compared with conventional directly excited cases.

2.5 Internal-resonance based VEHs

In MDOF systems, if there exist cubic and quadratic nonlinearities, and its natural frequencies are commensurable or nearly commensurable (e.g., $2\omega_1 \cong \omega_2; 3\omega_1 \cong \omega_3$), internal resonance phenomena may occur [64-66]. When an internal resonance is presented, modal interactions induce rich system dynamics and interesting phenomena such as periodic, quasi-periodic, chaotic responses, etc. For one of the typical phenomena that exists in the internal resonance, the frequency response bends to increasing and decreasing frequency directions from the centre frequency, which is also known as double-jump phenomenon. Compared with its linear counterpart (without internal-resonance phenomena), the double-jump phenomenon has the potential to broaden the frequency bandwidth as a broadband technique in two directions. In the presence of the energy exchanges between the coupled modes, excitation frequency at lower mode can trigger large-amplitude oscillations at higher modes, and vice versa. Initial applications based on the internal resonance worked as vibration absorbers in mechanical systems [67, 68]. The oscillations of the core element can be reduced and transferred to additionally designed sub-structures for structural protection purposes. In the last ten years, internal resonance has been considered as an energy harvesting method that has the potential to achieve broadband, low-frequency operation and high-efficiency energy conversion.

Chen and Wang [69] theoretically proposed an electromagnetic VEH based on an internal resonance. Under the same excitation conditions, the proposed device exhibited double-jump phenomena and had enhanced power level and effective bandwidth than the linear counterpart. Their theoretical investigations on internal-resonance-based VEHs also covered piezoelectric transducers [64], axially loaded beam [70] and VEHs coupled with energy sinks [71]. Numerical studies on three-to-one internal resonance such as dynamic behaviours of a parametrically excited VEH [60] and a piezoelectric VEH [72] demonstrated that, introducing internal-resonance phenomena to vibration-based energy harvesting is advantageous to increasing averaging power output and broadening bandwidth.

In order to obtain internal-resonance phenomena in a physical system/device, L-shaped beam structure is a simpler way to practically achieve commensurable natural frequencies than a single cantilever beam in clamped-free/clamped-clamped conditions. By altering the system parameters, such as dimensions of two beam components and mass blocks, internal-resonance phenomena can be obtained. Most experimental research works of L-shaped VEHs focused on two-to-one or three-to-one internal resonances between the first bending and second bending modes [73-75]. Harne et al. [74] investigated an L-shaped energy harvester with a two-to-one internal resonance under harmonic excitations with additive noise. Nie et al. [75] utilised a theoretical distributed-parameter model and the finite element method (FEM) to verify the experimental results. Similar to linear tuning techniques, magnetic coupling is an effective approach to facilitate internal resonance. Likewise, the magnetic restoring force in repulsive/attractive case, as an externally induced nonlinearity, could induce more distorted and complex dynamic behaviours, which is possible to further enhance the bandwidth/power performance of internal-resonance-based VEHs [76-82]. For instance, Xiong et al. [76] proposed a clamped-free piezoelectric energy harvester with an auxiliary oscillator and a tip magnet. By altering the distance between the tip and stationary magnet, a two-to-one internal resonance was revealed between the first two bending modes. Yang and Towfighian [77, 78] investigated internal-resonance-based VEH with magnetic couplings using multiple scales perturbation method and experiments, bistability could be revealed with a moving magnet attached on the main vibrating structure.

Compared with linear multi-mode/MDOF VEHs, internal-resonance-based VEHs require natural frequencies to be commensurable or nearly commensurable, which are more challenging to achieve in physical systems and require additional cost for fabrication. On the other hand, in the presence of internal resonance phenomena, energy exchanges between coupled modes enable more flexibilities to the system, such as large-amplitude oscillations at higher mode can be triggered by lower mode excitation frequency, vice versa. With the double-jump (or double-bend) frequency responses, the bandwidth can be broadened in both increasing and decreasing frequency directions. Yet, the extended resonance region due to internal resonance is still limited, compared with devices using softening/hardening responses. Generally, without considering the coexisting motions, restoring force has a greater impact on broadening the bandwidth. Still, Internal-resonance-based VEHs with multimodal, multi-directional and high power density characteristics,

deserve further evaluations and investigations, such as adding externally induced nonlinearities to broaden the bandwidth further.

2.6 Motion limiter (piecewise-linear restoring force)

The hardening frequency response in a system could also be induced by motion limiters (or mechanical stoppers). Figure 2-4 (a) depicts a linear piezoelectric VEH (see Figure 1-1) equipped with a two-side motion limiter. Motion limiter is generally made of rigid materials and locates at either/both side(s) of the cantilever beam; an adjustable gap distance Δ between the tip of the motion limiter and beam is determined by system parameters. Under a harmonic base excitation, when the excitation frequency in the up sweep is close to the resonance region of the device, the large-amplitude oscillations of the device lead the cantilever beam to strike the motion limiters. Accordingly, the effective stiffness instantly increases to a much higher value due to the piecewise linear restoring force, as illustrated in Figure 2-4 (b). Such that, an extended resonance regime due to external impacts can be formed simultaneously. Similar to nonlinear VEHs using magnetic restoring force, there are coexisting solutions in frequency responses (between up sweep and down sweep.)

(a)

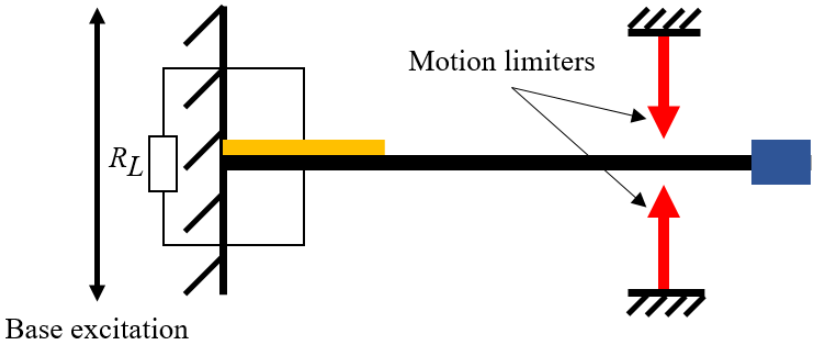

(b)

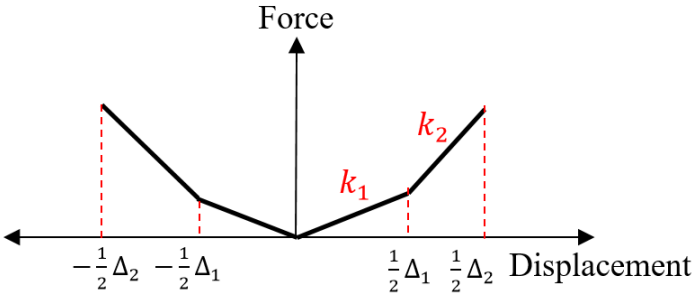

Figure 2-4. (a) Schematic of a piezoelectric energy harvester with motion limiters under a harmonic excitation. (b) The piecewise stiffness behaviour of the proposed device, Δ_1 and Δ_2 are the initial distances between contact positions and motion limiters.

The effects of motion limiter can sufficiently broaden the operational bandwidth, in some cases, the corresponding hardening response in the up sweep can be even broader than a VEH with magnetic restoring force. However, the power sacrifice due to motion limiter implies a trade-off between the operational bandwidth and peak power level. What is more, for conventional directly excited VEHs with motion limiters, large bifurcations in frequency responses exist between up and down sweep cases. Soliman et al. [83] presented a prototype of a MEMS-based VEH with motion limiters. Although the peak voltage level decreased, a 250% increase was found in bandwidth. A parameter study of the gap distance was performed to find the optimised value for maximum power generation. Different designs can be found in [84-88]. More recently, for theoretical modelling, two-DOF piezoelectric energy harvesters based on averaging perturbation method have been investigated by Liu et al. [89] and Hu et al. [90]. Zhou et al. [91] studied four types of motion limiters and considered geometric and inertia nonlinearities. Fan et al. [92] proposed a monostable VEH with combined motion limiter and magnetic restoring force effects. The ongoing concerns of VEHs using motion limiter are the dependence of excitation sources. For directly excited prototypes, the broadband performance based on the hardening response needs harmonic excitations with a certain excitation level. Under other conditions, the gap distance may need to be manually tuned to optimise the effective bandwidth and power level, which follows similar operating rules as tuning approaches to some extent.

2.7 Summary and research gaps

From the literature review, the centre of interest in state-of-the-art vibration-based energy harvesting techniques has been shifted from linear to nonlinear approaches, in order to deal with varying, time-dependent and realistic vibration sources. One of the most vital issues for VEHs from mechanical and structural perspectives is whether the proposed device is capable and efficient in harvesting the environmental vibration sources within a wideband frequency range. Borrowing concepts from nonlinear phenomena/techniques as structural or externally induced nonlinearities to VEHs have been exploited intensively to fulfil the needs/requirements in various conditions. Nonetheless, employing and combining nonlinear interactions between different techniques still deserve further studies and evaluations to tackle several critical issues in the aforementioned modern techniques in the stage of signal (i.e., environmental vibration sources) capturing. In particular:

- Parametrically excited VEHs provide an alternative solution to harvest energy at twice the primary resonance and could potentially have higher power output than directly excited counterparts. However, the nonlinear phenomenon is highly dependent on excitation level and the resonance region is rather narrow compared with VEHs that display softening/hardening frequency responses. Limited studies utilised externally induced nonlinearities to extend the resonance regime of the parametric resonance as a broadband technique.
- Further investigations on activating the threshold amplitude and broadening the resonance region of the parametric resonance shall be performed to justify if parametrically excited VEHs are truly advantageous under small excitations.
- The high-orbit oscillations due to interwell motion in multi-stable VEHs can greatly enhance the power output but also places restrictions on the excitation levels. As the ultimate goal of multi-stable VEHs is achieving continually periodic large-amplitude oscillations under varying vibration sources, insufficient investigations on optimising the depth/shape of the potential barriers can be found.
- Internal-resonance-based VEHs with high-efficient and multi-modal characteristics are more promising than linear multi-mode/MDOF VEHs. Limited experimental studies have been conducted to verify the broadband performance of internal-resonance-based VEHs.
- With the piezoelectric transduction method, the bending modes of the core vibrating elements are principally selected for strain rate-voltage conversion, though the

strain change rates in torsional modes can also be efficient with proper piezoelectric transducers. Minimal investigations on the dynamics of bending-torsion motions and the bandwidth/power performance in the presence of internal-resonance phenomena were found.

References

1. Shahruz, S.M., *Design of mechanical band-pass filters for energy scavenging.* Journal of Sound and Vibration, 2006. **292**(3): p. 987-998.
2. Fang, H.-B., J.-Q. Liu, Z.-Y. Xu, L. Dong, L. Wang, D. Chen, B.-C. Cai, and Y. Liu, *Fabrication and performance of mems-based piezoelectric power generator for vibration energy harvesting.* Microelectronics Journal, 2006. **37**(11): p. 1280-1284.
3. Liu, J.-Q., H.-B. Fang, Z.-Y. Xu, X.-H. Mao, X.-C. Shen, D. Chen, H. Liao, and B.-C. Cai, *A mems-based piezoelectric power generator array for vibration energy harvesting.* Microelectronics Journal, 2008. **39**(5): p. 802-806.
4. Abdelkefi, A., F. Najar, A.H. Nayfeh, and S.B. Ayed, *An energy harvester using piezoelectric cantilever beams undergoing coupled bending–torsion vibrations.* Smart Materials and Structures, 2011. **20**(11): p. 115007.
5. Li, X., D. Upadrashta, K. Yu, and Y. Yang, *Analytical modeling and validation of multi-mode piezoelectric energy harvester.* Mechanical Systems and Signal Processing, 2019. **124**: p. 613-631.
6. Dhote, S., Z. Yang, and J. Zu, *Modeling and experimental parametric study of a tri-leg compliant orthoplanar spring based multi-mode piezoelectric energy harvester.* Mechanical Systems and Signal Processing, 2018. **98**: p. 268-280.
7. Zhou, S., J.D. Hobeck, J. Cao, and D.J. Inman, *Analytical and experimental investigation of flexible longitudinal zigzag structures for enhanced multi-directional energy harvesting.* Smart Materials and Structures, 2017. **26**(3): p. 035008.
8. Wang, J., G. Hu, Z. Su, G. Li, W. Zhao, L. Tang, and L. Zhao, *A cross-coupled dual-beam for multi-directional energy harvesting from vortex induced vibrations.* Smart Materials and Structures, 2019. **28**(12): p. 12LT02.
9. Sun, R., Q. Li, J. Yao, F. Scarpa, and J. Rossiter, *Tunable, multi-modal, and multi-directional vibration energy harvester based on three-dimensional architected metastructures.* Applied Energy, 2020. **264**: p. 114615.
10. Toyabur, R.M., M. Salauddin, H. Cho, and J.Y. Park, *A multimodal hybrid energy harvester based on piezoelectric-electromagnetic mechanisms for low-frequency ambient vibrations.* Energy Conversion and Management, 2018. **168**: p. 454-466.
11. Hu, G., J. Liang, C. Lan, and L. Tang, *A twist piezoelectric beam for multi-directional energy harvesting.* Smart Materials and Structures, 2020. **29**(11): p. 11LT01.
12. Yang, T., Q. Cao, Q. Li, and H. Qiu, *A multi-directional multi-stable device: Modeling, experiment verification and applications.* Mechanical Systems and Signal Processing, 2021. **146**: p. 106986.
13. Mann, B.P. and N.D. Sims, *Energy harvesting from the nonlinear oscillations of magnetic levitation.* Journal of Sound and Vibration, 2009. **319**(1): p. 515-530.
14. Cottone, F., H. Vocca, and L. Gammaitoni, *Nonlinear energy harvesting.* Physical Review Letters, 2009. **102**(8): p. 080601.
15. Zou, H.-X., W.-m. Zhang, W.-B. Li, K.-X. Wei, Q.-H. Gao, Z.-K. Peng, and G. Meng, *Design and experimental investigation of a magnetically coupled vibration energy harvester using two inverted piezoelectric cantilever beams for rotational motion.* Energy Conversion and Management, 2017. **148**: p. 1391-1398.

16. Wang, J. and W.-H. Liao, *Attaining the high-energy orbit of nonlinear energy harvesters by load perturbation.* Energy Conversion and Management, 2019. **192**: p. 30-36.
17. Fang, S., X. Fu, and W.-H. Liao, *Asymmetric plucking bistable energy harvester: Modeling and experimental validation.* Journal of Sound and Vibration, 2019. **459**: p. 114852.
18. Mann, B.P., *Energy criterion for potential well escapes in a bistable magnetic pendulum.* Journal of Sound and Vibration, 2009. **323**(3): p. 864-876.
19. Pellegrini, S.P., N. Tolou, M. Schenk, and J.L. Herder, *Bistable vibration energy harvesters: A review.* Journal of Intelligent Material Systems and Structures, 2013. **24**(11): p. 1303-1312.
20. Daqaq, M.F., R. Masana, A. Erturk, and D. Dane Quinn, *On the role of nonlinearities in vibratory energy harvesting: A critical review and discussion.* Applied Mechanics Reviews, 2014. **66**(4).
21. Panyam, M. and M.F. Daqaq, *Characterizing the effective bandwidth of tri-stable energy harvesters.* Journal of Sound and Vibration, 2017. **386**: p. 336-358.
22. Zhou, S. and L. Zuo, *Nonlinear dynamic analysis of asymmetric tristable energy harvesters for enhanced energy harvesting.* Communications in Nonlinear Science and Numerical Simulation, 2018. **61**: p. 271-284.
23. Zhang, Y., Y. Jin, P. Xu, and S. Xiao, *Stochastic bifurcations in a nonlinear tri-stable energy harvester under colored noise.* Nonlinear Dynamics, 2020. **99**(2): p. 879-897.
24. Zhou, Z., W. Qin, and P. Zhu, *A broadband quad-stable energy harvester and its advantages over bi-stable harvester: Simulation and experiment verification.* Mechanical Systems and Signal Processing, 2017. **84**: p. 158-168.
25. Gao, M., Y. Wang, Y. Wang, Y. Yao, P. Wang, Y. Sun, and J. Xiao, *Modeling and experimental verification of a fractional damping quad-stable energy harvesting system for use in wireless sensor networks.* Energy, 2020. **190**: p. 116301.
26. Leadenham, S. and A. Erturk, *M-shaped asymmetric nonlinear oscillator for broadband vibration energy harvesting: Harmonic balance analysis and experimental validation.* Journal of Sound and Vibration, 2014. **333**(23): p. 6209-6223.
27. Andò, B., S. Baglio, A.R. Bulsara, and V. Marletta, *A bistable buckled beam based approach for vibrational energy harvesting.* Sensors and Actuators A: Physical, 2014. **211**: p. 153-161.
28. Cottone, F., L. Gammaitoni, H. Vocca, M. Ferrari, and V. Ferrari, *Piezoelectric buckled beams for random vibration energy harvesting.* Smart Materials and Structures, 2012. **21**(3): p. 035021.
29. Derakhshani, M., N. Momenzadeh, and T.A. Berfield, *Analytical and experimental study of a clamped-clamped, bistable buckled beam low-frequency pvdf vibration energy harvester.* Journal of Sound and Vibration, 2021. **497**: p. 115937.
30. Emam, S.A., J. Hobeck, and D.J. Inman, *Experimental investigation into the nonlinear dynamics of a bistable laminate.* Nonlinear Dynamics, 2019. **95**(4): p. 3019-3039.
31. Pan, D. and F. Dai, *Design and analysis of a broadband vibratory energy harvester using bi-stable piezoelectric composite laminate.* Energy Conversion and Management, 2018. **169**: p. 149-160.
32. Wu, M.Q., W. Zhang, and Y. Niu, *Experimental and numerical studies on nonlinear vibrations and dynamic snap-through phenomena of bistable asymmetric composite laminated shallow shell under center foundation excitation.* European Journal of Mechanics - A/Solids, 2021. **89**: p. 104303.
33. Cao, J., W. Wang, S. Zhou, D.J. Inman, and J. Lin, *Nonlinear time-varying potential bistable energy harvesting from human motion.* Applied Physics Letters, 2015. **107**(14): p. 143904.
34. Wang, W., J. Cao, C.R. Bowen, D.J. Inman, and J. Lin, *Performance enhancement of nonlinear asymmetric bistable energy harvesting from harmonic, random and human motion excitations.* Applied Physics Letters, 2018. **112**(21): p. 213903.
35. Zhao, S. and A. Erturk, *On the stochastic excitation of monostable and bistable electroelastic power generators: Relative advantages and tradeoffs in a physical system.* Applied Physics Letters, 2013. **102**(10): p. 103902.

36. Lan, C. and W. Qin, *Enhancing ability of harvesting energy from random vibration by decreasing the potential barrier of bistable harvester.* Mechanical Systems and Signal Processing, 2017. **85**: p. 71-81.
37. Wang, G.-Q. and W.-H. Liao, *A bistable piezoelectric oscillator with an elastic magnifier for energy harvesting enhancement.* Journal of Intelligent Material Systems and Structures, 2017. **28**(3): p. 392-407.
38. Cao, J., S. Zhou, W. Wang, and J. Lin, *Influence of potential well depth on nonlinear tristable energy harvesting.* Applied Physics Letters, 2015. **106**(17): p. 173903.
39. Chiacchiari, S., F. Romeo, D.M. McFarland, L.A. Bergman, and A.F. Vakakis, *Vibration energy harvesting from impulsive excitations via a bistable nonlinear attachment.* International Journal of Non-Linear Mechanics, 2017. **94**: p. 84-97.
40. Nayfeh, A.H. and D.T. Mook, *Nonlinear oscillations*. 1995: Wiley.
41. Ruby, L., *Applications of the mathieu equation.* American Journal of Physics, 1996. **64**(1): p. 39-44.
42. Hsieh, D.Y., *On mathieu equation with damping.* Journal of Mathematical Physics, 1980. **21**(4): p. 722-725.
43. Leven, R.W. and B.P. Koch, *Chaotic behaviour of a parametrically excited damped pendulum.* Physics Letters A, 1981. **86**(2): p. 71-74.
44. Watt, D. and M.P. Cartmell, *An externally loaded parametric oscillator.* Journal of Sound and Vibration, 1994. **170**(3): p. 339-364.
45. Clifford, M.J. and S.R. Bishop, *Rotating periodic orbits of the parametrically excited pendulum.* Physics Letters A, 1995. **201**(2): p. 191-196.
46. Horton, B., J. Sieber, J.M.T. Thompson, and M. Wiercigroch, *Dynamics of the nearly parametric pendulum.* International Journal of Non-Linear Mechanics, 2011. **46**(2): p. 436-442.
47. Xu, X., M. Wiercigroch, and M.P. Cartmell, *Rotating orbits of a parametrically-excited pendulum.* Chaos, Solitons & Fractals, 2005. **23**(5): p. 1537-1548.
48. Semenov, M.E., D.V. Shevlyakova, and P.A. Meleshenko, *Inverted pendulum under hysteretic control: Stability zones and periodic solutions.* Nonlinear Dynamics, 2014. **75**(1): p. 247-256.
49. Chen, X., Z. Jing, and X. Fu, *Chaos control in a pendulum system with excitations and phase shift.* Nonlinear Dynamics, 2014. **78**(1): p. 317-327.
50. Daqaq, M.F., C. Stabler, Y. Qaroush, and T. Seuaciuc-Osório, *Investigation of power harvesting via parametric excitations.* Journal of Intelligent Material Systems and Structures, 2009. **20**(5): p. 545-557.
51. Ma, T.-W., H. Zhang, and N.-S. Xu, *A novel parametrically excited non-linear energy harvester.* Mechanical Systems and Signal Processing, 2012. **28**: p. 323-332.
52. Abdelkefi, A., A.H. Nayfeh, and M.R. Hajj, *Global nonlinear distributed-parameter model of parametrically excited piezoelectric energy harvesters.* Nonlinear Dynamics, 2012. **67**(2): p. 1147-1160.
53. Yabuno, H., T. Murakami, J. Kawazoe, and N. Aoshima, *Suppression of parametric resonance in cantilever beam with a pendulum (effect of static friction at the supporting point of the pendulum).* Journal of Vibration and Acoustics, 2004. **126**(1): p. 149-162.
54. Sartorelli, J.C. and W. Lacarbonara, *Parametric resonances in a base-excited double pendulum.* Nonlinear Dynamics, 2012. **69**(4): p. 1679-1692.
55. Jia, Y., J. Yan, K. Soga, and A.A. Seshia, *Parametric resonance for vibration energy harvesting with design techniques to passively reduce the initiation threshold amplitude.* Smart Materials and Structures, 2014. **23**(6): p. 065011.
56. Yang, W. and S. Towfighian, *A parametric resonator with low threshold excitation for vibration energy harvesting.* Journal of Sound and Vibration, 2019. **446**: p. 129-143.
57. Panyam, M., M.F. Daqaq, and S.A. Emam, *Exploiting the subharmonic parametric resonances of a buckled beam for vibratory energy harvesting.* Meccanica, 2018. **53**(14): p. 3545-3564.
58. Kuang, Y. and M. Zhu, *Parametrically excited nonlinear magnetic rolling pendulum for broadband energy harvesting.* Applied Physics Letters, 2019. **114**(20): p. 203903.

59. Lajimi, S.A.M. and M.I. Friswell, *Dynamics of a non-linearly damped microresonator under parametric excitation and its application in developing sensitive inertial sensors with ultra-wide dynamic ranges.* International Journal of Non-Linear Mechanics, 2020. **123**: p. 103491.
60. Garg, A. and S.K. Dwivedy, *Nonlinear dynamics of parametrically excited piezoelectric energy harvester with 1:3 internal resonance.* International Journal of Non-Linear Mechanics, 2019. **111**: p. 82-94.
61. Daqaq, M.F. and D. Bode, *Exploring the parametric amplification phenomenon for energy harvesting.* Proceedings of the Institution of Mechanical Engineers, Part I: Journal of Systems and Control Engineering, 2011. **225**(4): p. 456-466.
62. Aghamohammadi, M., V. Sorokin, and B. Mace, *On the response attainable in nonlinear parametrically excited systems.* Applied Physics Letters, 2019. **115**(15): p. 154102.
63. Alevras, P., S. Theodossiades, and H. Rahnejat, *Broadband energy harvesting from parametric vibrations of a class of nonlinear mathieu systems.* Applied Physics Letters, 2017. **110**(23): p. 233901.
64. Chen, L. and W. Jiang, *A piezoelectric energy harvester based on internal resonance.* Acta Mechanica Sinica, 2015. **31**(2): p. 223-228.
65. Lee, C.L. and N.C. Perkins, *Nonlinear oscillations of suspended cables containing a two-to-one internal resonance.* Nonlinear Dynamics, 1992. **3**(6): p. 465-490.
66. Nayfeh, A.H. and B. Balachandran, *Modal interactions in dynamical and structural systems.* Applied Mechanics Reviews, 1989. **42**(11S): p. S175-S201.
67. El-Bassiouny, A.F., *Internal resonance of a nonlinear vibration absorber.* Physica Scripta, 2005. **72**(2-3): p. 203-211.
68. Sayed, M. and M. Kamel, *1:2 and 1:3 internal resonance active absorber for non-linear vibrating system.* Applied Mathematical Modelling, 2012. **36**(1): p. 310-332.
69. Chen, L.-Q. and W.-A. Jiang, *Internal resonance energy harvesting.* Journal of Applied Mechanics, 2015. **82**(3).
70. Jiang, W.-A., L.-Q. Chen, and H. Ding, *Internal resonance in axially loaded beam energy harvesters with an oscillator to enhance the bandwidth.* Nonlinear Dynamics, 2016. **85**(4): p. 2507-2520.
71. Li, X., Y.-W. Zhang, H. Ding, and L.-Q. Chen, *Dynamics and evaluation of a nonlinear energy sink integrated by a piezoelectric energy harvester under a harmonic excitation.* Journal of Vibration and Control, 2019. **25**(4): p. 851-867.
72. Aravindan, M. and S.F. Ali, *Exploring 1:3 internal resonance for broadband piezoelectric energy harvesting.* Mechanical Systems and Signal Processing, 2021. **153**: p. 107493.
73. Cao, D.X., S. Leadenham, and A. Erturk, *Internal resonance for nonlinear vibration energy harvesting.* The European Physical Journal Special Topics, 2015. **224**(14): p. 2867-2880.
74. Harne, R.L., A. Sun, and K.W. Wang, *Leveraging nonlinear saturation-based phenomena in an l-shaped vibration energy harvesting system.* Journal of Sound and Vibration, 2016. **363**: p. 517-531.
75. Nie, X., T. Tan, Z. Yan, Z. Yan, and M.R. Hajj, *Broadband and high-efficient l-shaped piezoelectric energy harvester based on internal resonance.* International Journal of Mechanical Sciences, 2019. **159**: p. 287-305.
76. Xiong, L., L. Tang, and B.R. Mace, *Internal resonance with commensurability induced by an auxiliary oscillator for broadband energy harvesting.* Applied Physics Letters, 2016. **108**(20): p. 203901.
77. Yang, W. and S. Towfighian, *A hybrid nonlinear vibration energy harvester.* Mechanical Systems and Signal Processing, 2017. **90**: p. 317-333.
78. Yang, W. and S. Towfighian, *Internal resonance and low frequency vibration energy harvesting.* Smart Materials and Structures, 2017. **26**(9): p. 095008.
79. Wu, Y., H. Ji, J. Qiu, W. Liu, and J. Zhao, *An internal resonance based frequency up-converting energy harvester.* Journal of Intelligent Material Systems and Structures, 2018. **29**(13): p. 2766-2781.

80. Xie, Z., B. Huang, K. Fan, S. Zhou, and W. Huang, *A magnetically coupled nonlinear t-shaped piezoelectric energy harvester with internal resonance.* Smart Materials and Structures, 2019. **28**(11): p. 11LT01.
81. Eshtehardiha, R., R. Tikani, and S. Ziaei-Rad, *Experimental and numerical investigation of energy harvesting from double cantilever beams with internal resonance.* Journal of Sound and Vibration, 2021. **500**: p. 116022.
82. Xia, C., D.F. Wang, T. Ono, T. Itoh, and M. Esashi, *Internal resonance in coupled oscillators – part i: A double amplification mass sensing scheme without duffing nonlinearity.* Mechanical Systems and Signal Processing, 2021. **159**: p. 107886.
83. Soliman, M.S.M., E.M. Abdel-Rahman, E.F. El-Saadany, and R.R. Mansour, *A wideband vibration-based energy harvester.* Journal of Micromechanics and Microengineering, 2008. **18**(11): p. 115021.
84. Gu, L. and C. Livermore, *Impact-driven, frequency up-converting coupled vibration energy harvesting device for low frequency operation.* Smart Materials and Structures, 2011. **20**(4): p. 045004.
85. Liu, H., C. Lee, T. Kobayashi, C.J. Tay, and C. Quan, *Investigation of a mems piezoelectric energy harvester system with a frequency-widened-bandwidth mechanism introduced by mechanical stoppers.* Smart Materials and Structures, 2012. **21**(3): p. 035005.
86. Giusa, F., A. Giuffrida, C. Trigona, B. Andò, A.R. Bulsara, and S. Baglio, *"Random mechanical switching harvesting on inductor": A novel approach to collect and store energy from weak random vibrations with zero voltage threshold.* Sensors and Actuators A: Physical, 2013. **198**: p. 35-45.
87. Dhakar, L., H. Liu, F.E.H. Tay, and C. Lee, *A new energy harvester design for high power output at low frequencies.* Sensors and Actuators A: Physical, 2013. **199**: p. 344-352.
88. Song, M., Y. Zhang, M. Peng, and J. Zhai, *Low frequency wideband nano generators for energy harvesting from natural environment.* Nano Energy, 2014. **6**: p. 66-72.
89. Liu, S., Q. Cheng, D. Zhao, and L. Feng, *Theoretical modeling and analysis of two-degree-of-freedom piezoelectric energy harvester with stopper.* Sensors and Actuators A: Physical, 2016. **245**: p. 97-105.
90. Hu, G., L. Tang, R. Das, and P. Marzocca, *A two-degree-of-freedom piezoelectric energy harvester with stoppers for achieving enhanced performance.* International Journal of Mechanical Sciences, 2018. **149**: p. 500-507.
91. Zhou, K., H.L. Dai, A. Abdelkefi, and Q. Ni, *Theoretical modeling and nonlinear analysis of piezoelectric energy harvesters with different stoppers.* International Journal of Mechanical Sciences, 2020. **166**: p. 105233.
92. Fan, K., Q. Tan, H. Liu, Y. Zhang, and M. Cai, *Improved energy harvesting from low-frequency small vibrations through a monostable piezoelectric energy harvester.* Mechanical Systems and Signal Processing, 2019. **117**: p. 594-608.

Chapter 3

Nonlinear Energy Harvesting using Combined Primary and Parametric Resonances

This chapter is based on the following published paper:

Fan, Y., M.H. Ghayesh, and T.-F. Lu, *Enhanced nonlinear energy harvesting using combined primary and parametric resonances: Experiments with theoretical verifications.* Energy Conversion and Management, 2020. **221**: p. 113061.

Statement of Authorship

Title of Paper	Enhanced nonlinear energy harvesting using combined primary and parametric resonances: Experiments with theoretical verifications
Publication Status	☑ Published ☐ Accepted for Publication ☐ Submitted for Publication ☐ Unpublished and Unsubmitted w ork w ritten in manuscript style
Publication Details	Fan, Y., M.H. Ghayesh, and T.-F. Lu, Enhanced nonlinear energy harvesting using combined primary and parametric resonances: Experiments with theoretical verifications. Energy Conversion and Management, 2020. 221: p. 113061.

Principal Author

Name of Principal Author (Candidate)	Mr. Yimin Fan		
Contribution to the Paper	Conceptualization, Investigation, Methodology, Validation, Writing - original draft, Software		
Overall percentage (%)	80%		
Certification:	This paper reports on original research I conducted during the period of my Higher Degree by Research candidature and is not subject to any obligations or contractual agreements with a third party that would constrain its inclusion in this thesis. I am the primary author of this paper.		
Signature		Date	27/01/2022

Co-Author Contributions

By signing the Statement of Authorship, each author certifies that:

i. the candidate's stated contribution to the publication is accurate (as detailed above);

ii. permission is granted for the candidate in include the publication in the thesis; and

iii. the sum of all co-author contributions is equal to 100% less the candidate's stated contribution.

Name of Co-Author	Dr. Mergen H. Ghayesh		
Contribution to the Paper	Conceptualization, Investigation, Methodology, Supervision, Writing - review & editing		
Signature		Date	01/02/2022

Name of Co-Author	Dr. Tien-Fu Lu		
Contribution to the Paper	Conceptualization, Investigation, Methodology, Supervision, Writing - review & editing		
Signature		Date	1/02/2022

Energy Conversion and Management 221 (2020) 113061

Contents lists available at ScienceDirect

Energy Conversion and Management

journal homepage: www.elsevier.com/locate/enconman

Enhanced nonlinear energy harvesting using combined primary and parametric resonances: Experiments with theoretical verifications

Yimin Fan, Mergen H. Ghayesh*, Tien-Fu Lu

School of Mechanical Engineering, University of Adelaide, South Australia 5005, Australia

ARTICLE INFO

Keywords:
Nonlinear energy
Energy harvester
Vibration
Experiment
Theory

ABSTRACT

Presented in this paper is harvested nonlinear energy from a vibration energy harvester device; the device has been designed, manufactured, and tested successfully – the device performance is verified theoretically to some extent. The design concept is on the basis of merging the nonlinearities of the building block (i.e. a beam) and those induced by the motion limiters, which for some design parameters leads to the combination of parametric and primary resonances of the device; these two resonances increase the operational frequency bandwidth by 118%. By introducing motion limiters to the proposed system, the overall frequency bandwidth of the primary and parametric resonances is able to be broadened even more – up to 178%. By varying the angle between the base (ambient) excitation and the length of the core element; the optimal angle for the largest possible frequency bandwidth is obtained. Theoretical investigations including the finite element method (FEM) using ANSYS and an averaging perturbation technique have been performed to verify the experimental results for few cases. An experimental parametric study on the performance of the device has also been conducted to highlight the limiter gap and type as well as orientation angle effects.

1. Introduction

Vibration energy harvesters convert/save environmental ambient vibration energy into/in-the-form-of electrical power [1–24]. Ambient vibration triggers the movement of the vibration energy harvester and then transducers on device such as piezoelectric layers or magnets can output electrical power. Numerous vibration sources such as car engines, clothes dryers, windows next to busy roads, base of 3-axis machine tools [25], heartbeats [26], etc., can be tapped into vibration energy harvesting. Transducing persistent and sustainable energy from real environment vibration sources makes ambient vibration energy harvesting technologies as an alternative solution, which can compensate for current battery limitations.

To date, the outlook of broadband energy harvesters seemed more practicable from the perspective of realistic vibration sources. Tuning approaches in nature aimed to adapt to the targeted ambient frequency required external input power; they were though limited by narrow tuneable bandwidths, which cannot be utilised in wideband vibrational sources. Although multi-array approaches [27–30] are counted as broadband, they suffered from poor power density and required external power for complex electrical circuit to adjust the phase differences.

1.1. Nonlinear techniques

To remedy the existing limitations, broadband energy harvesting gained more potential benefits and flexibilities to encounter with realistic excitations as random and time-varying frequencies. Multi-array approaches had the initial concept for broadband, however, size issues especially in remote sensing applications limited its practicability. *Nonlinear* techniques, on the other hand, offered a novel perspective to researchers in dealing with broadening the operational bandwidth; compared to linear approaches, nonlinear approaches were able to exhibit multiple equilibrium states and had expanded resonance regime which could be few times wider than the linear counterparts. Nonlinearities in energy harvesting could be categorised as *inherent nonlinearities* and *externally induced nonlinearities* [31]. Inherent nonlinearities mainly utilised nonlinear strain deformation from large bending of the core elements of the devices [32–35]. Externally induced nonlinearities, on the other hand, are due to nonlinearities in the applied forces to a vibrating system, such as nonlinear magnetics forces.

1.2. Parametric excitation and motion limiters

Conventional vibration energy harvester were designed to operate at primary resonances, where usually the excitation (ambient vibration)

* Corresponding author.
E-mail address: mergen.ghayesh@adelaide.edu.au (M.H. Ghayesh).

https://doi.org/10.1016/j.enconman.2020.113061
Received 12 February 2020; Received in revised form 8 May 2020; Accepted 3 June 2020
Available online 06 July 2020
0196-8904/

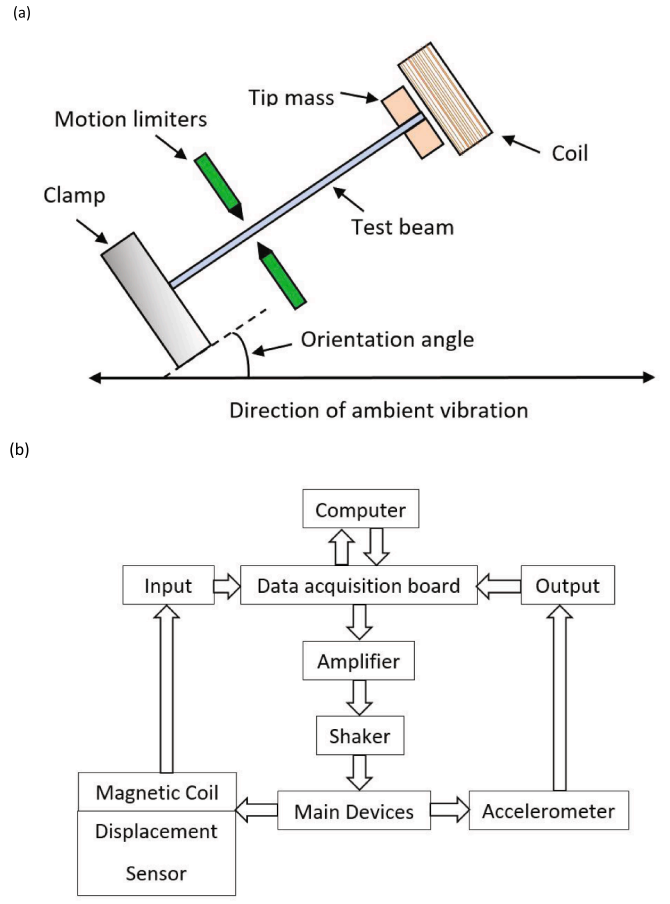

Fig. 1. Schematic of the device: a) the core element with motion limiters and the coil for transduction; b) measurement and data acquisition procedure.

direction is perpendicular to the core element (usually a beam structure). A *parametrically excited* beam has a parametric resonance locates at twice the fundamental frequency; by proper design parameter selections, the two adjacent resonances including both parametric and primary resonances could be merged, and it is different from conventional bi-stable energy harvesters. Abdelkefi et al. [36] proposed a distributed-parameter model which included the piezoelectric linear and nonlinear effects and workable for higher modes. Yildirim et al. [37] designed a beam subject to parametric loads with a centre-point magnetic mass.

Motion-limiter-based energy harvester were built upon a vibrating continuous core element (such as a beam [38–45]) which was constrained by mechanical motion limiters at either one or both sides; this lead to an instant increase in the effective stiffness of the device, and may help in broadening the operational bandwidth. Different designs had been reported [46–55] in this regard, for instance, Liu et al. and Ming et al. [47,50] proposed MEMS and nano-scale based designs; Liu et al. and Hu et al. [51,52] combined 2-DOF piezoelectric energy harvester with limiter; Liu et al. [56] proposed an external structure 'curve fixture' as a motion limiter.

1.3. Contributions of this article to the field

This paper is *the first* to utilise the concept of using a single element (and simultaneously benefiting from parametric and primary resonances of it) in the presence of motion limiter induced nonlinearities in vibration energy harvester; a FEM-based theoretical verification and an averaging perturbation technique are also given. The device based on this concept has been designed, manufactured, and tested showing 178% improvement in the operating frequency bandwidth. It is shown that merging nonlinearities due to the motion limiters and those due to large amplitude vibrations of the beam enhances the performance of the device substantially. It is also investigated that how the motion limiters as well as orientation angles alter the performance of the device.

2. Brief theoretical fundamentals

Consider a nonlinear system vibrating under an external force, the corresponding primary and parametric resonant motions can be described qualitatively by using a combined Duffing and Mathieu equation as [57,58]

$$\ddot{x} + [\omega - 2f_1 cos(2\Omega t)]x + \beta x^3 = f_2 cos(\Omega t) \quad (1)$$

where x is the displacement field, ω is the natural frequency, β is the nonlinear stiffness coefficient, Ω is the excitation frequency and f_1 and f_2 is the forcing amplitudes. In order to design a wideband energy harvester, this paper aims to utilise the combination of parametric and primary modes to achieve a wider operational bandwidth. To further increase the operational bandwidth, motion limiters, as externally induced nonlinearities are employed to merge the parametric and primary resonances together, such that, an even wider and continuous operational bandwidth can be formed. From the design perspectives, the core element of the device (i.e. a cantilever beam with tip mass) with a low primary resonance is preferred to fully merge the gap between the parametric and primary resonances.

3. Experimental setup and design

The system shown in Figs. 1(a) and 2 (a) is the schematic and fabricated vibration energy harvester, respectively. An aluminium (density 2700 kg/m^3) beam has [length = 125 mm; width = 9 mm; thickness = 0.5 mm] with one end fixed onto a supported structure and the other end attached to a pair of cylindrical neodymium magnets AMF21020 which weight 12.05 g on either side. A copper coil consisted 16 turns wired on a 36 mm diameter hollow cylindrical support structure was used as a transducer.

Figs. 1(b) and 2(b) show the measurement and data acquisition devices; the first one shows the flowchart and the former shows the actual one. A shaking table APS 113 was connected to power amplifier APS 115 to provide base excitation, an accelerometer Kistler 8774A50 measured the base acceleration and a displacement sensor Wenglor CP24MHT80 measured the beam deflection near the tip area, data acquisition board NI USB-6281 was used to collect the data from the accelerometer, displacement sensor and voltage from coil. LabVIEW 2014 and MATLAB 2017b were used for data monitoring and data post-processing, respectively. Due to system nonlinear frequency responses, both forward and backward sinusoid wave sweeps were conducted with 1 KHz sampling rate. With 0.05 Hz frequency increments, both primary and parametric resonances were fully captured. To eliminate the transient response, for each increment, the settling time was set to be 20 s to ensure the system was exhibiting steady state response. A constant base excitation acceleration 0.75 g peak to peak was employed for all the experiments.

In order to broaden the operational frequency bandwidth, motion limiters have been introduced to the experimental beam. Under base

(a)

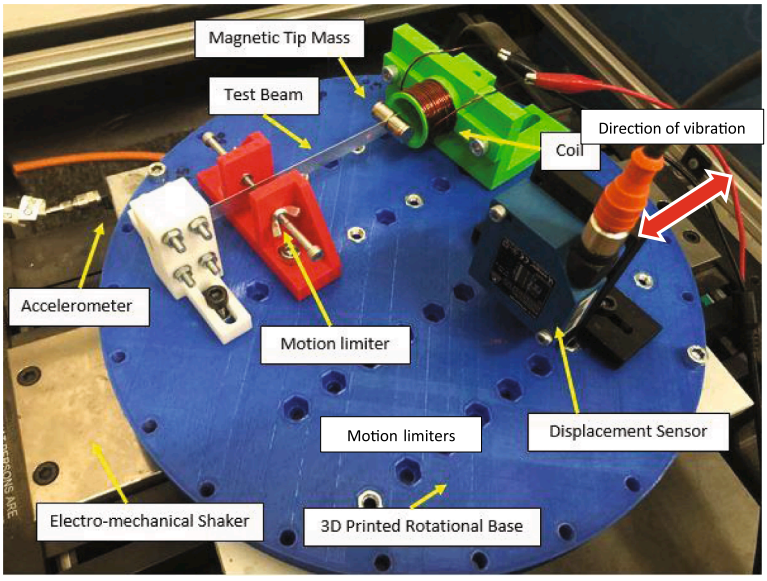

(b)

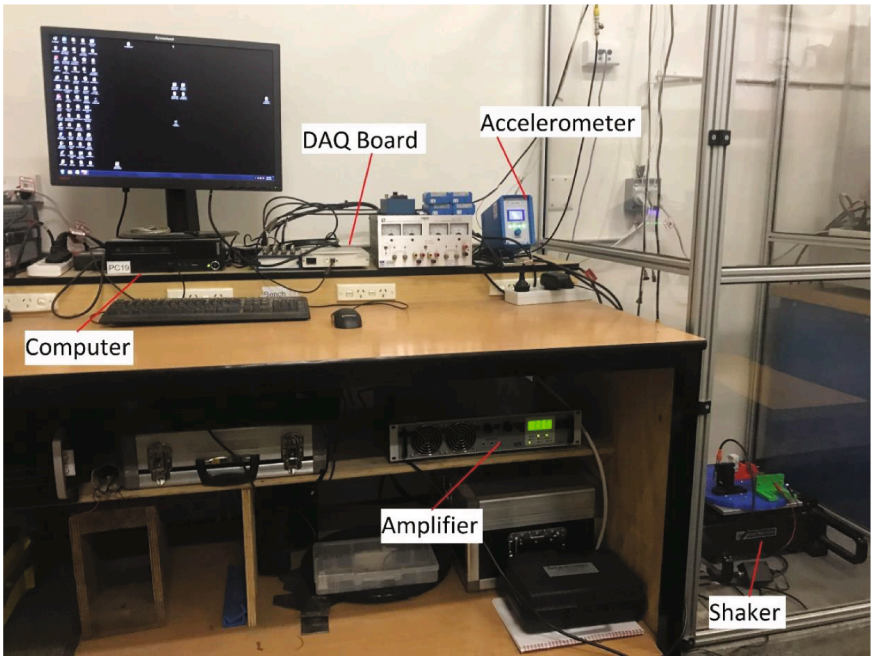

Fig. 2. Experimental setup: a) the vibration energy harvester with motion limiter; b) Overall Experimental Setup.

excitation, the beam engaged with the motion limiters due to large deflections, and beam effective stiffness suddenly changed to a higher value, hence changed its effective resonance. In the experiment, the motion limiters were located at 63 mm along the beam length from the fixed end and the gap between the limiters was 2.45 mm per side; see Figs. 1(a) and 2(a). Two different motion limiter configurations have been tested, 1-side limiter and 2-side limiter. A 3D-printed Acrylonitrile Butadiene Styrene (ABS) rotational base was used to fix the experimental setup including testing beam, motion limiters, coil and displacement sensor; by rotating the base, different orientation angles can be obtained from 0° to 90° with 15° increments, where 0° and 90° configurations represent a purely parametric excitation and a purely direct excitation, respectively.

4. Experimental results

In this section, the proposed energy harvester with no-limiter, 1-side limiter and 2-side limiter configurations were experimentally tested. The frequency-voltage and frequency-displacement curves collected through coil and displacement sensor, respectively, are discussed in

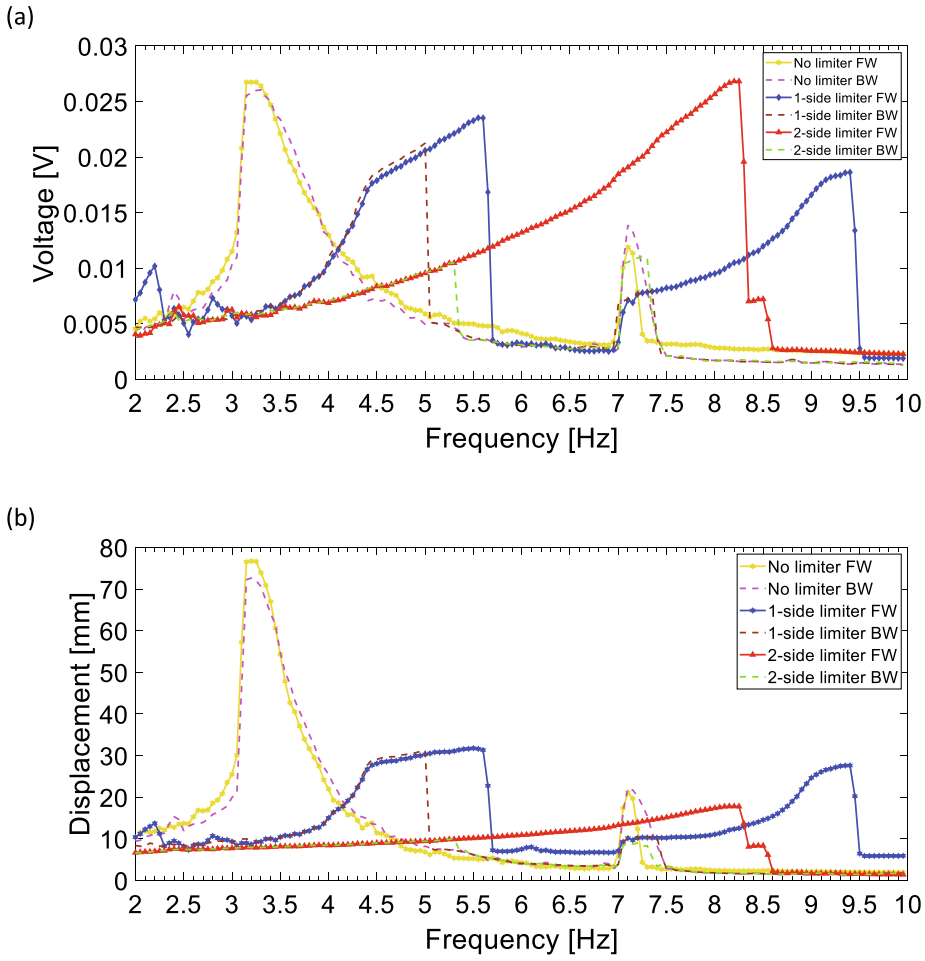

Fig. 3. Frequency response curve for the no-limiter, 1-side limiter and 2-side limiter configurations for both forward (FW) and backward (BW) sweeping at 45° orientation angle: a) frequency-voltage diagram; b) frequency-displacement diagram.

details.

To compare the effects of the configurations *with* and *without* motion limiters, the frequency-voltage response of no limiter, 1-side limiter and 2-side limiter configurations at 45° orientation angle is shown in Fig. 3. Figs. 4–6 display the (a) time trace; (b) phase-plane portraits and (c) Fast Fourier Transform (FFT) for no limiter configuration at 3.7 Hz, 1-side limiter configuration at 5.6 Hz and 2-side limiter configuration at 8.25 Hz, respectively. To illustrate and compare the performances among the three different configurations, the reference level of the effective bandwidth was set for output voltage equals 0.005 V condition.

As seen in Fig. 3, without the motion limiter engagement, the measured primary resonance occurred at 3.45 Hz, the parametric resonance occurred at 7.1 Hz and the operational bandwidth is 3.65 Hz. For forward sweeping plots, without limiter, system primary resonance was a weak softening response while both 1-side and 2-side limiter configurations' primary resonances were strong hardening responses. The 1-side limiter configuration had a lower peak voltage 0.0235 V at 5.6 Hz but a wider overall bandwidth 6 Hz compared to no limiter configuration, however, a 1.3 Hz gap due to bifurcation still existed between the two resonances. For the 2-side limiter configuration, it managed to merge the primary and parametric resonances together, which exhibited the strongest hardening response with a 6.5 Hz overall bandwidth and 0.0268 V peak voltage at 8.25 Hz. Compared to no limiter configuration, the 2-side limiter configuration increased overall bandwidth by 178%, while the obtained peak voltage remained at the same level. The 1-side limiter configuration could extend the parametric resonance to the highest frequency 9.4 Hz and had a 164% increased bandwidth compared to no limiter one. However, the voltage drop and the gap between the two resonances were the main concern for this configuration. For backward sweeping plots in Fig. 3, no limiter type indicated a small drop of the maximum displacement in primary resonance and the bandwidth of the parametric resonance was broader than forward sweeping plot which illustrated the nonlinear behaviour of parametric resonance. For both 1-side and 2-side limiter types, the bifurcations occurred at lower frequencies and dropped to off-resonance status, which indicated the hardening effects of motion limiter on backward frequency sweeping were insufficient.

For no limiter configuration, it can be seen from Fig. 7(a) the frequency-voltage response and b) the frequency displacement curve, the amplitude of primary resonance was a weakly softening response and the nonlinear behaviour increased with the increasing orientation angles. While for the parametric resonance, the amplitude slightly decreased with increasing orientation angles, the peak voltage occurred at 30° and 45°. The positions that parametric resonances occurred were within a 0.7 Hz range, this was due to the geometric imperfection while rotating the 3D-printed base to obtain different orientation angles.

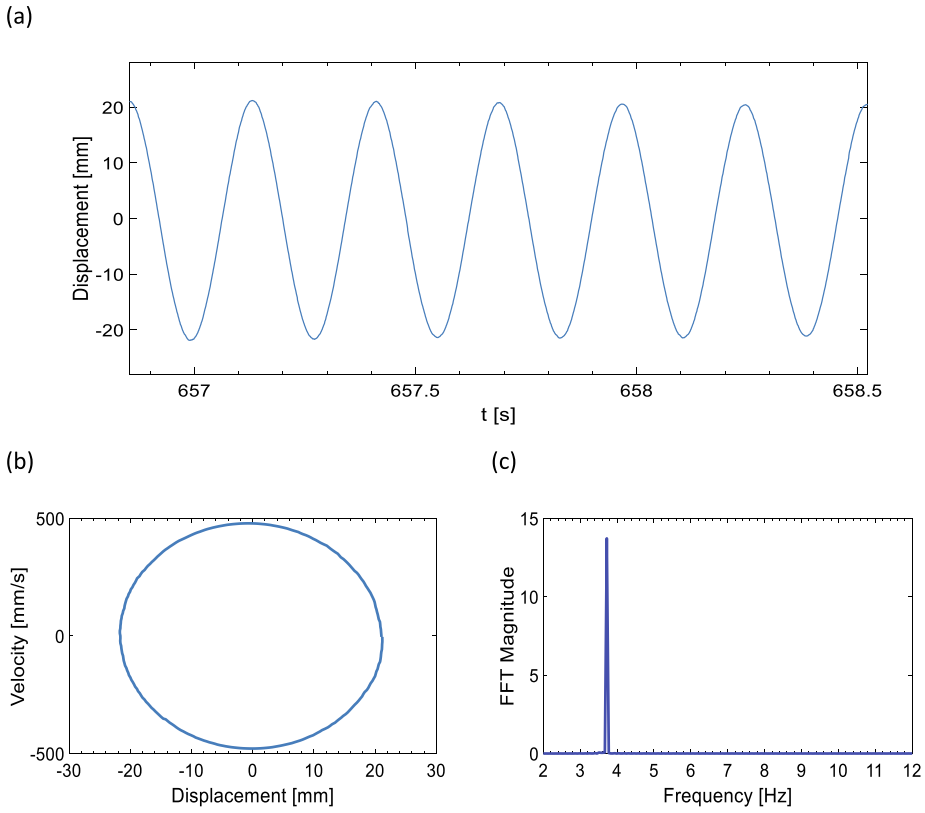

Fig. 4. No limiter configuration at 45° orientation angle: a) time trace; b) phase portrait; c) FFT.

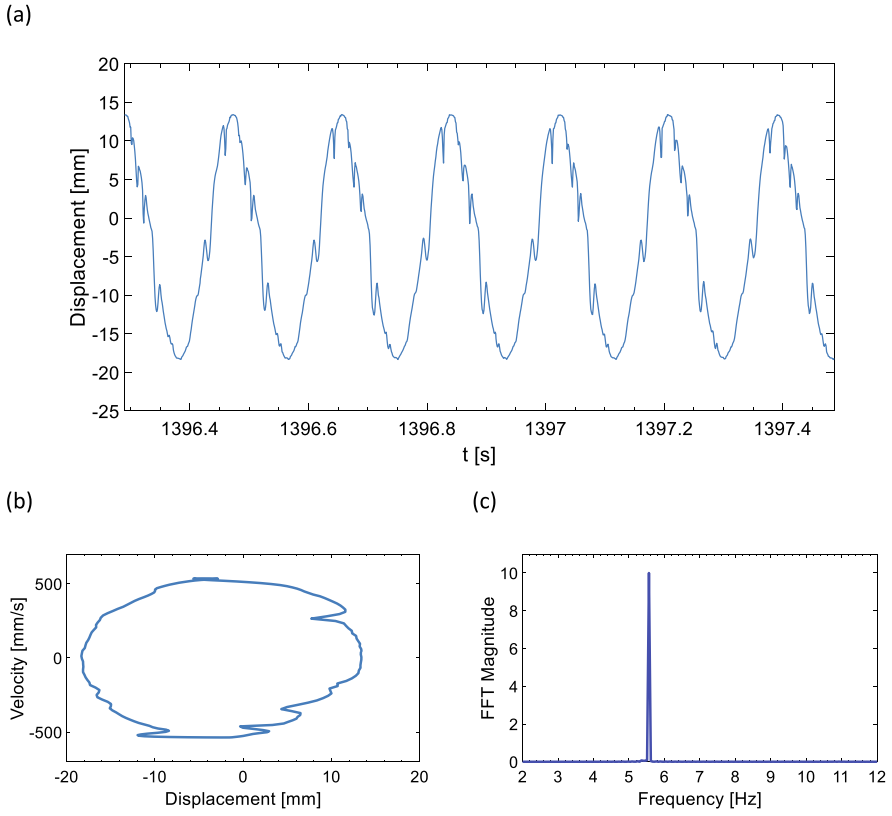

Fig. 5. 1-side limiter configuration at 45° orientation angle: a) time trace; b) phase portrait; c) FFT.

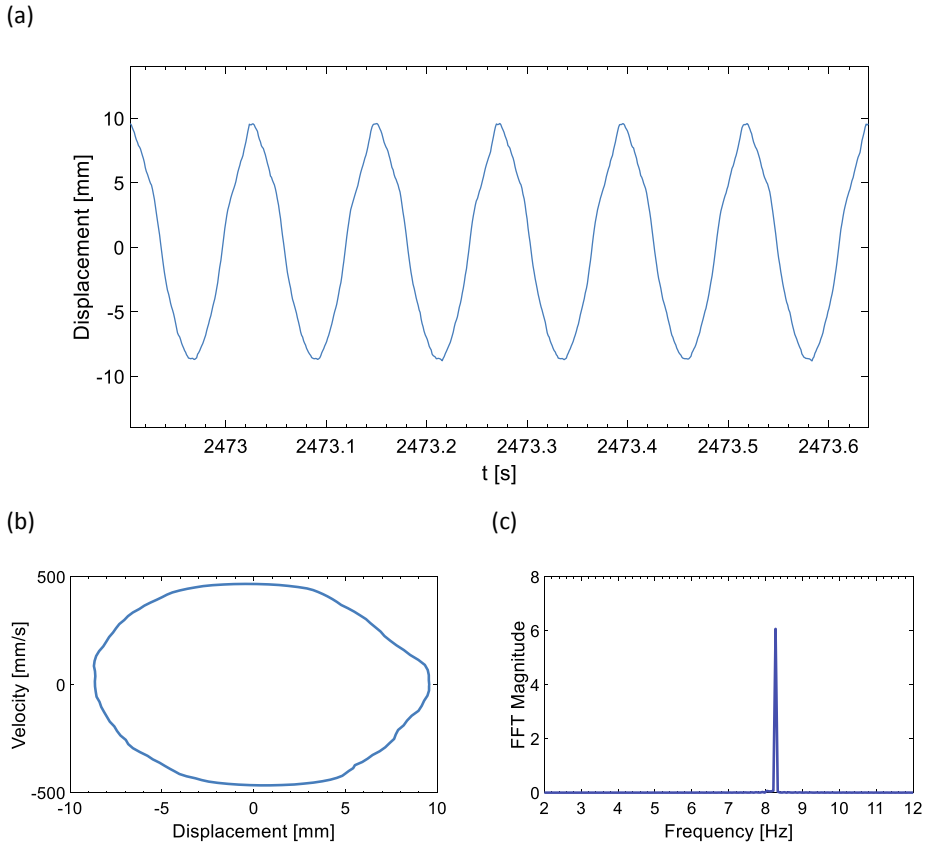

Fig. 6. 2-side limiter configuration at 45° orientation angle: a) time trace; b) phase portrait; c) FFT.

Compared to the primary resonance, the amplitude of parametric resonance was at a relatively similar position, the frequency-displacement response shown in Fig. 7(b) evidently proved the trend of parametric resonance with varying orientation angles remained at almost the same amplitude.

The effects of orientation angle (see Fig. 1(a)) in 1-side and 2-side limiter configurations are shown in Figs. 8 and 9, respectively. When the experimental beam engaged with limiters, the system exhibited strong hardening responses for both primary and parametric resonances with a wider bandwidth. In Fig. 8(a), 0.005 V was set to be the reference level, for 30° orientation angle, the primary resonance, parametric resonance, the bandwidth of primary resonance and parametric resonance were 6.55 Hz, 9.9 Hz, 3.35 Hz and 3 Hz, respectively; compared to without limiter 30° orientation angle configuration, the primary resonance, parametric resonance, the bandwidth of primary resonance and parametric resonance were 3.2 Hz, 6.9 Hz, 2.1 Hz and 0.3 Hz, respectively, which was 159% increase in primary resonance mode and 1000% increase in parametric resonance. For 1-side limiter configuration, the 30° configuration had the widest overall bandwidth 6.35 Hz, however, a bifurcation still existed between the primary and parametric resonances which resulted a 0.35 Hz gap. In order to merge the two modes together hence collect the effective voltages within a continuously effective bandwidth, 2-side limiter configuration was introduced.

Fig. 9(a) shows the 2-side limiter configuration managed to eliminate the bifurcation between primary and parametric mode with varying orientation angles except the 0° and 15° configurations, because the parametric excitation setting limited the maximum deflection at its primary resonance which caused the system cannot engage with the limiters, the resulting off-resonance status reached minimum voltage level. Fig. 8(b) and 9(b) show the comparison between the tip deflection of 1-side limiter and 2-side limiter, the latter had smaller deflections since deflection of both sides of the experimental beam were limited by the motion limiter; however, Fig. 8(a) and 9(a) indicate the average output voltage from 2-side limiter configuration was higher than 1-side limiter configuration.

Fig. 10(a) and (b) show the comparison of peak voltages and operating frequency bandwidth among the no limiter, 1-side limiter and 2-side limiter configurations with different orientation angles, respectively. Fig. 10(a) indicated the no limiter configuration had lower peak voltages compared to with limiter configurations; 2-side limiter configurations with various angles had a slightly higher average peak voltage over 1-side limiter configuration – Fig. 10(b) shows that both with limiter configurations doubled the effective bandwidth compared to no limiter configuration, while the merit of 1-side limiter has the capability of reaching higher operational frequency and the merit of 2-side limiter was merging the two resonances together hence harvest energy within a continuous effective bandwidth.

5. Theoretical verification

In this section, two different approaches are employed to theoretically verify the experimental results. First, a finite element method (FEM) is used for a linear model analysis, both modal and harmonic

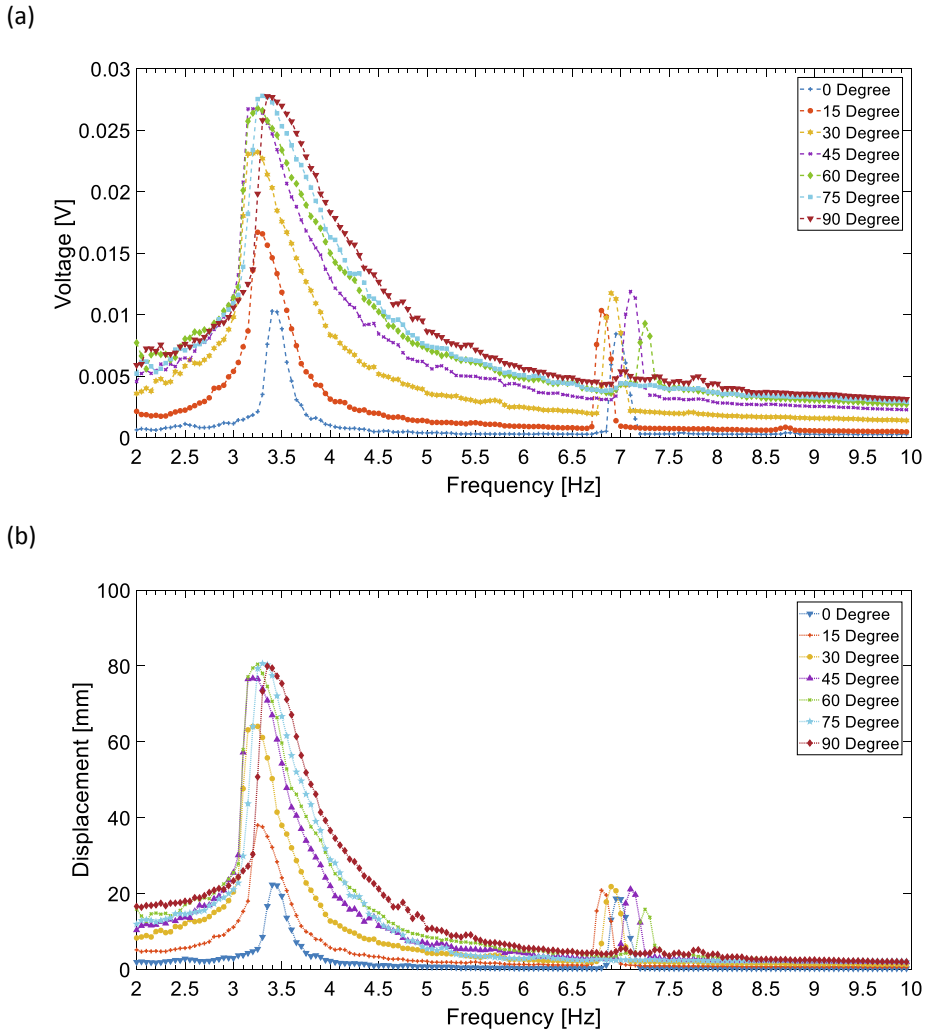

Fig. 7. No limiter configuration a) frequency-voltage diagram and b) frequency-displacement diagram at different orientation angles from 0° to 90°.

modules have been employed to validate the mode shape of the proposed device and the first mode frequency response, respectively; due to the strong softening behaviour caused by large base excitation, for the comparison, we chose the 0°case to eliminate the nonlinear effect between experimental and numerical results, which can be found in Fig. 7 (0°plot); due to geometric imperfection, the 0°case exhibited a slight directly excited component which caused a 22 mm maximum deflection on primary resonance. Second, an averaging perturbation technique is employed for the system subject to limiters and the nonlinear frequency responses are validated for some cases.

FEM via ANSYS Workbench 18.2 was conducted for preliminary theoretical verification, Figs. 11 and 12 show the mode shape of the proposed beam and the comparison between theoretical and experimental obtained primary resonance, respectively. By using the modal analysis module, the first mode of the testing beam was at 3.59 Hz, which was only 3.9% discrepancy compared to the primary resonance in no limiter configuration (3.45 Hz vs 3.59 Hz); this small discrepancy was due to the initial geometric imperfection. A fine mesh with 1196 elements has been applied for the geometry meshing; the selected measuring point of the directional amplitude analysis in ANSYS had the similar longitudinal distance along the beam from the clamped end as the measuring point of the displacement sensor; by using the harmonic analysis module with 0.05 Hz frequency increment, as seen in Fig. 12, the theoretical and experimental results are within good agreement.

As the second approach, to further investigate the experimental results and validate the nonlinear frequency response of the proposed design, the governing equation of 2-side limiter configuration can be written as [59]

$$\begin{cases} m\ddot{z} + (c_0 + c_1)\dot{z} + (k_0 + k_1)z - k_1\Delta_1 = -m\ddot{y}(z \geq \Delta_1), \\ m\ddot{z} + c_0\dot{z} + k_0 z = -m\ddot{y}(-\Delta_2 \leq z \leq \Delta_1), \\ m\ddot{z} + (c_0 + c_2)\dot{z} + (k_0 + k_2)z + k_1\Delta_2 = -m\ddot{y}(z \leq -\Delta_2), \end{cases} \quad (2)$$

where m is the equivalent mass, c_0, c_1, c_2 are the damping coefficients for no limiter, left limiter engaged and right limiter engaged scenarios, respectively; k_0, k_1, k_2 are the stiffness coefficients for no limiter, left limiter engaged and right limiter engaged scenarios, respectively; z is the tip mass displacement, $y = Ysin(\omega t)$ is the base excitation displacement, where Y is the base excitation amplitude: Δ_1 and Δ_2 represent the gap distance for left and right side motion limiter, respectively. The dimensionless equation can be defined as [59]

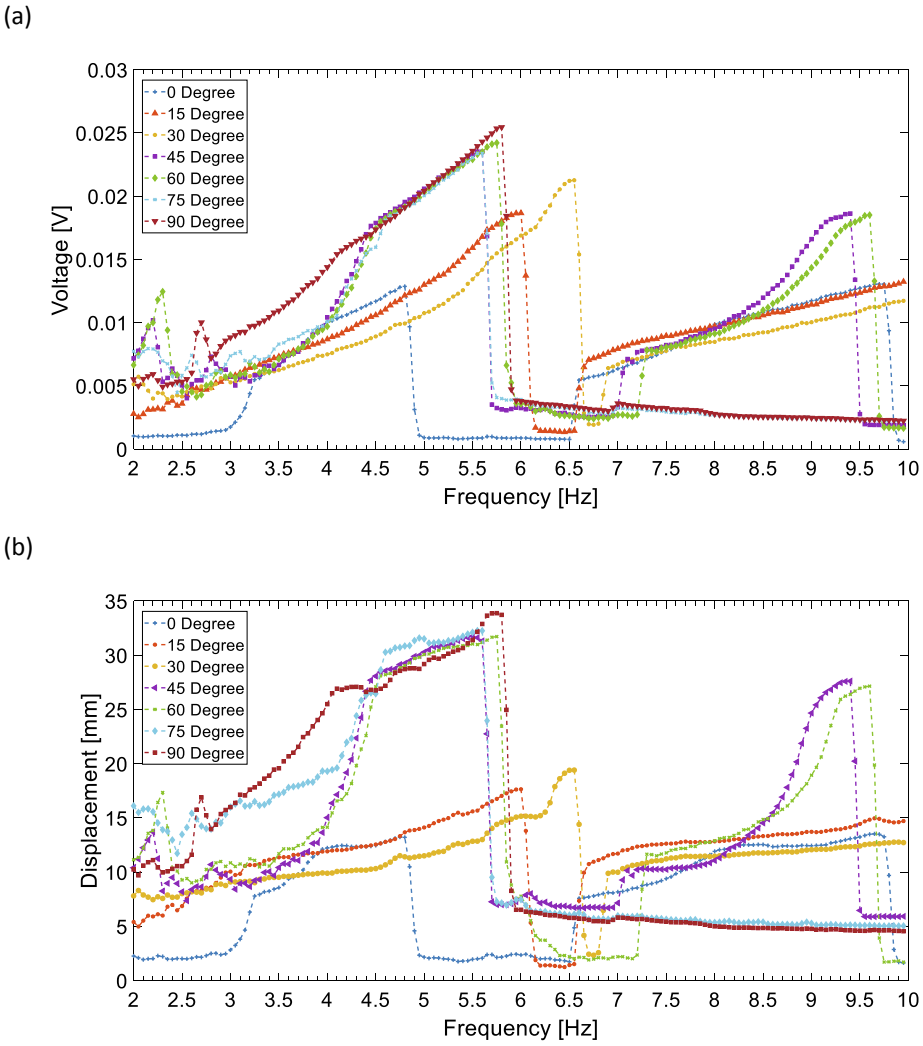

Fig. 8. 1-side limiter configuration a) frequency-voltage curve and b) frequency-displacement curve at different orientation angles from 0° to 90°.

$$\begin{cases} \ddot{u} + (2\xi_0 + 2r_1\xi_1)\dot{u} + (1 + {r_1}^2)u - {r_1}^2\delta_1 = r^2 sin(r\tau), & (u \geq \delta_1), \\ \ddot{u} + 2\xi_0\dot{u} + u = r^2 sin(r\tau), & (-\delta_2 < u < \delta_1), \\ \ddot{u} + (2\xi_0 + 2r_2\xi_2)\dot{u} + (1 + {r_2}^2)u + {r_2}^2\delta_2 = r^2 sin(r\tau), & (u \leq -\delta_2), \end{cases} \tag{3}$$

where $\xi_0 = c_0/2m\omega_0$, $\xi_1 = c_1/2m\omega_1$, $\xi_2 = c_2/2m\omega_2$, ${\omega_0}^2 = k_0/m$, ${\omega_1}^2 = k_1/m$, ${\omega_2}^2 = k_2/m$ and ω is the excitation frequency characteristic, $u = z/Y$, $r = \omega/\omega_0$, $r_1 = \omega_1/\omega_0$, $r_2 = \omega_2/\omega_0$, $\tau = \omega_0 t$, $\delta_1 = \Delta_1/Y$, $\delta_2 = \Delta_2/Y$. To separate the terms of impact force due to motion limiter, Eq. (3) can be rearranged as [59]

$$\ddot{u} + 2\xi_0\dot{u} + u = r^2 sin(r\tau) + F(u, \dot{u}), \tag{4}$$

where

$$F(u, \dot{u}) = \begin{cases} -2\xi_1 r_1\dot{u} - {r_1}^2 u + {r_1}^2\delta_1 & (u \geq \delta_1), \\ 0 & (-\delta_2 < u < \delta_1), \\ -2\xi_2 r_2\dot{u} - {r_2}^2 u - {r_2}^2\delta_2 & (u < -\delta_2), \end{cases} \tag{5}$$

To obtain an analytical approximation for Eq. (4), the method of averaging is adopted. The solution for Eq. (4) is assumed to be [59]

$$u = a(\tau)sin(r\tau + \beta(\tau)) \tag{6}$$

where $a(\tau)$ and $\beta(\tau)$ are expected to be slowly varying functions of τ. To find out the steady state response, by substituting Eq. (6) into Eq. (4) and applying averaging, the Eq. (4) can be defined as [59]

$$\pi r^2 sin(\beta) = -2\xi_0 ar\pi + arr_1\xi_1(2\varphi_1 - \pi + sin(2\varphi_1)) + arr_2\xi_2(2\varphi_2 - \pi + sin(2\varphi_2)) \tag{7}$$

$$\begin{aligned} &\pi r^2 cos(\beta) \\ &= -\pi a(r^2 - 1) - (\frac{1}{2}{r_1}^2 a(2\varphi_1 - \pi - sin(2\varphi_1)) + 4\delta_1 cos(\varphi_1)) - (\frac{1}{2}{r_2}^2 a \\ &\quad (2\varphi_2 - \pi - sin(2\varphi_2)) + 4\delta_1 cos(\varphi_2)) \end{aligned} \tag{8}$$

where $\varphi_1 = sin^{-1}(\delta_1/a)$ and $\varphi_2 = sin^{-1}(\delta_2/a)$. Eqs. (7) and (8) can be numerically solved, hence the motion of the 2-side motion limiter system can be obtained.

To compare the analytical and experimental results, the base acceleration level was set to be constant 0.21 g peak to peak; the beam was set to be directly excited condition to avoid the effects of parametric resonance; four different configurations has been conducted including no

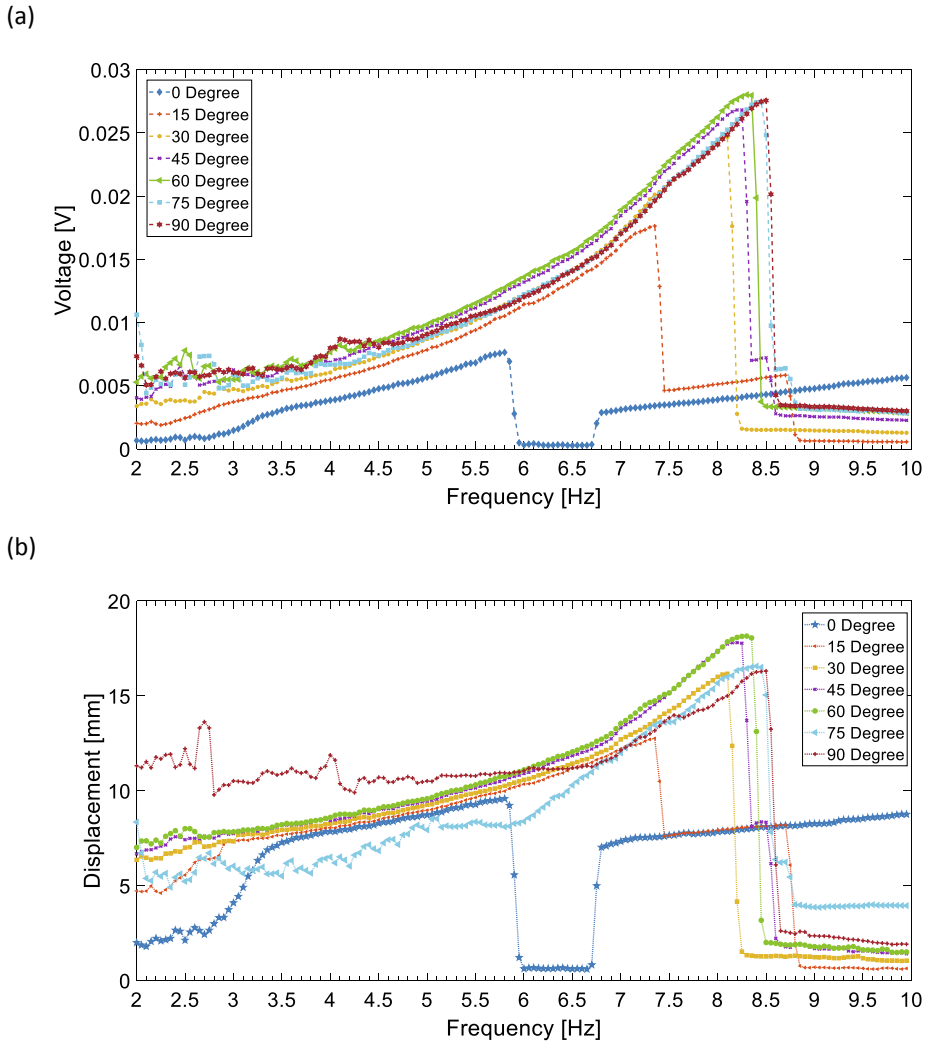

Fig. 9. 2-side limiter Configuration a) frequency-voltage curve and b) frequency-displacement curve at different orientation angles from 0° to 90°.

limiter configuration and with limiter configurations with 2.58 mm 3.85 mm and 4.59 mm gap distance per side. For the analytical equations, the parameters were: $\xi_0 = 0.039$, $\xi_1 = \xi_2 = 0.01$, $f_0 = 3.35Hz$, $f_1 = f_2 = 5Hz$. Fig. 13(a)–(c) show the comparison between analytical and experimental results of motion limiter gap distance 2.58 mm, 3.85 mm and 4.59 mm, respectively. For no motion limiter configuration, since the measuring point of the displacement sensor was located at 94.7 mm from the clamped end, the measured maximum amplitude was supposed to be smaller than simulated one. With constant base acceleration, analytical plot of no limiter configuration indicated a consistently higher amplitude at low frequency (e.g. 2.5–3.2 Hz) comparing to experimental one, which was mainly due to the effects of the ratio of tip and beam mass and the mass moment of inertia. For with motion limiter configurations, a larger limiter gap distance resulted in an increase in the amplitude and a smaller bandwidth, which implied the trade-off between peak amplitude and effective bandwidth. Based on the aforementioned measuring point setup, the experimental plots of with limiter configurations were expected to have a lower overall amplitude near the resonance. However, the measuring points could be inconsistent due to the large deflection near resonance which caused a slightly higher amplitude. Overall, the analytical results were in very good agreement with experimental results for 2-side stopper configurations.

6. Conclusions

An energy harvester with motion limiters subject to both direct and parametric excitations has been designed, manufactured, and experimentally tested. Based the design concept, for the core element (i.e. test beam), the combination of parametric and primary resonances broadens the operational bandwidth by an increasing of 118%. To further broaden the frequency bandwidth and eliminate the gap between parametric and primary modes, motion limiters were employed to merge the parametric and primary resonances by strong hardening frequency response effects, hence a 178% increase in the frequency bandwidth. A theoretical study by using FEM in ANSYS and an averaging perturbation technique have been conducted to verify the linear and nonlinear frequency responses, respectively. Parametric studies including the orientation angles between the purely direct excitation and purely parametric excitation, the length of the core element and the gap between the motion limiters have been conducted to carry out the optimal performance of the proposed vibration energy harvester.

Under a base excitation, no limiter configuration exhibited weakly softening frequency responses while both 1-side and 2-side limiter configurations exhibited strongly hardening frequency responses due to the presence of motion limiters. Comparison of the cantilever beam tip

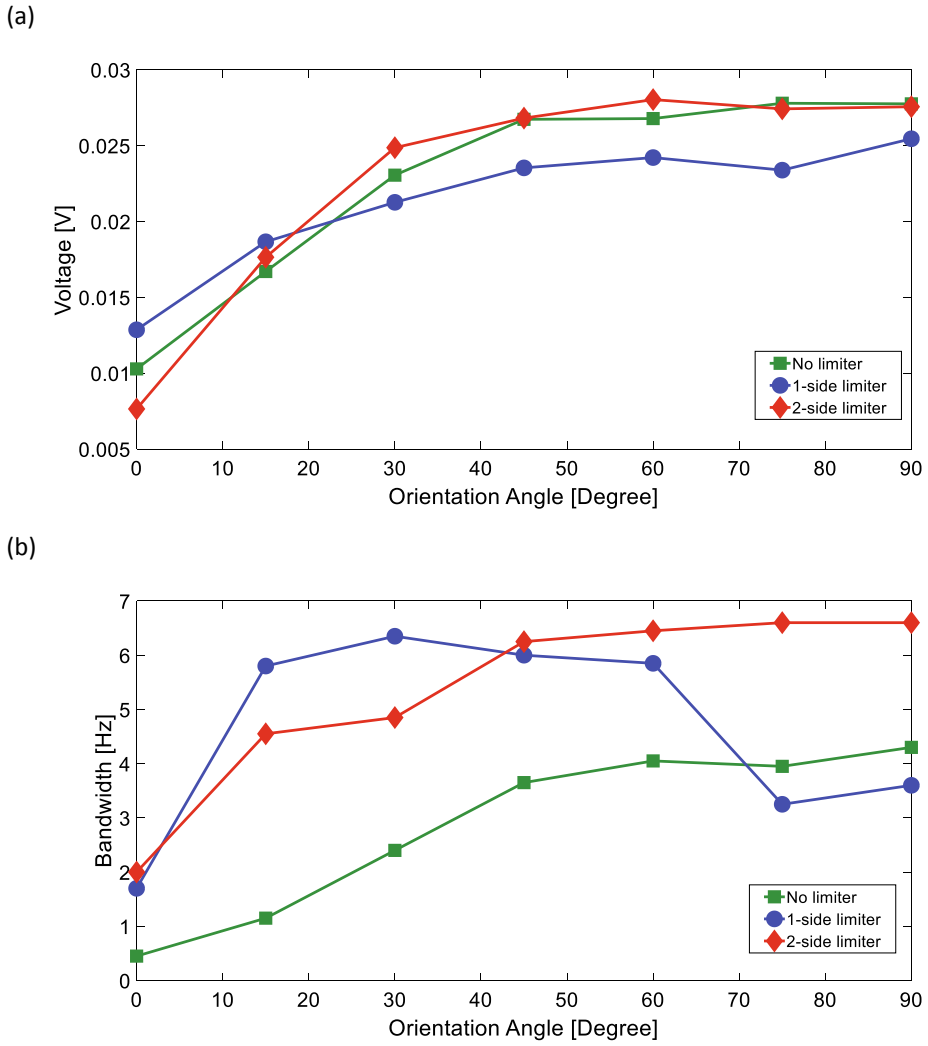

Fig. 10. The comparison of a) peak voltages and b) bandwidth among no limiter, 1-side limiter and 2-side limiter configurations with different orientation angles from 0° to 90°.

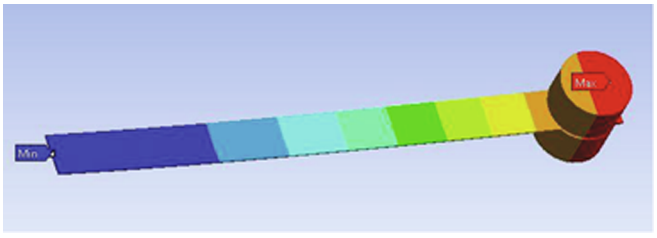

Fig. 11. Theoretical mode shape of the primary resonance.

deflections among with and without limiter configurations indicated no-limiter configuration had the largest deflection and followed by 1-side limiter; 2-side limiter configuration had the smallest deflection which were consistent with the function of motion limiter. However, from the voltage-frequency curves, 2-side limiter had the largest peak voltage, followed by no limiter, the 1-side limiter had the smallest peak voltage. With limiter configurations had wider bandwidth, comparing with no limiter configuration, at 45° orientation angle, 1-side limiter configuration had 164% increased bandwidth (6 Hz vs 3.65 Hz) and 2-side limiter configuration had 178% increased bandwidth (6.5 Hz vs 3.65 Hz). However, 1-side limiter configuration exhibited a bifurcation between the primary and parametric resonances which caused the discontinuity of the overall operational bandwidth; the primary and parametric resonances in 2-side limiter configuration were successfully merged together hence formed a continuous bandwidth for energy harvesting from 2 Hz to 8.6 Hz. For theoretical verification, both linear (without motion limiter) and nonlinear (with motion limiter) frequency responses were obtained theoretically through FEM and the averaging perturbation method, respectively, highlighting very good agreement.

Under a multi-directional base excitation, by adapting the hardening frequency response from motion limiters to the primary and parametric resonances, the two resonances are managed to be merged together, hence form a broad and continuous resonance regime; with transducers (e.g. tip magnets and coil) on the core element, the resulting overall voltage output is significantly enhanced.

CRediT authorship contribution statement

Yimin Fan: Conceptualization, Investigation, Methodology, Validation, Writing - original draft, Software. **Mergen H. Ghayesh:** Conceptualization, Investigation, Methodology, Supervision, Writing -

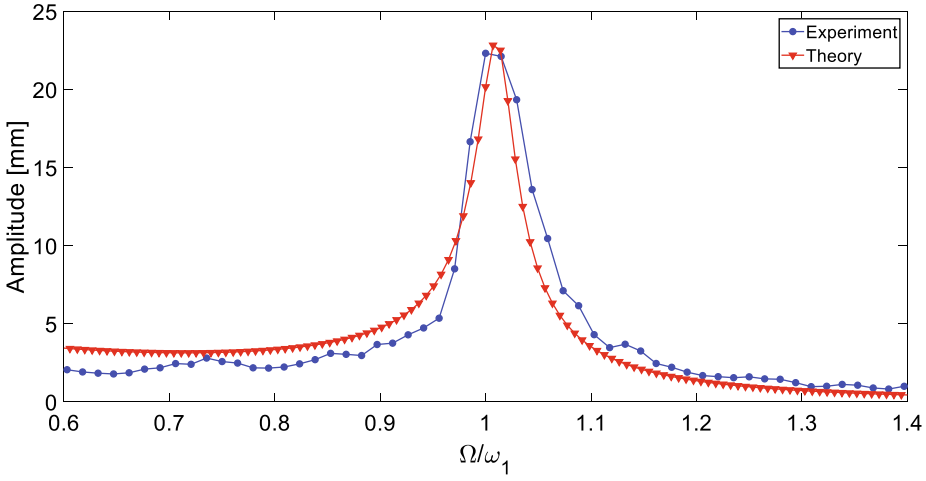

Fig. 12. Comparison between theoretical and experimental obtained primary resonance.

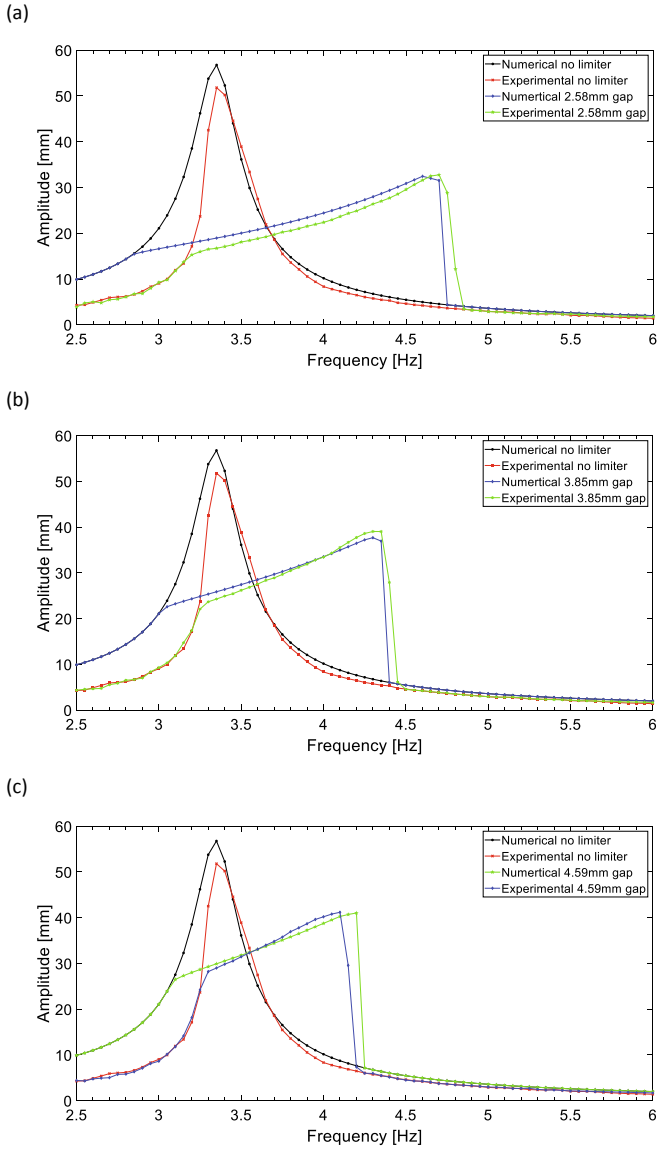

Fig. 13. Comparison between analytical and experimental results of a) limiter gap distance 2.58 mm; b) limiter gap distance 3.85 mm and c) limiter gap distance 4.59 mm.

review & editing. **Tien-Fu Lu:** Conceptualization, Investigation, Supervision, Writing - review & editing.

Declaration of Competing Interest

The authors declare that they have no known competing financial interests or personal relationships that could have appeared to influence the work reported in this paper.

Acknowledgment

This work has been supported by the Australian Government Research Training Program Scholarship. The support is greatly appreciated.

References

[1] Fan K, Cai M, Wang F, Tang L, Liang J, Wu Y, et al. A string-suspended and driven rotor for efficient ultra-low frequency mechanical energy harvesting. Energy Convers Manage 2019;198.
[2] Febbo M, Machado SP, Gatti CD, Ramirez JM. An out-of-plane rotational energy harvesting system for low frequency environments. Energy Convers Manage 2017;152:166–75.
[3] Guo X, Zhang Y, Fan K, Lee C, Wang F. A comprehensive study of non-linear air damping and “pull-in” effects on the electrostatic energy harvesters. Energy Convers Manage 2020;203.
[4] Hu Y, Yang B, Chen X, Wang X, Liu J. Modeling and experimental study of a piezoelectric energy harvester from vortex shedding-induced vibration. Energy Convers Manage 2018;162:145–58.
[5] Iqbal M, Khan FU. Hybrid vibration and wind energy harvesting using combined piezoelectric and electromagnetic conversion for bridge health monitoring applications. Energy Convers Manage 2018;172:611–8.
[6] Kumar S, Singh HH, Khare N. Flexible hybrid piezoelectric-thermoelectric generator for harnessing electrical energy from mechanical and thermal energy. Energy Convers Manage 2019;198.
[7] Li H, Liu D, Wang J, Shang X, Hajj MR. Broadband bimorph piezoelectric energy harvesting by exploiting bending-torsion of L-shaped structure. Energy Convers Manage 2020;206.
[8] Li X, Upadrashta D, Yu K, Yang Y. Sandwich piezoelectric energy harvester: analytical modeling and experimental validation. Energy Convers Manage 2018;176:69–85.
[9] Li Z, Saadatnia Z, Yang Z, Naguib H. A hybrid piezoelectric-triboelectric generator for low-frequency and broad-bandwidth energy harvesting. Energy Convers Manage 2018;174:188–97.
[10] Li Z, Yan Z, Luo J, Yang Z. Performance comparison of electromagnetic energy harvesters based on magnet arrays of alternating polarity and configuration. Energy Convers Manage 2019;179:132–40.
[11] Pan D, Dai F. Design and analysis of a broadband vibratory energy harvester using bi-stable piezoelectric composite laminate. Energy Convers Manage 2018;169:149–60.
[12] Rajarathinam M, Ali SF. Energy generation in a hybrid harvester under harmonic excitation. Energy Convers Manage 2018;155:10–9.
[13] Stamatellou AM, Kalfas AI. Experimental investigation of energy harvesting from swirling flows using a piezoelectric film transducer. Energy Convers Manage

2018;171:1405–15.
[14] Stamatellou AM, Kalfas AI. Testing of piezoelectric energy harvesters isolated from base vibrations. Energy Convers Manage 2019;196:717–28.
[15] Sun W, Guo F, Seok J. Development of a novel vibro-wind galloping energy harvester with high power density incorporated with a nested bluff-body structure. Energy Convers Manage 2019;197.
[16] Sun W, Seok J. A novel self-tuning wind energy harvester with a slidable bluff body using vortex-induced vibration. Energy Convers Manage 2020;205.
[17] Thomson G, Yurchenko D, Val DV, Zhang Z. Predicting energy output of a stochastic nonlinear dielectric elastomer generator. Energy Convers Manage 2019;196:1445–52.
[18] Toyabur RM, Salauddin M, Cho H, Park JY. A multimodal hybrid energy harvester based on piezoelectric-electromagnetic mechanisms for low-frequency ambient vibrations. Energy Convers Manage 2018;168:454–66.
[19] Wang DW, Mo JL, Wang XF, Ouyang H, Zhou ZR. Experimental and numerical investigations of the piezoelectric energy harvesting via friction-induced vibration. Energy Convers Manage 2018;171:1134–49.
[20] Wang J, Zhou S, Zhang Z, Yurchenko D. High-performance piezoelectric wind energy harvester with Y-shaped attachments. Energy Convers Manage 2019;181:645–52.
[21] Wang W, Cao J, Zhang N, Lin J, Liao WH. Magnetic-spring based energy harvesting from human motions: design, modeling and experiments. Energy Convers Manage 2017;132:189–97.
[22] Zhang LB, Dai HL, Yang YW, Wang L. Design of high-efficiency electromagnetic energy harvester based on a rolling magnet. Energy Convers Manage 2019;185:202–10.
[23] Zhang Z, Xiang H, Shi Z, Zhan J. Experimental investigation on piezoelectric energy harvesting from vehicle-bridge coupling vibration. Energy Convers Manage 2018;163:169–79.
[24] Zhao J, Li X. A review of polymer electrolyte membrane fuel cell durability for vehicular applications: degradation modes and experimental techniques. Energy Convers Manage 2019;199.
[25] Roundy S, Wright PK, Rabaey J. A study of low level vibrations as a power source for wireless sensor nodes. Comput Commun 2003;26:1131–44.
[26] Karami MA, Inman DJ. Powering pacemakers from heartbeat vibrations using linear and nonlinear energy harvesters. Appl Phys Lett 2012;100:042901.
[27] Bin Y, Chengkuo L, Wenfeng X, Jin X, Johnny Han H, Rama Krishna K, et al. Electromagnetic energy harvesting from vibrations of multiple frequencies. J Micromech Microeng 2009;19:035001.
[28] Roundy S, Leland ES, Baker J, Carleton E, Reilly E, Lai E, et al. Improving power output for vibration-based energy scavengers. IEEE Pervas Comput 2005;4:28–36.
[29] Jiang XY, Zou HX, Zhang WM. Design and analysis of a multi-step piezoelectric energy harvester using buckled beam driven by magnetic excitation. Energy Convers Manage 2017;145:129–37.
[30] Salauddin M, Rasel MS, Kim JW, Park JY. Design and experiment of hybridized electromagnetic-triboelectric energy harvester using Halbach magnet array from handshaking vibration. Energy Convers Manage 2017;153:1–11.
[31] Daqaq MF, Masana R, Erturk A, Dane Quinn D. On the role of nonlinearities in vibratory rnergy harvesting: a critical review and discussion. Appl Mech Rev 2014;66:040801–40823.
[32] Cottone F, Gammaitoni L, Vocca H, Ferrari M, Ferrari V. Piezoelectric buckled beams for random vibration energy harvesting. Smart Mater Struct 2012;21:035021.
[33] Masana R, Daqaq MF. Relative performance of a vibratory energy harvester in mono- and bi-stable potentials. J Sound Vib 2011;330:6036–52.
[34] Xu C, Liang Z, Ren B, Di W, Luo H, Wang D, et al. Bi-stable energy harvesting based on a simply supported piezoelectric buckled beam. J Appl Phys 2013;114:114507.
[35] Li HT, Qin WY, Zu J, Yang Z. Modeling and experimental validation of a buckled compressive-mode piezoelectric energy harvester. Nonlinear Dyn 2018;92:1761–80.
[36] Abdelkefi A, Nayfeh AH, Hajj MR. Global nonlinear distributed-parameter model of parametrically excited piezoelectric energy harvesters. Nonlinear Dyn 2012;67:1147–60.
[37] Yildirim T, Ghayesh MH, Li W, Alici G. Design and development of a parametrically excited nonlinear energy harvester. Energy Convers Manage 2016;126:247–55.
[38] Akbaş ŞD. Wave propagation of a functionally graded beam in thermal environments. Steel Compos Struct 2015;19:1421–47.
[39] Akbaş SD. Vibration and static analysis of functionally graded porous plates. J Appl Comput Mech 2017;3:199–207.
[40] Akbaş SD. Wave propagation in edge cracked functionally graded beams under impact force. JVC/J Vibrat Control 2016;22:2443–57.
[41] Akbaş SD. Thermal effects on the vibration of functionally graded deep beams with porosity. Int J Appl Mech 2017;9.
[42] Akbaš ŞD. Large deflection analysis of edge cracked simple supported beams. Struct Eng Mech 2015;54:433–51.
[43] Akbaş SD. Post-buckling analysis of edge cracked columns under axial compression loads. Int J Appl Mech 2016;8.
[44] Akbaş ŞD. Large post-buckling behavior of Timoshenko beams under axial compression loads. Struct Eng Mech 2014;51:955–71.
[45] Akbas SD. Geometrically nonlinear analysis of functionally graded porous beams Wind and Structures. Int J 2018;27:59–70.
[46] Lei G, Carol L. Impact-driven, frequency up-converting coupled vibration energy harvesting device for low frequency operation. Smart Mater Struct 2011;20:045004.
[47] Huicong L, Chengkuo L, Takeshi K, Cho Jui T, Chenggen Q. Investigation of a MEMS piezoelectric energy harvester system with a frequency-widened-bandwidth mechanism introduced by mechanical stoppers. Smart Mater Struct 2012;21:035005.
[48] Giusa F, Giuffrida A, Trigona C, Andò B, Bulsara AR, Baglio S. "Random Mechanical Switching Harvesting on Inductor": a novel approach to collect and store energy from weak random vibrations with zero voltage threshold. Sens Actuat A 2013;198:35–45.
[49] Dhakar L, Liu H, Tay FEH, Lee C. A new energy harvester design for high power output at low frequencies. Sens Actuat A 2013;199:344–52.
[50] Song M, Zhang Y, Peng M, Zhai J. Low frequency wideband nano generators for energy harvesting from natural environment. Nano Energy 2014;6:66–72.
[51] Liu S, Cheng Q, Zhao D, Feng L. Theoretical modeling and analysis of two-degree-of-freedom piezoelectric energy harvester with stopper. Sens Actuat A 2016;245:97–105.
[52] Hu G, Tang L, Das R, Marzocca P. A two-degree-of-freedom piezoelectric energy harvester with stoppers for achieving enhanced performance. Int J Mech Sci 2018;149:500–7.
[53] Fan K, Tan Q, Zhang Y, Liu S, Cai M, Zhu Y. A monostable piezoelectric energy harvester for broadband low-level excitations. Appl Phys Lett 2018;112:123901.
[54] Fan K, Tan Q, Liu H, Zhang Y, Cai M. Improved energy harvesting from low-frequency small vibrations through a monostable piezoelectric energy harvester. Mech Syst Sig Process 2019;117:594–608.
[55] Wang C, Zhang Q, Wang W. Low-frequency wideband vibration energy harvesting by using frequency up-conversion and quin-stable nonlinearity. J Sound Vib 2017;399:169–81.
[56] Liu W, Liu C, Ren B, Zhu Q, Hu G, Yang W. Bandwidth increasing mechanism by introducing a curve fixture to the cantilever generator. Appl Phys Lett 2016;109:043905.
[57] Cottone F, Vocca H, Gammaitoni L. Nonlinear energy harvesting. Phys Rev Lett 2009;102:080601.
[58] J. Peña-Ramírez, R.H.B. Fey, H. Nijmeijer. An Introduction to Parametric Resonance. in: T.I. Fossen, H. Nijmeijer, (Eds.), Parametric Resonance in Dynamical Systems. Springer New York, New York, NY, 2012. pp. 1-13.
[59] Narimani A, Golnaraghi ME, Jazar GN. Frequency response of a piecewise linear vibration isolator. J Vib Control 2004;10:1775–94.

Chapter 4

A Nonlinear Energy Harvester via Piezoelectric Arrays and Motion Limiters

This chapter is based on the following accepted paper (in Journal production process):

Fan, Y., M.H. Ghayesh, T.-F. Lu and M. Amabili, *Design, development, and theoretical and experimental tests of a nonlinear energy harvester via piezoelectric arrays and motion limiters*. International Journal of Non-Linear Mechanics, 2022

Statement of Authorship

Title of Paper	Design, development, and theoretical and experimental tests of a nonlinear energy harvester via piezoelectric arrays and motion limiters
Publication Status	☐ Published ☑ Accepted for Publication ☐ Submitted for Publication ☐ Unpublished and Unsubmitted w ork w ritten in manuscript style
Publication Details	This paper has been accepted for publication in International Journal of Non-Linear Mechanics and is waiting for journal production.

Principal Author

Name of Principal Author (Candidate)	Mr. Yimin Fan		
Contribution to the Paper	Conceptualization, Investigation, Methodology, Validation, Writing - original draft, Software		
Overall percentage (%)	70%		
Certification:	This paper reports on original research I conducted during the period of my Higher Degree by Research candidature and is not subject to any obligations or contractual agreements with a third party that would constrain its inclusion in this thesis. I am the primary author of this paper.		
Signature		Date	15 | 02 | 2022

Co-Author Contributions

By signing the Statement of Authorship, each author certifies that:

i. the candidate's stated contribution to the publication is accurate (as detailed above);

ii. permission is granted for the candidate in include the publication in the thesis; and

iii. the sum of all co-author contributions is equal to 100% less the candidate's stated contribution.

Name of Co-Author	Dr. Mergen H. Ghayesh		
Contribution to the Paper	Conceptualization, Investigation, Methodology, Supervision, Writing - review & editing		
Signature		Date	17/02/2022

Name of Co-Author	Dr. Tien-Fu Lu		
Contribution to the Paper	Conceptualization, Investigation, Methodology, Supervision, Writing - review & editing		
Signature		Date	15/02/2022

Name of Co-Author	Prof. Marco Amabili		
Contribution to the Paper	Conceptualization, Investigation, Methodology, Supervision, Writing - review & editing		
Signature		Date	17/2/2022

International Journal of Non-Linear Mechanics 142 (2022) 103974

Contents lists available at ScienceDirect

International Journal of Non-Linear Mechanics

journal homepage: www.elsevier.com/locate/nlm

Design, development, and theoretical and experimental tests of a nonlinear energy harvester via piezoelectric arrays and motion limiters

Yimin Fan [a,*], Mergen H. Ghayesh [a,*], Tien-Fu Lu [a], Marco Amabili [b]

[a] School of Mechanical Engineering, University of Adelaide, South Australia, 5005, Australia
[b] Department of Mechanical Engineering, McGill University, 817 Sherbrooke Street, West, Montréal H3A 0C3, Québec, Canada

ARTICLE INFO

Keywords:
Energy harvester
Vibration
Motion limiter
Nonlinear energy
Parametric resonance

ABSTRACT

This paper presents the design, development and test of a nonlinear piezoelectric energy harvesting array with wideband performance under directly and parametrically excited conditions; theoretical verifications of equation-type as well as finite-element-methods are also provided. The array, as the core element, consists of four cantilever beams with attached piezoelectric layers and individual tip masses; two pairs of motion limiters were designed to limit the cantilever motions. By introducing 1-pair motion limiters, a strong hardening frequency response extended the system resonance regime and generated an enhanced bandwidth; when the monotonically increased system response triggered engagement with 2-pair motion limiters, the operational bandwidth was even further extended and formed a fully merged resonance regime for energy harvesting purposes. With motion limiters, the directly excited device achieved a continuous operational frequency bandwidth from 5.7 Hz to 12.3 Hz, which is a frequency bandwidth increase of 240%; by introducing the nonlinear frequency response in parametric resonance to the proposed device, the operational frequency bandwidth is increased by 579%. The corresponding piezoelectric voltage output of the proposed device is compared with conventional no limiter and one limiter counterparts. Theoretical investigations using an equation for the motion of the system along with a time-integration solution, as well as a finite element method using ANSYS, have been carried out to verify the results, showing good agreement. The results reveal that the proposed device has potential for dealing with different excitation levels and low frequency applications while broadening the frequency bandwidth.

1. Introduction

With recent developments in wireless sensors and remote/portable electronic devices, the application ranges of green energy harvesters have varied from laboratory levels to applications in construction, medical health, transportation and civil engineering. Typically, wireless sensors are limited by volume and size; therefore, a conventional chemical battery power supply is not suitable for these long-term and remote applications. To remedy the current bottleneck, energy harvesting techniques, can not only compensate energy for consumable power supplies, but also replace expensive and polluting sources with environmentally friendly power sources. Mechanical vibration is one form of energy that is ubiquitous in ambient environments; the vibration energy is converted to electrical power by devices called vibration energy harvesters.

In dealing with ambient vibration sources, which are naturally time-varying and random within certain frequency ranges, the main challenge for energy harvesting techniques is forming an effective wideband frequency range at efficiently high output voltage/power levels. To achieve wideband energy harvesting, nonlinear techniques such as externally induced and inherent nonlinearities, were adopted comprehensively by researchers. The inherent nonlinearities generally utilise the large deformations from bending and preloading methods [1–6]. For instance, Friswell et al. [1] reported an inverted beam type energy harvester under a pre-buckling condition. Li et al. [3] proposed a buckled double-clamped beam-based element for energy harvesting purpose under both random and harmonic excitations. By combining magnetic coupling mechanism in pre-loading methods, more external nonlinearities are induced. Zhu and Zu [7] proposed a buckled beam-based energy harvester with magnetic repulsive couplings. Derakhshani et al. [8] studied a clamped–clamped buckled bistable energy harvester works in low frequency excitation. The inherent nonlinearities have the potential to broaden the operational frequency bandwidth to a certain range. However, devices under pre-buckling or post-buckling conditions are prone to be damaged on structures (i.e., cantilever beams) alongside the piezoelectric ceramic transducers [9]. For cantilever beam-based energy harvesters, the repulsive magnetic restoring

* Corresponding authors.
E-mail addresses: yimin.fan@adelaide.edu.au (Y. Fan), mergen.ghayesh@adelaide.edu.au (M.H. Ghayesh).

https://doi.org/10.1016/j.ijnonlinmec.2022.103974
Received 12 August 2021; Received in revised form 1 February 2022; Accepted 14 February 2022
Available online 18 February 2022

force approach is commonly utilised to achieve system multiple equivalent stable stages [10–14]. Typically, novel modifications revolve around the different arrangements between the magnetic tip mass and the external stationary magnet(s). Although multi-stable energy harvesters are capable to achieve large oscillations known as interwell motion, the types of motion highly depend on external excitation levels. To further extend the system resonance regime, impact-based energy harvesting techniques have been drawing attention. The external impacts are introduced by motion limiters (or mechanical stoppers). As the system engages with the motion limiters, the instantly increased effective stiffness alters the system resonance to higher values; hence, an overall extended resonance regime can be formed. Soliman et al. [15] first proposed an impacted-based energy harvester with 1-side motion limiters; different designs have been reported in [16–19], with scale, limiter shape and multi-stable stage modifications. Zhou et al. [20] theoretically investigated and modelled a piezoelectric energy harvester with different mechanical stopper types. More recently, wind energy harvesters also utilised impact-based features to broaden the bandwidth [21]. Li et al. [22] utilised generated contact forces between a mass and stopper to induce nonlinear dynamics behaviours, hence achieving broadband energy harvesting. For the aforementioned approaches, the base excitation directions are always perpendicular to the beam length; to introduce parametric resonance, the chosen base excitation direction is in parallel to the beam length — the principal parametric resonance is about twice the primary one. Abdelkefi et al. [23] analysed a piezoelectric energy harvester operating at parametric resonance; other investigations into parametrically excited systems for energy harvesting purposes are reported in [24–30], which typically focus on reducing the initial threshold amplitude of the parametric resonance. As a subclass of the parametric resonance, researchers have also exploited autoparametric resonance based energy harvesting techniques [31–33]. Zhang et al. [34] investigated a pendulum-like energy harvester based on autoparametric resonance and magnetic coupling effects. Tan et al. [33] studied an autoparametric vibration energy harvester coupled by a nonlinear energy sink analytically and experimentally.

Under a direct force, the nonlinear dynamic behaviour of a system of its fundamental mode can be described by the Duffing equation [35]:

$$\ddot{x} + 2\zeta\omega_n\dot{x} + {\omega_n}^2 x + \beta x^3 = f cos(\Omega t), \tag{1}$$

where $f cos(\Omega t)$ is the external forcing term including forcing amplitude f, excitation frequency Ω and time domain t; x denotes the displacement, ζ is the damping ratio, ω_n denotes the natural frequency and β denotes the nonlinear stiffness coefficient. The dynamic behaviour of a parametrically excited system of its principal parametric mode can be described by using the Mathieu equation [36]:

$$\ddot{x} + 2\zeta\omega_n\dot{x} + \gamma x^3 + \left[{\omega_n}^2 - \epsilon f cos(\Omega t)\right] x = 0, \tag{2}$$

where x, ζ, ω_n, γ, Ω, ϵf are the displacement field, damping ratio, natural frequency, nonlinear stiffness coefficient, the excitation frequency and the magnitude of parametric excitation, respectively. Directly excited system exhibits shorter transient status and requires a lower base excitation level; while a parametrically excited system has time-dependent variables and needs a certain threshold amplitude to trigger the movement. However, in dealing with particular vibration sources, the amplitude growth in a parametrically excited energy harvester is able to maximise the output voltage/power even more than a directly excited device. The performances of the proposed device have been examined under both directly excited and parametrically excited conditions.

In this paper, a report on the design, fabrication, theoretical and experimental test of an impact-based piezoelectric nonlinear energy harvesting array with two pairs of motion limiters is presented. When subject to both primary and parametric excitations, the proposed device had enhanced broadband performance at both its fundamental and parametric resonances. Firstly, under a conventional direct base excitation, the proposed device exhibited a broad and continuous effective frequency bandwidth; the obtained frequency response of the system implies the advantages of the second pair of motion limiters. Secondly, under a parametric excitation, the proposed device demonstrated the merit of combining a nonlinear frequency response in parametric resonance and the motion limiters; both the operational frequency bandwidth and the peak voltage level were increased. Both directly and parametrically excited conditions of the proposed device are compared with the conventional linear and one (single-side or double-side) motion limiter counterparts, highlighting the effectiveness of the device proposed in this paper.

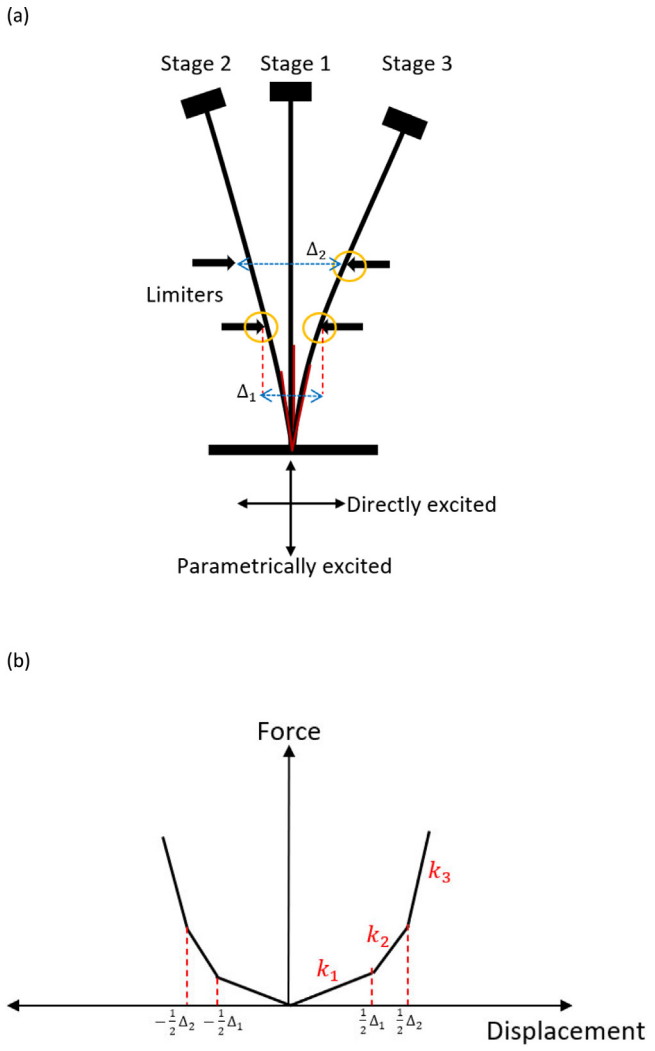

Fig. 1. Schematic of the motion of the proposed device: (a) three stages of the proposed device; (b) the piecewise stiffness behaviour of the proposed device.

2. Experiments

2.1. Design and experimental setup

In this section, the experimental setup and test procedure for both directly excited and parametrically excited scenarios are discussed. The detailed dimensions of the fabricated array and the working principle of the proposed device are also given.

The proposed nonlinear energy harvesting array has been designed and fabricated based on four cantilever beams as the core vibrating elements, and two pairs of two-side motion limiters as the externally induced nonlinearity. The schematics shown in Fig. 1(a) and (b) are

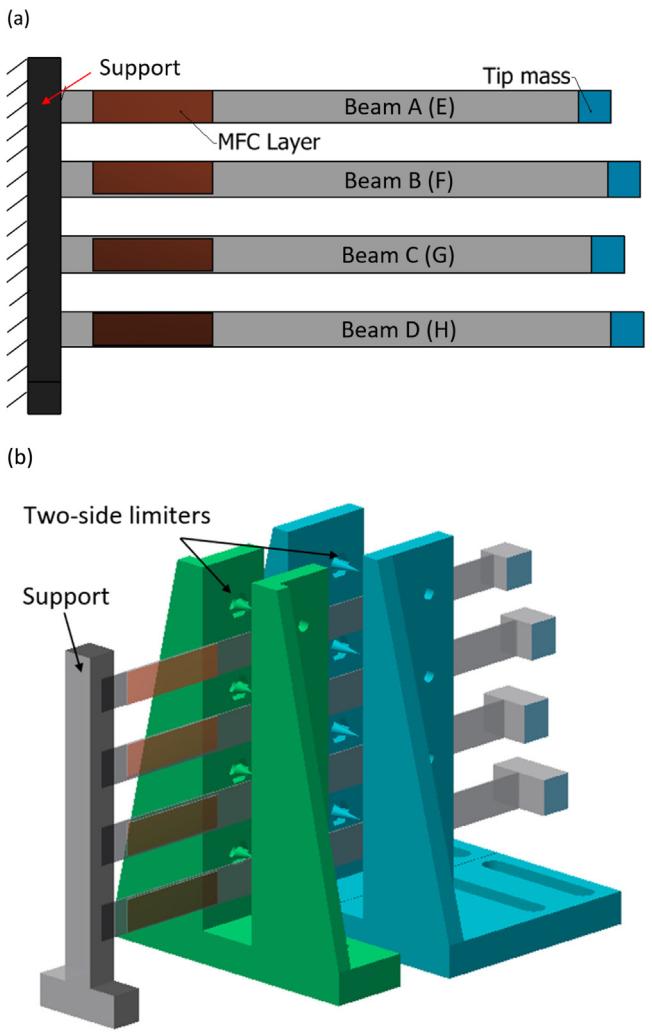

Fig. 2. Schematic of the device: (a) device without motion limiters; (b) device with two pairs of motion limiters.

Table 1
Proposed device for directly excited scenario: (a) beam dimensions; (b) gap distance of the first and second pairs of two-side limiters.

(a)		
Beam	Length × width × thickness	Tip mass m_t
A	170 × 11.5 × 0.5 (mm)	0.972 (gram)
B	179 × 11.8 × 0.5 (mm)	0.964 (gram)
C	174 × 11.5 × 0.5 (mm)	1.931 (gram)
D	180 × 10.8 × 0.5 (mm)	3.169 (gram)
(b)		
Beam	Gap distance Δ_1 of First two-side limiter	Gap distance Δ_2 of Second two-side limiter
A	3.67 (mm)	8.53 (mm)
B	4.81 (mm)	10.24 (mm)
C	4.69 (mm)	11.37 (mm)
D	5.00 (mm)	14.34 (mm)

Table 2
Proposed device for parametrically excited scenario: (a) beam dimensions; (b) gap distance of the first and second pairs of two-side limiters.

(a)		
Beam	Length × width × thickness	Tip mass m_t
E	165 × 11.7 × 0.5 (mm)	5.58 (gram)
F	165 × 11.5 × 0.5 (mm)	7.34 (gram)
G	162 × 11.6 × 0.5 (mm)	11.24 (gram)
H	175 × 12.5 × 0.5 (mm)	11.74 (gram)
(b)		
Beam	Gap distance Δ_1 of First two-side limiter	Gap distance Δ_2 of Second two-side limiter
E	12.37 (mm)	30.45 (mm)
F	12.88 (mm)	36.25 (mm)
G	12.84 (mm)	36.83 (mm)
H	8.7 (mm)	32.27 (mm)

the working principle and the displacement-effective stiffness plot, respectively, of the proposed device, which is presented in Fig. 2. Under a base excitation, the motion of the test beam can be divided into three operational stages. At the off-resonance regime, the system undergoes a low amplitude frequency response. At resonance regime, the increasing displacement leads the system to engage with the first pair of double-side limiters. A periodic impact alters the system effective stiffness to a higher value, and the resultant resonance is shifted to a much higher value during the impact. Consequently, a wider resonance range can be formed with the rapid impacts. When the displacement triggers the second pair of the double-side limiters, the effective stiffness can be increased even further, hence the resonance regime can be extended even more.

The systems shown in Fig. 2(a) and Fig. 3(a) are the schematic and the fabricated device without motion limiter configurations, respectively; Fig. 2(b) and Fig. 3(b) show the schematic and the fabricated devices with 2 pairs of two-side motion limiters configurations, respectively. The dimensions (length, width, thickness and tip mass) of the four clamped–free aluminium beams (density 2700 kg/m^3) used for directly excited and parametrically excited scenarios are shown in Table 1(a) and Table 2(a), respectively. Table 1(b) and Table 2(b) are the selected gap distances between the two pairs of motion limiters used for directly excited and parametrically excited scenarios, respectively. The locations of the 2-pair motion limiters were selected based on preliminary experimental tests to ensure the wideband behaviours can be achieved and a relatively higher overall power level can still be obtained. In addition, the locations of the motion limiters were set to be closer to the first half length from the clamped end to avoid structural fatigue, as the sharpened tips of the motion limiters can potentially damage the test beam during contacting in rapid high-amplitude oscillations near the free end. The experimental measurement and data acquisition devices are shown in Fig. 4(a). A base excitation was provided by a shaking table, APS 113, and its associated power amplifier, APS 115. The base acceleration was monitored by an accelerometer, Kistler 8774A50, and its coupler, Kistler 5134B. A Macro Fibre Composite (MFC) layer M2807-P2 (a piezoelectric layer) was attached to each of the test beams as the transduction method, and the voltage divider circuit shown in Fig. 4(b) was employed to reduce the input signal level to the allowable voltage range of data acquisition board NI USB-6281.

To fully capture the system's nonlinear response, the frequency sampling rate was set to be 1 kHz; both forward (FW) and backward (BW) frequency sweeps with a 0.05 Hz frequency increment were adopted to reveal the nonlinear frequency responses in fundamental and parametric resonances adequately. A preliminary test in the vicinity of a primary resonance were conducted for a single ambient frequency–time history (plotted in Fig. 5) to decide the minimum settling time (4.1 s) required to reach a system steady-state response for each frequency increment. However, for the parametric resonance, the time-dependent variable results in a wider transient status, hence the settling time was set to be 20 s.

(a)

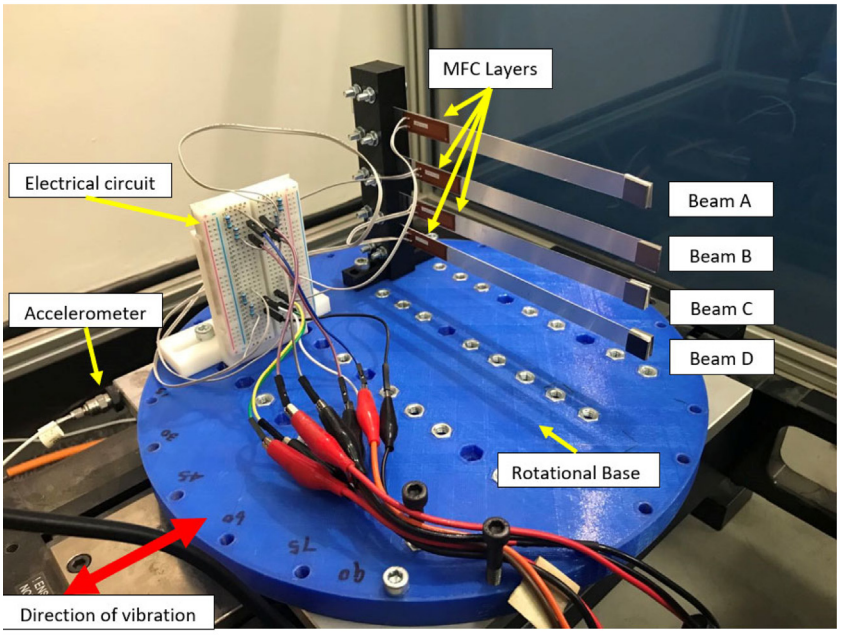

(b)

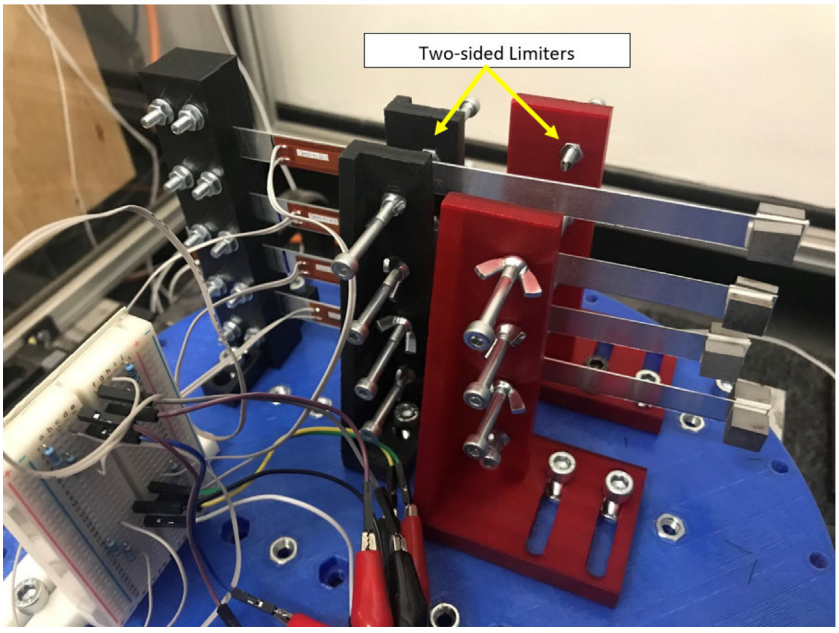

Fig. 3. Fabricated device: (a) No limiter configuration; (b) with two pairs two-side limiters.

2.2. Primary resonance scenario

In this section, the proposed device was tested experimentally by utilising the fundamental primary resonance under a directly excited scenario (i.e., the beam length is perpendicular to the base excitation direction). Four beams with tip masses (see Table 1) were employed as an energy harvesting array. Three different configurations were tested: (i) no motion limiter, (ii), with 1-pair double-side motion limiters and (iii) with 2-pair double-side motion limiters configurations; the longitudinal positions for 1-pair limiters and 2-pair limiters configurations were located at 68 mm and 105.6 mm from the clamped end, respectively. A constant base acceleration was set to be 0.22 g peak to peak for all directly excited experiments. To study and compare the device performance of an effective frequency bandwidth, the effective voltage level was set to be 0.3 V throughout the directly excited experiments.

As shown in Fig. 6, the frequency voltage plot of the no limiter configuration indicated the linear (or weakly nonlinear) system behaviour within the fundamental primary resonance regime for both the forward and backward frequency sweeps. The fabricated test beams A, B, C and D have their fundamental primary resonance frequencies at 10.1 Hz, 9.1 Hz, 7.6 Hz, and 5.95 Hz, respectively; and the corresponding effective frequency bandwidths are 0.8 Hz, 0.65 Hz, 0.65 Hz and 0.65 Hz, respectively. For the sake of demonstration, the experimental results of test beam C were adopted to investigate the time history, phase-plane diagram and Fast-Fourier-Transform (FFT) plots, as shown in Figs. 7, 9 and 11 for no limiter, 1-pairs limiter and 2-pair limiters configurations, respectively.

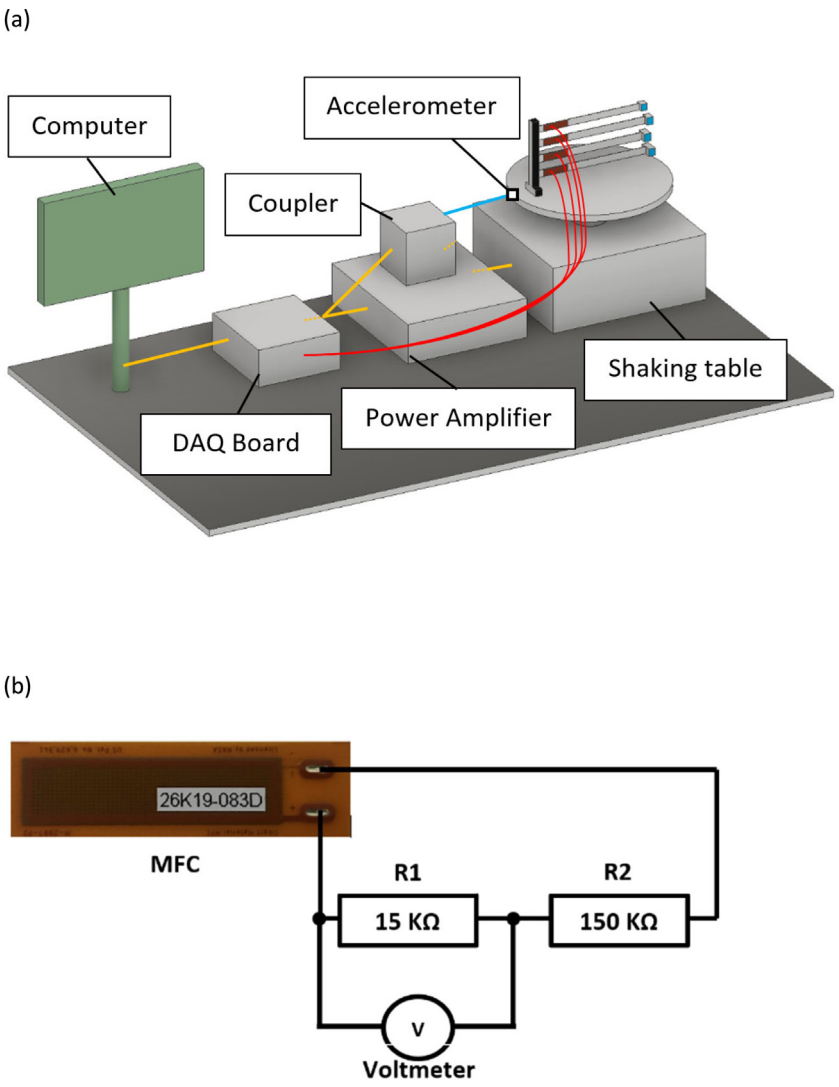

Fig. 4. Schematics of experimental setup: (a) testing and data acquisition devices; (b) voltage divider circuit diagram of each MFC layer.

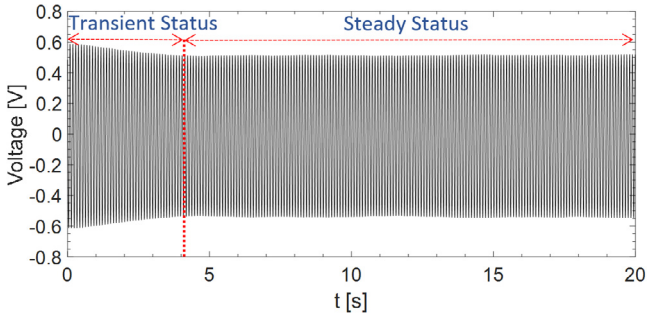

Fig. 5. Experimental tested system transient and steady state responses under a single ambient frequency.

With 1-pair limiters, as shown in Fig. 8, the externally induced nonlinearity was managed to engage with the device at the resonance regime. The strong hardening response altered the effective fundamental resonance frequencies to higher values, hence reducing the off-resonance regimes between the adjacent test beams. The frequency bandwidths of the test beams (A; B; C; D) were increased (1.45; 1.2; 1.65; 1.75) Hz. It can be seen that the forward and backward sweeps increased monotonically first, then bifurcated at 10.4 Hz, 9.25 Hz, 7.9 Hz and 6.2 Hz for test beams A, B, C and D, respectively. The reason for this phenomenon is that the hardening response can only alter the device to a more rigid effective stiffness; hence, the nonlinear region of backward frequency sweep can only be triggered at the linear resonance regime. As seen in Fig. 8, Beam D had a sharper slope in the forward sweep plot, which is due to the effects of the equipped large end mass. Given that the support structure of the motion limiters was made in 3-D printed plastic material (PLA), the large impact force can cause a transient deformation on the structure, which broadened the initial gap distance, hence leading to a higher voltage level.

To fully eliminate the off-resonance regime between adjacent test beams, another pair of motion limiters was adopted. As seen in Fig. 10, at the resonance regime, the test beam (i.e., test beam C) engaged with the first pair of motion limiters at 7.45 Hz. As the beam displacement continued to increase, at 8.1 Hz, the test beam was able to further engage with the second pair of motion limiters as a more rigid boundary condition, leading to the hardening frequency regime being further extended to 9.35 Hz, which fully merged the off-resonance regime. Hence, a continuous effective bandwidth has been formed from 5.7 Hz to 12.3 Hz; the effective bandwidths of beam (A; B; C; D) were (2.55; 1.65; 2.1; 2.4) Hz. Compared with the linear counterpart (the no limiter configuration in Fig. 6), the overall frequency bandwidth was increased by 240%. Comparing no limiter and with limiter configurations, it can be seen that the time trace and phase plane diagram in Figs. 9(a) and 11(a) and Figs. 13(b) and 13(b) exhibited external impacts, respectively. This phenomenon was mainly due to the hardening frequency response of the adjacent test beam. Both Figs. 9 and 11 display a dominant periodic

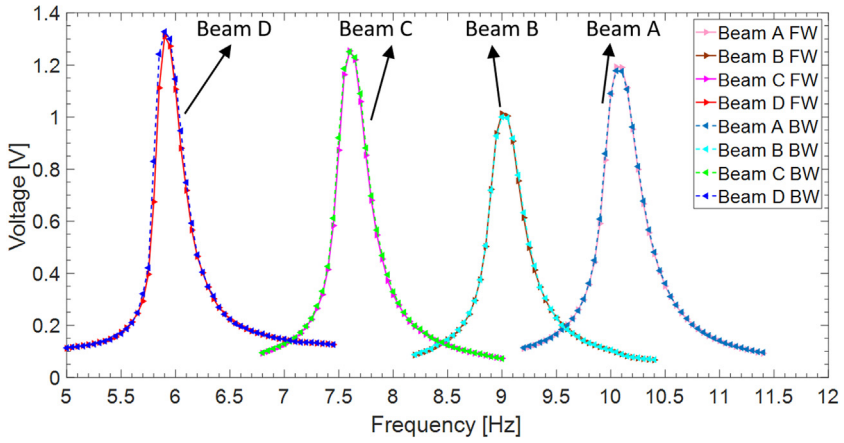

Fig. 6. Frequency–voltage diagram for the no limiter configuration for primary resonance scenario.

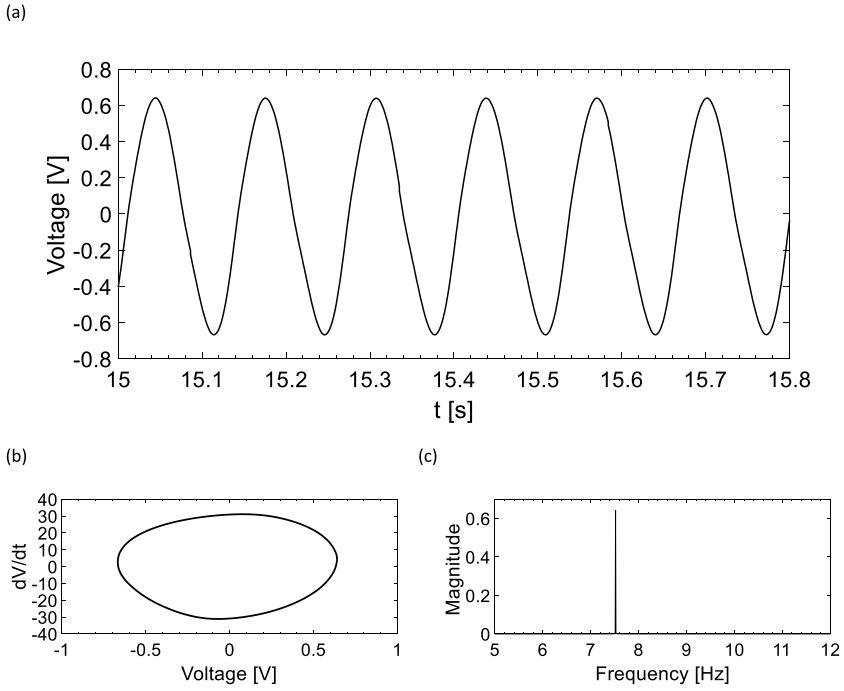

Fig. 7. At 7.6 Hz, the test Beam C without limiter configuration: (a) time trace; (b) phase plane diagram; (c) FFT.

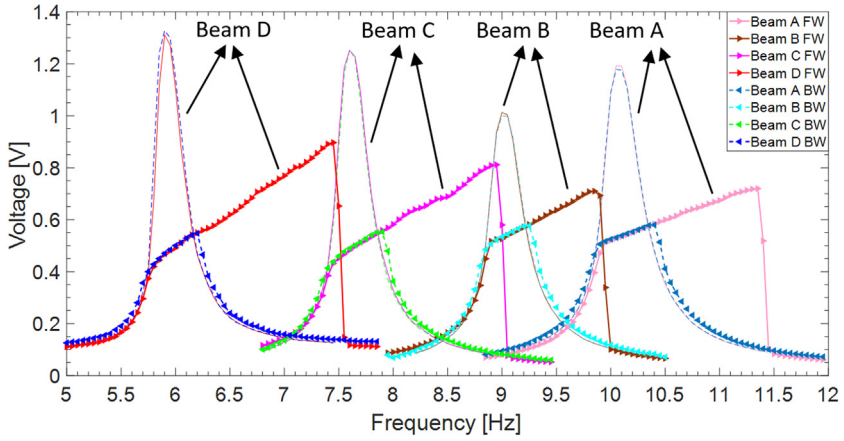

Fig. 8. Frequency–voltage diagram for the 1-pair double-side limiters configuration for primary resonance scenario.

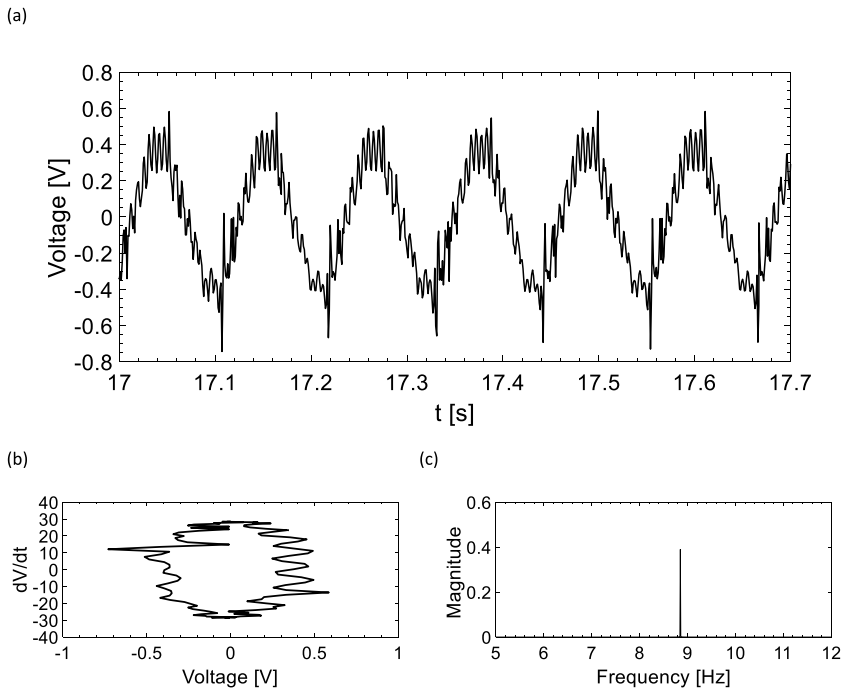

Fig. 9. At 8.8 Hz, the test Beam C with 1-pair double-side limiters configuration: (a) time trace; (b) phase plane diagram; (c) FFT, display a dominant periodic characteristic together with small disturbances.

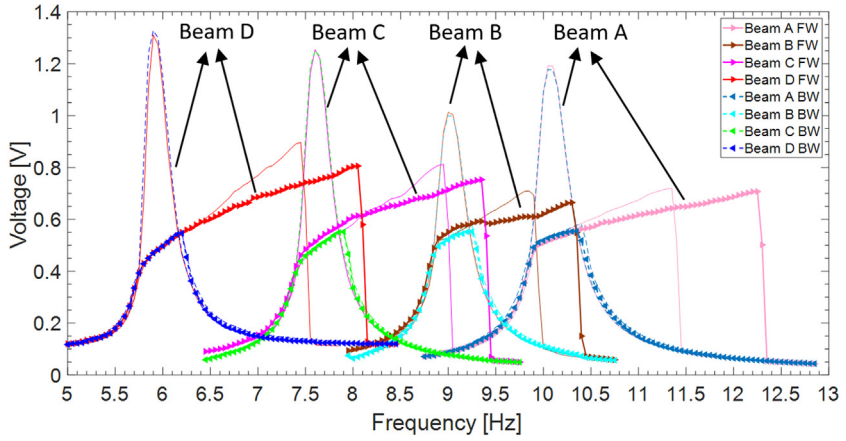

Fig. 10. Frequency–voltage diagram for the 2-pair double-side limiters configuration for primary resonance scenario.

characteristic plus small disturbances; this phenomenon was possibly caused by the piezoelectric effects and limiters features.

2.3. Parametric resonance scenario

In this section, the proposed device was tested experimentally by utilising the principal parametric resonance under a parametrically excited scenario (where the beam length is parallel to the base excitation direction). The principal parametric resonance is about twice the principal fundamental resonance; thus, the four test beams (E, F, G and H) were fabricated and attached with larger tip masses to shift the fundamental resonances to lower values (see Table 2). Similar to the primary resonance cases, three different configurations were considered for testing the device's performance on effective frequency bandwidths: (i) no motion limiter, (ii) 1-pair double-side motion limiters and (iii) 2-pair double-side motion limiters configurations. The longitudinal distances of the limiters remained at the same positions as for the primary resonance cases.

As a certain threshold excitation amplitude is needed to trigger the parametric resonance phenomenon, the selected base excitation level needs to be higher than for the primary resonance cases. Moreover, the test beams were coupled with piezoelectric layers, so the external damping effects from piezoelectricity are taken into consideration. Based on preliminary testings, a 1.34 g peak to peak base acceleration level was sufficient to trigger the parametric resonance as well as revealing the nonlinear frequency responses. The effective voltage level was set to be 0.1 V through all parametrically excited experiments, as the off-resonance regime in parametrically excited experiments displayed an almost zero-amplitude frequency response.

As shown in Fig. 12, the frequency–voltage curve of the no limiter configuration reveals a nonlinear frequency response from the system under a high base excitation level. The resonance regime bandwidth in the backward sweep was doubled compared with the forward sweep. The frequency bandwidths in forward and backward sweeps of the test beams (E; F; G; H) were 0.3 Hz vs 0.6 Hz, 0.35 Hz vs 0.65 Hz, 0.35 Hz vs 0.7 Hz and 0.45 Hz vs 0.75 Hz, respectively. The corresponding resonance peaks of beams E to H were 0.56 V vs 1.28 V, 0.47 V vs

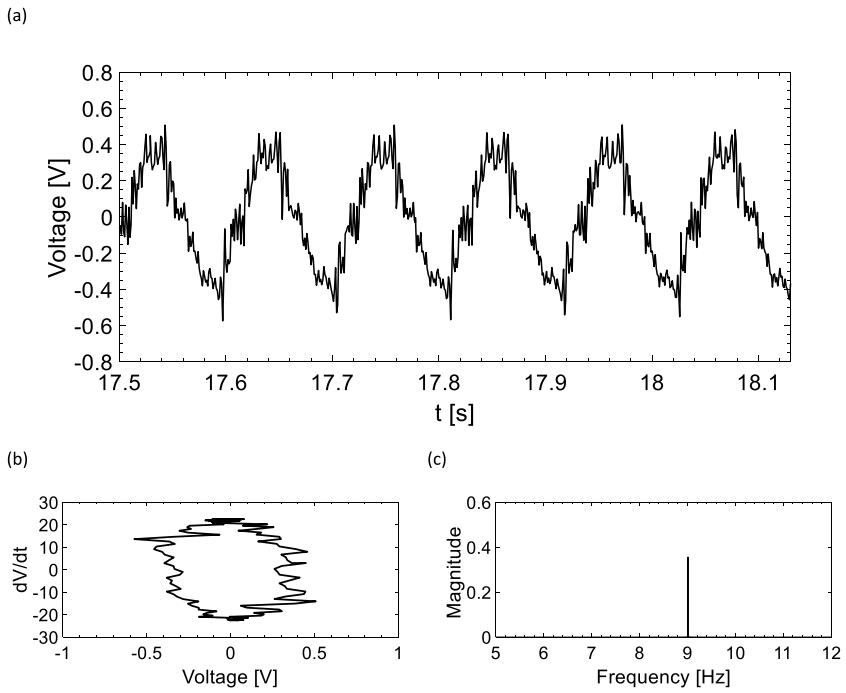

Fig. 11. At 9 Hz, the test Beam C with 2-pair double-side limiters configuration: (a) time trace; (b) phase plane diagram; (c) FFT, display a dominant periodic characteristic together with small disturbances.

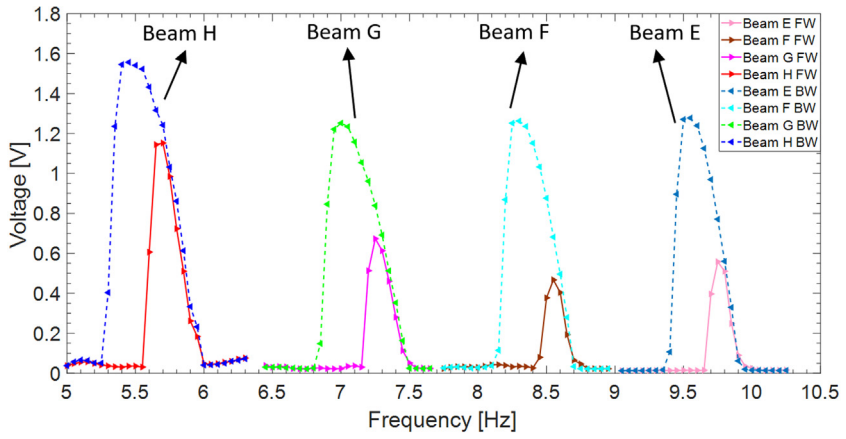

Fig. 12. Frequency–voltage diagram for the no limiter configuration for parametric resonance scenario.

1.26 V, 0.67 V vs 1.25 V and 1.15 V vs 1.56 V, respectively. Different from directly excited case, the parametrically excited device can have a broader frequency bandwidth and higher amplitude in the backward sweep for no limiter configuration. It can be seen that the beam H had a relatively higher voltage amplitude in both the forward and backward sweeps, which was due to the impact of the tip mass. In order to fabricate a beam with its parametric resonance occurring at 5.7 Hz, a large tip mass (11.75 gram) was utilised to shift the fundamental primary resonance to an ultra-low value (around 2.8 Hz).

Comparing the time trace and phase plane diagrams between directly excited (in Fig. 7(a) and (b), respectively) and parametrically excited (in Fig. 13(a) and (b), respectively) scenarios, the directly excited cases exhibited more smooth and rounded paths. Slightly saw-tooth shaped paths were seen at the peaks in the parametrically excited scenarios. However, since the base acceleration levels were inconsistent between the two experiments, parametrically excited experiments under high base excitation levels may cause more external impacts, such as insured clamped ends and inherent geometric nonlinearities. Fig. 14 shows the frequency response of the 1-pair limiters configuration. With 1-pair motion limiters, the effective frequency bandwidths of beams E to H were increased to 1.35 Hz, 1.25 Hz, 1.1 Hz and 1.35 Hz, respectively. Different from the primary resonance scenario (with motion limiters), the peak voltage of the system was maintained at the same level as for the no limiter configuration. For beams E and F, the peak voltage levels were even higher than no limiter configurations. As shown in Fig. 16, by introducing the second pair of motion limiters, the off-resonance regimes between the four test beams were eliminated and the effective frequency bandwidths of beams E to H were further increased to 1.7 Hz, 2.05 Hz, 2.3 Hz and 2.35 Hz, respectively. Hence, the overall effective bandwidths were increased by 579% and 311% compared with their no limiter counterpart, for forward and backward sweeps, respectively.

It can be seen that test beams F, G and H reached higher resonance peaks with the second pair of motion limiters. When beam F engaged with the second pair of motion limiters at 8.85 Hz, the instant frequency response slope became smaller than for the 1-pair limiters' configuration. However, the second pair limiters induced external stiffness, which extended the effective resonance regime to 10.45 Hz (9.55 Hz for the 1-pair limiters configuration), and resulted in a higher peak voltage

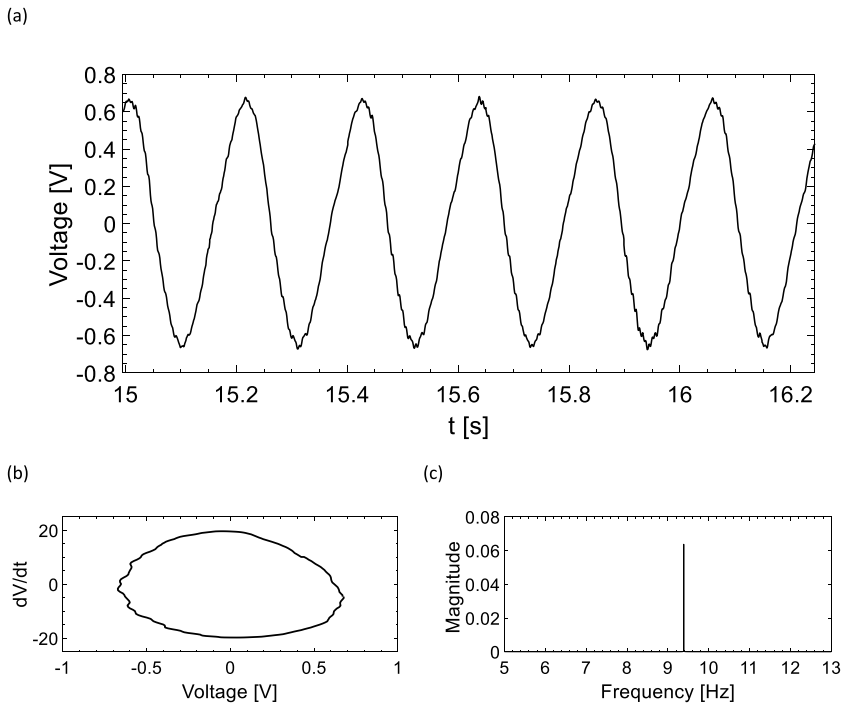

Fig. 13. At 9.4 Hz, the test Beam F without limiter configuration: (a) time trace; (b) phase plane diagram; (c) FFT.

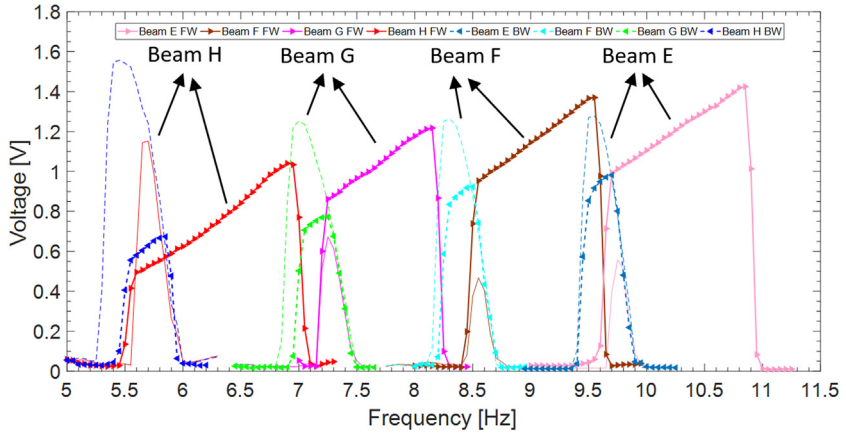

Fig. 14. Frequency–voltage diagram for the 1-pair double-side limiters configuration for parametric resonance scenario.

level (1.384 V) than for the 1-pair limiters configuration (1.37 V). The time history, phase-plane diagram and FFT for the 1-pair limiters and 2-pair limiters configurations are shown in Fig. 15(a), (b) and (c) and Fig. 17(a), (b) and (c), respectively. Both the phase plane diagrams show coincident paths. The saw-tooth motion (i.e., slight amplitude disturbances) can be revealed in the positive half circle; however, the trend in the negative voltage region was not conspicuous. This was mainly caused by the partially attached unimorph MFC layer as the asymmetrically located MFC layer induced the system initial geometric imperfection.

3. Theoretical verification

In order to verify the experimental results theoretically and numerically, in this section, equations for the lumped model of the system along with the adaptive step-size Runge–Kutta method and the finite element method (FEM) have been utilised to compare the experimental results of a reference piezoelectric cantilever beam without a motion limiter at its primary resonance regime. Table 3 shows the system parameters used for the FEM and Runge–Kutta method. A low constant base acceleration 0.2 g peak to peak is employed in this section.

Table 3
Structural parameters and geometry for analytical and numerical verifications of the proposed piezoelectric energy harvester.

Aluminium beam	
Dimension $l_b \times w_b \times h_b$ (mm)	$180 \times 12.5 \times 0.5$
Elastic Modulus E_b (GPa)	68.9
Poisson's Ratio	0.31
Mass density (kg/m^3)	2770
Tip mass m_t (g)	3.169
MFC-2807-P2 patch	
Dimension $l_p \times w_p \times h_p$ (mm)	$28 \times 7 \times 0.3$
Elastic Modulus E_p (GPa)	30.33
Poisson's Ratio	0.33
Mass density (kg/m^3)	5440
Capacitance c_p (nF)	15.11
Load Resistance R (Ohm)	1.65×10^5
Piezoelectric constant d_{31} (m/V)	-170×10^{-10}
Piezoelectric constant g_{31} (Vm/N)	1.2×10^{-4}
electromechanical coupling coefficient φ (N/V)	-5.996×10^{-5}

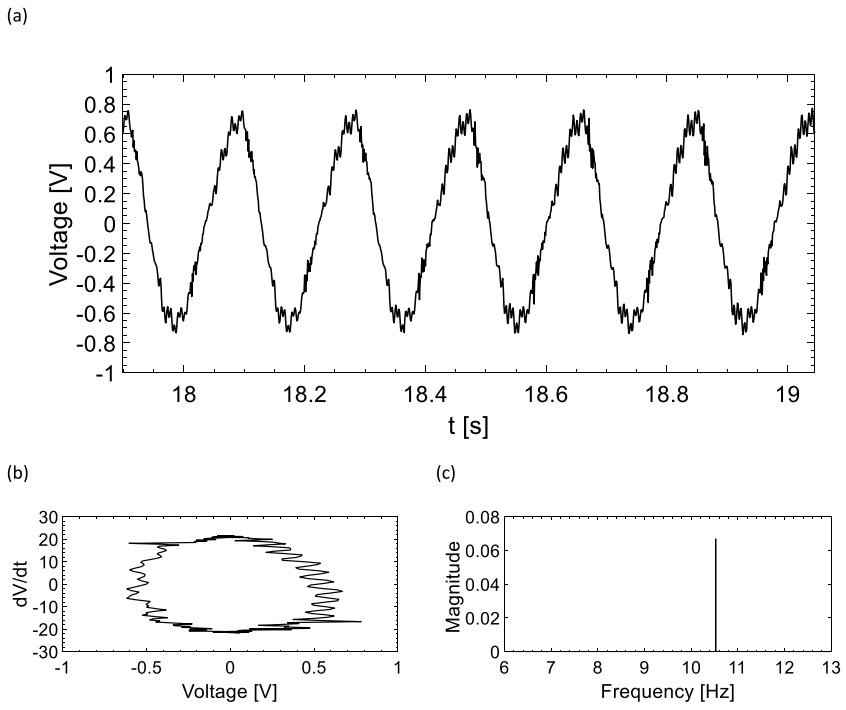

Fig. 15. At 10.55 Hz, the test Beam F with 1-pair double-side limiters configuration: (a) time trace; (b) phase plane diagram; (c) FFT, display a dominant periodic characteristic together with small disturbances.

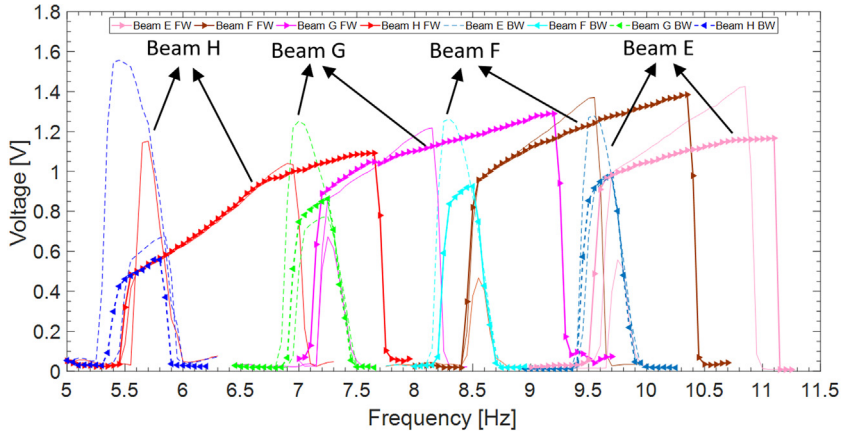

Fig. 16. Frequency–voltage diagram for the 2-pair double-side limiters configuration for parametric resonance scenario.

FEM is performed by the FEA package ANSYS Workbench 18.2. The mode shape, piezoelectric effects and frequency response of the first mode of the testing beam have been simulated in modal and harmonic analysis modules. An adequately fine mesh contains 14723 hexahedral elements and 90810 nodes and it has been applied for modelling as shown in Fig. 18. In Fig. 19(a), the FEM and experimental results indicate a very good agreement on the natural frequency, showing a discrepancy of 1.27% (6.2 Hz vs 6.28 Hz), which was mainly due to the impacts of the thin adhesive layer between the piezoelectric layer and the aluminium beam, which can induce insufficient effective stiffness to the system. As in the harmonic analysis module, the steady-state response of the linear system neglected the transient effects, the 0.08 Hz difference between FEM and experimental results indicates the slightly softening behaviour of the system. The FEM voltage output from the piezoelectric bender is based on the FEM results [37]:

$$v\left(\frac{d}{L_b}\right) = g_{31} E\varepsilon \left(\frac{d}{L_b}\right) L_p, \tag{3}$$

where d is the longitudinal position of the partially attached piezoelectric bender; $L_b, L_p, g_{31}, E\varepsilon$ are the length of the test beam, length of the piezoelectric bender, piezoelectric voltage constant and the stress at that position, respectively. The governing electro-mechanical equations of the piezoelectric cantilever beam can be described as:

$$m\ddot{x}(t) + c\dot{x}(t) + k_1 x(t) + k_3 x(t)^3 + \varphi v(t) = f(t), \tag{4}$$

$$c_p \dot{v}(t) + v/R - \varphi \dot{x}(t) = 0, \tag{5}$$

where $f(t)$ is the external forcing term; x is the displacement field; m, c, k_1 and k_3 denote the equivalent mass, damping, linear and

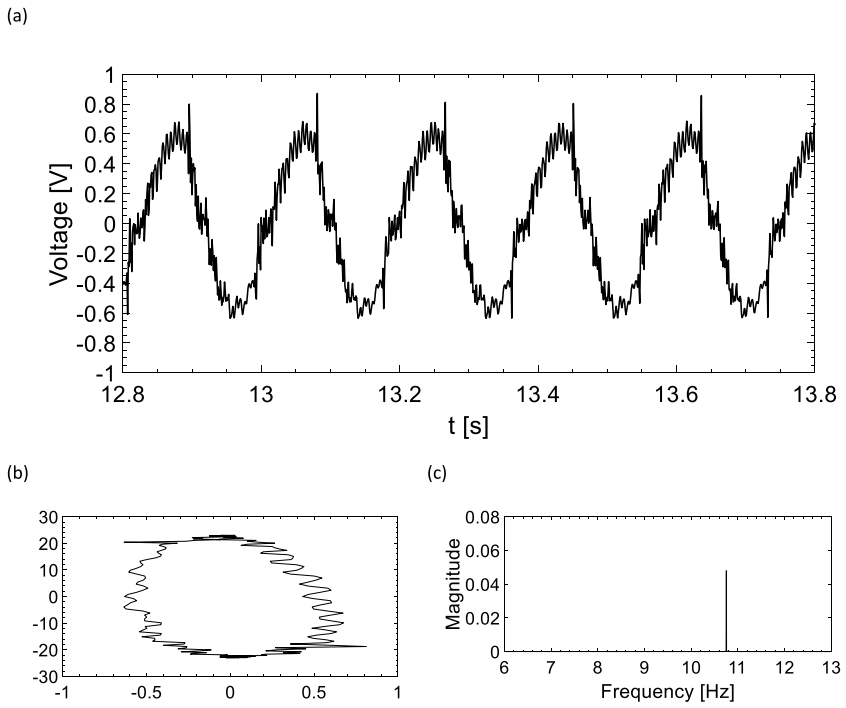

Fig. 17. At 10.75 Hz, the test Beam F with 2-pair double-side limiters configuration: (a) time trace; (b) phase plane diagram; (c) FFT, display a dominant periodic characteristic together with small disturbances.

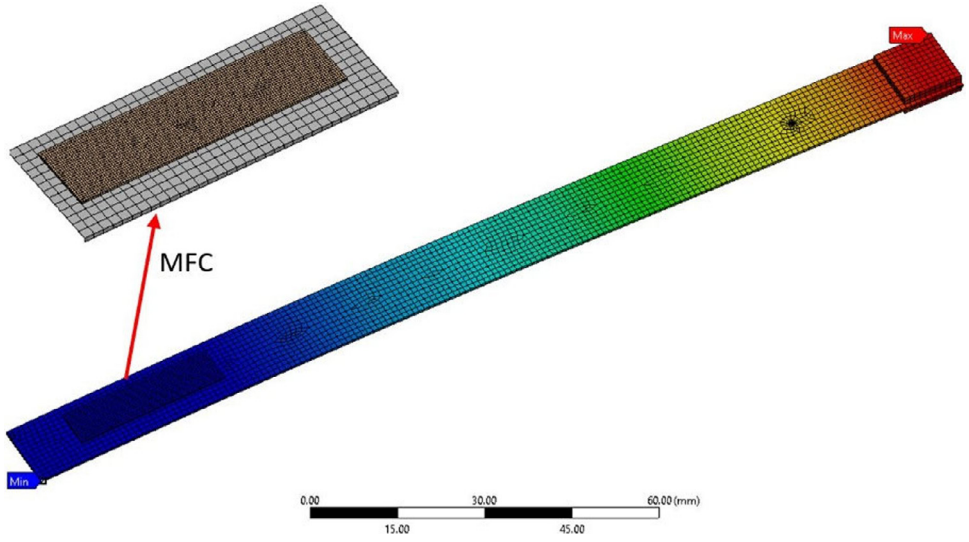

Fig. 18. The mode shape of the testing beam of its primary resonance.

nonlinear stiffness coefficients, respectively. υ is the voltage across resistor R, c_p is the capacitance of the piezoelectric bender and φ is the electromechanical coupling coefficient.

The equivalent mass and stiffness are defined as [38]:

$$m = \frac{33}{140}\left(m_b + m_p\right) + m_t, \tag{6}$$

$$k_1 = \frac{3E_bI_b}{{l_b}^3} + \varepsilon\frac{3E_pI_p}{{l_p}^3}, \tag{7}$$

$$c = 2\xi\omega_n m, \tag{8}$$

where ε is the correction factor as the beam is not fully covered by the piezoelectric bender; ω_n denotes the natural frequency and ξ denotes the damping ratio. Based on the system parameters given in Table 3 and Eqs. (6)–(8), the calculated parameters for the analytical model are: $m = 3.96$ g, $c = 0.0064$ Ns/m, $k_1 = 6.18$ N/m, $k_3 = -321.4$ N/m^3. The Runge–Kutta method in MATLAB was employed to simulate the frequency response of the proposed piezoelectric energy harvester.

Fig. 19(a) and (b) depict the displacement voltage comparison across the theoretical, numerical and experimental results for the testing beam, respectively. The results present a good agreement of the natural frequency between the theoretical and experimental resonances, which indicates that the system owns a nonlinear stiffness term as the system exhibited slight softening behaviour in the primary resonance. To decide the optimal load resistance across the piezoelectric bender, Fig. 20 illustrates the average power as a function of load resistance under different excitation levels when the system is excited at its natural frequency. $R = 10^6\Omega$ seems to be the optimal load resistance value under different base acceleration levels (i.e., 0.1 g, 0.2 g and 0.3 g

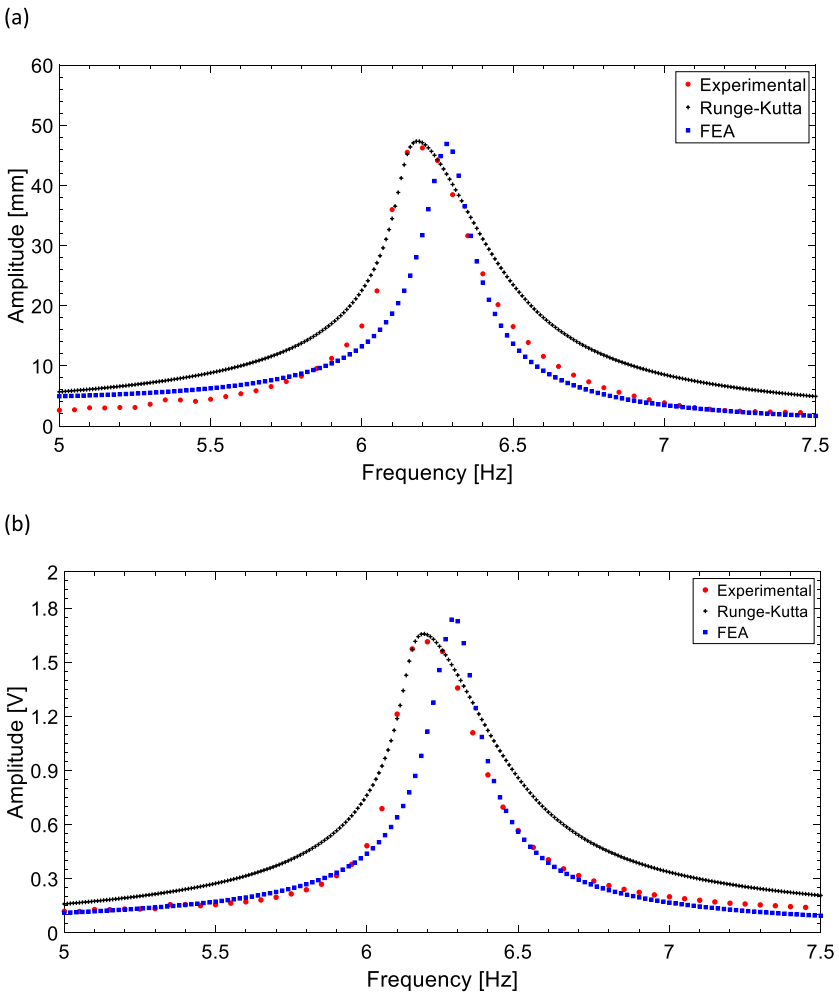

Fig. 19. The comparison between experimental, analytical and numerical results: (a) displacement; (b) voltage.

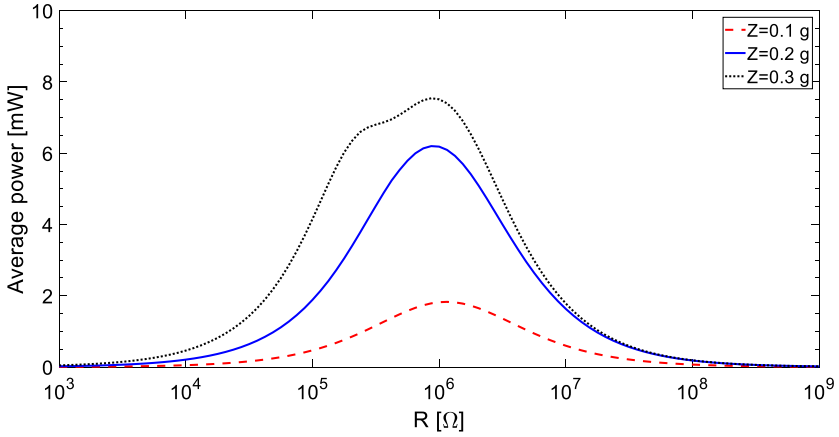

Fig. 20. The average power as a function of load resistance under different excitation levels.

peak to peak), which indicates the slight impacts of base excitation levels on the load resistance.

4. Conclusion

This paper has proposed an impact-based piezoelectric energy harvesting array for both conventional directly excited and parametrically excited scenarios. The working principle is based on the externally induced nonlinearity from the two pairs double-side motion limiters. The device has been built and the experimental validations have been carried out, and the results imply that for both cases, the proposed device exhibited extended continuous effective frequency bandwidths. For the theoretical verification, comparisons of the resonance peak, tip displacement and generated voltage across the theoretical, numerical

and experimental results indicate their good agreement. For the directly excited cantilever array, the overall frequency bandwidth was increased by 240% as compared with the no limiter configuration, while the peak voltage level exhibited a reduction. This implies a certain trade-off between the gap distance of the motion limiters and the extended resonance regime in the directly excited condition at the fundamental primary resonance. For the parametrically excited cantilever array, the overall frequency bandwidth was increased significantly; i.e., 579% in the forward sweep and 311% in the backward sweep cases, as compared with those without limiter configurations. For the second pair motion limiters, the peak voltage level of some test beams was even higher than for the no limiter configuration. Without a limiter, the directly excited array exhibited a linear frequency response due to the relatively small acceleration level. In order to trigger and overcome a certain threshold amplitude in principal parametric resonance, the base acceleration was set to be larger, which led the parametrically excited beams to exhibit nonlinear frequency responses; as the parametric resonance is sensitive to damping, a proper transducer was suggested (i.e., piezoelectric elements or magnet-coil structures) to adapt a selected base excitation level. Compared to conventional impact-based energy harvesting devices (without limiter and with one (one-side or double-side) limiters configuration), the proposed directly excited device achieved an increase in the effective frequency bandwidth. When the device was under the parametrically excited condition at the principal parametric resonance, both the peak voltage level and the effective bandwidth were enhanced.

CRediT authorship contribution statement

Yimin Fan: Conceptualisation, Investigation, Methodology, Validation, Writing – original draft, Software. **Mergen H. Ghayesh:** Conceptualisation, Investigation, Methodology, Supervision, Writing – review & editing. **Tien-Fu Lu:** Conceptualisation, Investigation, Methodology, Supervision, Writing – review & editing. **Marco Amabili:** Conceptualisation, Investigation, Methodology, Supervision, Writing – review & editing.

Declaration of competing interest

The authors declare that they have no known competing financial interests or personal relationships that could have appeared to influence the work reported in this paper.

Acknowledgement

This work has been supported by the Australian Government Research Training Program. The support is greatly appreciated.

References

[1] M.I. Friswell, S.F. Ali, O. Bilgen, S. Adhikari, A.W. Lees, G. Litak, Non-linear piezoelectric vibration energy harvesting from a vertical cantilever beam with tip mass, J. Intell. Mater. Syst. Struct. 23 (2012) 1505–1521.

[2] X.-Y. Jiang, H.-X. Zou, W.-M. Zhang, Design and analysis of a multi-step piezoelectric energy harvester using buckled beam driven by magnetic excitation, Energy Convers. Manage. 145 (2017) 129–137.

[3] H.T. Li, W.Y. Qin, J. Zu, Z. Yang, Modeling and experimental validation of a buckled compressive-mode piezoelectric energy harvester, Nonlinear Dynam. 92 (2018) 1761–1780.

[4] Z. Yi, Y. Hu, B. Ji, J. Liu, B. Yang, Broad bandwidth piezoelectric energy harvester by a flexible buckled bridge, Appl. Phys. Lett. 113 (2018) 183901.

[5] C. Liu, R. Zhao, K. Yu, H.P. Lee, B. Liao, A quasi-zero-stiffness device capable of vibration isolation and energy harvesting using piezoelectric buckled beams, Energy 233 (2021) 121146.

[6] M.A. Ben Hassena, H. Samaali, H.M. Ouakad, F. Najar, 2D electrostatic energy harvesting device using a single shallow arched microbeam, Int. J. Non-Linear Mech. 132 (2021) 103700.

[7] Y. Zhu, J. Zu, A magnet-induced buckled-beam piezoelectric generator for wideband vibration-based energy harvesting, J. Intell. Mater. Syst. Struct. 25 (2014) 1890–1901.

[8] M. Derakhshani, N. Momenzadeh, T.A. Berfield, Analytical and experimental study of a clamped-clamped, bistable buckled beam low-frequency PVDF vibration energy harvester, J. Sound Vib. 497 (2021) 115937.

[9] E. Beltramo, B. Balachandran, S. Preidikman, Three-dimensional formulation of a strain-based geometrically nonlinear piezoelectric beam for energy harvesting, J. Intell. Mater. Syst. Struct. 32 (2021) 2153–2173.

[10] S. Chiacchiari, F. Romeo, D.M. McFarland, L.A. Bergman, A.F. Vakakis, Vibration energy harvesting from impulsive excitations via a bistable nonlinear attachment, Int. J. Non-Linear Mech. 94 (2017) 84–97.

[11] M. Lallart, S. Zhou, Z. Yang, L. Yan, K. Li, Y. Chen, Coupling mechanical and electrical nonlinearities: The effect of synchronized discharging on tristable energy harvesters, Appl. Energy 266 (2020) 114516.

[12] G. Wang, H. Wu, W.-H. Liao, S. Cui, Z. Zhao, J. Tan, A modified magnetic force model and experimental validation of a tri-stable piezoelectric energy harvester, J. Intell. Mater. Syst. Struct. 31 (2020) 967–979.

[13] S. Roy, D. Das, D. Banerjee, Vibrational resonance in a bistable van der Pol–Mathieu–Duffing oscillator, Int. J. Non-Linear Mech. 135 (2021) 103771.

[14] S. Li, H. Wu, X. Zhou, T. Wang, W. Zhang, Theoretical and experimental studies of global dynamics for a class of bistable nonlinear impact oscillators with bilateral rigid constraints, Int. J. Non-Linear Mech. 133 (2021) 103720.

[15] M.S.M. Soliman, E.M. Abdel-Rahman, E.F. El-Saadany, R.R. Mansour, A wideband vibration-based energy harvester, J. Micromech. Microeng. 18 (2008) 115021.

[16] W. Liu, C. Liu, B. Ren, Q. Zhu, G. Hu, W. Yang, Bandwidth increasing mechanism by introducing a curve fixture to the cantilever generator, Appl. Phys. Lett. 109 (2016) 043905.

[17] X. Wang, C. Chen, N. Wang, H. San, Y. Yu, E. Halvorsen, X. Chen, A frequency and bandwidth tunable piezoelectric vibration energy harvester using multiple nonlinear techniques, Appl. Energy 190 (2017) 368–375.

[18] G. Hu, L. Tang, R. Das, P. Marzocca, A two-degree-of-freedom piezoelectric energy harvester with stoppers for achieving enhanced performance, Int. J. Mech. Sci. 149 (2018) 500–507.

[19] W. Jiang, L. Wang, L. Zhao, G. Luo, P. Yang, S. Ning, D. Lu, Q. Lin, Modeling and design of V-shaped piezoelectric vibration energy harvester with stopper for low-frequency broadband and shock excitation, Sensors Actuators A 317 (2021) 112458.

[20] K. Zhou, H.L. Dai, A. Abdelkefi, Q. Ni, Theoretical modeling and nonlinear analysis of piezoelectric energy harvesters with different stoppers, Int. J. Mech. Sci. 166 (2020) 105233.

[21] L. Zhao, Y. Yang, An impact-based broadband aeroelastic energy harvester for concurrent wind and base vibration energy harvesting, Appl. Energy 212 (2018) 233–243.

[22] Z. Li, Z. Saadatnia, Z. Yang, H. Naguib, A hybrid piezoelectric-triboelectric generator for low-frequency and broad-bandwidth energy harvesting, Energy Convers. Manage. 174 (2018) 188–197.

[23] A. Abdelkefi, A.H. Nayfeh, M.R. Hajj, Global nonlinear distributed-parameter model of parametrically excited piezoelectric energy harvesters, Nonlinear Dynam. 67 (2012) 1147–1160.

[24] Y. Jia, J. Yan, K. Soga, A.A. Seshia, Parametrically excited MEMS vibration energy harvesters with design approaches to overcome the initiation threshold amplitude, J. Micromech. Microeng. 23 (2013) 114007.

[25] M. Marszal, B. Witkowski, K. Jankowski, P. Perlikowski, T. Kapitaniak, Energy harvesting from pendulum oscillations, Int. J. Non-Linear Mech. 94 (2017) 251–256.

[26] P. Alevras, S. Theodossiades, H. Rahnejat, Broadband energy harvesting from parametric vibrations of a class of nonlinear Mathieu systems, Appl. Phys. Lett. 110 (2017) 233901.

[27] A. Garg, S.K. Dwivedy, Nonlinear dynamics of parametrically excited piezoelectric energy harvester with 1:3 internal resonance, Int. J. Non-Linear Mech. 111 (2019) 82–94.

[28] Y. Fan, M.H. Ghayesh, T.-F. Lu, Enhanced nonlinear energy harvesting using combined primary and parametric resonances: Experiments with theoretical verifications, Energy Convers. Manage. 221 (2020) 113061.

[29] S.A.M. Lajimi, M.I. Friswell, Dynamics of a non-linearly damped microresonator under parametric excitation and its application in developing sensitive inertial sensors with ultra-wide dynamic ranges, Int. J. Non-Linear Mech. 123 (2020) 103491.

[30] Y. Fan, M.H. Ghayesh, T.-F. Lu, A broadband magnetically coupled bistable energy harvester via parametric excitation, Energy Convers. Manage. 244 (2021) 114505.

[31] Z. Yan, M.R. Hajj, Energy harvesting from an autoparametric vibration absorber, Smart Mater. Struct. 24 (2015) 115012.

[32] S. Mahmoudkhani, H. Soleymani Meymand, Effects of nonlinear interactions of flexural modes on the performance of a beam autoparametric vibration absorber, J. Vib. Control 26 (2019) 459–474.

[33] T. Tan, Z. Wang, L. Zhang, W.-H. Liao, Z. Yan, Piezoelectric autoparametric vibration energy harvesting with chaos control feature, Mech. Syst. Signal Process. 161 (2021) 107989.

[34] A. Zhang, V. Sorokin, H. Li, Energy harvesting using a novel autoparametric pendulum absorber-harvester, J. Sound Vib. 499 (2021) 116014.
[35] F. Cottone, H. Vocca, L. Gammaitoni, Nonlinear energy harvesting, Phys. Rev. Lett. 102 (2009) 080601.
[36] J. Peña Ramírez, R.H.B. Fey, H. Nijmeijer, An introduction to parametric resonance, in: T.I. Fossen, H. Nijmeijer (Eds.), Springer New York, New York, NY, 2012, pp. 1–13.
[37] H. Kim, Y. Tadesse, S. Priya, Piezoelectric energy harvesting, in: D.J. Inman S. Priya (Ed.), Energy Harvesting Technologies, Springer, US, Boston, MA, 2009, pp. 3–39.
[38] A. Erturk, D.J. Inman, On mechanical modeling of cantilevered piezoelectric vibration energy harvesters, J. Intell. Mater. Syst. Struct. 19 (2008) 1311–1325.

Chapter 5

A Broadband Magnetically Coupled Bistable Energy Harvester via Parametric Excitation

This chapter is based on the following published paper:

Fan, Y., M.H. Ghayesh, and T.-F. Lu, *A broadband magnetically coupled bistable energy harvester via parametric excitation.* Energy Conversion and Management, 2021. **244**: p. 114505.

Statement of Authorship

Title of Paper	A broadband magnetically coupled bistable energy harvester via parametric excitation
Publication Status	☑ Published ☐ Accepted for Publication ☐ Submitted for Publication ☐ Unpublished and Unsubmitted w ork w ritten in manuscript style
Publication Details	Fan, Y., M.H. Ghayesh, and T.-F. Lu, A broadband magnetically coupled bistable energy harvester via parametric excitation. Energy Conversion and Management, 2021. 244: p. 114505.

Principal Author

Name of Principal Author (Candidate)	Mr. Yimin Fan		
Contribution to the Paper	Conceptualization, Investigation, Methodology, Validation, Writing - original draft, Software		
Overall percentage (%)	80%		
Certification:	This paper reports on original research I conducted during the period of my Higher Degree by Research candidature and is not subject to any obligations or contractual agreements with a third party that would constrain its inclusion in this thesis. I am the primary author of this paper.		
Signature		Date	27/01/2022

Co-Author Contributions

By signing the Statement of Authorship, each author certifies that:

i. the candidate's stated contribution to the publication is accurate (as detailed above);

ii. permission is granted for the candidate in include the publication in the thesis; and

iii. the sum of all co-author contributions is equal to 100% less the candidate's stated contribution.

Name of Co-Author	Dr. Mergen H. Ghayesh		
Contribution to the Paper	Conceptualization, Investigation, Methodology, Supervision, Writing - review & editing		
Signature		Date	01/02/2022

Name of Co-Author	Dr. Tien-Fu Lu		
Contribution to the Paper	Conceptualization, Investigation, Methodology, Supervision, Writing - review & editing		
Signature		Date	1/02/2022

Energy Conversion and Management 244 (2021) 114505

Contents lists available at ScienceDirect

Energy Conversion and Management

journal homepage: www.elsevier.com/locate/enconman

A broadband magnetically coupled bistable energy harvester via parametric excitation

Yimin Fan *, Mergen H. Ghayesh, Tien-Fu Lu

School of Mechanical Engineering, University of Adelaide, South Australia 5005, Australia

ARTICLE INFO

Keywords:
Nonlinear energy harvesting
Vibration
Parametrically excited
Bistable
Wideband technique

ABSTRACT

Owing to the excitation level of ambient vibrations, the wideband performance of multi-stable energy harvesters and parametrically excited energy harvesters is restricted. The bistable periodic interwell motion and parametric resonance initial threshold amplitude primarily depend on the base excitation level. In this paper, a wideband two-element piezoelectric energy harvester with both bistability and parametric resonance characteristics is presented (i.e. designed, theoretically tested, fabricated and experimentally tested) to tackle the issue of reducing the potential barrier and triggering the parametric threshold amplitude. This device is the first to utilise a directly excited element as an external oscillation source to trigger the large amplitude oscillation of a parametrically excited element through magnetic coupling effects; the periodic interwell motion revealed in the parametrically excited device infers its bistability feature; and a continuously effective operational bandwidth (10–17.3 Hz) is achieved for both elements, which infers the high-energy orbit motions. Theoretical modelling of the proposed device and the expression of the magnetic coupling effects are presented to predict the dynamics of the system, as well as verifying the experimental results. The effects of the base excitation level and the gap distance between magnets are also analysed to shed light on the flexibilities and limitations of the device.

1. Introduction

With the rapid development of Internet of Things (IoT) devices including wearable electronic devices, wireless sensors, implantable medical devices and remote smart monitors, battery power consumption is an unavoidable issue that limiting their performance. As a natural energy source, vibration energy is renewable and has diverse forms, and is therefore considered to be one of the promising methods for mitigating battery power limitations. Of keen interest for vibration energy harvesting (VEH) techniques is converting vibration energy into electrical energy, thereby aiming to provide a sustainable and efficient energy supply for the daily use of electronic devices.

The initial concept of VEH is to utilise tuning techniques to match ambient and designed system resonances, so-called linear resonators, which are only applicable to single harmonic input frequency sources. In dealing with varying excitation frequency sources and stochastic environments, nonlinear energy harvesting (NVEH) techniques aim to broaden the effective frequency bandwidth. The resultant expanded resonance regime should enable the system to be operational within a certain effective bandwidth. In order to achieve a broadband system, softening and hardening frequency responses caused by magnetic restoring forces are commonly introduced by researchers. In early applications, Mann and Sims [1] proposed a magnetic levitation system with a hardening frequency response, the results demonstrated that the nonlinear phenomenon had potential to enhance the bandwidth performance. Cottone, Vocca and Gammaitoni [2] investigated an inverted pendulum with tip magnets subjected to a stationary magnet: potential wells were formed through repulsive magnetic interaction, by altering the distance between the magnets, two equilibrium stable positions of the cantilever have been found and the feature of this energy harvester is known as a bistable oscillator. Differing from a linear resonator, a bistable Duffing energy harvester moves between two potential wells, and its interwell motion under large excitation levels has the potential to outperform its linear or monostable counterparts [3]. For multi-stable energy harvesters, typical modifications are based on the magnetic restoring force [4–6] or initially curved structures [7–9]. The magnetic interaction mainly decides the system behaviours whether it is linear, monostable or bistable; based on the design parameters, the gap distance between the two magnets (e.g., a tip magnet on a core element interacts with a stationary one) affects the frequency bandwidth and the output power/amplitude levels. With alternative magnet designs, the

* Corresponding author.
E-mail addresses: yimin.fan@adelaide.edu.au (Y. Fan), mergen.ghayesh@adelaide.edu.au (M.H. Ghayesh), tien-fu.lu@adelaide.edu.au (T.-F. Lu).

https://doi.org/10.1016/j.enconman.2021.114505
Received 25 March 2021; Accepted 2 July 2021
Available online 20 July 2021

Nomenclature

Z	excitation force amplitude
ω	excitation frequency
m_d	equivalent mass of directly excited beam
m_p	equivalent mass of parametrically excited beam
c_d	damping coefficient of directly excited beam
c_p	damping coefficient of parametrically excited beam
k_d	linear stiffness coefficient of directly excited beam
k_p	linear stiffness coefficient of parametrically excited beam
α	nonlinear stiffness coefficient of directly excited beam
β	nonlinear stiffness coefficient of parametrically excited beam
x	displacement component of directly excited beam
y	displacement component of parametrically excited beam
φ_d	electromechanical coupling coefficient of directly excited beam
φ_p	electromechanical coupling coefficient of parametrically excited beam
R_L	load resistance
C_p	capacitance of the piezoelectric element
v	output voltage
U_m	potential energy field caused by magnetic interaction
M	density of magnetization
B_{rj}	residual magnetic flux density
μ_0	permeability of vacuum
V	volume of magnet
θ	rotational angle of the parametrically excited cantilever beam

equilibrium states of these proposed systems can reach tristable [10–12] and even quadstable states [13,14]. For multi-stable energy harvesting techniques, the types of motion including intrawell and interwell motions, which are highly dependent on the external excitation level. Based on the vibration sources, Cao et al. studied a nonlinear bistable energy harvester from human motion [15]; Qian et al. numerically and experimentally investigated a piezoelectric footwear energy harvester [16]; Izadgoshasb et al. proposed a double pendulum structure for vibration energy harvesting purpose from human motions [17]. To evaluate and optimise the performances of multi-stable energy harvesters under random excitations, Lan and Qin studied a bistable energy harvester with both magnetic repulsion and attraction effects under weak base excitation levels [18]; Leng et al. analytically and experimentally investigated a tristable energy harvester with a different arrangement of magnets, the experimental results demonstrated a higher voltage level compared with its bistable counterpart under filtered Gaussian noise [19]. As another broadband technique, multi degrees of freedom (DOFs) structures with more than one effective resonance have been investigated theoretically and experimentally by researchers, typically in L-shaped energy harvesters [20–22]; by combining with the bistability feature, multi DOFs bistable energy harvesters can further broaden the operational bandwidth [23,24]. Although the aforementioned multi-stable energy harvesters brought an advanced outlook in dealing with realistic problems, crossing the potential barrier between each potential well remains an unfulfilled issue since the external excitation level is exceedingly important for triggering the periodic interwell motion. Mann and Owens investigated a nonlinear energy harvester with magnetic interactions induced bistable potential well, both the theoretical and experimental results showed broadband performance due to interwell motion [25]. In order to decrease the potential barrier between potential wells, Wang and Liao proposed a bistable piezoelectric oscillator with an elastic magnifier [26]; Cao et al. investigated the potential well depth in a tristable energy harvester [27]; Chiacchiari et al. presented numerical studies on a 2-DOF bistable energy harvester [28].

Unlike directly excited energy harvesters, parametrically excited energy harvesters mostly utilise the principal parametric resonance that occurs commonly at twice the principal fundamental resonance to extract energy, requiring the excitation direction to be paralleled to the core element length (e.g., a clamped-free cantilever beam). Daqaq et al. presented analytical and experimental investigations of a parametrically excited energy harvester [29]. Their results indicated there was a critical excitation level (or a certain threshold amplitude) exists in a parametrically excited device, which depends on the system damping coefficient. Different from directly excited devices, the off-resonance regime exhibited an almost zero-amplitude frequency response. Consequently, reducing the threshold amplitude of parametrically excited devices is the most critical issue in the view of energy harvesting [30–34], especially for piezoelectric transducers [35,36], where inherent damping from ceramics are used, which makes triggering even more difficult.

Based on the points mentioned above, the base excitation level is the common constraint for broadening the effective frequency bandwidth in both multi-stable energy harvesting and parametrically excited energy harvesting techniques. A certain excitation level is required to overcome the potential barriers between potential wells and trigger the threshold amplitude for achieving interwell motion in bistable energy harvesters and the parametric resonance in parametrically excited devices, respectively. This paper attempts to address this issue by employing magnetic coupling effects between a parametrically excited beam and a directly excited beam. By tailoring the system parameters, the strong hardening frequency response from the directly excited beam as an external vibration source managed to trigger the principal parametric resonance of the parametrically excited beam, even under a low excitation level.

The paper is organised as follows. In Section 2, the proposed two-element magnetically coupled device is modelled theoretically. The magnetic dipole method is introduced for analysing the magnetic interactions between the two core elements. Section 3 describes the specific experimental setup, data processing approaches as well as preliminary tests on the device including revealing the equilibrium stable positions and resonances of the uncoupled system. Theoretical and experimental results are given in Section 4 along with discussion and comparison. Parametric studies of key system parameters such as the base acceleration level and gap distance between magnets are also presented. The major findings are discussed in details in Section 5.

2. Theoretical modelling

Consider a system with magnetic coupling between a parametrically excited beam and a directly excited beam under a certain base excitation, as shown in Fig. 1. Each beam attaches with a laminated piezoelectric layer that is connected to a resistance for energy harvesting purposes; each beam is modelled as a mass-spring-damper system, with an external magnetic coupling term from the interactions of the magnets as well as an electromechanical coupling term induced by piezoelectric layers. The governing equations can be described as

$$m_d\ddot{x} + c_d\dot{x} + k_d x + \alpha x^3 - \varphi_d v_d + \frac{\partial U_m}{\partial x} = -m_d Z\cos(\omega t), \tag{1}$$

$$C_p\dot{v}_d + \frac{v_d}{R_L} + \varphi_d\dot{x} = 0, \tag{2}$$

$$m_p\ddot{y} + c_p\dot{y} + \left(k_p - hZ\cos(\omega t)\right)y + \beta y^3 - \varphi_p v_p + \frac{\partial U_m}{\partial y} = 0, \tag{3}$$

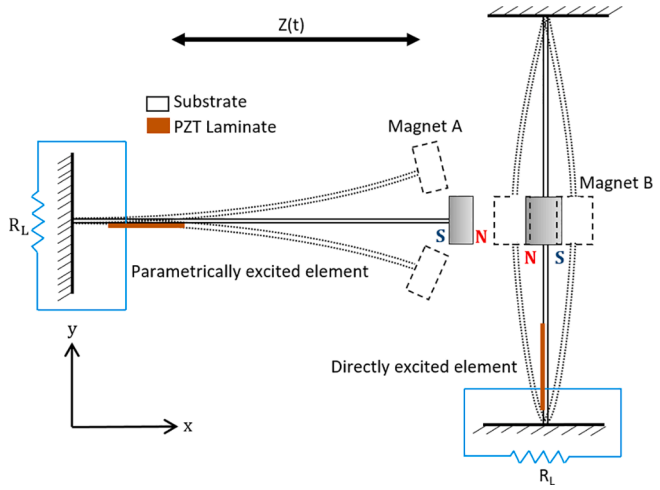

Fig. 1. Schematic of the proposed bistable wideband energy harvesting device.

$$C_p\dot{v}_p + \frac{v_p}{R_L} + \varphi_p\dot{y} = 0, \tag{4}$$

where m_d and m_p are the equivalent masses of directly excited beam and parametrically excited beam, respectively; c_d and c_p are the damping coefficients; k_d and k_p are the linear stiffness coefficients;α and β are the nonlinear stiffness coefficients;φ_d and φ_p are the electromechanical coupling coefficients for directly excited and parametrically excited beams, respectively; $Zcos(\omega t)$ is the base acceleration term, ω is the excitation frequency; R_L and C_p are the load resistance and capacitance of the piezoelectric element, respectively; x and y are the displacement components of the directly excited beam and parametrically excited beam, respectively; v_d and v_p are the output voltages from the piezoelectric layer of directly and parametrically excited beams, respectively; h is the scaling factor of the parametric excitation term; U_m is the potential energy field caused by the magnetic interactions between the two magnets, A and B.

To model the magnetic coupling between these two beams theoretically, the magnetic dipole method is employed. The two magnets are assumed to be point dipoles, and the magnetic field generated by A upon B is expressed as [37]

$$B_{AB} = -\frac{\mu_0}{4\pi}\nabla\frac{\mu_A \bullet r_{AB}}{{r_{AB}}^3} = -\frac{\mu_0}{4\pi}\left(\frac{\mu_A}{{r_{AB}}^3} - (\mu_A \bullet r_{AB})\frac{3r_{AB}}{{r_{AB}}^5}\right), \tag{5}$$

where μ_0 is the permeability of the vacuum; μ_A is the magnetic moment vector of dipole A; r_{AB} is the distance vector from dipole B to dipole A; and ∇ represents the Euclidean Norm. The magnetic moment vectors of dipole A and B and the distance vector r_{AB} can be determined from Fig. 2 as

$$\mu_A = \begin{pmatrix} M_A V_A \cos\theta \\ M_A V_A \sin\theta \end{pmatrix}, \tag{6a}$$

$$\mu_B = \begin{pmatrix} -M_B V_B \\ 0 \end{pmatrix}, \tag{6b}$$

$$r_{AB} = \begin{pmatrix} -d - x - l_p(1-\cos\theta) \\ y \end{pmatrix}, \tag{6c}$$

where M_A and M_B are the densities of magnetization of dipole A and dipole B, respectively ($M_j = B_{rj}/\mu_0$, B_{rj} is the residual magnetic flux density); V_A and V_B are the volumes of magnets A and B, respectively; d is the initial distance between two dipoles along the x axis; and l_p and θ are the length and the rotational angle ($\theta = \dot{y}$) of the parametrically excited cantilever beam, respectively. The magnetic vector μ_B in the y direction is assumed to be zero as the magnet on the clamped–clamped beam is attached at the centre of the beam. Thus, the potential energy induced by these two dipoles can be expressed as

$$U_m = -B_{AB} \bullet \mu_B = -\frac{\mu_0 M_A V_A M_B V_B cos\theta}{4\pi}\left((D^2+y^2)^{-\frac{3}{2}} - 3D^2\left((D^2+y^2)^{-\frac{5}{2}}\right)\right), \tag{7a}$$

$$D = d + x - l_p(\cos\theta - 1) \tag{7b}$$

Eqns. (7a) and (7b) are the derived magnetic potential energy induced by dipoles A and B. Thus, the magnetic restoring forces in Eqns. (1) and (3) can be calculated by taking partial derivatives with respect to x and y for directly excited and parametrically excited beams, respectively:

$$F_d = \frac{\partial U_m}{\partial x} = -\frac{\mu_0 M_A V_A M_B V_B \cos\theta}{4\pi}(9D(D^2+y^2)^{-\frac{5}{2}} - 15D^3(D^2+y^2)^{-\frac{7}{2}}), \tag{8a}$$

$$F_p = \frac{\partial U_m}{\partial y} = -\frac{\mu_0 M_A V_A M_B V_B \cos\theta y}{4\pi}\left(3(D^2+y^2)^{-\frac{5}{2}} - 15D^2(D^2+y^2)^{-\frac{7}{2}}\right) \tag{8b}$$

Eqns. (8a) and (8b) indicate the difference between the derived magnetic restoring forces on directly and parametrically excited beam.

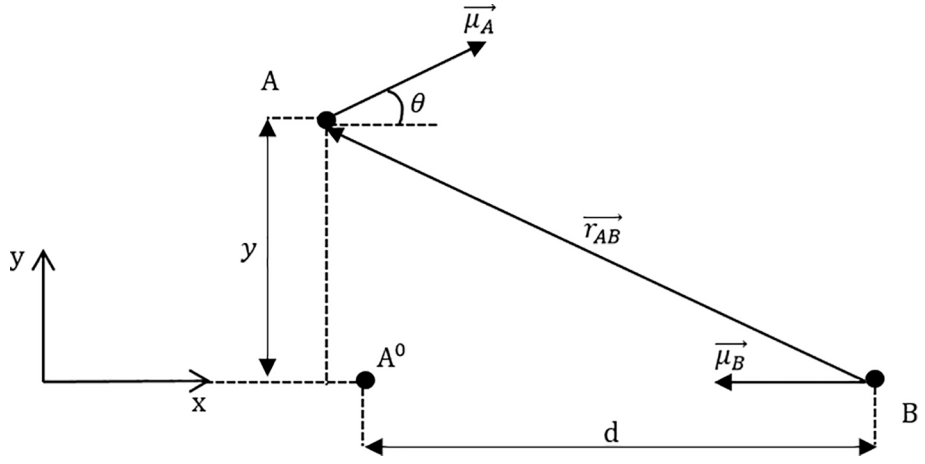

Fig. 2. Geometric configuration of the dipole–dipole model between the tip magnet A on the parametrically excited beam and the middle magnet B on the directly excited beam.

A parametrically excited beam, is more dependent on its displacement; since the magnetic moment μ_B omits the vector along the y axis, the oscillations of parametrically excited beam have fewer effects on F_d. Based on Eqns. ((1)–(4)), (8a) and (8b), the voltage outputs of the proposed energy harvester can be obtained numerically by employing the Runge-Kutta Method in MATLAB; the system parameters are derived based on the geometric and material properties listed in Table 1.

3. Experimental setup

The corresponding experimental tests are performed to validate the theoretical model of the proposed device. A picture of the experimental setup is shown in Fig. 3(a) and the system parameters are listed in Table 1. The core element consists of a parametrically excited beam (clamped-free) and a directly excited beam (clamped–clamped). Both of them are made of aluminium and attached with laminated piezoelectric benders (Macro Fiber Composite MFC2807-P2 from Smart Material Corporation) for energy conversion. To introduce magnetic coupling effects to the system, a tip magnet with a plastic holder and a middle magnet (neodymium) are attached to the parametrically excited and directly excited beams, respectively. The base excitation is provided by a shaking table, APS 113, and its power amplifier, APS 115. An accelerometer, Kistler 8774A50, is used to monitor the real-time acceleration level. A displacement sensor, Wenglor CP24MHT80, is used to record the transverse deflection of the parametrically excited beam near the free end and an electrical circuit serves as a voltage divider to ensure the maximum output voltage is within the allowable range of data acquisition board NI USB-6281. With a 1 kHz sampling rate, 0.05 Hz step size and 20 s settling time, the proposed device reaches the stable states thoroughly for both the parametrically excited and directly excited beams. Constant base acceleration amplitudes are adopted for all experiments. By altering the gap distance between the two magnets, the system is able to undergo linear, monostable, or bistable status. The bistability of parametrically excited beam is displayed in Fig. 3(b); these two equilibrium positions indicate that the initial positions of the parametrically excited beam varying with different gap distances (the longitudinal distance between the tip and the mid magnets).

Table 1
Material and geometric parameters of the proposed system.

Directly excited cantilever beam	
Dimension $l_d \times w_d \times h_d$ (mm)	175 X 11 X 0.5
Mid mass m_{dt} (g)	33.0
Parametrically excited cantilever beam	
Dimension $l_p \times w_p \times h_p$ (mm)	159 X 11 X 0.5
Tip mass m_{pt} (g)	2.1 (magnet 1.15 g, plastic holder 0.95 g)
Aluminium property	
Elastic Modulus E_{Al} (GPa)	68.9
Poisson's Ratio	0.31
Mass density ρ_{Al} (kg/m^3)	2770
Piezoelectric patch property	
Dimension $l_{pzt} \times w_{pzt} \times h_{pzt}$ (mm)	28 X 7 X 0.3
Elastic Modulus E_p (GPa)	30.33
Poisson's Ratio	0.33
Mass density ρ_{pzt} (kg/m^3)	5440
Capacitance c_p (nF)	15.11
Load Resistance R (Ohm)	1.65×10^5
Piezoelectric constant d_{31} (m/V)	-1.7×10^{-10}
electromechanical coupling coefficient φ_d (N/V)	-1.1×10^{-4}
electromechanical coupling coefficient φ_p (N/V)	-8.3×10^{-5}
Magnet property	
Residual magnetic flux density B_r (T)	1.057
Permeability of vacuum μ_0 (H/m)	$4\pi \times 10^{-7}$
Volume of magnet A V_A (m^3)	1.5708×10^{-7}
Volume of magnet B V_B (m^3)	4.459×10^{-6}

Since the directly excited beam works as an external vibration source that enhances the operational bandwidth performance of the parametrically excited beam, the ratio of the fundamental primary resonances between parametrically and directly excited beam without magnetic coupling effects should be around 1:2. By considering the repulsive magnetic coupling effects on each beam, the designed fundamental primary resonances of the uncoupled parametrically excited and directly excited beams are 6.9 Hz and 17.9 Hz, respectively. In preliminary testing, the directly excited beam with clamped–clamped boundary conditions exhibited a strong hardening frequency response with a relatively wider resonance range as expected. Thus, for the parametrically excited beam, its predicted parametric resonance should occur around 13.8 Hz, which is within the range of the directly excited beam resonance regime. It should also be noted that the piezoelectric layers attached to the testing beams induced external mechanical/electrical damping to the system; for conventional parametrically excited devices (e.g., simply clamped-free cantilever with piezoelectric elements), the parametric resonance phenomenon could only be revealed under a much higher base excitation level.

4. Results

The first test was to examine the performance of the proposed device in terms of the voltage level and compare it with the corresponding theoretical results. The longitudinal distance between the two magnets is set to be 55 mm for the main experiments. The theoretical and experimental voltage-frequency plots of both forward (FW) and backward (BW) sweeps of the coupled system under a 0.5 g base excitation are shown in Fig. 4(a) and Fig. 4(b), respectively, as well as a comparison plot in Fig. 4(c). The theoretical and experimental results are within good agreements for both operational frequency bandwidth and output voltage level. Under a 0.5 g base acceleration level, both the parametrically excited and directly excited beams exhibit a strong hardening frequency response with a continually effective frequency bandwidth from 10 Hz to 17.3 Hz. In Fig. 4(b), the directly excited plots reveal a considerable peak occurred at 14.0 Hz, which demonstrate the existence of the principal parametric resonance for the parametrically excited beam, as well as its positive effects on the directly excited component.

For a conventional uncoupled parametrically excited device, the resonance regime suffers from a narrow effective bandwidth and its off-resonance regime is obtained as a zero-amplitude response. However, in the proposed device, as the directly excited beam exhibits a strong hardening frequency response due to the clamped–clamped condition, the magnetic coupling between these two beams induces rapid interactions between the mid magnet (on the directly excited beam) and the tip magnet (on the parametrically excited beam). As a result, the initial boundary conditions of the parametrically excited beam have been changed, and this triggers and overcomes the threshold amplitudes for both the bistable and parametric resonance characteristics in consequence. The parametrically excited beam maintains on its high energy orbit and displays periodic interwell motions synchronously with the directly excited beam untill 17.3 Hz where the resonance regime of directly excited beam ends, the parametric resonance of parametrically excited beam is also terminated. In term of the voltage level, a higher overall voltage level shows in the parametrically excited beam plot (see Fig. 4(a), (b) and (c)). Since the directly excited clamped–clamped beam has a smaller amplitude than the parametrically excited beam in a clamped-free condition, the positive proportional relationship between the deformation and output voltage of the piezoelectric layer implies the higher overall voltage level of the parametrically excited beam.

As one of the most important features of this proposed device is triggering and observing the bistability in the parametrically excited

(a)

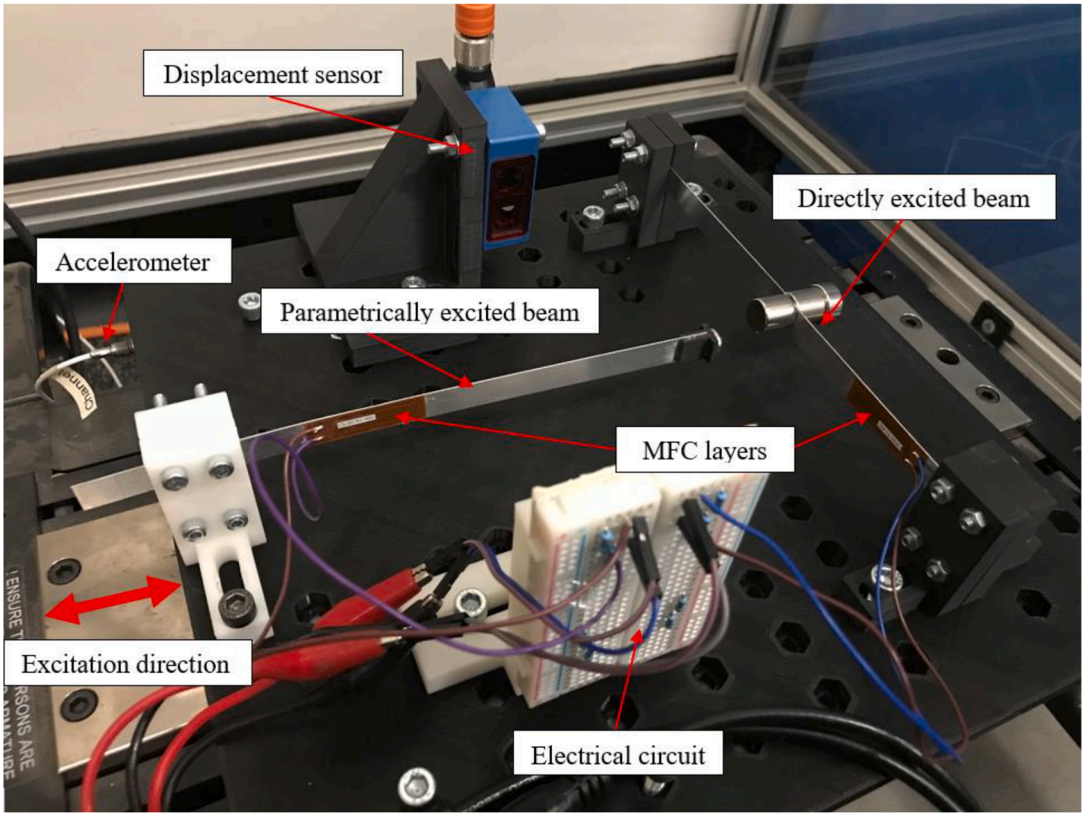

(b)

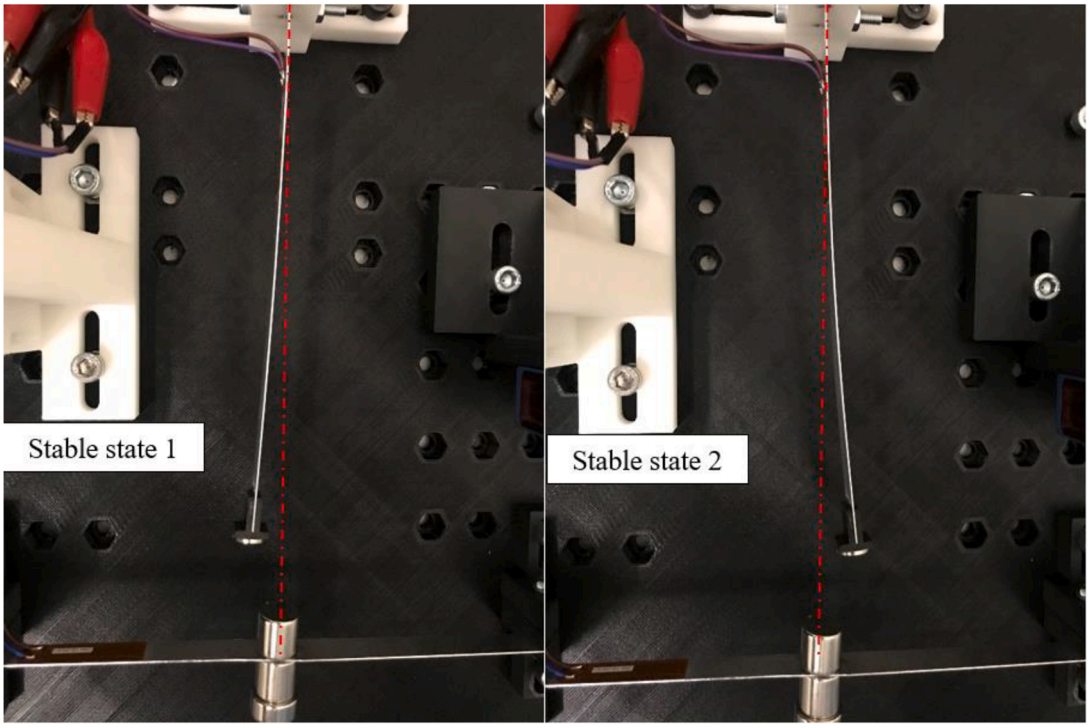

Fig. 3. a) Experimental setup; b) the two stable equilibrium positions of the parametrically excited beam.

(a)

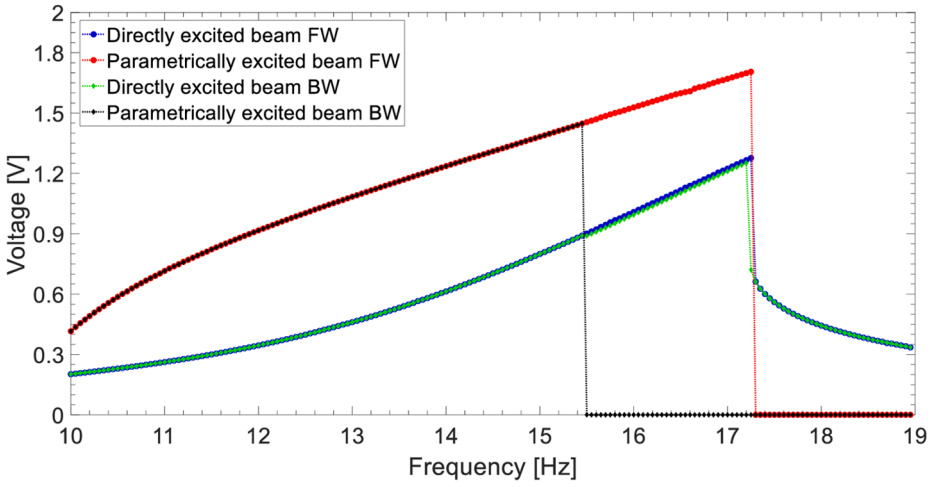

(b)

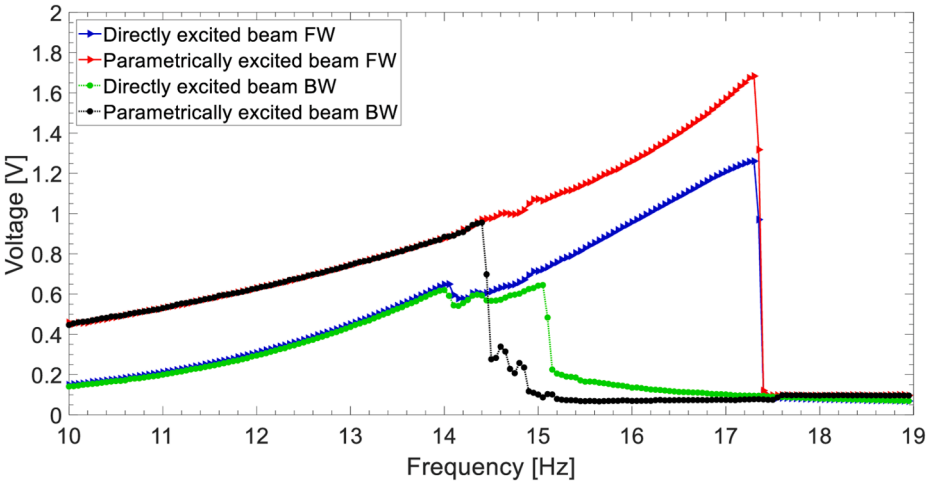

(c)

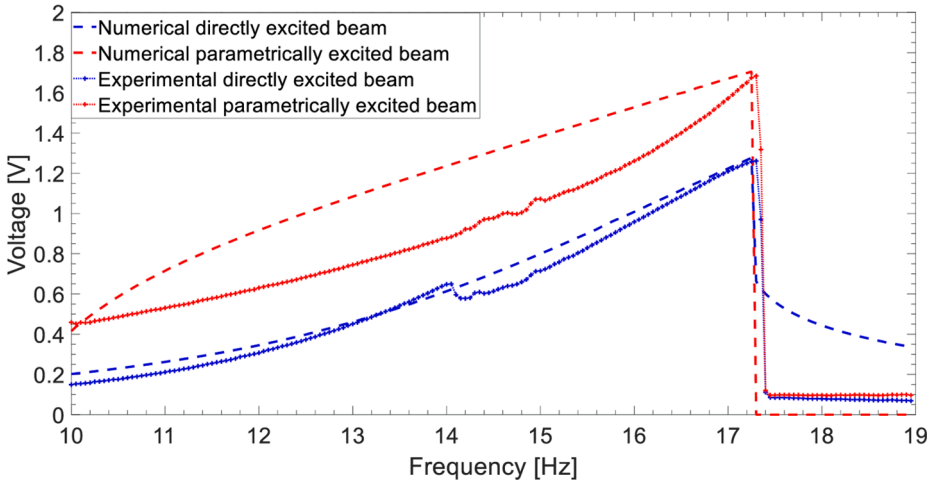

Fig. 4. The voltage-frequency plots of both forward and backward sweeps of the coupled system under a 0.5 g base excitation: a) theoretical results; b) experimental results; c) comparison between theoretical and experimental results.

system. For the second test, a smaller base excitation 0.36 g is adopted to expose the uncertain dynamic behaviours of the proposed system. The overall time trace for output voltage of the coupled system in the forward sweep case is shown in Fig. 5(a), Fig. 5(b) depicts the time trace of displacement of the parametrically excited beam in the forward sweep case. Based on the dynamic behaviours, the system motions are categorised into four regions: monostable I, bistable, chaotic and monostable II. For each region, the corresponding time trace, probability density function (PDF), voltage phase portrait, and the displacement phase portrait are plotted in Fig. 6(a)-(d), Fig. 7(a)-(d), Fig. 8(a)-(d) and Fig. 9(a)-(d), respectively.

Unlike the 0.5 g base excitation case, the parametrically excited beam was not able to cross the potential barrier with a 0.36 g base excitation that started at 10 Hz. An intrawell movement is observed in Fig. 5(b) and the displacement phase portrait in Fig. 6(d) indicates its motion in one potential well, which was around its one equilibrium attractor. Without the parametric resonance, the motion of the parametrically excited beam was almost consistent with the directly excited beam, which further proves the effects of the proposed magnetic coupling enhanced the motion, as well as the voltage level of parametrically excited devices in its off-resonance regime. With an increased excitation frequency, the parametric resonance was triggered at 740 s (11.85 Hz). A periodic interwell movement was formed and the voltage levels for both beams were increased significantly. In the presence of the parametric resonance, the motion of the parametrically excited beam no longer followed the directly excited beam synchronously. Fig. 7(a) shows the period of parametrically excited beam movement was doubled comparing to the directly excited beam. Fig. 7(c) reveals the effects of parametric resonance on direct excited beam, there are bifurcations near the peaks of directly excited beam. With the large oscillation, a clean high-energy periodic interwell motion is shown in Fig. 7(d). It is clear to see the average peak to peak displacement amplitude of the interwell motion shown in Fig. 5(b) is 11.7 times larger than the one in first monostable region (27 mm vs 2.3 mm), which implies the merit of a fully triggered bistable energy harvester; in terms of voltage level, a 730% increase is observed (0.73 V vs 0.1 V) by comparing the average peak to peak voltage of the bistable region and the first monostable region. In the bistable region, the potential barrier seems to be neutralised because of the externally induced oscillation from the directly excited beam through the magnetic coupling; the threshold amplitude for the parametric resonance has also been triggered; in most bistable or parametrically excited devices, a piezoelectric

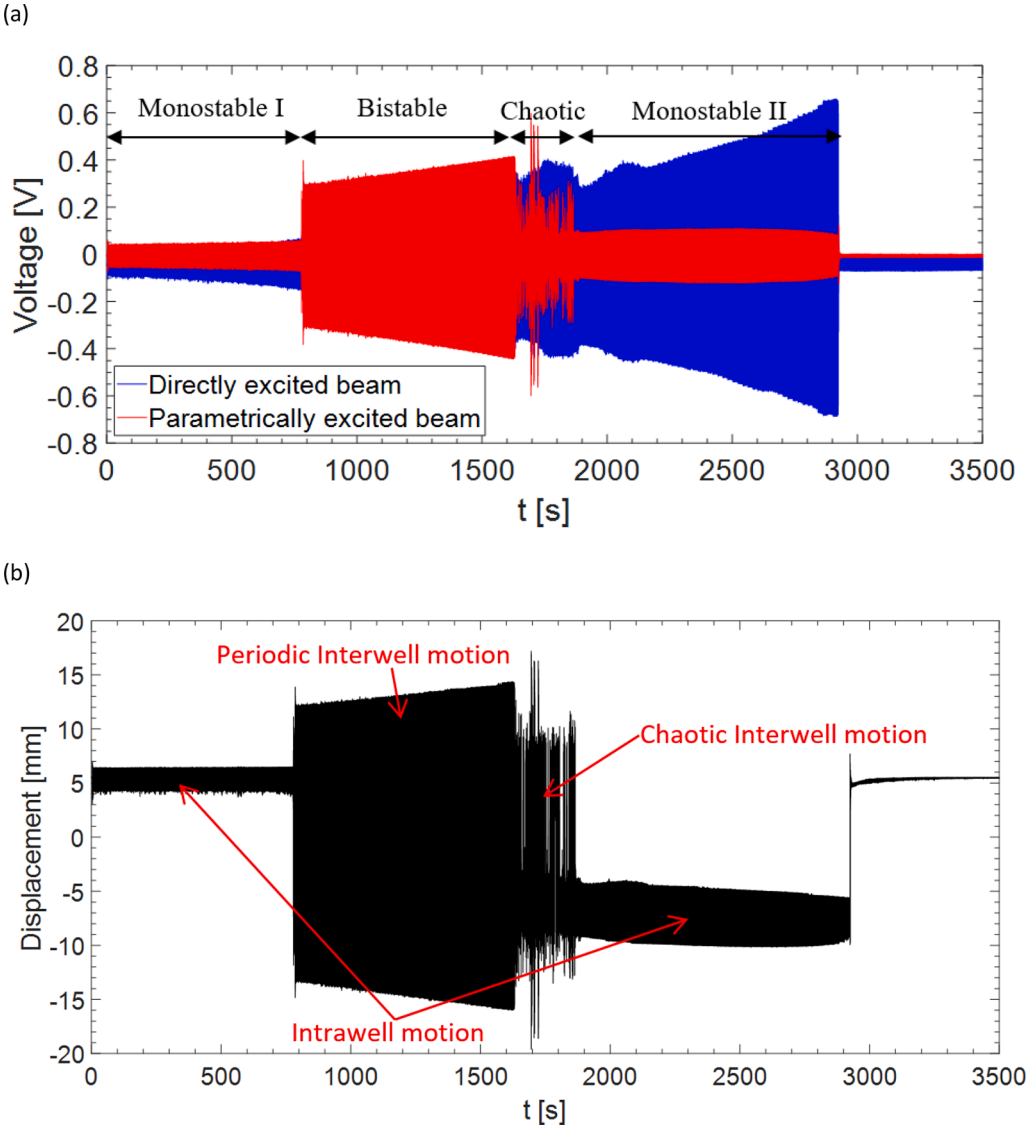

Fig. 5. Experimental time trace of the coupled system in forward sweep under a 0.36 g base excitation: a) the voltage-frequency plots of both the directly and parametrically excited beams; b) displacement-frequency plot of the parametrically excited beam.

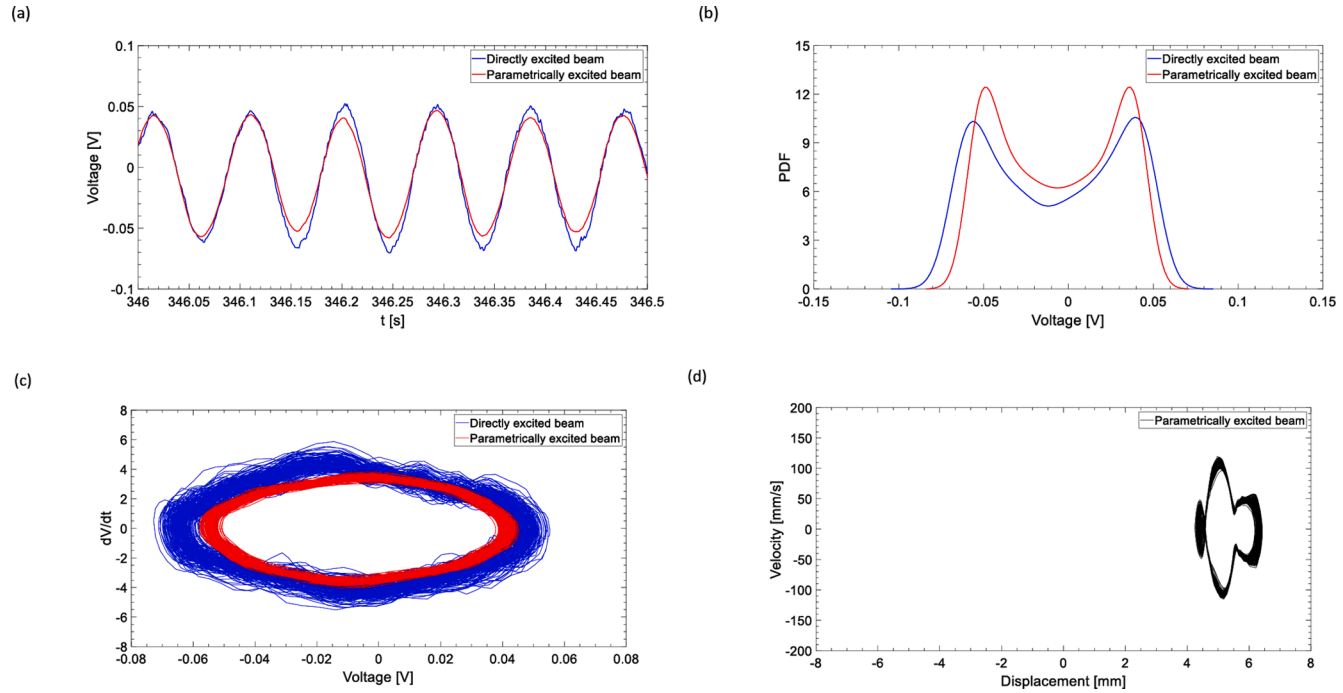

Fig. 6. Experimental results of the proposed system in monostable I region under a 0.36 g base excitation: a) time history at 10.85 Hz; b) probability density function (PDF); c) phase portrait of voltage; d) phase portrait of displacement.

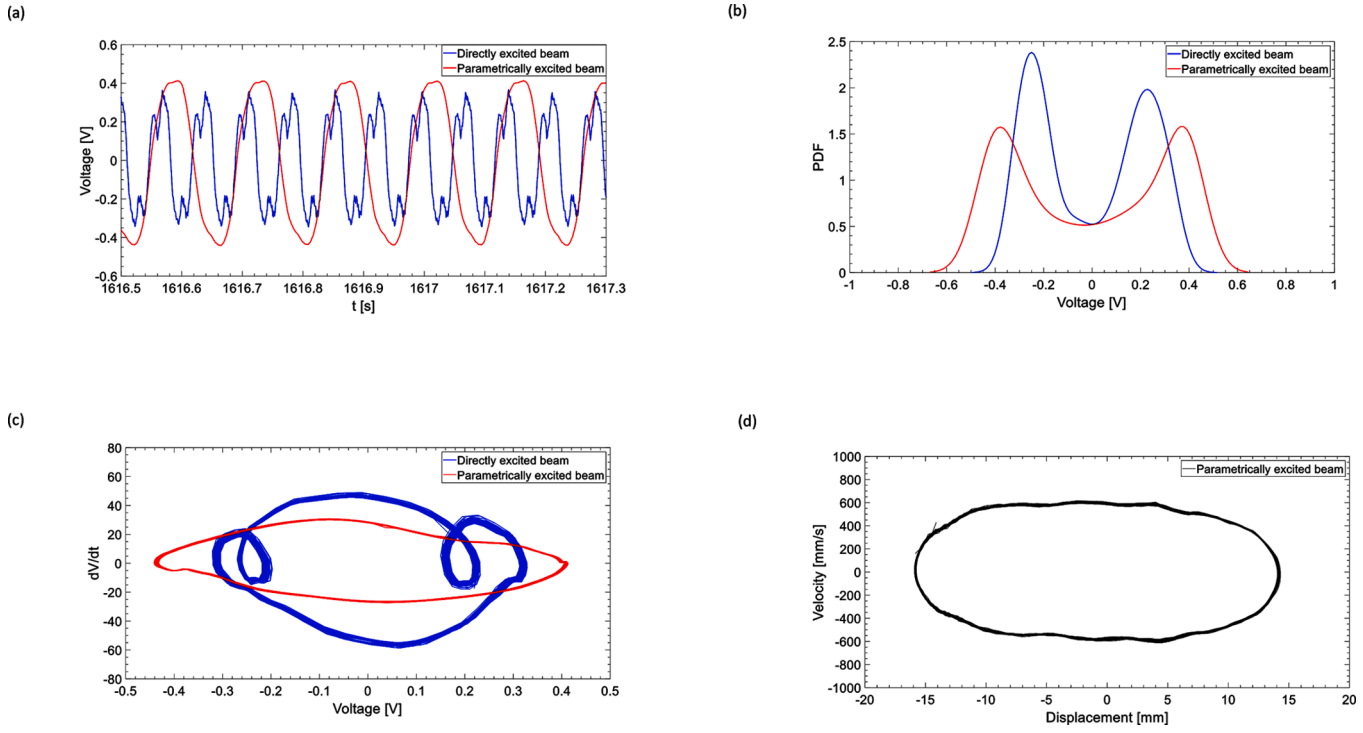

Fig. 7. Experimental results of the proposed system in bistable region under a 0.36 g base excitation: a) time history at 14.0 Hz; b) probability density function (PDF); c) phase portrait of voltage; d) phase portrait of displacement.

layer attached on cantilever beam requires a much larger excitation level to get triggered. The chaotic region shows that the parametrically excited beam exhibits both intrawell and interwell motions randomly when its parametric resonance gets closer to the upper limit (which mainly depends on the base excitation level), or receives insufficient oscillation support from the directly excited beam. The unpredictable motions can be found in Fig. 5(a), (b) and Fig. 8(a)-(d). The motions of the parametrically excited beam have random orbit jumps and brought uncertainties to the system; nevertheless, the two potential wells and the mixed motions of the parametrically excited beam can clearly be seen in Fig. 8(d). Similar to the first monostable region, the second monostable region occurs after the chaotic region, which implies the movement of the parametrically excited beam in this region is only driven by the rapid movement of the directly excited beam through magnetic coupling.

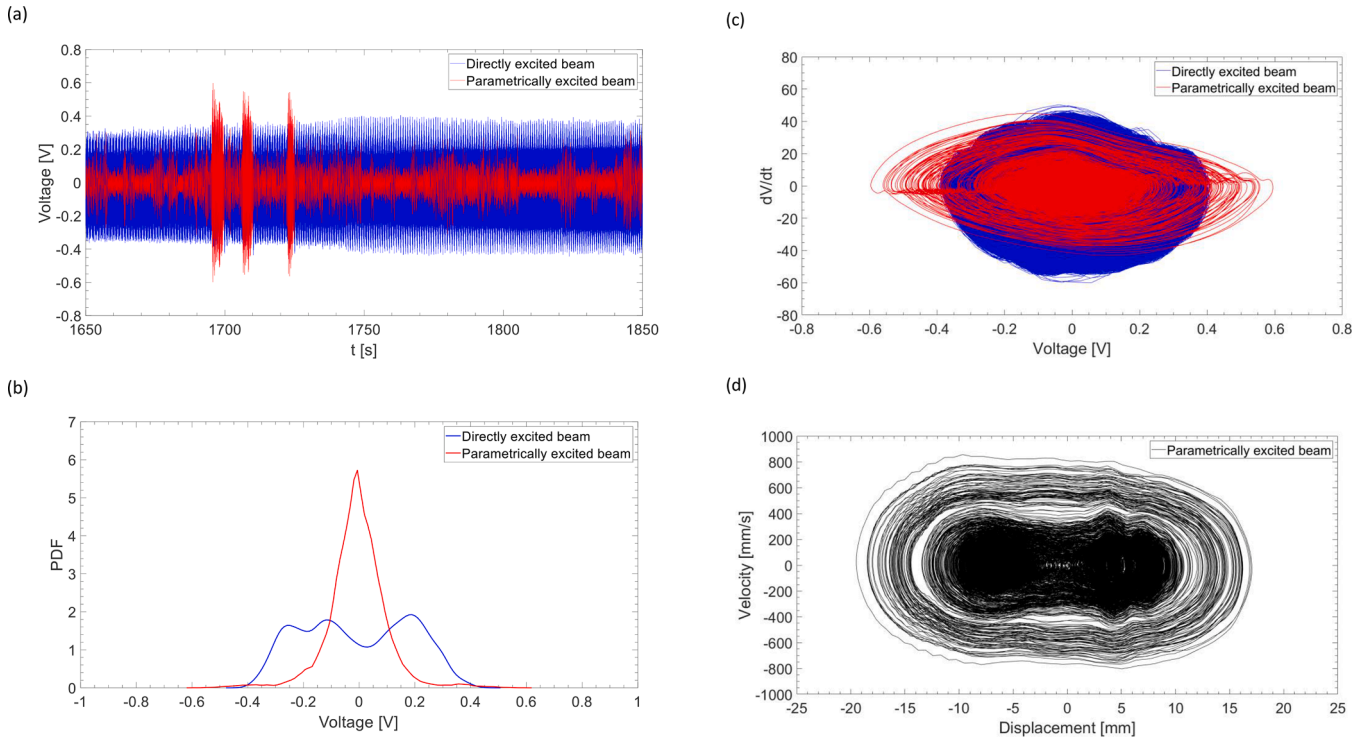

Fig. 8. Experimental results of the proposed system in chaotic region under a 0.36 g base excitation: a) time history of the chaotic region; b) probability density function (PDF); c) phase portrait of voltage; d) phase portrait of displacement.

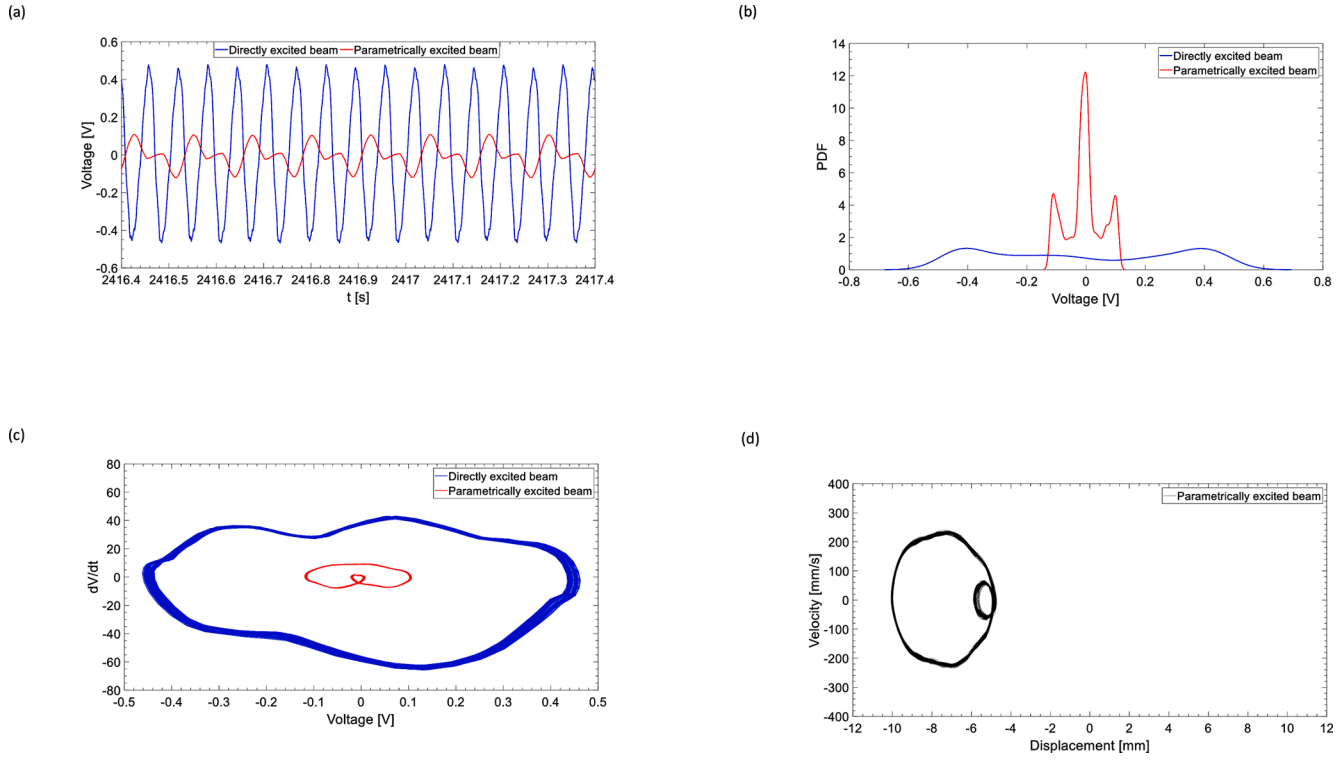

Fig. 9. Experimental results of the proposed system in monostable II region under a 0.36 g base excitation: a) time history at 16.0 Hz; b) probability density function (PDF); c) phase portrait of voltage; d) phase portrait of displacement.

Comparing between the two monostable regions, two equilibrium positions can be found in Fig. 5(b). The average displacement amplitude in the second monostable region is higher than the first region, which is due to the gradually rising peaks of the hardening frequency response from the directly excited beam. This external oscillation vibration source enhances the motions the parametrically excited element. Considering the dynamic behaviours of the second monostable region, in Fig. 9(a), the voltage level of directly excited beam was 0.93 V, which was 7.75

times greater than the level in the first monostable region (see Fig. 6(a)). Fig. 9(c) and (d) indicate the intrawell motion of parametrically excited device that exhibits irregular circular-like trajectories near the potential barrier wall. Owing to the strong magnetic interaction, a larger velocity amplitude has brought the parametrically excited beam closer to the upper boundary position of the potential barrier and has almost stimulated the interwell motion.

The effects of the base acceleration level substantially decide the effective bandwidth (or power level) of both multi-stable and parametrically excited systems. In order to illustrate the proposed device's performance under different excitation levels, as well as validating the accuracy of the theoretical model, three different base excitation levels (0.36 g, 0.5 g, 0.6 g) were employed for the parametric studies, including both forward and backward frequency sweeps. For the parametrically excited beam, the forward and backward theoretical results are plotted in Fig. 10(a) and (d), respectively. The forward and backward experimental results are also shown in Fig. 10(b) and (e), respectively. A comparison plot is shown in Fig. 10(c). Beyond the 0.36 g base excitation, the parametrically excited beam exhibits an effective frequency bandwidth for both theoretical and experimental results. Under a 0.6 g base excitation, the upper peak in the theoretical results occurs at 17.8 Hz, which has 0.55 Hz difference compared with the 0.5 g case. However, in the experimental results, the peaks and overall trend of these two cases are highly consistent with one another. In Fig. 10(b), even under a 0.36 g small base excitation, the interwell motion for the bistable region between 11.95 Hz and 14.05 Hz has a similar peak-to-peak amplitude for the 0.5 g or 0.6 g cases. It can be inferred from this phenomenon, with the proposed magnetic coupling, that the bandwidth/voltage level of the parametrically excited beam does not primarily depend on the base excitation level except that the threshold amplitude of the parametric resonance has yet to be triggered. In comparison to the parametrically excited beam frequency response curves under different excitation levels, Fig. 11(a)-(e) show the theoretical and experimental voltage-frequency results of the directly excited beam. Theoretically, a clamped–clamped formed beam induces more nonlinearities into the system, and an increased base excitation level delivers a stronger hardening response even with the effects of the parametrically excited beam movement through magnetic coupling as shown in Fig. 11(a). The experimental results of the directly excited beam in Fig. 11(b) showing slight differences across three base excitation cases, and the hardening trend from the frequency response curve can be observed. The effects of parametric resonance on the directly

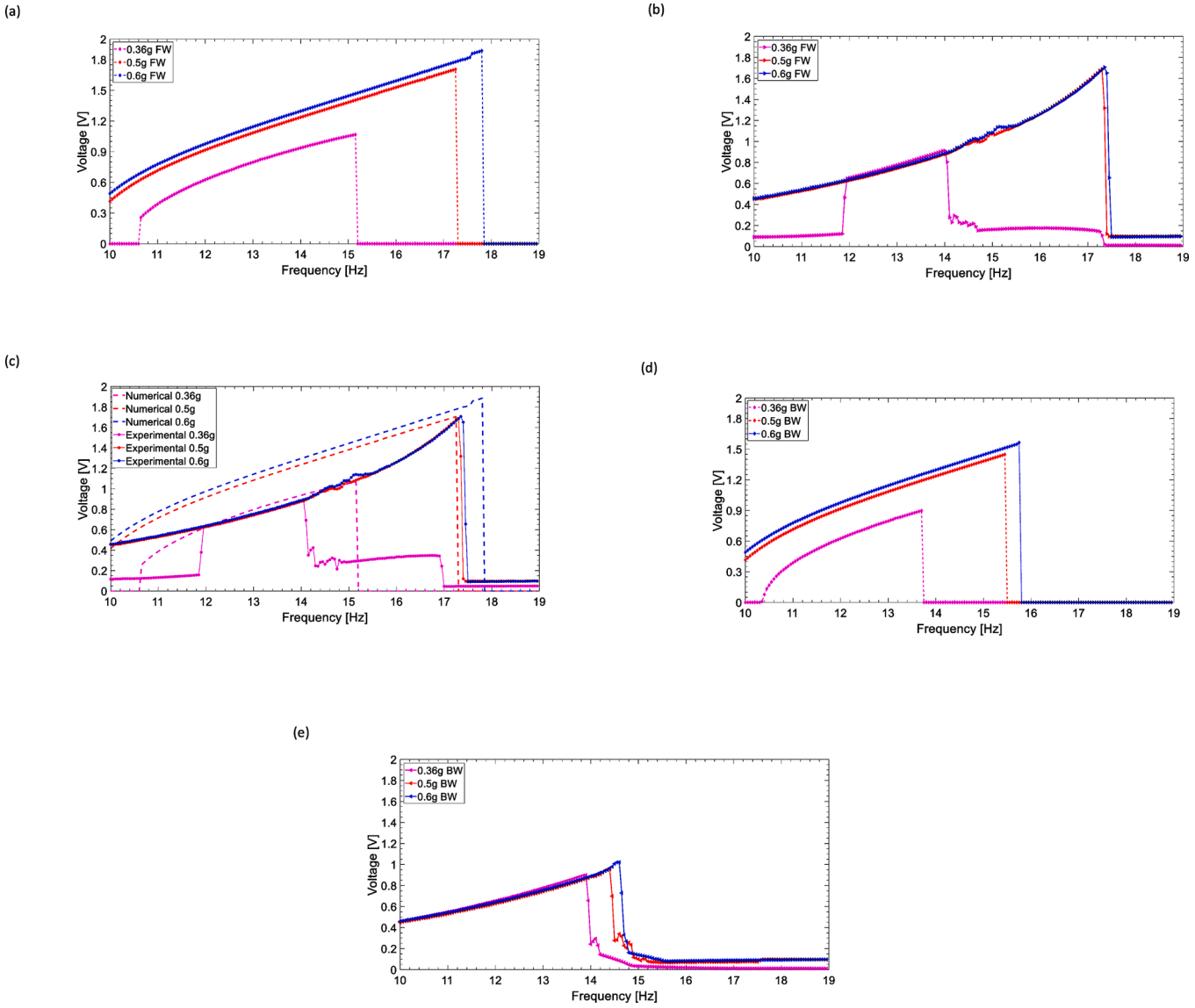

Fig. 10. The voltage-frequency plots of the parametrically excited beam under different base excitation levels. Theoretical results: a) forward sweep; d) backward sweep; experimental results: b) forward sweep; e) backward sweep; c) comparison between theoretical and experimental results.

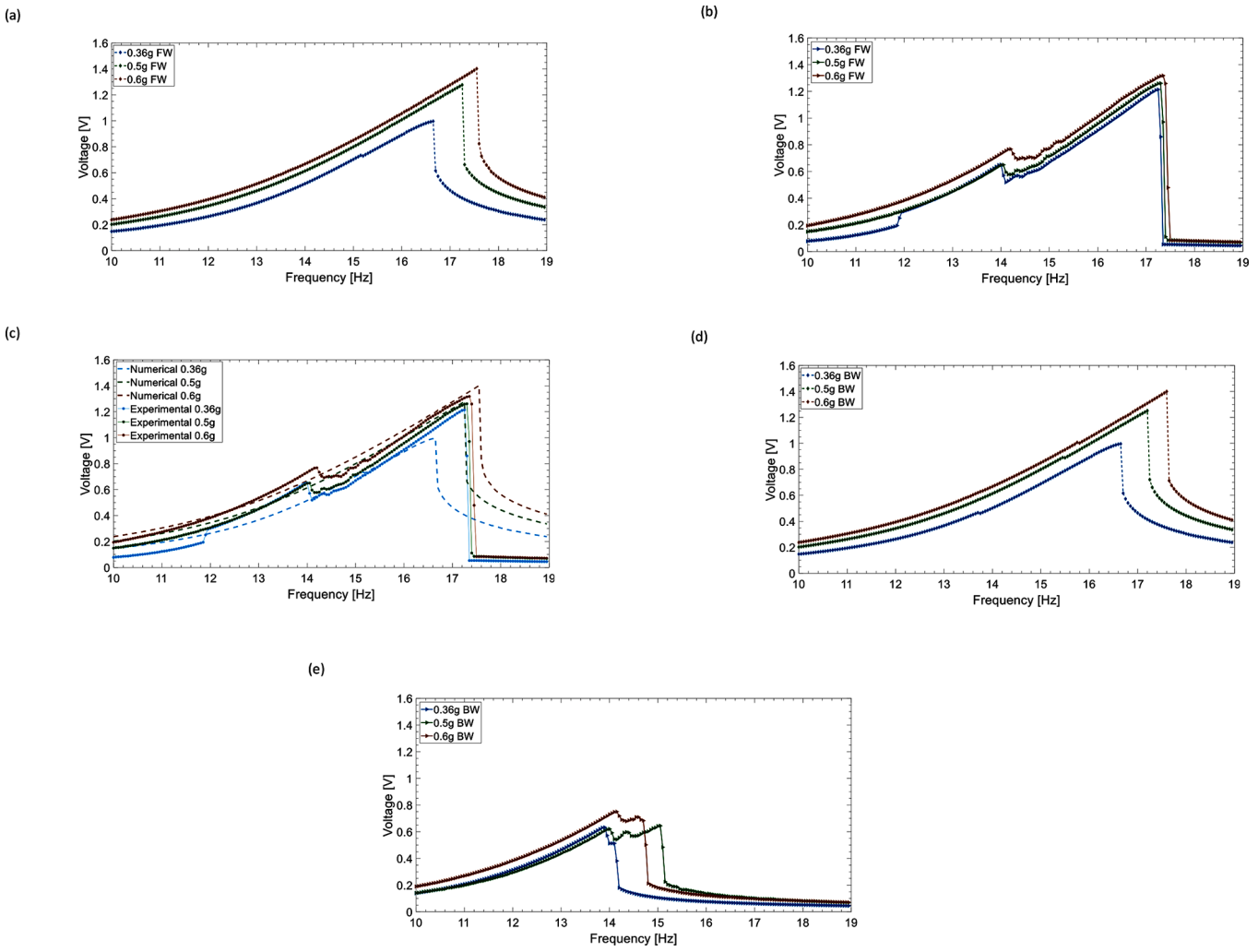

Fig. 11. The voltage-frequency plots of the directly excited beam under different base excitation levels. Theoretical results: a) forward sweep; d) backward sweep; experimental results: b) forward sweep; e) backward sweep; c) comparison between theoretical and experimental results.

excited beam are shown in Fig. 11(b) and (e), which indicate the effects of parametric resonance through magnetic coupling on the directly excited beams are positive proportional in terms of peak amplitude.

Under a smaller excitation level, the parametrically excited beam is prone to settle in one potential well due to insufficient energy to move across the potential barrier; as the magnetically coupling effects not only serve as an additional source of vibration, but it is also a vital factor of achieving bistability. Thus, the analyses of gap distance between the tip and mid magnets are conducted. Fig. 12(a) and (b) display the theoretical frequency response results for different gap distances d between the two magnets for the parametrically excited beam and directly excited beam, respectively. As seen in Fig. 12(a), the gap distance determines the initial amplitude of the parametrically excited beam. The equilibrium stable position is further from the origin with smaller d; the peaks have considerable increases in amplitude but their positions in the frequency domain are maintained at almost the same location. Fig. 12(b) indicates the magnetic coupling on the directly excited beam has relatively lower impacts compared with the parametrically excited beam. This is in agreement with the theoretical expression of magnetic coupling, the magnetic moment vectors of dipole B in the y direction are omitted as it is a centre magnet on a clamped–clamped beam.

5. Conclusion

This paper presents theoretical and experimental investigations to analyse the dynamic responses of a designed two-element parametrically excited bistable energy harvester for broadening operational frequency bandwidth, as well as reducing the potential barrier and initial threshold amplitude that are required for bistability and parametric resonance characteristics, respectively. The device consists of two core elements, a parametrically excited clamped-free beam and a directly excited clamped–clamped beam. In the presence of the magnetic coupling between the tip magnet (on the parametric beam) and the mid magnet (on the direct beam), both the beams exhibit strong hardening frequency responses that form a wide resonance regime from 10 Hz to 17.3 Hz, which is a substantial increase when compared with a single parametrically excited case – its parametric resonance cannot be triggered unless a much higher base acceleration is adopted.

In order to examine the bistability feature of the proposed device, different base excitation levels are adopted. The experimental results illustrate that 0.36 g is the critical base excitation level of the proposed device, as its time trace shows all types of motion including monostable, bistable and chaotic motions. For any smaller excitation level, a proper piezoelectric layer is suggested to adjust the system damping characteristics. The bistable region in Fig. 5(a) and (b) illustrates that even under a small base acceleration level, the periodic large interwell motion of the parametrically excited beam can be observed, which infers the merits of the proposed system – the proposed design enables periodic interwell motion, as well as triggers the parametric resonance threshold amplitude through the magnetic coupling effects. The monostable

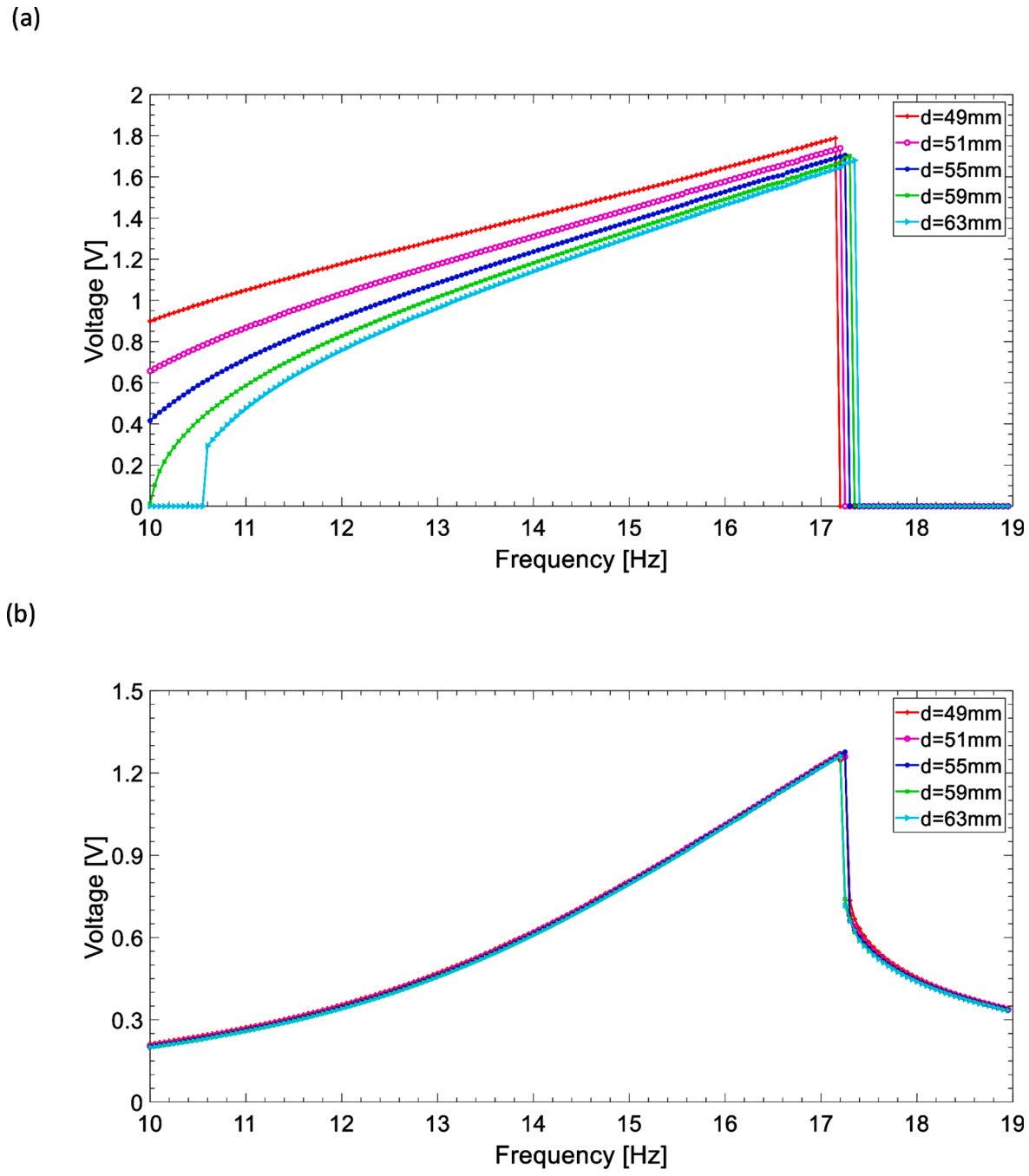

Fig. 12. Theoretical results of the coupled system with different gap distances between the two magnets under a 0.5 g base excitation: a) the parametrically excited beam; b) the directly excited beam.

motion implies the off-resonance regime of the parametrically excited beam exhibits a non-zero amplitude-frequency response. The periodic intrawell motion enhances the displacement as well as the harvested voltage levels at its off-resonance regime. With the magnetic coupling effects, the output voltage level of the directly excitation beam has also been enhanced. The directly excited beam acts as an energy-harvesting element, as well as an external vibration source that aims to lower the potential barrier and threshold amplitude of the parametrically excited bistable element. Future work could also focus on optimising the designs of the directly excited beam (e.g., obtaining a larger mid-point deflection design or utilising hybrid transducers as magnet-coil structures) in order to achieve lower-excitation levels as well as high-power applications. The theoretical model is presented to predict the dynamics of the proposed device, showing good agreement with the experimental results. The effects of the base excitation level and magnet gap distance were also measured in the parametric studies. Of keen interest to parametrically excited and bistable energy harvesting devices, the proposed device provides a new broadband technique for nonlinear energy harvesting applications under low excitation levels.

CRediT authorship contribution statement

Yimin Fan: Conceptualization, Investigation, Methodology, Validation, Writing - original draft, Software. **Mergen H. Ghayesh:** Conceptualization, Investigation, Methodology, Supervision, Writing - review & editing. **Tien-Fu Lu:** Conceptualization, Investigation, Supervision, Writing - review & editing.

Declaration of Competing Interest

The authors declare that they have no known competing financial interests or personal relationships that could have appeared to influence the work reported in this paper.

Acknowledgement

This work has been supported by the Australian Government Research Training Program. The support is greatly appreciated.

References

[1] Mann BP, Sims ND. Energy harvesting from the nonlinear oscillations of magnetic levitation. J Sound Vib 2009;319:515–30.
[2] Cottone F, Vocca H, Gammaitoni L. Nonlinear energy harvesting. Phys Rev Lett 2009;102:080601.
[3] Tang L, Yang Y, Soh CK. Toward broadband vibration-based energy harvesting. J Intell Mater Syst Struct 2010;21(18):1867–97.
[4] Zou H-X, Zhang W-M, Li W-B, Wei K-X, Gao Q-H, Peng Z-K, et al. Design and experimental investigation of a magnetically coupled vibration energy harvester using two inverted piezoelectric cantilever beams for rotational motion. Energy Convers Manage 2017;148:1391–8.
[5] Fang S, Fu X, Liao W-H. Asymmetric plucking bistable energy harvester: Modeling and experimental validation. J Sound Vib 2019;459:114852. https://doi.org/10.1016/j.jsv.2019.114852.
[6] Wang J, Liao W-H. Attaining the high-energy orbit of nonlinear energy harvesters by load perturbation. Energy Convers Manage 2019;192:30–6.
[7] Pan D, Dai F. Design and analysis of a broadband vibratory energy harvester using bi-stable piezoelectric composite laminate. Energy Convers Manage 2018;169:149–60.
[8] Qian F, Hajj MR, Zuo L. Bio-inspired bi-stable piezoelectric harvester for broadband vibration energy harvesting. Energy Convers Manage 2020;222:113174.
[9] Chillara VSC, Ramanathan AK, Dapino MJ. Self-sensing piezoelectric bistable laminates for morphing structures. Smart Mater Struct 2020;29:085008.
[10] Panyam M, Daqaq MF. Characterizing the effective bandwidth of tri-stable energy harvesters. J Sound Vib 2017;386:336–58.
[11] Zhou S, Zuo L. Nonlinear dynamic analysis of asymmetric tristable energy harvesters for enhanced energy harvesting. Commun Nonlinear Sci Numer Simul 2018;61:271–84.
[12] Zhang Y, Jin Y, Xu P, Xiao S. Stochastic bifurcations in a nonlinear tri-stable energy harvester under colored noise. Nonlinear Dyn 2020;99:879–97.
[13] Zhou Z, Qin W, Zhu P. A broadband quad-stable energy harvester and its advantages over bi-stable harvester: Simulation and experiment verification. Mech Syst Sig Process 2017;84:158–68.
[14] Gao M, Wang Y, Wang Y, Yao Y, Wang P, Sun Y, et al. Modeling and experimental verification of a fractional damping quad-stable energy harvesting system for use in wireless sensor networks. Energy 2020;190:116301.
[15] Cao J, Wang W, Zhou S, Inman DJ, Lin J. Nonlinear time-varying potential bistable energy harvesting from human motion. Appl Phys Lett 2015;107:143904.
[16] Qian F, Xu T-B, Zuo L. Design, optimization, modeling and testing of a piezoelectric footwear energy harvester. Energy Convers Manage 2018;171:1352–64.
[17] Izadgoshasb I, Lim YY, Tang L, Padilla RV, Tang ZS, Sedighi M. Improving efficiency of piezoelectric based energy harvesting from human motions using double pendulum system. Energy Convers Manage 2019;184:559–70.
[18] Lan C, Qin W. Enhancing ability of harvesting energy from random vibration by decreasing the potential barrier of bistable harvester. Mech Syst Sig Process 2017;85:71–81.
[19] Leng Y, Tan D, Liu J, Zhang Y, Fan S. Magnetic force analysis and performance of a tri-stable piezoelectric energy harvester under random excitation. J Sound Vib 2017;406:146–60.
[20] Li H, Liu D, Wang J, Shang X, Hajj MR. Broadband bimorph piezoelectric energy harvesting by exploiting bending-torsion of L-shaped structure. Energy Convers Manage 2020;206:112503.
[21] Xie X, Wang Z, Liu D, Du G, Zhang J. An experimental study on a novel cylinder harvester made of L-shaped piezoelectric coupled beams with a high efficiency. Energy 2020;212:118752.
[22] Tian W, Shi Y, Cui H, Shi J. Research on piezoelectric energy harvester based on coupled oscillator model for vehicle vibration utilizing a L-shaped cantilever beam. Smart Mater Struct 2020;29:075014.
[23] Yu N, Ma H, Wu C, Yu G, Yan B. Modeling and experimental investigation of a novel bistable two-degree-of-freedom electromagnetic energy harvester. Mech Syst Sig Process 2021;156:107608.
[24] Wang H, Tang L. Modeling and experiment of bistable two-degree-of-freedom energy harvester with magnetic coupling. Mech Syst Sig Process 2017;86:29–39.
[25] Mann BP, Owens BA. Investigations of a nonlinear energy harvester with a bistable potential well. J Sound Vib 2010;329:1215–26.
[26] Wang G-Q, Liao W-H. A bistable piezoelectric oscillator with an elastic magnifier for energy harvesting enhancement. J Intell Mater Syst Struct 2017;28:392–407.
[27] Cao J, Zhou S, Wang W, Lin J. Influence of potential well depth on nonlinear tristable energy harvesting. Appl Phys Lett 2015;106:173903.
[28] Chiacchiari S, Romeo F, McFarland DM, Bergman LA, Vakakis AF. Vibration energy harvesting from impulsive excitations via a bistable nonlinear attachment. Int J Non Linear Mech 2017;94:84–97.
[29] Daqaq MF, Stabler C, Qaroush Y, Seuaciuc-Osório T. Investigation of Power Harvesting via Parametric Excitations. J Intell Mater Syst Struct 2009;20:545–57.
[30] Jia Y, Yan J, Soga K, Seshia AA. Parametric resonance for vibration energy harvesting with design techniques to passively reduce the initiation threshold amplitude. Smart Mater Struct 2014;23:065011.
[31] Panyam M, Daqaq MF, Emam SA. Exploiting the subharmonic parametric resonances of a buckled beam for vibratory energy harvesting. Meccanica 2018;53:3545–64.
[32] Garg A, Dwivedy SK. Nonlinear dynamics of parametrically excited piezoelectric energy harvester with 1:3 internal resonance. Int J Non Linear Mech 2019;111:82–94.
[33] Fan Y, Ghayesh MH, Lu T-F. Enhanced nonlinear energy harvesting using combined primary and parametric resonances: experiments with theoretical verifications. Energy Convers Manage 2020;221:113061. https://doi.org/10.1016/j.enconman.2020.113061.
[34] Lajimi SAM, Friswell MI. Dynamics of a non-linearly damped microresonator under parametric excitation and its application in developing sensitive inertial sensors with ultra-wide dynamic ranges. Int J Non Linear Mech 2020;123:103491.
[35] Garg A, Dwivedy SK. Piezoelectric energy harvester under parametric excitation: A theoretical and experimental investigation. J Intell Mater Syst Struct 2020;31(4):612–31.
[36] Bobryk RV, Yurchenko D. On enhancement of vibration-based energy harvesting by a random parametric excitation. J Sound Vib 2016;366:407–17.
[37] Tan D, Leng YG, Gao YJ. Magnetic force of piezoelectric cantilever energy harvesters with external magnetic field. Eur Phys J Special Top 2015;224:2839–53.

Chapter 6

High-Efficient Internal Resonance Energy Harvesting

This chapter is based on the following submitted paper (under review, April 2022):

Fan, Y., M.H. Ghayesh, and T.-F. Lu, *High-efficient internal resonance energy harvesting: Modelling and experimental study*. Submitted to: Mechanical Systems and Signal processing.

Statement of Authorship

Title of Paper	High-efficient internal resonance energy harvesting Modelling and experimental study
Publication Status	☐ Published ☐ Accepted for Publication ☑ Submitted for Publication ☐ Unpublished and Unsubmitted w ork w ritten in manuscript style
Publication Details	

Principal Author

Name of Principal Author (Candidate)	Mr. Yimin Fan
Contribution to the Paper	Conceptualization, Investigation, Methodology, Validation, Writing - original draft, Software
Overall percentage (%)	80%
Certification:	This paper reports on original research I conducted during the period of my Higher Degree by Research candidature and is not subject to any obligations or contractual agreements with a third party that would constrain its inclusion in this thesis. I am the primary author of this paper.
Signature	Date 27/01/2022

Co-Author Contributions

By signing the Statement of Authorship, each author certifies that:

i. the candidate's stated contribution to the publication is accurate (as detailed above);

ii. permission is granted for the candidate in include the publication in the thesis; and

iii. the sum of all co-author contributions is equal to 100% less the candidate's stated contribution.

Name of Co-Author	Dr. Mergen H. Ghayesh
Contribution to the Paper	Conceptualization, Investigation, Methodology, Supervision, Writing - review & editing
Signature	te 01/02/2022

Name of Co-Author	Dr. [illegible]
Contribution to the Paper	Conceptualization, Investigation, Methodology, Supervision, Writing - review & editing
Signature	Date 1/02/2022

High-efficient internal resonance energy harvesting: Modelling and experimental study

Yimin Fan*, Mergen H. Ghayesh, Tien-Fu Lu

School of Mechanical Engineering, University of Adelaide, South Australia, 5005, Australia

*Corresponding Author: yimin.fan@adelaide.edu.au

Abstract

This research investigates a U-shaped vibration-based energy harvester with broadband and bi-directional features via an internal resonance. The proposed U-shaped structure has been tailored in a way that displays a two-to-one internal resonance between the selected transverse modes. The resonant modes and mode shapes of the proposed device have been designed and validated through an analytical method, the finite-element simulations as well as experimental tests, showing good agreement. The experimental tests imply the benefits of energy transfer between two modes, as resonance phenomena in all segments have been successfully triggered to obtain large-amplitude oscillations for high-efficient energy conversion via piezoelectric effects. Under harmonic excitations, different from conventional multi-mode vibration energy harvesters, the proposed device presented broadened resonance regions for both modes, and exhibited equally effective bandwidths under forward/backward sweeps. Moreover, the device is capable of being excited in two orthogonal directions as a bi-directional energy harvester. Parametric studies on the acceleration levels are also presented to evaluate the system performance and reveal the critical excitation level for triggering the internal resonance. It has been found that even under a 0.1 g acceleration level, the internal resonance phenomenon can still be observed between the first and second modes, which implies the feasibility of the proposed device even for ambient vibration sources with low energies.

Highlights

- The proposed device consists of bi-directional, multi-mode and internal resonance features.
- Theoretical investigations are presented to predict the resonant modes and mode shapes.
- Experimental results depict a two-to-one internal resonance between the first and second transverse modes.
- High-efficient and broadband operations are achieved at both the first and second transverse modes.

1. Introduction

The designed size of wireless electronic devices is foreseeably more compact with the developments of integrated circuits. With limited battery sizes and capacities, the functionality of devices primarily depends on the power supply. A device that utilises energy conversion between environmental vibration sources and electric power offers an alternative perspective on how to achieve clean and sustainable energy scavenging, is known as an energy harvester. Various types of vibration sources such as ocean waves, streams and wind are capable of achieving efficient energy harvesting. For wearable electronic devices, as well as remote monitoring devices, mechanical vibration is seen to be the most promising vibration source in a low ambient frequency range.

In recent research, to settle the narrow operational bandwidth issue in linear energy harvesting techniques (i.e., to utilise a single-mode and tuning approach), broadband techniques are one of the most promising approaches that are capable of obtaining a specific range of natural vibration sources for efficient energy harvesting purpose. In early applications, the general investigations into linear energy harvesters focused on fundamental resonant modes that could only adapt ambient vibration sources in limited working ranges. Later, adjacent resonant modes, which may have the potential to broaden the operational frequency bandwidth, were considered. Multi-degree-of-freedom (MDOF) and multi-mode energy harvesting techniques utilise multiple resonant modes to improve the system of energy harvesting efficiency, and have therefore been introduced by various

researchers. Common approaches utilise cantilever beam-based structures with main and secondary elements through cut out methods [1-3]. For instance, Li et al. [3] proposed a multi-mode energy harvester consisting of a main beam and three sub-beams placed at its tip. By attaching selected tip masses on the main and sub-structures, three resonant modes were close enough to narrow the off-resonance regimes between each other; the energy harvesting efficiency was therefore improved. In recent studies, Dhote et al. [4] proposed multi-mode energy harvesters with an orthoplanar spring structure. A broad bandwidth was achieved by the proposed structure, as the designed sub-structures enabled multiple close peaks. By dealing with most of the environmental vibration sources, which are naturally multi-directional, on the basis of multi-mode energy harvesters, their feasibility for adding multi-directional features have also been studied [5-8]. Zhou et al. [5] studied a piezoelectric energy harvester with a zigzag structure, which was capable of outputting energy under different excitation directions. Yang et al. [8] combined multi-directional and multi-stable features on a spring-mass-based structure as a low operation frequency energy harvester.

Considering an MDOF system with its resonant modes that are commensurable or nearly commensurable (e.g., $2\omega_1 \cong \omega_2; 3\omega_1 \cong \omega_3;\ \omega_1 + \omega_2 \cong \omega_3$), internal resonance phenomena could be revealed [9, 10]. When an internal resonance is presented, a common frequency response gets distorted and becomes complex to satisfy the energy transfer conditions. Compared with its linear counterpart, the energy transfer between the resonant modes enables nonlinear regimes in the system, which has the potential to broaden the frequency bandwidth as a broadband technique. As internal resonance can only be triggered with two or more resonant modes, to obtain the internal resonance phenomenon, it is essential to tune the resonant modes to be commensurable. To obtain energy harvesting that utilises internal resonances, L-shaped beam structures have been exploited comprehensively by researchers [11-14]. With the designed system parameters, by adding the side and end masses, as well as altering the two beam lengths, two-to-one or three-to-one internal resonances (or in general any higher mode internal resonances) can be obtained. Nie et al. [13] investigated an L-shaped piezoelectric energy harvester. By altering the side and end masses, a two-to-one internal resonance was obtained, which enhances the energy and bandwidth performance. A theoretical distributed-parameter model and the finite element method (FEM) were conducted to verify the experimental results.

Magnetic coupling is another approach to achieve resonant modes tuning, as well as inducing more nonlinearities into the system. Combining internal resonance and magnetic coupling characteristics, researchers such as Chen et al. [15] studied an L-shaped energy harvester with magnetic coupling between a stationary magnet and a magnet at the tip of the side beam. Xiong et al. [16] experimentally investigated a magnetically coupled L-shaped energy harvester with an auxiliary oscillator. Yang and Towfighian [17] proposed a dual beam energy harvester consist of one vertical and one horizontal beam, both attached with tip magnets and interacted with each other so as to achieve an internal resonance. Under a certain base excitation, the internal resonance phenomenon can be revealed by altering the distances between the magnets. Other investigations of dual-beam structures with magnetic coupling effects can also be found in [18-20]. To induce more external nonlinearities, axially loaded approaches have been investigated to obtain monostable or bistable features [21-23]. Several recent investigations have provided theoretical and analytical perspectives of energy harvesters based on internal resonance, such as a 2-DOF bistable device [24], a clamped-free piezoelectric cantilever with lumped mass [25], and gravity effects on internal resonance [26]. Apart from conventional bending modes, torsion modes can also provide high power levels for energy harvesting purpose, such as a zigzag structure [27] or L-shaped structure utilised both bending and torsion modes [28].

Based on the aforementioned literature, this paper investigates a U-shaped energy harvester with some critical features to enhance the bandwidth and power level performance. In spite of existing research studies on U-shaped energy harvesters such as [29-31], investigations into the modal coupling effects and internal resonance phenomenon remain unfulfilled. Although Rocha et al. [32] have investigated a portal frame based (or U-shaped) energy harvester with one piezoelectric element analytically via the multi-scale method, to author's best knowledge, experimental validations and explanations of the rich dynamics involving internal resonances are not yet available.

Recently, Fan et al. [33] examined a low operational frequency multi-directional vibration energy harvester with combined primary and parametric resonances by utilising motion limiters. They then designed an energy harvesting array by considering double-type motion limiters when subjected to direct and parametric excitations [34]. With externally induced magnetic coupling effects, they proposed a parametrically excited energy harvester to achieve bistable and wideband features [35].

In this paper, we consider the two-to-one internal resonance in a bi-directional U-shaped piezoelectric energy harvester. In Section 2, to predict the natural modes of the U-shaped structure, an analytical model is analysed to investigate the mode shapes of the device, and to validate the findings using finite-element methods (FEM). Experimental tests and a FEM model with piezoelectric effects have been conducted to tune and optimise the modal coupling between two selected resonant modes, thereby introducing a two-to-one internal resonance. In Section 3, the experimental results of the proposed device under harmonic excitations are discussed to justify its performance in terms of bandwidth and voltage level. Effects of base acceleration levels are also studied experimentally as a parametric study. Section 4 concludes the main findings of this study and provides the directions for future study.

2. Design and modelling for internal resonance

In order to obtain an internal resonance, two or more resonant modes should be commensurable or nearly commensurable. Thus, locating and predicting the natural frequencies of the proposed device will be tested and validated preliminarily. A U-shaped cantilever beam-based structure is utilised as the core vibrating element (as shown in Fig. 1). The device consists of three beams, including two identical side beams and one mid beam with a small mid mass located at its centre position for resonance tuning purposes. Each beam attaches with a micro fibre composite as the transducer.

With the aim of achieving an ambient multi-directional and internal resonance based energy harvesting technique, we focus on the analysis of its first and second resonant modes to find out about the system characteristics associated with the targeted internal resonance. For the reference and preliminary simulation via FEM, as shown in Fig. 2, the base excitation direction is perpendicular and parallel to the length of the mid beam for the first and second modes to obtain peak amplitude, respectively. For energy harvesting devices that utilise internal resonance phenomena, because the phenomena can only be achieved if the selected modes are highly commensurable, an accurate frequency ratio needs to be obtained theoretically between the selected modes for prediction before design and manufacture for lab-use or industrial purposes. Therefore, an analytical model based on Euler-Bernoulli beam theory is given in this section to predict the mode shapes of such device and FEM method is used to compare with the analytical results. To derive

the mode shapes of the proposed device, the effects of the piezoelectric layers are neglected; the corner between each segment is assumed to be 90 degrees; all segments have similar width and thickness. As shown in Fig. 1 (b), all segments (i.e., $i = 1, 2, 3, 4$) are assumed to be uniform, and the axial motions of such slender structures can be neglected; hence, we are only interested in transverse $v_i(s_i, t)$ components for this structure. The small mid mass m_t located at the centre position of the mid beam for frequency tuning purposes is assumed to be a point mass and the rotatory inertia effects are neglected. Based on the Euler-Bernoulli beam theory, the equation of motion for transverse direction can be written as

$$E_b I_b \frac{\partial^4 v_i(s_i, t)}{\partial s_i^4} + \rho_b A_b \frac{\partial^2 v_i(s_i, t)}{\partial t^2} = 0, \qquad 0 < s_i < L_i \tag{1}$$

where ρ_b, E_b, A_b and I_b are the density, elastic modulus, area of cross section and area moment of the cross section of the substrate, respectively. By using the separable solution $v_i(s_i, t) = W_i(s_i)e^{j\omega t}$, Eqns. (1) can be expressed as [36]:

$$W_i''''(s_i) - \beta_i{}^4 W_i(s_i) = 0 \tag{2}$$

where

$$\beta_i = \sqrt[4]{\frac{\rho_b A_b \omega_r{}^2}{E_b I_b}}$$

ω_r is the natural frequency of *r*-th vibration mode. The general mode shape function of the transverse motions for each segment can be expressed as [37, 38]

$$W_i(S_i) = a_i \sin(\beta_i S_i) + b_i \cos(\beta_i S_i) + c_i \sinh(\beta_i S_i) + d_i \cosh(\beta_i S_i) \tag{3}$$

where the coefficients a_i, b_i, c_i, d_i can be determined by the system boundary conditions. The boundary conditions based on assumptions and following [36, 39], can be expressed as

$$v_1(0, t) = 0 \tag{4.1}$$

$$v_1'(0, t) = 0 \tag{4.2}$$

$$v_4(L_4, t) = 0 \tag{4.3}$$

$$v_4'(L_4, t) = 0 \tag{4.4}$$

$$v_2(0,t) = 0 \tag{4.5}$$

$$v_1'(L_1,t) = v_2'(0,t) \tag{4.6}$$

$$E_b I_b v_1''(L_1,t) = E_b I_b v_2''(0,t) \tag{4.7}$$

$$v_2(L_2,t) = v_3(0,t) \tag{4.8}$$

$$v_2'(L_2,t) = v_3'(0,t) \tag{4.9}$$

$$E_b I_b v_2''(L_2,t) = E_b I_b v_3''(0,t) \tag{4.10}$$

$$E_b I_b v_2'''(L_2,t) = m_t \ddot{v}_2(L_2,t) + E_b I_b v_3'''(0,t) \tag{4.11}$$

$$v_3(L_3,t) = 0 \tag{4.12}$$

$$v_3'(L_3,t) = v_4'(0,t) \tag{4.13}$$

$$E_b I_b v_3''(L_3,t) = E_b I_b v_4''(0,t) \tag{4.14}$$

$$v_1(L_1,t) = -v_4(0,t) \tag{4.15}$$

$$E_b I_b v_1'''(L_1,t) + E_b I_b v_3'''(0,t) = (\rho_b A_b (L_2 + L_3) + m_t)\ddot{v}_1(L_1,t) \tag{4.16}$$

By substituting the defined boundary conditions listed in Eqns. 4.1 – 4.16 into Eqn 3, the resulting sixteen equations can be rewritten into a matrix form as:

$$M \cdot \begin{bmatrix} a_1 \\ b_1 \\ \vdots \\ d_4 \end{bmatrix} = \begin{bmatrix} 0 \\ 0 \\ \vdots \\ 0 \end{bmatrix} \tag{5}$$

where *M* is a 16 by 16 matrix. The zeros of the determinant of *M* can be numerically solved, and the natural frequencies of the system can be obtained. As β_i is directly related to the system natural frequencies, the unknown coefficients in the mode shape functions of all segments can be determined numerically.

To validate the calculated resonant modes, a corresponding FEM model via commercial software ANSYS (version 18.2, ANSYS, Inc., Cannonsburg, PA) was adopted for the comparison. The system parameters and material properties used for the experiments and FEM can be found in Table 1, and Table 2 illustrates the comparison (121.9 mm side beam case) between the calculated and simulated frequency results of the first six resonant modes, which are in very good agreement. The comparison reveals the accuracy of the derived mode shape functions, as well as the defined boundary conditions.

As the first and second mode shapes of the U-shaped structure mainly depend on the side beams and the mid beam, respectively, to further tune the two resonant modes, the mid mass and side beams' lengths were selected as the changing variables to obtain a two-to-one internal resonance. The experimental setup and measurement devices are shown in Figs. 3 (a) and (b). An aluminium beam was bent into a right-angled U-shaped structure. An MFC 0714-P2 layer was attached to each segment and the voltage of each MFC layer was measured across an identical loading resistance. Two laser sensors, Wenglor CP24MHT80 were utilised to obtain the transverse displacement of the right-side beam near the right-angled area, as well as recording the transverse displacement of the mid beam at its centre position. A shaking table (APS 113) with its amplifier (APS 115) produced external base excitation and was monitored by an accelerometer, Kistler 8774A50, and its coupler, 5134B, to obtain constant base acceleration levels. A data acquisition board, NI USB-6281 was adopted for data collection. LabVIEW 2014 and MATLAB 2017b were used to monitor real-time data and data processing, respectively. A 1 kHz sampling rate was adopted for all experiments including forward and backward cases; 0.05 Hz frequency interval and 10 seconds settling time were sufficient to reach the system steady-state response.

To illustrate the sensitivity of the internal resonance phenomenon, the side beam length is set as a changing variable from 115 mm to 128mm, and the responses of the device with different side beam length have been experimentally tested under base excitations within the resonance ranges of the first and second transverse modes. As depicted in Fig. 4, the system internal resonance occurs when the side beam length is 121.9 mm. For the first mode under base excitation $Y_1 cos\omega t$, the frequency response of the side beam 121.9 mm case (Fig. 4 (a)) illustrates a classic internal resonance phenomenon with centre frequency at 18.1 Hz. The frequency response bends in two directions from the centre, and for the mid beam shown in Fig. 4 (b), the internal resonance occurs with various lengths. However, the 121.9 mm case shows more symmetric peaks, as well as much higher peak displacements. To examine the coupling between the first and second modes through internal resonance, Figs. 4 (c) and (d) show the frequency response of the side beam and mid beam within the second resonance regime under the base excitation $Y_2 cos\omega t$, respectively. Without an internal resonance, the motion of the side beam is limited to less than 1 mm, which illustrates more sensitivities of revealing saturated dynamics in the side beam. When the internal

resonance has been triggered, five times larger maximum displacement of the side beam can be observed. As opposed to the system responses at its first mode, Fig. 4 (c) depicts clear jump phenomena between its forward and backward plots, while in Fig 4 (d), the frequency response of the mid beam displays hardening and softening responses in forward and backward plots, respectively. In order to examine if the frequency ratio between the first two transverse modes is commensurable, a comparison of the first two resonant modes between experimental and FEM results with different side beam lengths is shown in Fig. 5, which depicts a good match between the FEM and experimental results. 121.9 mm is the overlapping position that denotes the perfect 1:2 resonant modes ratio. Thus, from the theoretical investigations and experimental tests, the two adjacent modes (i.e., first and second transverse modes) were managed to be coupled as a two-to-one internal resonance by tailored system parameters. Comparing Table 2 and Fig. 5, the discrepancies of the first transverse mode (0.84 Hz between calculated and experimental results, 0.57 Hz between FEM with and without MFC layers results) illustrate that the MFC layers induced additional stiffness and mechanical damping to the system; in addition, the adhesive used for surface bonding of MFC layers can possibly cause additional damping that shifts the resonant modes to higher values.

3. Results and discussions

The mode shapes and natural frequencies can be predicted and calculated accurately through preliminary tests and theoretical validations. Thus, the internal resonance phenomenon can be obtained between the first and second resonant modes. In this section, the experimental results of the proposed device are discussed to reveal the merits of a U-shaped internal resonance-based energy harvester. For clarity, both displacement-frequency and voltage-frequency responses are adopted as the main figures to examine the device's performance in terms of bandwidth and voltage/power level.

With an excitation direction parallel to the mid beam length, as shown in Fig. 6, the device was excited in the vicinity of its first resonant mode. The displacement-frequency responses in Fig. 6 (a) illustrate the different dynamic behaviours between side and mid beams under 0.6 g base acceleration. The two side beams, as the core vibrating segments, displayed two peaks occurring at 17.85 Hz and 18.75 Hz. The two jumps led the system to exhibit a continuously operational bandwidth of 0.9 Hz. The displacement-frequency

response of the mid beam shows a flat peak. The initial and ending positions of the resonance region are equal to the locations of the left and right peaks of the side beam, respectively. Figs. 6 (c) and (d) depict the overall time trace including both forward and backward sweeps for mid and side beams, respectively; it should be noted that the two peaks of the side beam are asymmetric: right peak has a higher amplitude, which suggests the system may exhibit initial geometric imperfections. From Figs. 7 (a), (b) and (c), the time trace and the FFT plots illustrate and prove the modal coupling between the first and second modes – even the side and mid beams share a similar resonance region, the time domain and frequency domain results both show the 2:1 ratio between the mid and side beams. Compared between Figs. 7 (b) and (c), the FFT of the side beam denotes a slight but notable peak at the second mode, while there is almost no response from the mid beam in the first mode. In terms of voltage levels, as shown in Fig. 6 (b), peak voltage can reach to 8.28 V, and the power dissipated in the resistor can be calculated by $P = V^2/R_L$, which is 0.46 mW. Both beams have coincident voltage-frequency responses, which are coherent with the features of piezoelectric elements. As the laser sensors could only record the transverse displacements of the side and mid beams, the longitudinal motions may cause additional deformations to the structure, and there are additional deformations caused by longitudinal motions in the piezoelectric layers. Although both forward and backward plots were conducted for all the experiments, the system frequency responses of the first mode show few differences between them. There is no obvious frequency jumps between the two directional sweeps when the system is excited within the first transverse mode, which is different from most nonlinear energy harvesters that utilise soft/hardening dynamic behaviours: large bifurcations may occur when the directions of harmonic excitations change.

To analyse the system responses at its second resonant mode, the device was excited with the direction perpendicular to the mid beam length to obtain higher oscillation amplitudes. Displacement-frequency responses shown in Figs. 8 (a), (c) and (d) reveal nonlinear responses in the forward and backward plots. Both beams' frequency responses and time traces depict jump phenomena in the forward and backward plots. The corresponding left and right branches (peaks) were able to extend even further in the backward and forward sweep cases, respectively. Although the two branches were asymmetric due to initial geometric nonlinearities, the extended regions, due to the double jump phenomena, have almost equally increased bandwidth. Based on derived mode

shape functions and FEM results, the core vibrating element in system's second resonant mode is the mid beam. However, in the presence of the two-to-one internal resonance, large oscillations of the two side beams have been triggered, with a peak amplitude up to 9.5 mm. Compared with the mid beam, the side beam has an overall higher amplitude at resonance, while the mid beam displays a non-zero amplitude response at the off-resonance regime. Figs. 9 (a), (b) and (c) describe the time trace and FFT plots of mid and side beams, respectively, at system second resonant mode. Similar to the first mode (see Fig. 7), by introducing internal resonance to couple the first two modes, the two FFT figures prove the 2:1 ratio between mid and side segments. The voltage-frequency responses shown in Fig. 8 (b) illustrate the same trend and resonant region as the displacement-frequency responses shown in Fig. 8 (a). The peak voltage was up to 4.29 V and the power dissipated in the resistor was 0.12 mW.

Comparing the first and second modes, the core elements (i.e., the side beams for the first mode and the mid beam for the second mode) exhibited internal resonance phenomenon that the two peaks were bent in two opposite directions from the centre. In comparison, the coupled elements (the mid beam for the first mode and the side beam for the second mode) exhibited flatter resonance regions with a much higher amplitude near the central position and had similar zero-like off-resonance regimes, respectively.

To distinguish the differences between input frequency signals and system responses, Figs. 10 (a)-(h) illustrate the overall input base acceleration signals and the response spectrograms of both mid and side beams. Figs. 10 (a) and (b) show the overall time trace plots and the frequency spectrums of the measured input base acceleration within the system's first and second transverse resonant ranges, respectively. With the input harmonic base excitation frequencies within the system's first transverse mode (Figs. 10 (a) and (c)), the response of the mid beam implies the effects of modal coupling that convert the low input frequency signal to high frequency oscillation. On the contrary, with a high input frequency shown in Figs. 10 (b) and (d), the response of the side beam reveals the energy exchanges from higher frequency to lower, especially between the resonant range from 17.8 Hz to 18.75 Hz (Fig. 10 (h)). The overall response spectrograms of the mid and side beams are consistent with the spectrums provided in Figs. 7 and 9.

To further study the performance of the proposed energy harvester in terms of the bandwidth and the voltage level, the base excitation level, as the most vital factor in

dealing with realistic ambient energy harvesting applications, was adopted for the parameter studies. The proposed device under six base acceleration levels, from 0.1 g to 0.6 g, peak to peak, was investigated experimentally. Fig. 11 depicts the system responses at the first mode. Displacement-frequency responses of the mid and side beams are shown in Figs. 11 (a) and (c), respectively. Under a 0.1 g acceleration level, the left peak of the side beam can hardly be found. However, the mid beam's response illustrates the existence of the internal resonance as it exhibited two notable resonant peaks that bend in opposite directions from the centre, which has a similar resonant region to the side beam. Even though the 0.1 g case can be considered as the critical excitation level to trigger internal resonance, a peak voltage of 2.1 V and power of 0.03 mW can still be generated. With increasing excitation levels, the frequency jump becomes larger between the two peaks are shown in the mid beam displacement-frequency plot as expected, which broadens the operational bandwidth, and increases the overall peak amplitudes of displacement and voltage levels. The system responses at its second mode shown in Figs. 12 and 13, illustrate nonlinear dynamic behaviours in the forward and backward frequency responses. Unlike in the first mode case, even under a 0.1 g acceleration level, there is a 0.2 Hz symmetric frequency jump as shown in Figs. 12 (c) and 13 (c). Compared with most nonlinear energy harvesters which utilised hardening or softening responses, the bandwidth of their device is only effective in one direction (i.e., forward or backward sweeps). For the proposed devices, under a harmonic excitation, the broadband performance is not limited to one direction. As a U-shaped structure, the two side beams (segment 1 and segment 4) are considered to be symmetrical with the same material properties, as well as the mechanical-electrical coupling effects between the substrate and the MFC layer. To further validate the dynamic responses of the two side beams, Figs. 14 (a) and (b) depict their voltage-frequency responses at the first and second modes, respectively. The results imply that the motions of the two side beams are almost consistent with each other, which agree with the assumptions. It should be noted, although the two side beams are considered to be symmetrical, the overall device is not, as the MFC layer attached to the mid beam was not placed on the centre position.

4. Conclusion

This research exploited a U-shaped piezoelectric energy harvester utilising an internal resonance to achieve broadband and bi-directional features. An analytical method was presented to predict and locate the resonant modes of the proposed device. The derived mode shape functions were validated with FEM simulations, showing less than 2% errors for the first six modes. The first two adjacent modes (i.e., the first and second modes) were managed to be coupled as a two-to-one internal resonance by introducing a mid-mass and adjusting the side beams' lengths as tuning methods, both experimentally and theoretically. Under harmonic excitations, the experimental tests illustrate the internal resonance phenomenon between the first and second modes, providing a peak power level of 0.46 mW and 0.12 mW, respectively. The effective operational bandwidths in either forward or backward sweeps for all segments (i.e., two side beams and one mid beam) are 1.5 Hz and 1.4 Hz in the first and second modes, respectively. Compared with conventional multi-mode and multi-DOFs energy harvesters that have substructures suffering low amplitude vibrations, the internal resonance phenomenon leads all segments of the proposed device exhibit large amplitude oscillations at both the first and second transverse modes. Thus, high-efficient energy conversion can be achieved. Compared with cases without an internal resonance, the side beam exhibited an almost zero amplitude response at its second mode. Compared with energy harvesters utilise softening or hardening features, which exhibit large frequency bifurcations under forward and backward harmonic excitations and the effective bandwidth depends on the directions of harmonic excitation, the operational bandwidth of the proposed device are effective for both directional harmonic excitations (e.g., forward and backward directions). As a prototype design and test, to optimise the power level, a fully covered unimorph or bimorph cantilever is suggested for future studies. Based on the characteristics of its first two transverse modes, the device is applicable under bi-directional base excitations. Parametric studies on acceleration levels suggest the critical excitation level is below 0.1 g, which imply its feasibility under a small level of excitations from ambient vibrations.

Declaration of Competing Interest

The authors declare that they have no known competing financial interests or personal relationships that could have appeared to influence the work reported in this paper.

Acknowledgement

This work has been supported by the Australian Government Research Training Program.

The support is greatly appreciated.

References

[1] Q. Tang, X. Li, Two-Stage Wideband Energy Harvester Driven by Multimode Coupled Vibration, IEEE/ASME Transactions on Mechatronics, 20 (2015) 115-121.
[2] X. Li, K. Yu, D. Upadrashta, Y. Yang, Comparative study of core materials and multi-degree-of-freedom sandwich piezoelectric energy harvester with inner cantilevered beams, Journal of Physics D: Applied Physics, 52 (2019) 235501.
[3] X. Li, D. Upadrashta, K. Yu, Y. Yang, Analytical modeling and validation of multi-mode piezoelectric energy harvester, Mechanical Systems and Signal Processing, 124 (2019) 613-631.
[4] S. Dhote, Z. Yang, J. Zu, Modeling and experimental parametric study of a tri-leg compliant orthoplanar spring based multi-mode piezoelectric energy harvester, Mechanical Systems and Signal Processing, 98 (2018) 268-280.
[5] S. Zhou, J.D. Hobeck, J. Cao, D.J. Inman, Analytical and experimental investigation of flexible longitudinal zigzag structures for enhanced multi-directional energy harvesting, Smart Materials and Structures, 26 (2017) 035008.
[6] J. Wang, G. Hu, Z. Su, G. Li, W. Zhao, L. Tang, L. Zhao, A cross-coupled dual-beam for multi-directional energy harvesting from vortex induced vibrations, Smart Materials and Structures, 28 (2019) 12LT02.
[7] R. Sun, Q. Li, J. Yao, F. Scarpa, J. Rossiter, Tunable, multi-modal, and multi-directional vibration energy harvester based on three-dimensional architected metastructures, Applied Energy, 264 (2020) 114615.
[8] T. Yang, Q. Cao, Q. Li, H. Qiu, A multi-directional multi-stable device: Modeling, experiment verification and applications, Mechanical Systems and Signal Processing, 146 (2021) 106986.
[9] L. Chen, W. Jiang, A piezoelectric energy harvester based on internal resonance, Acta Mechanica Sinica, 31 (2015) 223-228.
[10] C.L. Lee, N.C. Perkins, Nonlinear oscillations of suspended cables containing a two-to-one internal resonance, Nonlinear Dynamics, 3 (1992) 465-490.
[11] D.X. Cao, S. Leadenham, A. Erturk, Internal resonance for nonlinear vibration energy harvesting, The European Physical Journal Special Topics, 224 (2015) 2867-2880.
[12] R.L. Harne, A. Sun, K.W. Wang, Leveraging nonlinear saturation-based phenomena in an L-shaped vibration energy harvesting system, Journal of Sound and Vibration, 363 (2016) 517-531.
[13] X. Nie, T. Tan, Z. Yan, Z. Yan, M.R. Hajj, Broadband and high-efficient L-shaped piezoelectric energy harvester based on internal resonance, International Journal of Mechanical Sciences, 159 (2019) 287-305.
[14] H. Li, H. Sun, B. Song, D. Zhang, X. Shang, D. Liu, Nonlinear dynamic response of an L-shaped beam-mass piezoelectric energy harvester, Journal of Sound and Vibration, 499 (2021) 116004.
[15] L.-Q. Chen, W.-A. Jiang, M. Panyam, M.F. Daqaq, A Broadband Internally Resonant Vibratory Energy Harvester, Journal of Vibration and Acoustics, 138 (2016).
[16] L. Xiong, L. Tang, B.R. Mace, Internal resonance with commensurability induced by an auxiliary oscillator for broadband energy harvesting, Applied Physics Letters, 108 (2016) 203901.
[17] W. Yang, S. Towfighian, Internal resonance and low frequency vibration energy harvesting, Smart Materials and Structures, 26 (2017) 095008.

[18] R. Eshtehardiha, R. Tikani, S. Ziaei-Rad, Experimental and numerical investigation of energy harvesting from double cantilever beams with internal resonance, Journal of Sound and Vibration, 500 (2021) 116022.
[19] C. Xia, D.F. Wang, T. Ono, T. Itoh, M. Esashi, Internal resonance in coupled oscillators – Part I: A double amplification mass sensing scheme without Duffing nonlinearity, Mechanical Systems and Signal Processing, 159 (2021) 107886.
[20] Y. Wu, S. Li, K. Fan, H. Ji, J. Qiu, Investigation of an ultra-low frequency piezoelectric energy harvester with high frequency up-conversion factor caused by internal resonance mechanism, Mechanical Systems and Signal Processing, 162 (2022) 108038.
[21] W.-A. Jiang, L.-Q. Chen, H. Ding, Internal resonance in axially loaded beam energy harvesters with an oscillator to enhance the bandwidth, Nonlinear Dynamics, 85 (2016) 2507-2520.
[22] A.Z. Hajjaj, F.K. Alfosail, M.I. Younis, Two-to-one internal resonance of MEMS arch resonators, International Journal of Non-Linear Mechanics, 107 (2018) 64-72.
[23] Z. Xie, B. Huang, K. Fan, S. Zhou, W. Huang, A magnetically coupled nonlinear T-shaped piezoelectric energy harvester with internal resonance, Smart Materials and Structures, 28 (2019) 11LT01.
[24] J. Zhang, X. Li, R. Li, L. Dai, W. Wang, K. Yang, Internal resonance of a two-degree-of-freedom tuned bistable electromagnetic actuator, Chaos, Solitons & Fractals, 143 (2021) 110612.
[25] M. Aravindan, S.F. Ali, Exploring 1:3 internal resonance for broadband piezoelectric energy harvesting, Mechanical Systems and Signal Processing, 153 (2021) 107493.
[26] G.-X. Wang, H. Ding, L.-Q. Chen, Dynamic effect of internal resonance caused by gravity on the nonlinear vibration of vertical cantilever beams, Journal of Sound and Vibration, 474 (2020) 115265.
[27] H. Abdelmoula, N. Sharpes, A. Abdelkefi, H. Lee, S. Priya, Low-frequency Zigzag energy harvesters operating in torsion-dominant mode, Applied Energy, 204 (2017) 413-419.
[28] H. Li, D. Liu, J. Wang, X. Shang, M.R. Hajj, Broadband bimorph piezoelectric energy harvesting by exploiting bending-torsion of L-shaped structure, Energy Conversion and Management, 206 (2020) 112503.
[29] W.-J. Su, H.-A. Shih, A U-shaped multi-modal bi-directional piezoelectric energy harvester, Applied Physics Letters, 113 (2018) 071905.
[30] X. Hu, Y. Li, X. Xie, A study on a U-shaped piezoelectric coupled beam and its corresponding ingenious harvester, Energy, 185 (2019) 938-950.
[31] X. Xie, J. Zhang, Z. Wang, G. Song, An experimental study on a high-efficient multifunctional U-shaped piezoelectric coupled beam, Energy Conversion and Management, 224 (2020) 113330.
[32] R.T. Rocha, J.M. Balthazar, A.M. Tusset, V. Piccirillo, J.L.P. Felix, Nonlinear piezoelectric vibration energy harvesting from a portal frame with two-to-one internal resonance, Meccanica, 52 (2017) 2583-2602.
[33] Y. Fan, M.H. Ghayesh, T.-F. Lu, Enhanced nonlinear energy harvesting using combined primary and parametric resonances: Experiments with theoretical verifications, Energy Conversion and Management, 221 (2020) 113061.
[34] Y. Fan, M.H. Ghayesh, T.-F. Lu, M. Amabili, Design, development, and theoretical and experimental tests of a nonlinear energy harvester via piezoelectric arrays and motion limiters, International Journal of Non-Linear Mechanics, 142 (2022) 103974.
[35] Y. Fan, M.H. Ghayesh, T.-F. Lu, A broadband magnetically coupled bistable energy harvester via parametric excitation, Energy Conversion and Management, 244 (2021) 114505.
[36] H.P. Lin, J. Ro, Vibration analysis of planar serial-frame structures, Journal of Sound and Vibration, 262 (2003) 1113-1131.
[37] D.J. Inman, Vibration with control, John Wiley & Sons, 2017.
[38] S.S. Rao, Vibration of Continuous Systems, John Wiley & Sons, New Jersey, 2007.
[39] A. Erturk, J.M. Renno, D.J. Inman, Modeling of Piezoelectric Energy Harvesting from an L-shaped Beam-mass Structure with an Application to UAVs, Journal of Intelligent Material Systems and Structures, 20 (2008) 529-544.

Table 1. System parameters and material properties

Substrate (Aluminium)	
Side beam (Segment 1) Dimension $l_{b1} \times b_{b1} \times h_{b1}$ [mm]	121.9×17×0.5
Mid beam Dimension $l_{b2} \times b_{b2} \times h_{b2}$ [mm]	180.0×17×0.5
Side beam (Segment 4) Dimension $l_{b3} \times b_{b3} \times h_{b3}$ [mm]	121.9×17×0.5
Elastic Modulus E_b [GPa]	68.9
Poisson's Ratio	0.33
Mass density ρ_b [kg/m^3]	2700
Mid mass m_t at centre of the horizontal beam [g]	2.8
MFC Patch	
Dimension $l_p \times b_p \times h_p$ [mm]	7×14×0.3
Location from fixed end [mm]	18.28
Location from connection point between segments 3 and 4	15.71
Location from fixed end [mm]	18.28
Elastic Modulus E_p [GPa]	30.3
Poisson's Ratio	0.31
Mass density ρ_p [kg/m^3]	5440
Load resistance on each MFC patch R_L [Ohm]	1.5×10^5

Table 2. Comparisons between calculated and simulated system natural frequencies. Side beam length is 121.9 mm and a 2.8 g point mass is attached on the centre position of mid beam.

Modes	Calculated results [Hz]	FEM results (without MFC layers)[Hz]	Error [%]
1	17.26	17.46	1.15
2	35.15	35.33	0.51
3	132.36	132.91	0.41
4	144.54	146.11	1.08
5	202.79	205.02	1.09
6	293.77	295.59	0.62

(a)

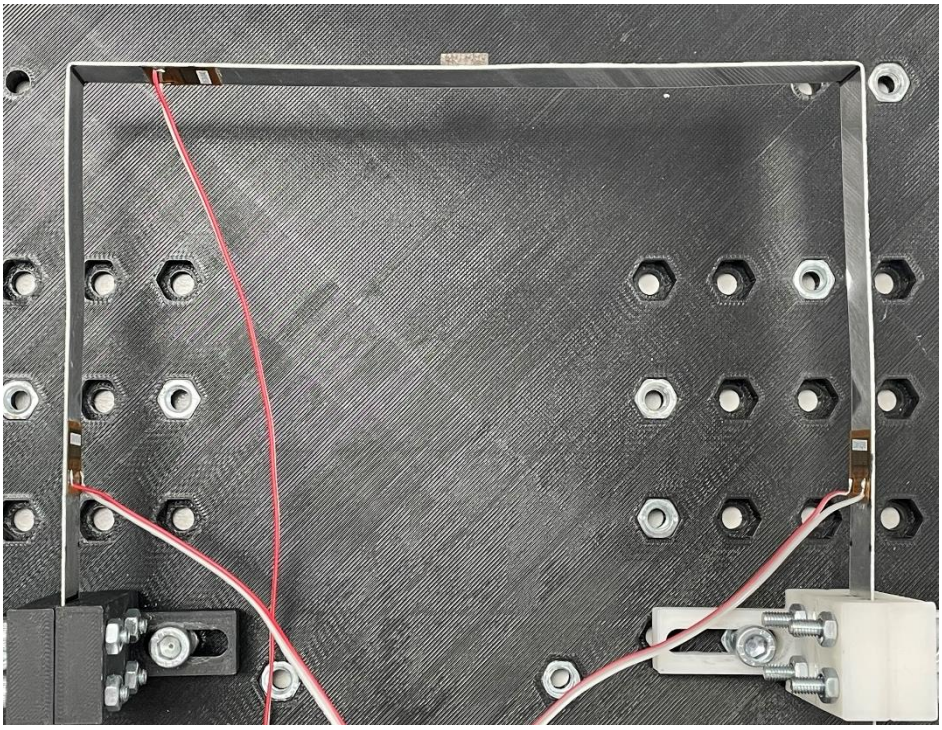

(b)

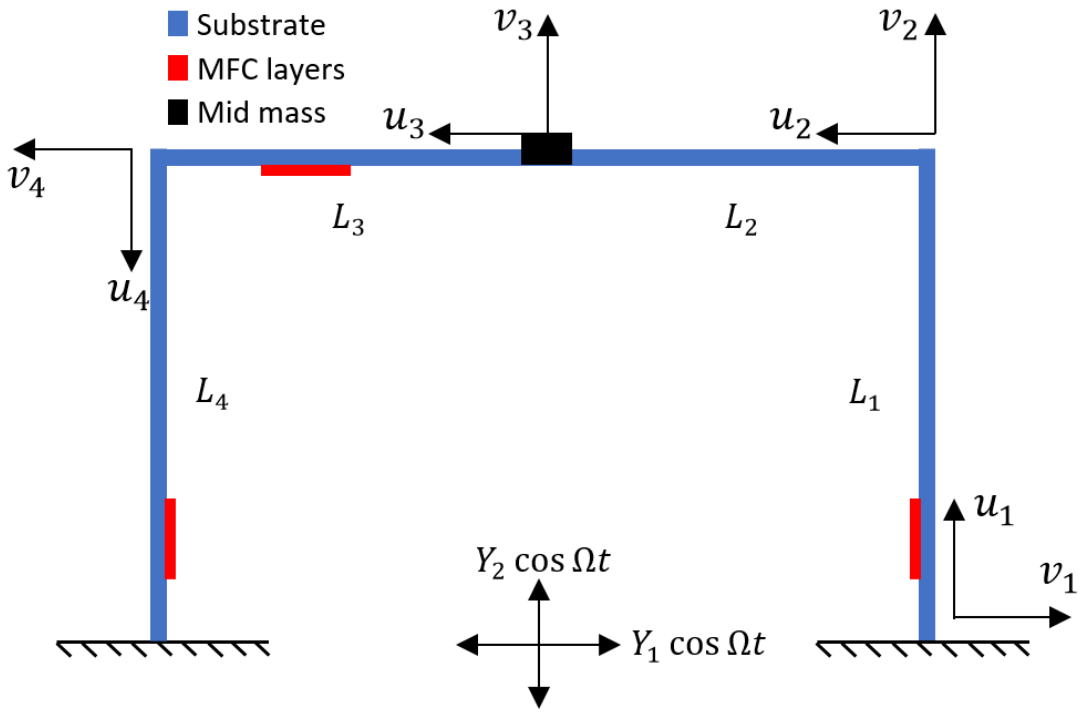

Figure 1. Proposed U-shaped piezoelectric energy harvester: a) fabricated device; b) schematics.

(a)

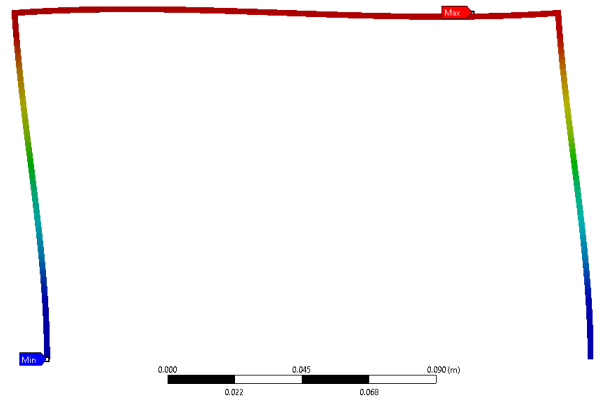

(b)

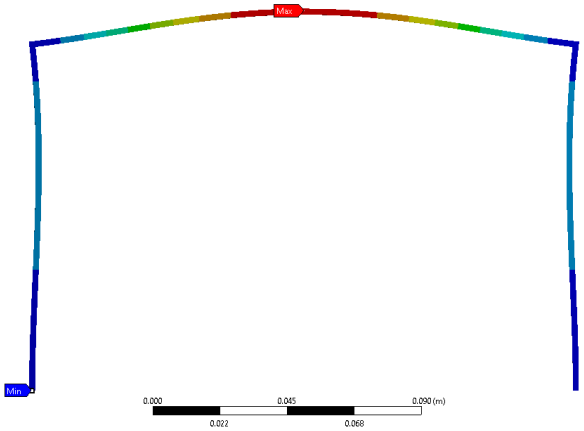

Figure 2. FEM simulated the first two resonant mode shapes of the proposed device.

(a)

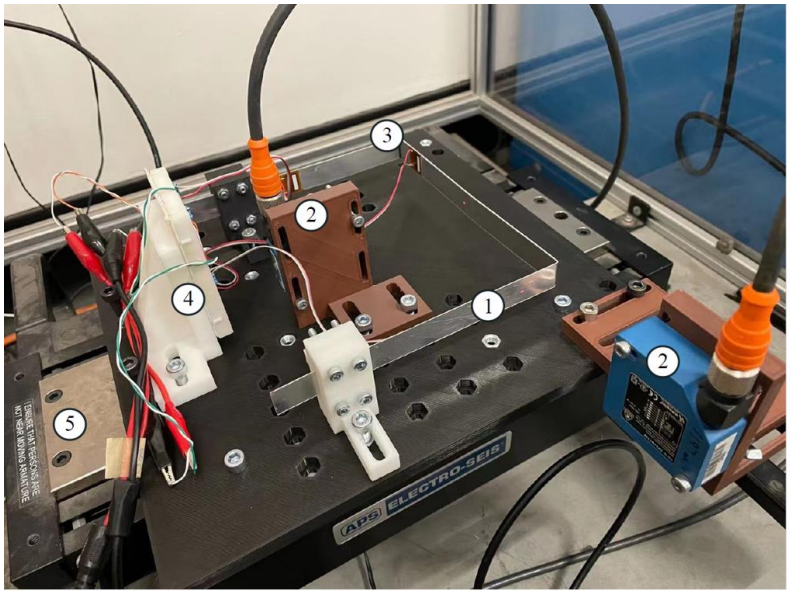

(b)

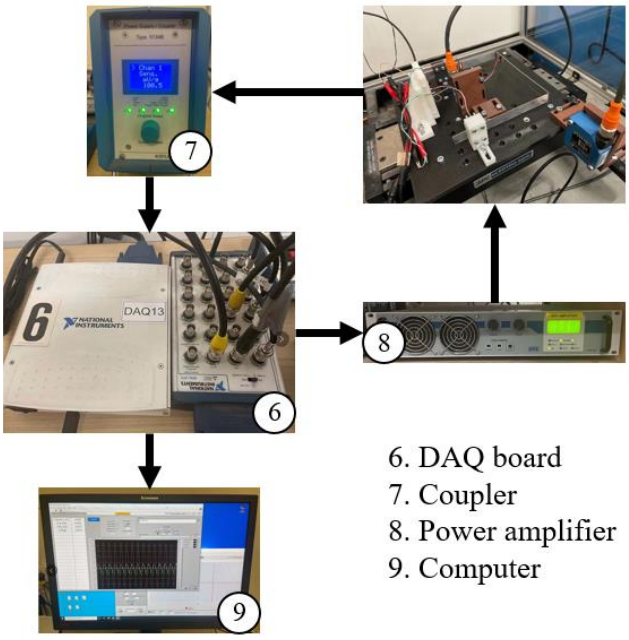

Figure 3. Experimental setup: a) main vibrating setup; b) flowchart of the experimental procedure.

(a)

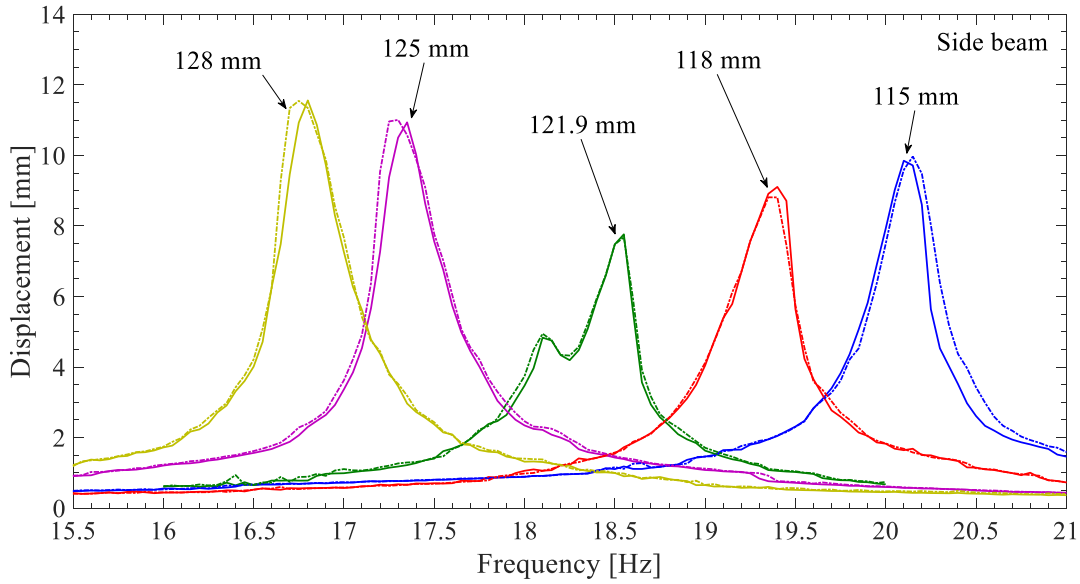
Side beam
128 mm
125 mm
121.9 mm
118 mm
115 mm
Displacement [mm]
Frequency [Hz]
0
2
4
6
8
10
12
14
15.5
16
16.5
17
17.5
18
18.5
19
19.5
20
20.5
21

(b)

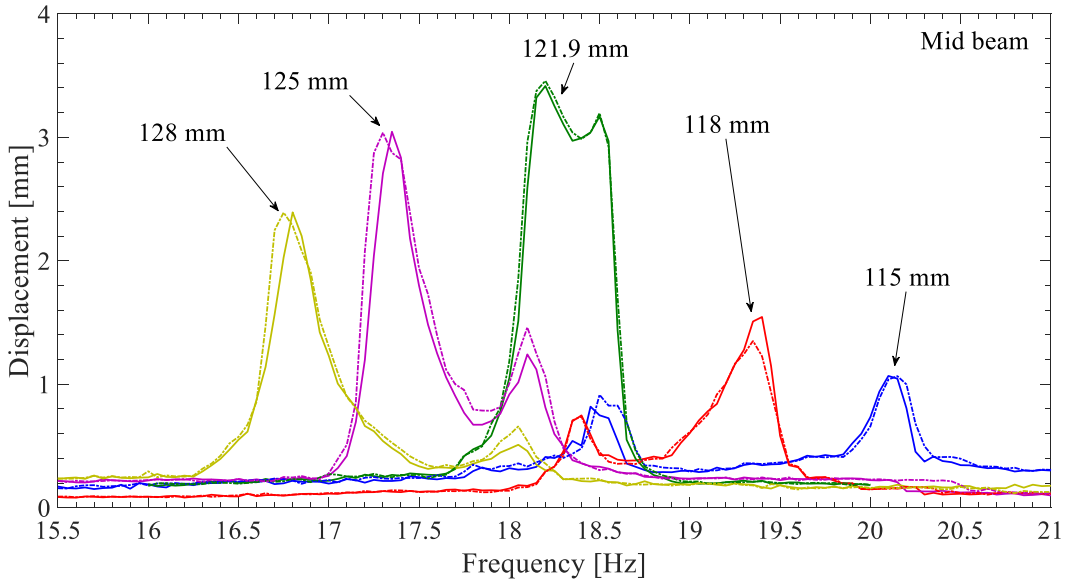
Mid beam
128 mm
125 mm
121.9 mm
118 mm
115 mm
Displacement [mm]
Frequency [Hz]
0
1
2
3
4
15.5
16
16.5
17
17.5
18
18.5
19
19.5
20
20.5
21

(c)

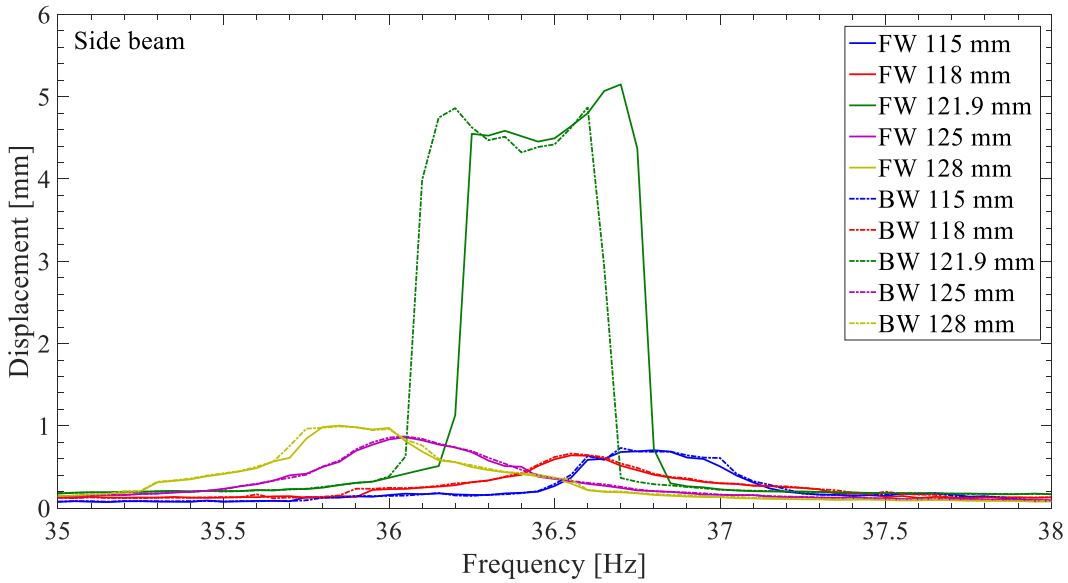

(d)

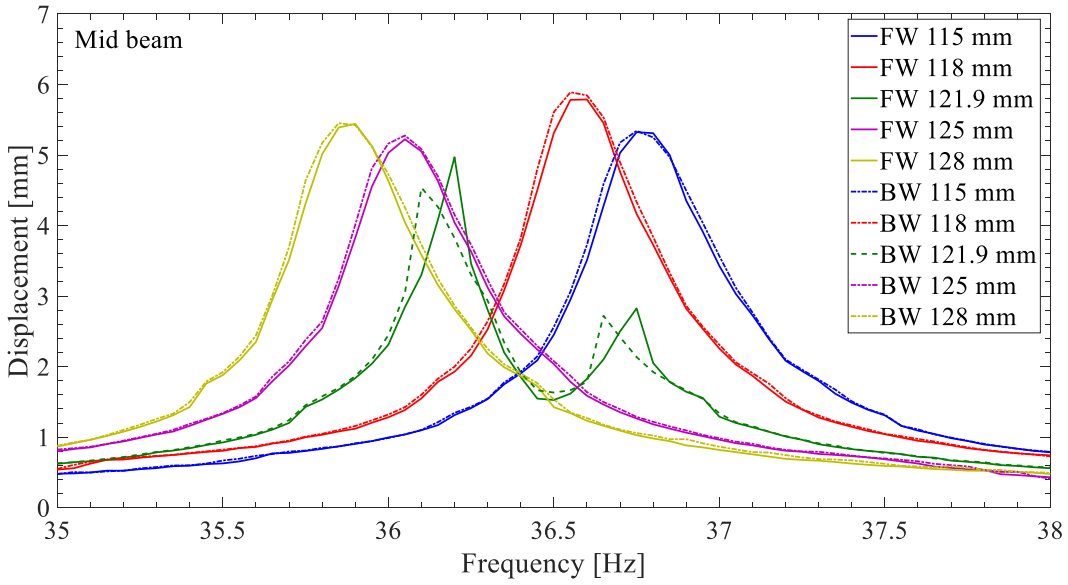

Figure 4. With 2.8 gram mid mass, frequency responses of the selected side beam (segment 1) and the mid beam for different side beam length. For the first mode: a) side beam; b) mid beam. For the second mode: c) side beam; d) mid beam.

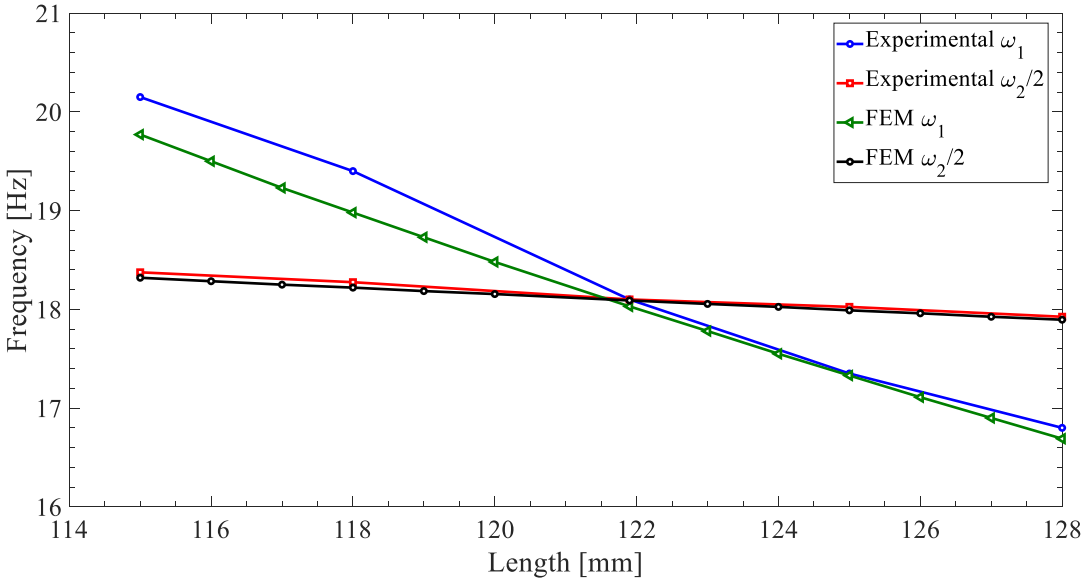

Figure 5. Comparison of the frequency ratios of the first two transverse modes between Experimental and FEM results (including MFC layers) with different side beam lengths.

(a)

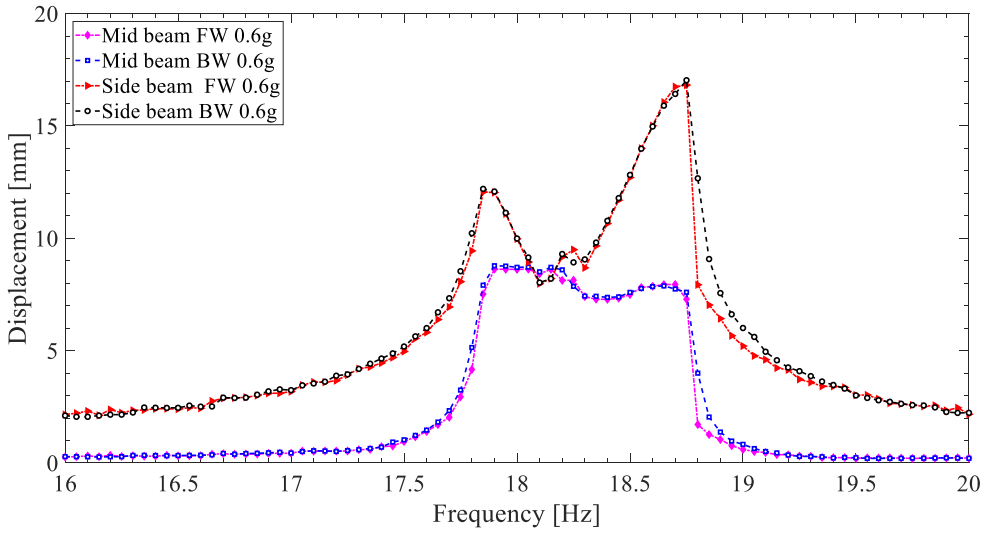

(b)

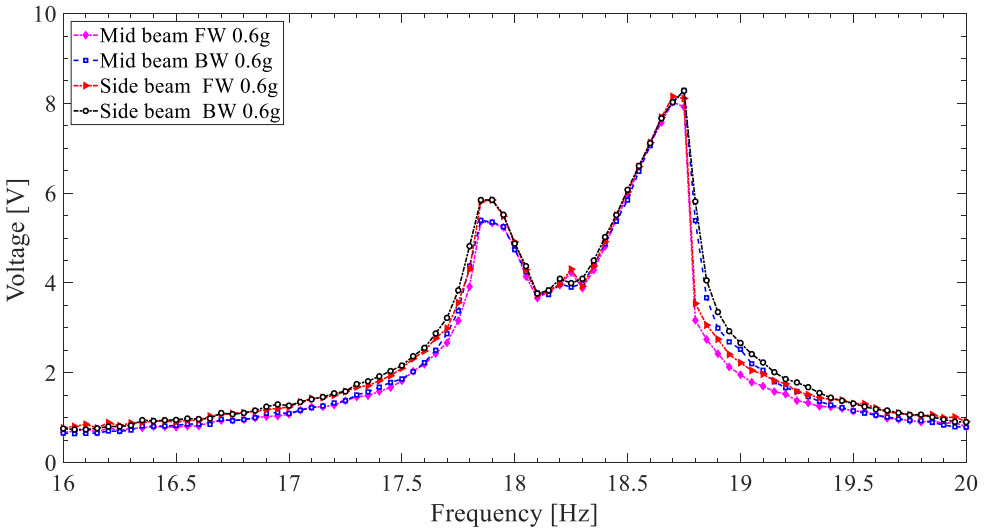

Figure 6. Frequency responses of the side and the mid beams under 0.6 g base acceleration at the first transverse mode, where the excitation direction is parallel to the mid beam length. a) displacement-frequency response; b) voltage-frequency response.

(a)

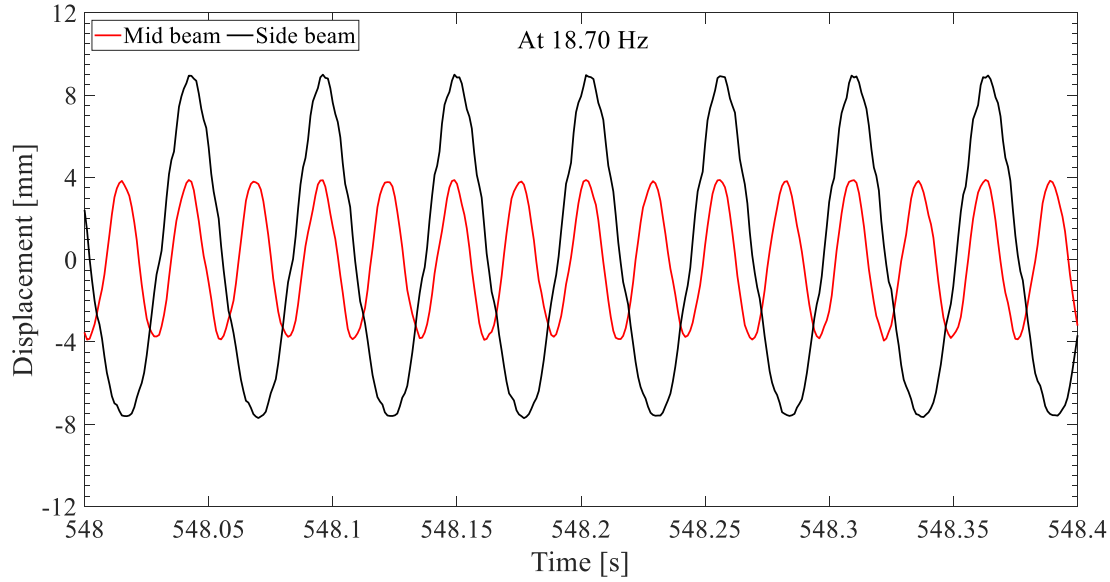

(b)

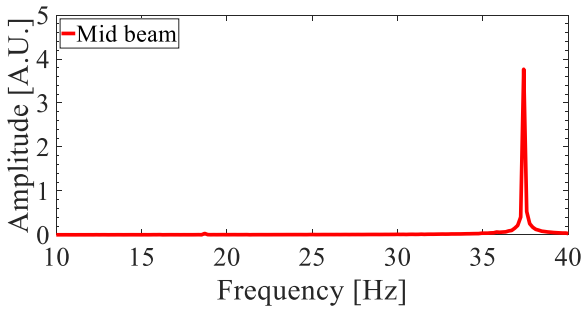

(c)

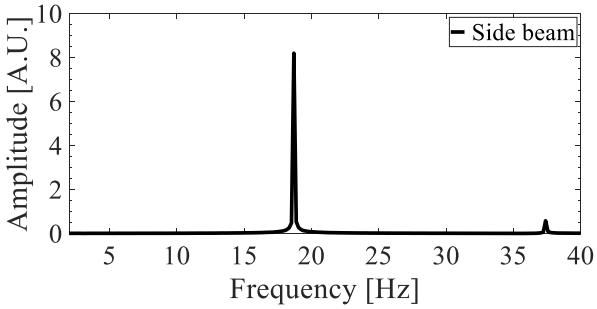

Figure 7. System responses at the right peak position (18.70 Hz): a) time trace; b) FFT of the mid beam and c) FFT of the side beam.

(a)

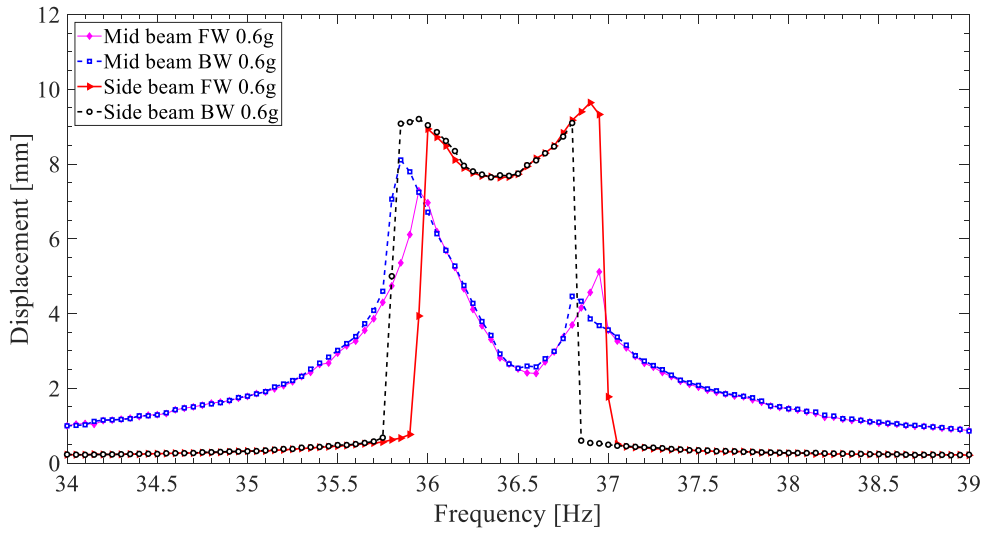

(b)

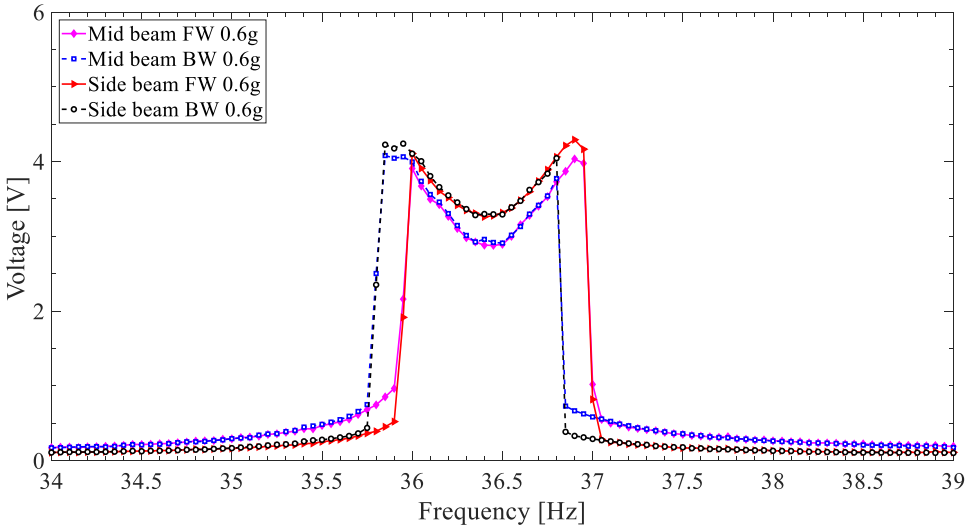

Figure 8. Frequency responses of the side and the mid beams under 0.6 g base acceleration at the second transverse mode, where the excitation direction is perpendicular to the mid beam length. a) displacement-frequency response; b) voltage-frequency response.

(a)

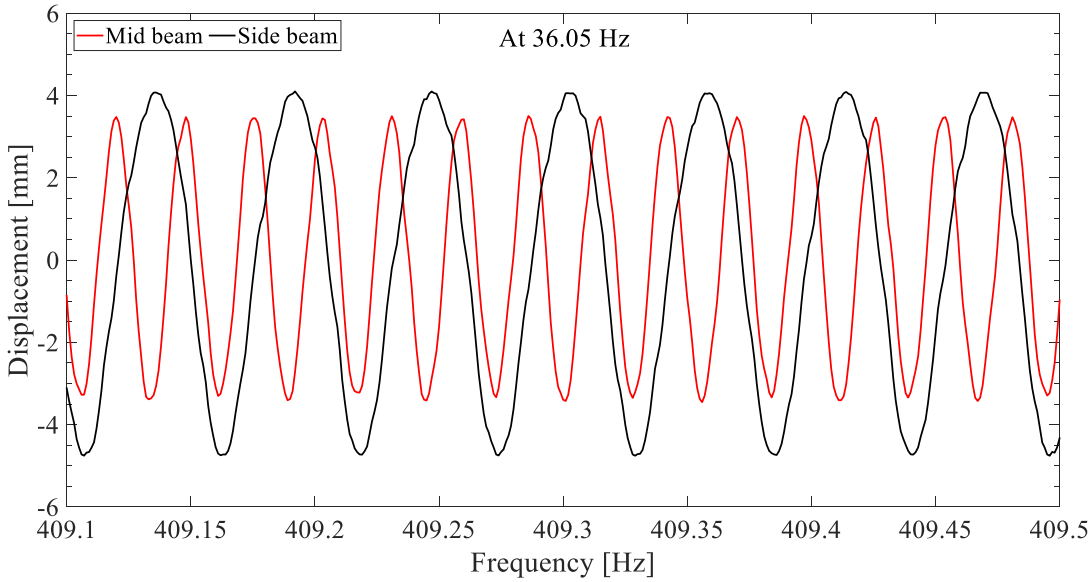

(b)

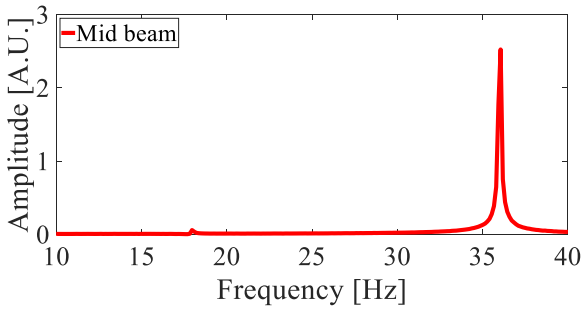

(c)

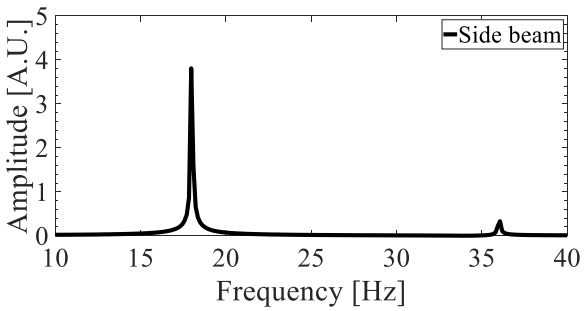

Figure 9. System responses at left peak position (36.05 Hz): a) time trace; b) FFT of the mid beam and c) FFT of the side beam.

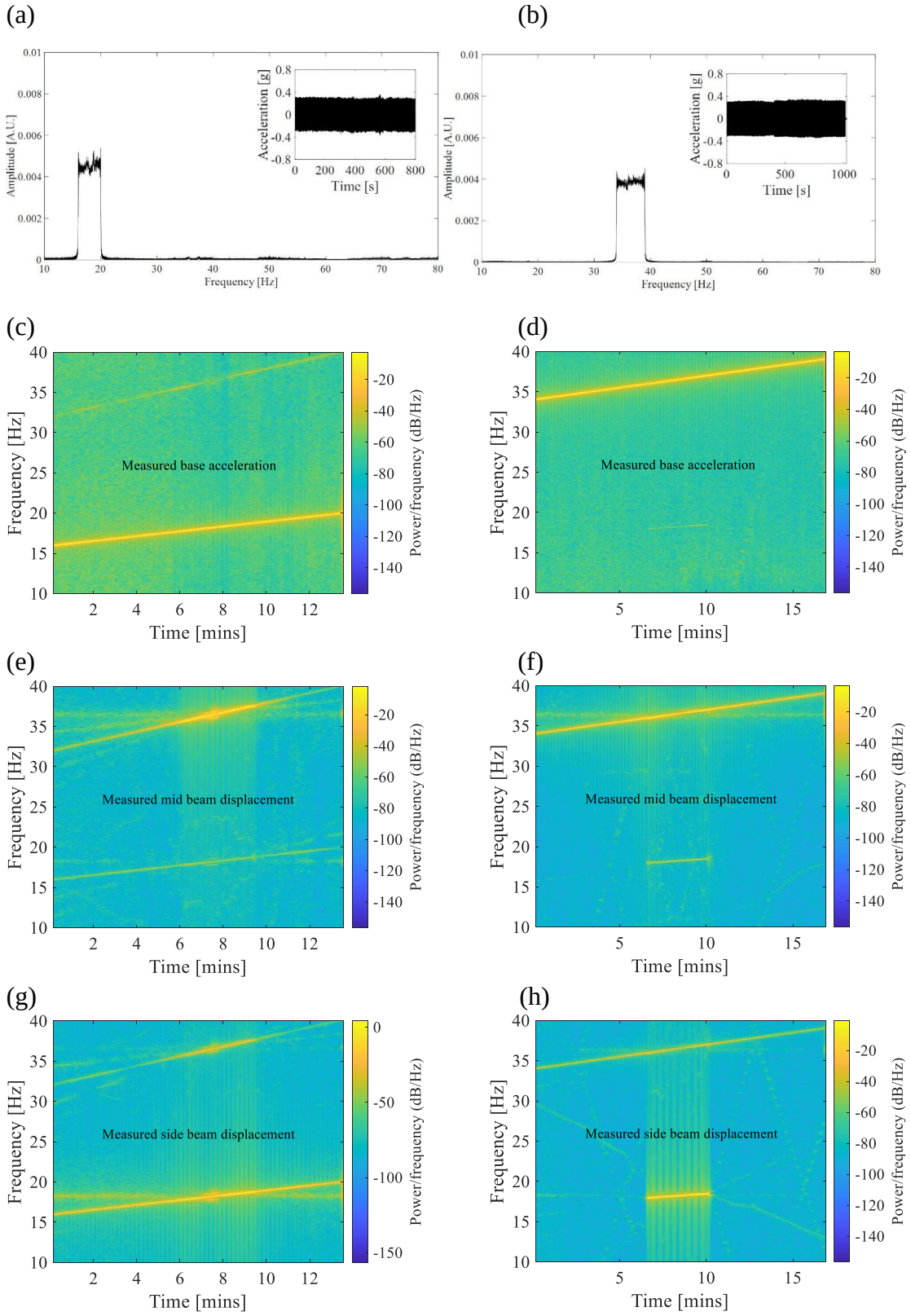

Figure 10. Measured input base acceleration signals and displacement response spectrograms. First transverse mode: (a), (c), (e) and (g); second transverse mode: (b), (d), (f) and (h).

(a)

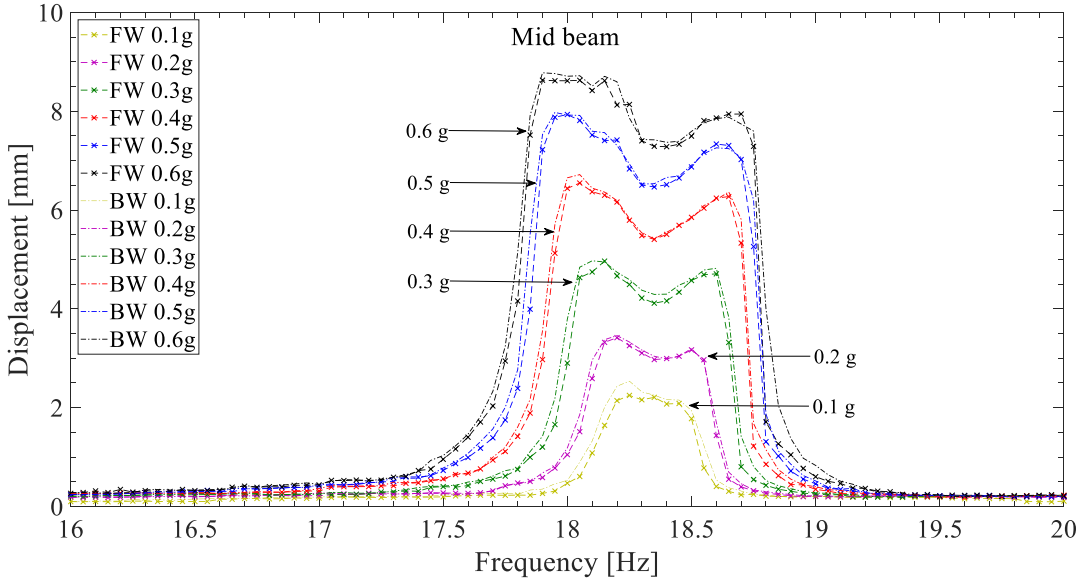
Mid beam
FW 0.1g
FW 0.2g
FW 0.3g
FW 0.4g
FW 0.5g
FW 0.6g
BW 0.1g
BW 0.2g
BW 0.3g
BW 0.4g
BW 0.5g
BW 0.6g
0.6 g
0.5 g
0.4 g
0.3 g
0.2 g
0.1 g
Displacement [mm]
Frequency [Hz]

(b)

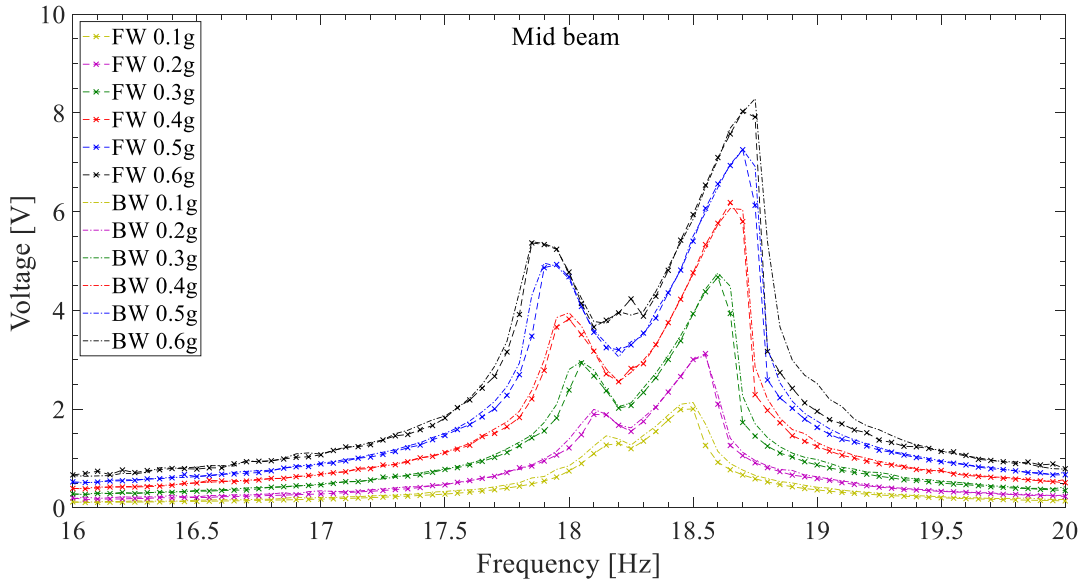
Mid beam
FW 0.1g
FW 0.2g
FW 0.3g
FW 0.4g
FW 0.5g
FW 0.6g
BW 0.1g
BW 0.2g
BW 0.3g
BW 0.4g
BW 0.5g
BW 0.6g
Voltage [V]
Frequency [Hz]

(c)

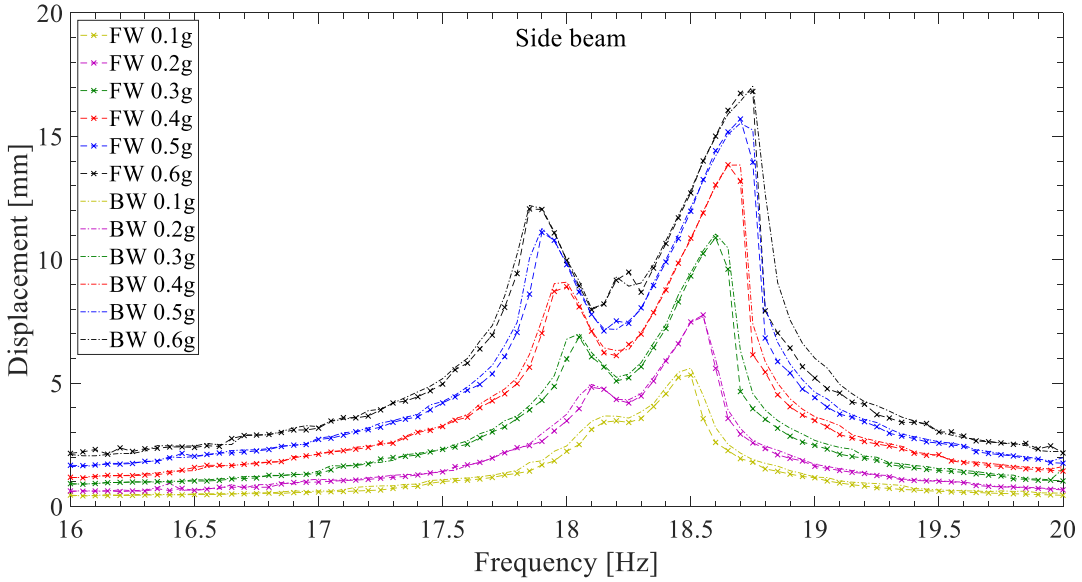

(d)

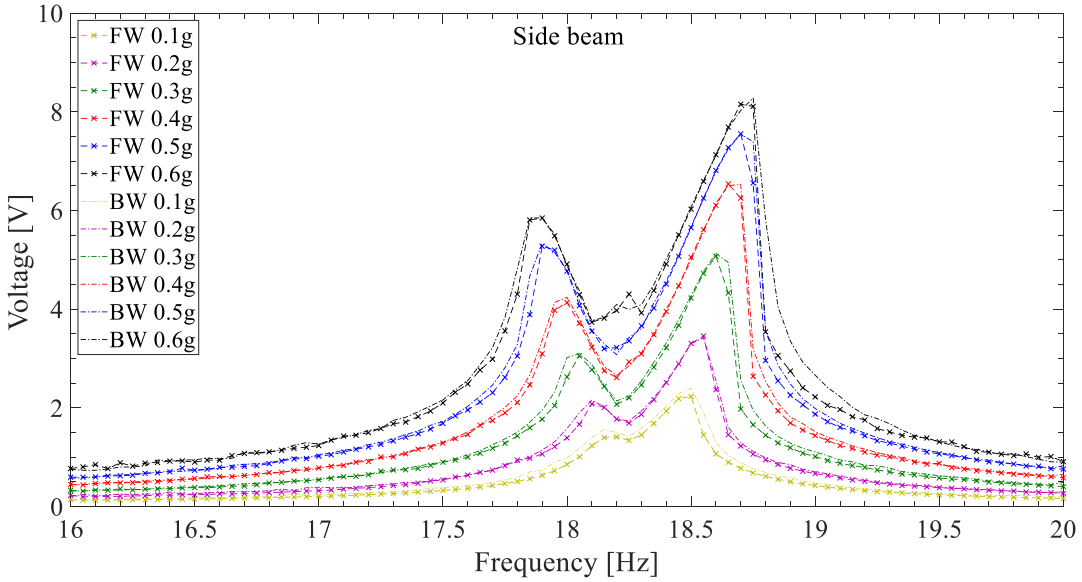

Figure 11. Under different base excitation levels, the system responses at the first transverse mode. Displacement-frequency responses a) the mid beam and b) the side beam; voltage-frequency responses c) the mid beam and d) the side beam.

(a)

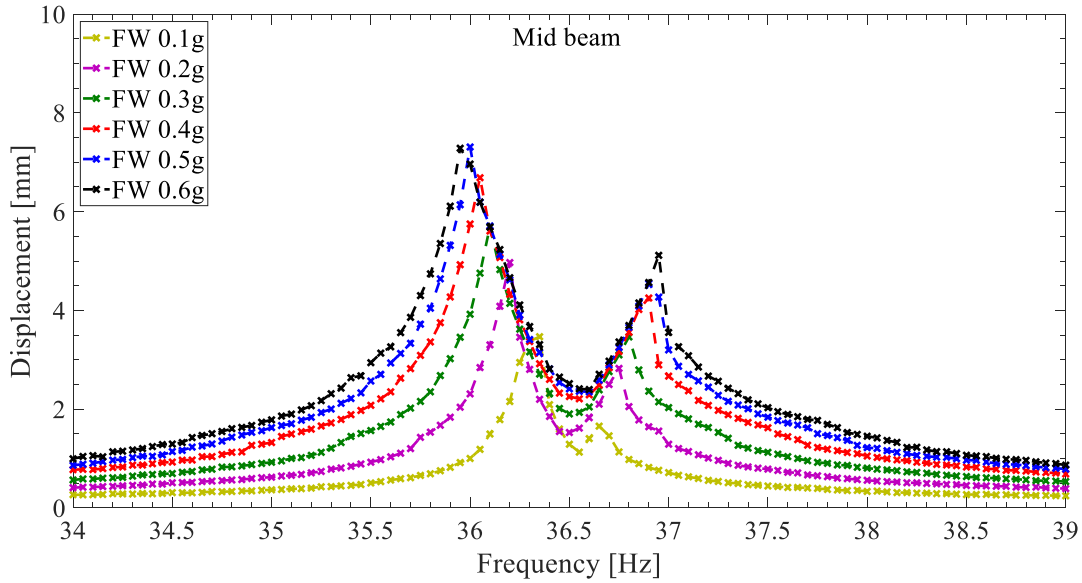
Mid beam
FW 0.1g
FW 0.2g
FW 0.3g
FW 0.4g
FW 0.5g
FW 0.6g
Displacement [mm]
Frequency [Hz]
0
2
4
6
8
10
34
34.5
35
35.5
36
36.5
37
37.5
38
38.5
39

(b)

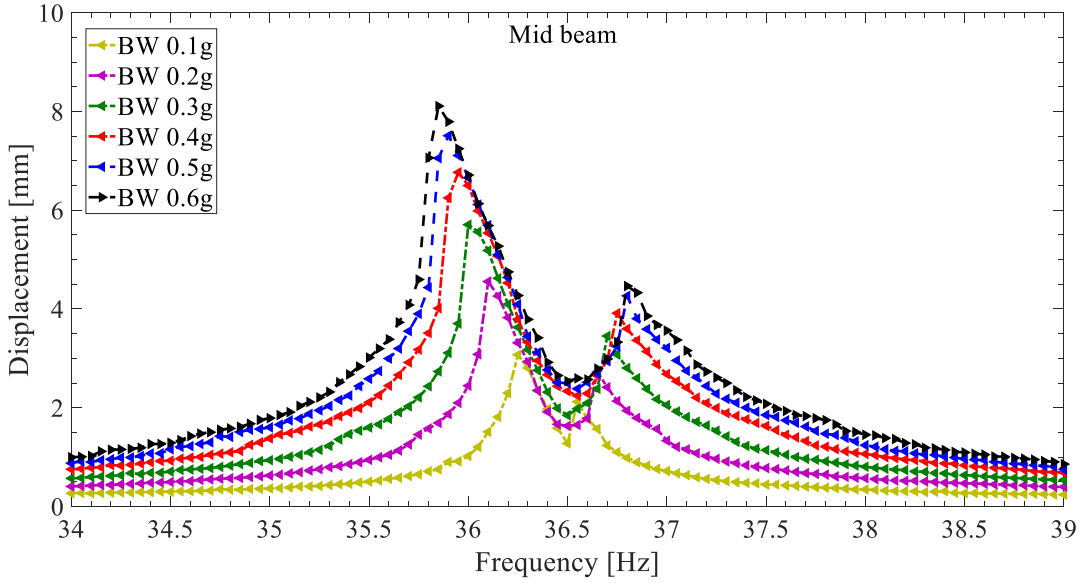
Mid beam
BW 0.1g
BW 0.2g
BW 0.3g
BW 0.4g
BW 0.5g
BW 0.6g
Displacement [mm]
Frequency [Hz]
0
2
4
6
8
10
34
34.5
35
35.5
36
36.5
37
37.5
38
38.5
39

(c)

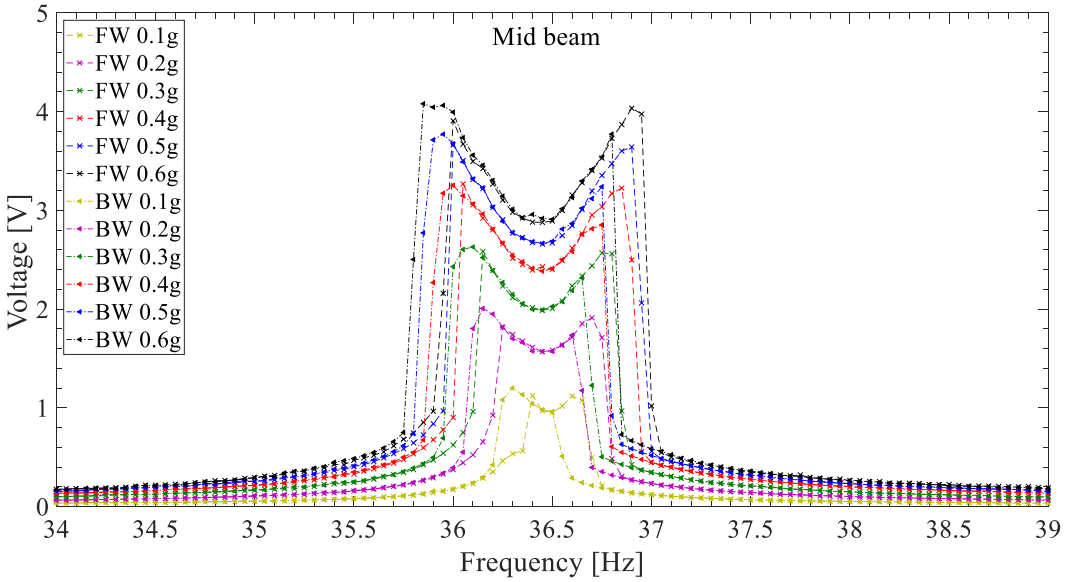

Figure 12. Under different base excitation level, the mid beam responses at the second transverse mode. Displacement-frequency responses a) forward plot and b) backward plot; c) voltage-frequency responses including both forward and backward plots.

(a)

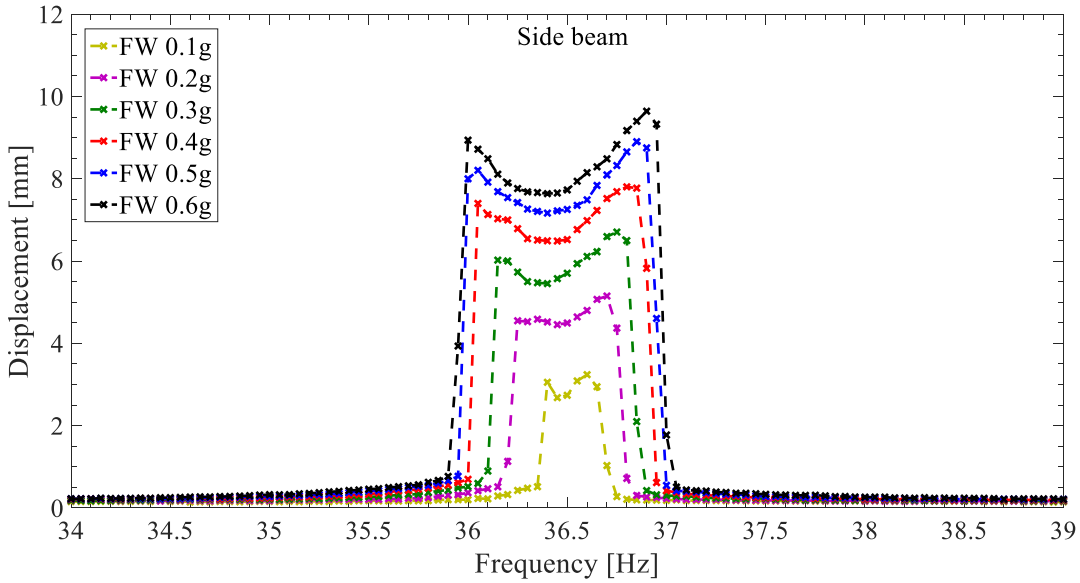
Side beam
FW 0.1g
FW 0.2g
FW 0.3g
FW 0.4g
FW 0.5g
FW 0.6g
Displacement [mm]
Frequency [Hz]
0
2
4
6
8
10
12
34
34.5
35
35.5
36
36.5
37
37.5
38
38.5
39

(b)

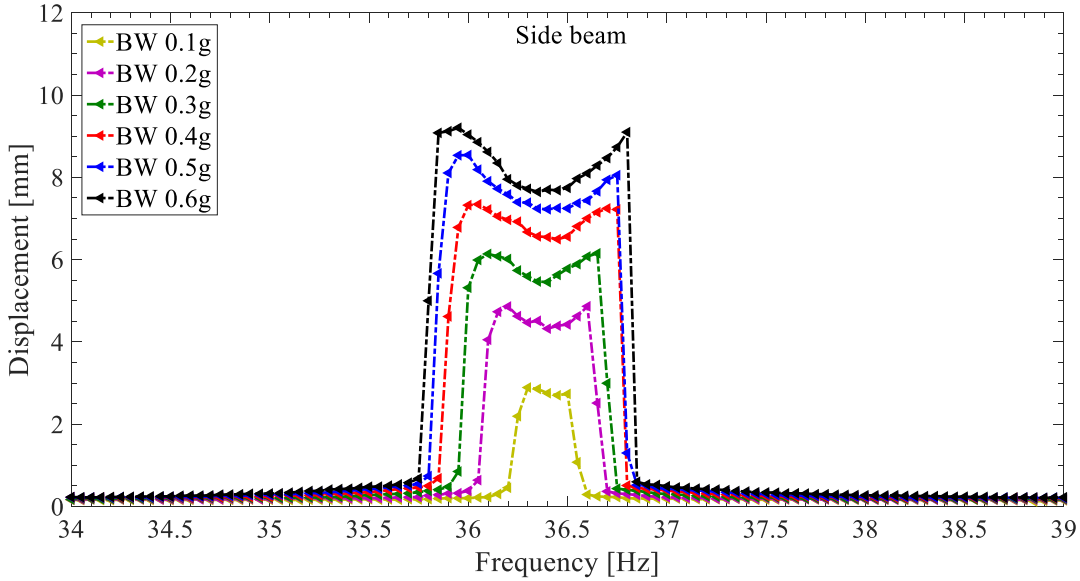
Side beam
BW 0.1g
BW 0.2g
BW 0.3g
BW 0.4g
BW 0.5g
BW 0.6g
Displacement [mm]
Frequency [Hz]
0
2
4
6
8
10
12
34
34.5
35
35.5
36
36.5
37
37.5
38
38.5
39

(c)

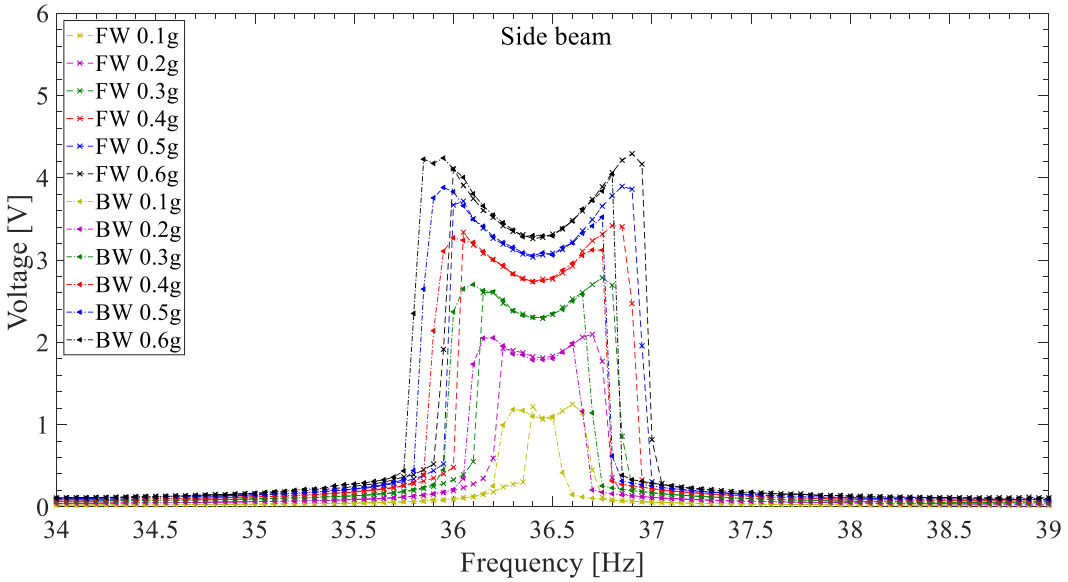

Figure 13. Under different base excitation level, the side beam responses at second resonant mode. Displacement-frequency responses a) forward plot and b) backward plot; c) voltage-frequency responses including both forward and backward plots.

(a)

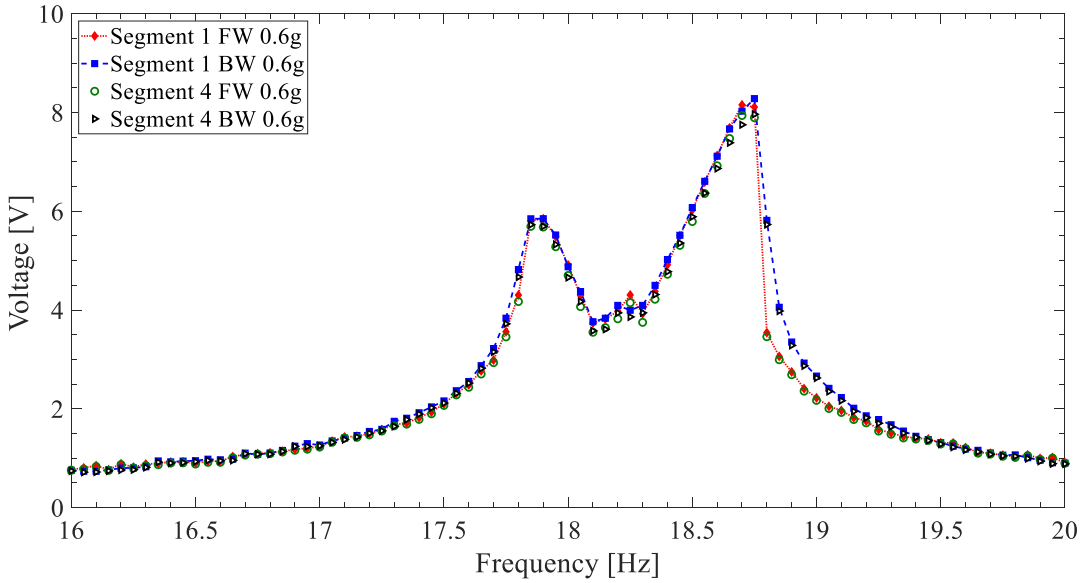

(b)

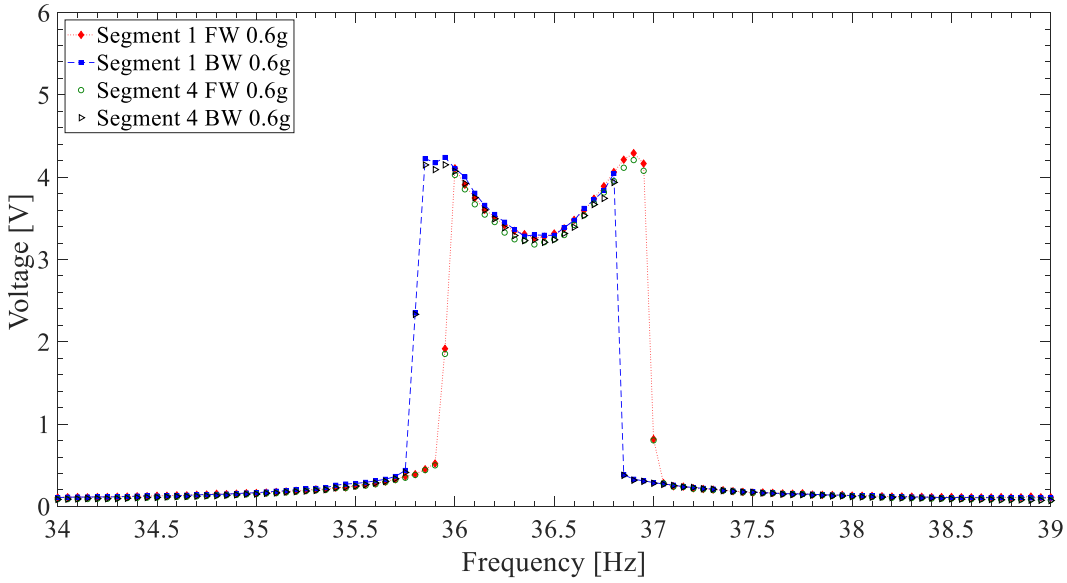

Figure 14. Comparison of voltage-frequency responses between two side beams (segments 1 and 4) at a) the first transverse mode and b) the second transverse mode.

Chapter 7

An Internal-Resonance based Piezoelectric Energy Harvester with Coupled Three-Dimensional Bending-Torsion Motions

This chapter is based on the following submitted paper (under review, April 2022):

Fan, Y., M.H. Ghayesh and T.-F. Lu, *A proof-of-concept study on an internal-resonance based piezoelectric energy harvester with coupled three-dimensional bending-torsion motions.* Submitted to: ASME Journal of Vibration and Acoustics..

Statement of Authorship

Title of Paper	A proof-of-concept study on an internal-resonance based piezoelectric energy harvester with coupled three-dimensional bending-torsion motions
Publication Status	☐ Published ☐ Accepted for Publication ☑ Submitted for Publication ☐ Unpublished and Unsubmitted w ork w ritten in manuscript style
Publication Details	

Principal Author

Name of Principal Author (Candidate)	Mr. Yimin Fan
Contribution to the Paper	Conceptualization, Investigation, Methodology, Validation, Writing - original draft, Software
Overall percentage (%)	80%
Certification:	This paper reports on original research I conducted during the period of my Higher Degree by Research candidature and is not subject to any obligations or contractual agreements with a third party that would constrain its inclusion in this thesis. I am the primary author of this paper.
Signature	Date: 27/01/2022

Co-Author Contributions

By signing the Statement of Authorship, each author certifies that:

i. the candidate's stated contribution to the publication is accurate (as detailed above);

ii. permission is granted for the candidate in include the publication in the thesis; and

iii. the sum of all co-author contributions is equal to 100% less the candidate's stated contribution.

Name of Co-Author	Dr. Mergen H. Ghayesh
Contribution to the Paper	Conceptualization, Investigation, Methodology, Supervision, Writing - review & editing
Signature	Date: 01/02/2022

Name of Co-Author	Dr. Tien-Fu Lu
Contribution to the Paper	Conceptualization, Investigation, Methodology, Supervision, Writing - review & editing
Signature	Date: 1/02/2022

A proof-of-concept study on an internal-resonance based piezoelectric energy harvester with coupled three-dimensional bending-torsion motions

Yimin Fan*, Mergen H. Ghayesh*, Tien-Fu Lu

School of Mechanical Engineering, University of Adelaide, South Australia, 5005, Australia

*Corresponding Author: yimin.fan@adelaide.edu.au; mergen.ghayesh@adelaide.edu.au

Highlights

- Both bending and shear strain changes can be captured for high-efficient energy conversion.
- An internal-resonance phenomenon is presented between bending and torsion modes for broadband energy harvesting, for the first time
- Multi-directional ambient vibration sources can be captured by the proposed device.
- Low excitation frequencies can trigger large-amplitude oscillations at higher modes.
- Quasi-periodic region exists near the centre frequencies of the coupled modes.

Abstract

Internal resonance based energy harvesters, by exchanging the internal energy between coupled vibration modes, may provide an effective solution to broadening and enhancing bandwidth and power performance in dealing with realistic vibration sources. With the development of piezoelectric-based transducers, cantilever-based energy harvesters which focus on bending modes, cannot utilise the shear deformation for energy conversion to sufficiently improve the power density. In this paper, we present an internal-resonance based piezoelectric energy harvester with three-dimensional coupled bending and torsional modes, for the first time. The fine-tuned system leverages a two-to-one internal resonance between its first torsion and second bending modes. The

dynamic behaviour implies the coexistence of in-plane and out-of-plane motions under a single excitation frequency, and the corresponding strain changes in the bending and shear directions are captured by bonded piezoelectric transducers. Dependence between excitation levels and the internal-resonance phenomenon is justified as a key system parameter study; the results also indicate an intriguing quasi-periodic region exists near the centre frequency. The outcomes of this study feature a multi-directional and multi-modal energy harvester that displays rich dynamic behaviours with coupled bending and torsional motions, and is promising for broadband energy harvesting, as well as enhancing the output voltage from both in-plane and out-of-plane motions.

1. Introduction

1.1 A brief review on vibration energy harvesters

As the trend of state-of-the-art electronic devices progressively becomes miniaturised and wireless, it is doubtful whether conventional electrochemical batteries are still promising in such low-power consumption devices. To achieve targeted applications such as powering up Internet of Things (IoT) sensor networks [1, 2] and medical implants [3], routine replacement and relatively high expense of conventional batteries limit the continuous and long-term usage performance of the devices. With the required power level of these devices reducing to sub-milliwatt, vibration-based energy harvesting techniques are feasible to provide continuous power supplies by converting environmental vibration sources into electrical energy. Nonlinear vibration-based energy harvesting has recently been shown to be an effective means of improving energy harvesting efficiency by broadening effective bandwidth and capturing a certain frequency range of vibration sources. The selected/designed nonlinear techniques, which should be effective for the specific themes, are primarily determined by the characteristics of ambient vibration sources including the excitation level and direction.

Multi-stable energy harvesting is a typical approach for broadening the operational bandwidth. Yan et al. [4] utilised magnetic restoring forces as externally induced nonlinearities to introduce bistability. By altering the system design parameters such as the distance between tip magnet on vibrating structure and stationary magnets, the system displayed softening and hardening frequency responses. bistability can also be achieved

by pre-loading approaches on beam-mass structures [5-9] and snap-through phenomena of laminated plate structures [10, 11]. The motion types of multi-stable energy harvester are highly dependent on acceleration levels. Periodic inter-well motion need a sufficient high excitation level to obtain enough energy for crossing the potential barrier between the two wells [12]. Under insufficient excitation levels, monostable systems surpassed bistable systems for both operational bandwidth and peak power level [13-15]. In dealing with small ambient excitation levels, parametrically excited energy harvester also need design techniques to reduce the initial threshold amplitudes [16-19]. In addition, piezoelectric materials with high power density compared with electromagnetic type transducers, are commonly utilised as strain-charge converters in vibration-based energy harvesting devices [20-22]. On the other hand, with additional damping effects, large-amplitude oscillations are even difficult to be triggered when the piezoelectric benders are bonded on the vibrating structure (i.e., a cantilever beam). To scavenge naturally varying vibration sources, multi-modal and multi-degree-of-freedom (MDOF) devices aim to utilise multiple adjacent natural frequencies to attain multiple peaks over a certain frequency range [23-26]. Energy harvesters with multiple close natural frequencies can provide a broader operational bandwidth, and some prototypes are also efficient under multi-directional ambient environmental vibration sources. However, the concerns are the complexity of design, as well as the sacrifice of power density. For some of the multi-modal energy harvesters, when the primary resonances are either commensurable or nearly commensurable, a nonlinear phenomenon named internal resonance can be possessed, which can potentially be used for energy harvesting optimisation.

1.2. Internal resonance benefits for energy harvesting

One of the typical phenomena is that the frequency response bends to increasing and decreasing frequency directions from the centre frequency as a double-jump phenomenon, which is considered an alternative solution within the broadband techniques [27]. Such a dynamic response can broaden the resonance regime in the presence of internal resonances [28, 29]. However, in most cases, a two-to-one (or three-to-one) internal resonance in fabricated simple cantilever beam structures can be difficult to achieve for the first few primary resonances. Thus, tuning techniques such as inducing external magnetic coupling effects are employed simultaneously [30-33]. By changing the

distance between the coupled magnets, the natural frequencies of the device can be tuned into designed values. Alternatively, a fine-tuned structure can be obtained by adding auxiliary structures to the main structure as an MDOF system [34]; for instance, an L-shaped beam and mass structure [35-38]. L-shaped structures are seem to be more practical than simple clamped-free beam-mass structures, with tailored system parameters such as beam dimensions and tip/side masses, commensurable natural frequencies can be obtained accordingly.

In spite of in-depth investigations on L-shaped energy harvesting deviced by using internal resonance phenomena, achieving internal resonances *between the first two bending modes* requires a sufficiently large ratio between the attached masses and the beam itself. For some cases, a large side mass block is essential to connect the two orthogonal beams because of the mismatched thicknesses and widths, which introduces more complexity into the system. On the other hand, for L-shaped energy harvesters with internal resonance phenomena, the mode couplings between natural frequencies is always between two bending modes (i.e., the first two transverse modes), and the harvested electrical energy is therefore limited to in-plane motions only. Such devices have raised a practical concern, with the rapid development of piezoelectric transducers that are capable of capturing both bending and torsional strain changes simultaneously, the out-of-plane motions are vital to optimise the power level.

1.3. Contributions of this work to the field

To provide an insight into the *internal resonance phenomenon between bending and torsional modes*, this paper, for the first time, proposes an internal-resonance based energy harvester with coupled in-plane and out-of-plane motions (i.e., torsion and bending modes couplings). Specifically, we study the responses of a multi-mode energy harvesting device (i.e., an L-shaped beam-mass structure with bonded piezoelectric elements as transducers) that exhibits *a two-to-one internal resonance between its first torsional and second bending modes* under external harmonic excitations. It is of interest to explore the feasibility of combining both in-plane and out-of-plane motions together under one single excitation frequency, as well as the possibility of enhancing the harvested voltage/power from piezoelectric transducers from both bending and torsional

motions and broadening the overall operational bandwidth by an internal resonance phenomenon.

2. Experimental setup and design

The first torsion and second bending modes are shown in Figs. 1 (a) and (b). A finite element method (FEM) via ANSYS (version 18.2, ANSYS, Inc., Cannonsburg, PA) were adopted for simulation and pre-testing of the proposed device. The results display in Figs. 1 (a) and (b) show that, without an internal resonance phenomenon, the first and second bending modes exhibit in-plane motions (Y-Z plane) and out-of-plane motions (X-Z plane) occur at the first torsion mode. Although most L-shaped energy harvesters with internal resonance focus on the first bending mode, for the sake of demonstration, we look into its second bending and first torsional modes and examine the functionality of coupling them together to possess internal resonance phenomena. The designed device, with its first bending mode occurring at 6.7 Hz, could also be utilised for energy harvesting as a linear resonator. The out-of-plane (torsion) motion of the L-shaped device is predominantly determined by the inertia of the horizontal beam and the tip mass: the torsional deformation of the vertical beam in the first three natural frequencies can therefore be neglected. The preliminary tests demonstrates that the optimising base excitation $W_b(t)$ is in the X-direction and the Y-direction for the first torsional and second bending modes, respectively. A schematic of the proposed device undergoes both bending and torsional motions is shown in Fig. 1 (c). Because the strain changes of the horizontal beam contain both bending and twisting deformations, piezoelectric transducers are chosen to be bonded onto the horizontal beam for high-efficient strain-voltage conversion.

Fig. 1 (d) presents the fabricated device and the main experimental setup. To tune an internal resonance between the first torsional and second bending modes, a 0.5 mm thick, 15.2 mm wide aluminium ($\rho_{Al} = 2650\ kg/m^3$) beam is bent into an L-shaped (right-angled) structure, with a 79.5 mm (l_h) horizontal beam (clamped end) and 74 mm (l_v) vertical beam (free end). A 9.5 gram tip mass is fixed onto the free end for tuning purposes. To obtain both bending and torsional motions for energy harvesting purpose, two MFC 0714-P2 (macro fibre composite) made of piezoelectric (PZT) material CTS3222HD are bonded onto the horizontal beam. The one with the fibres parallel to the horizontal beam

length measures the bending motion and the other with the fibres perpendicular to the horizontal beam length measures the torsional motion. Two Wenglor CP24MHT80 laser sensors measure the bending displacement at the centre line position along the horizontal beam length in the Z-direction and the torsional displacement in the X-direction by attaching an external plane that is placed parallel to the Z-direction (see Fig. 1 (d)). A shaking table APS 113, which is driven by an APS 115 amplifier, provides harmonic excitations $W_b(t) = Fcos(\omega t)$, where F is the forcing amplitude and ω is the excitation frequency. The acceleration amplitude of the base excitation is recorded by an accelerometer Kistler 8774A50 and its coupler Kistler 5134B, and the generated voltage from each of the PZT layers are measured across a resistive load of $R_L = 150$ kΩ. All the measured signals are recorded to a data acquisition board NI USB-6281. The steady state frequency response of the proposed device is obtained by employing both an upward and a downward sweep with 0.05 Hz frequency internal, 10 seconds of settling time, a 1 kHz sampling rate and constant base acceleration levels.

(a)

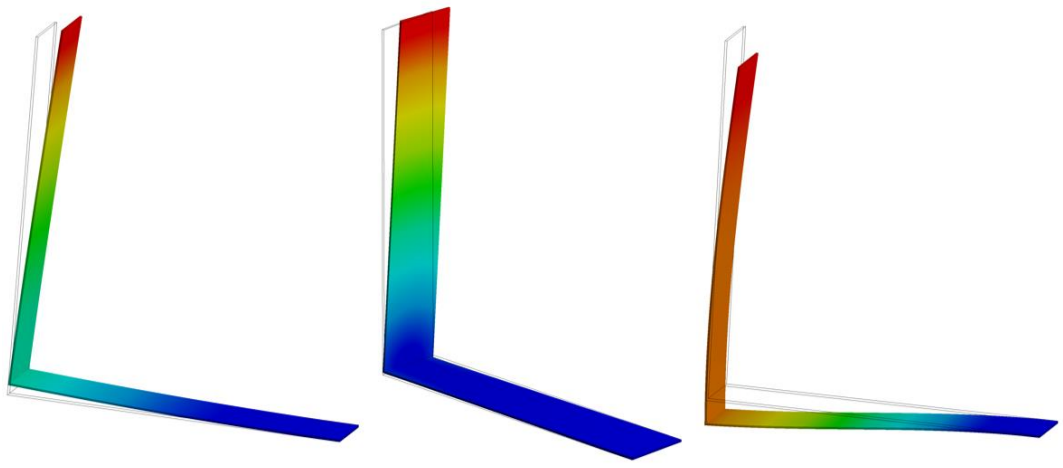

First bending mode First torsion mode second bending mode

(b)

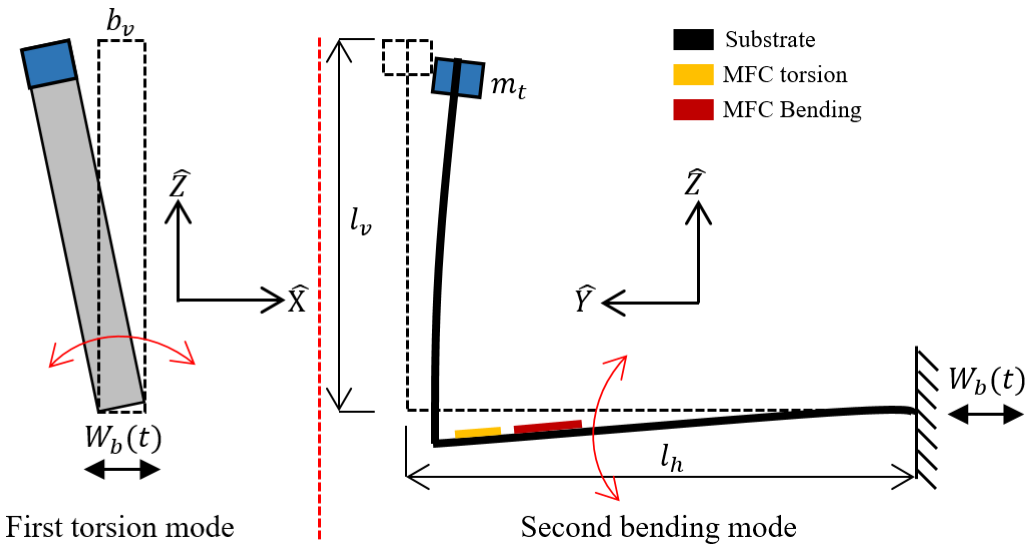
b_v
$\hat{Z}$
$\hat{X}$
$W_b(t)$
l_v
m_t
Substrate
MFC torsion
MFC Bending
$\hat{Z}$
$\hat{Y}$
$W_b(t)$
l_h
First torsion mode
Second bending mode

(c)

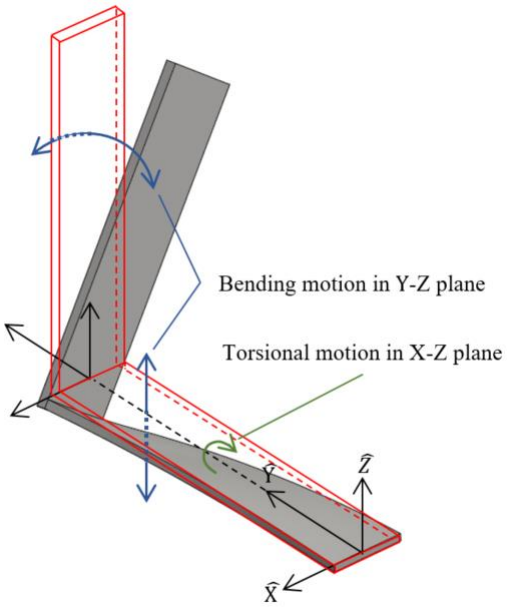
Bending motion in Y-Z plane
Torsional motion in X-Z plane
$\hat{Z}$
$\hat{Y}$
$\hat{X}$

(d)

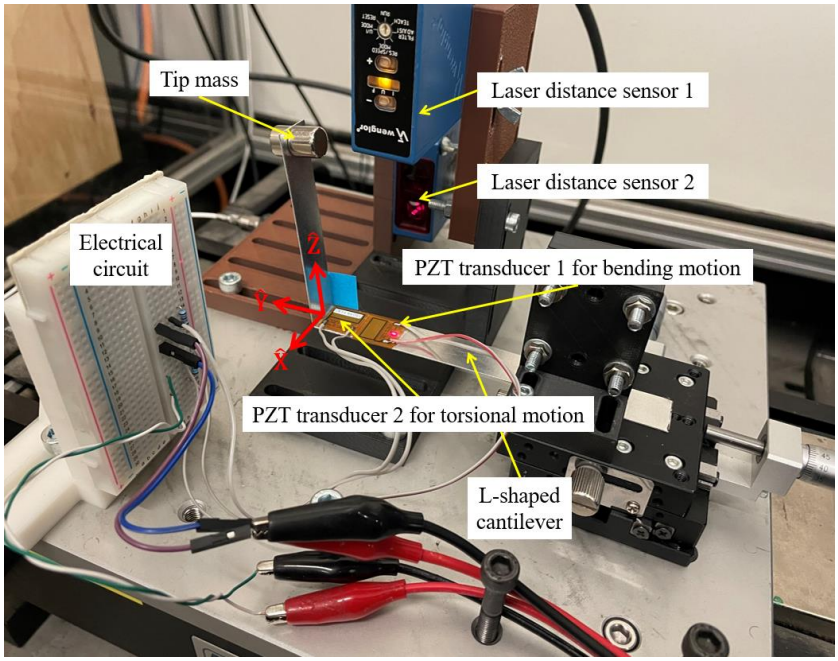

Figure 1. (a) Simulated results of the first three modes of proposed devices by FEM. (b) Schematics of the mode shapes of an L-shaped energy harvesting device of its first torsional mode (top left) and second bending mode (top right). (c) Schematics of the proposed device with coupled bending-torsion motions. (d) Experimental setup of the core elements.

3. Results and discussion

With preliminary testings and optimisations completed, the measured first three modes of the L-shaped device are $\omega_1 = 6.7$ Hz, $\omega_2 = 10.9$ Hz and $\omega_3 = 22.1$ Hz. The proposed structure leverages the relationship between ω_2 and ω_3 of a 1:2 ratio for inducing a two-to-one internal resonance. The device is firstly excited under 0.4 g peak-to-peak ($g = 9.81\, N/s^2$) up (from 9 Hz to 14 Hz) and down (from 14 Hz to 9 Hz) base accelerations in X-direction as out-of-plane excitations within its first torsional mode ($\omega \cong \omega_2$). Fig. 2 depicts the voltage-frequency and displacement-frequency responses from the PZT and laser sensors, respectively. Two peaks are revealed at 10.15 Hz to 12.2 Hz in both bending and torsion motions, which implies there is an internal resonance phenomenon between the torsional and bending modes and resonance energy is transferred to the second bending mode. The frequency responses show that the two branches are asymmetrical and there exists a quasi-periodic region between the left peak and the centre frequency region (Figs. 2 (a) and (b)). The right branch has an upward

jump at 11.65 Hz, but the peak of on the left occurs at 10.95 Hz, which is within the quasi-periodic region.

Compared with the bending motion, the torsional motion distinguishes the left branch and the quasi-periodic region in the frequency response. It is particularly important to see that although the energy transfers between the two coupled modes in the presence of an internal resonance phenomenon, there is no obvious jump phenomenon occur between the upward and downward harmonic excitations, except a narrow 0.1 Hz bifurcation near the left peak. For the system behaviours at the off-resonance regime, the bending motions (in Y-Z plane) have an almost zero response while torsion motions (X-Z plane) exhibit a non-zero response, which is due to the direction of the base excitation. When the direction of excitation is parallel to the torsional motion, the device is prone to oscillate in the X-Z plane because of the inertia of the tip mass block and horizontal beam. Figs. 2 (c) and (d) depict the harvested voltages from the bending and torsional PZT layers, respectively. Based on the level of displacement, the bending motion results in a larger peak voltage, which is consistent with the measured results from the laser sensors. The peak-to-peak voltages V_{p-p} of bending and torsion motions are up to 9.15 V and 6.52 V, respectively. It can be seen that the output voltage from the torsional motion is resemble to the bending motion. Although the torsional PZT is bonded in perpendicular to the beam length, it still generates charges in the fibre perpendicular direction. Hence, the output voltages in Figs. 2 (c) and (d) consist of both bending and torsional motions.

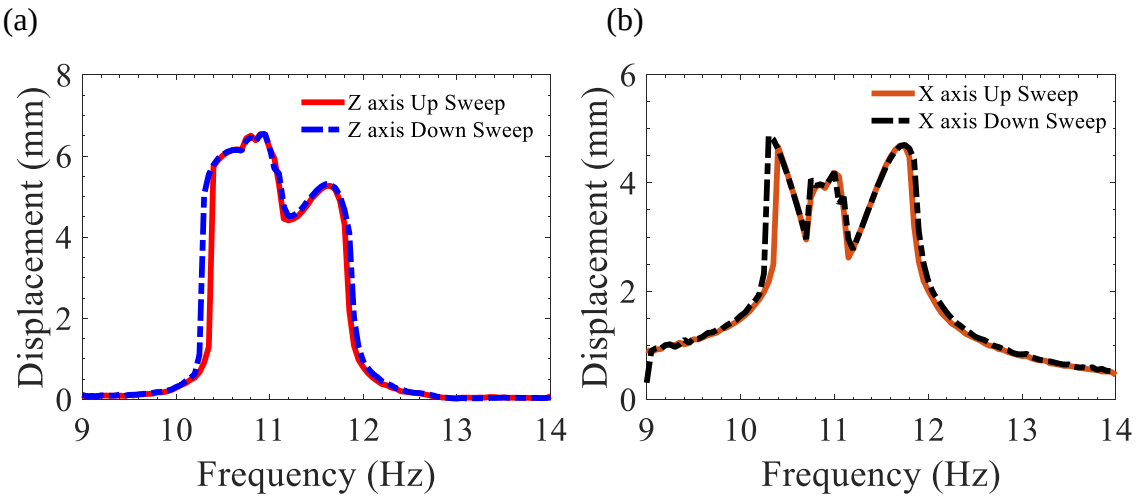

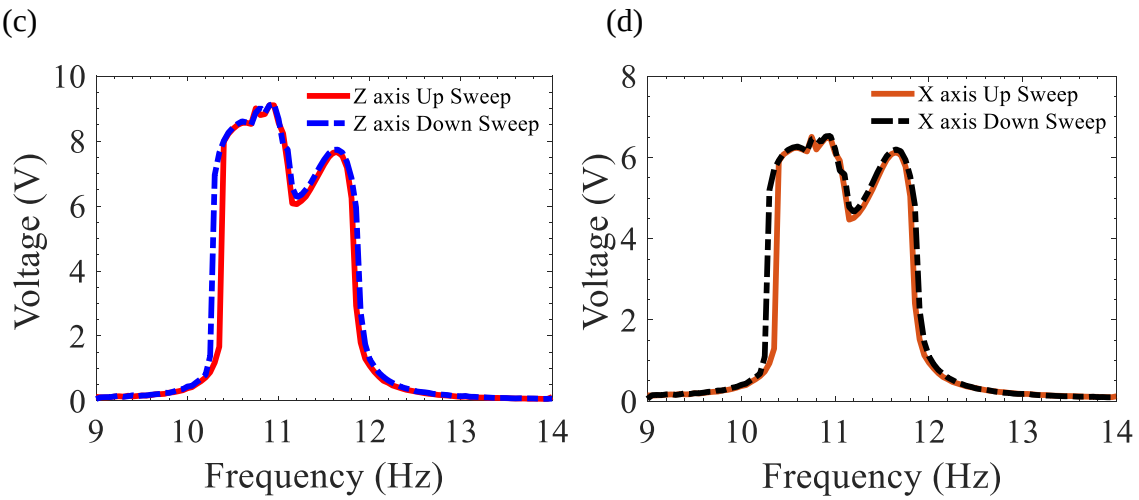

Figure. 2. The proposed device excited at its first torsion mode under a 0.4 g base acceleration. Frequency responses from laser sensors of (a) bending motion and (b) torsional motion; output voltages from (c) bending PZT and (d) torsional PZT.

The steady-state responses of the proposed device under 0.4 g in-plane (Y-axis) base excitations within its second bending mode are shown in Fig. 3. The experimental results present a large amplitude double-jump phenomenon, and the two branches are bent into opposite directions from the centre frequency. The overall resonance regime is from 21.1 Hz to 23.3 Hz. The results shown in Figs. 2 and 3 demonstrate that, the dynamic responses provide key evidence that the device exhibits a two-to-one internal resonance between its first torsional and second bending modes. Between the coupled two modes, excitation frequency at lower mode can trigger large-amplitude oscillations at higher modes, and vice versa. With piezoelectric transducers in both bending and torsional directions, the power density of the device is greatly enhanced. As shown in Fig. 3 (a), the bending motion undergoes an upward jump at 22.8 Hz and a downward jump at 21.65 Hz, ending at 23.25 Hz and 21.1 Hz, respectively. The downward response displays asymmetric branches that suggests the left branch has a much higher peak than the right one in downward sweep case, and the bandwidths due to bifurcation, are slightly broader than for the upward case (0.55 Hz vs 0.45 Hz). The frequency responses of the bending motion shown in Fig. 3 (b) depict a more symmetric resonance region in terms of bandwidth and amplitude. The peak-to-peak voltages from bending (Fig. 3 (c)) and torsional (Fig. 3 (d)) PZTs are 6.63 V and 4.69 V respectively.

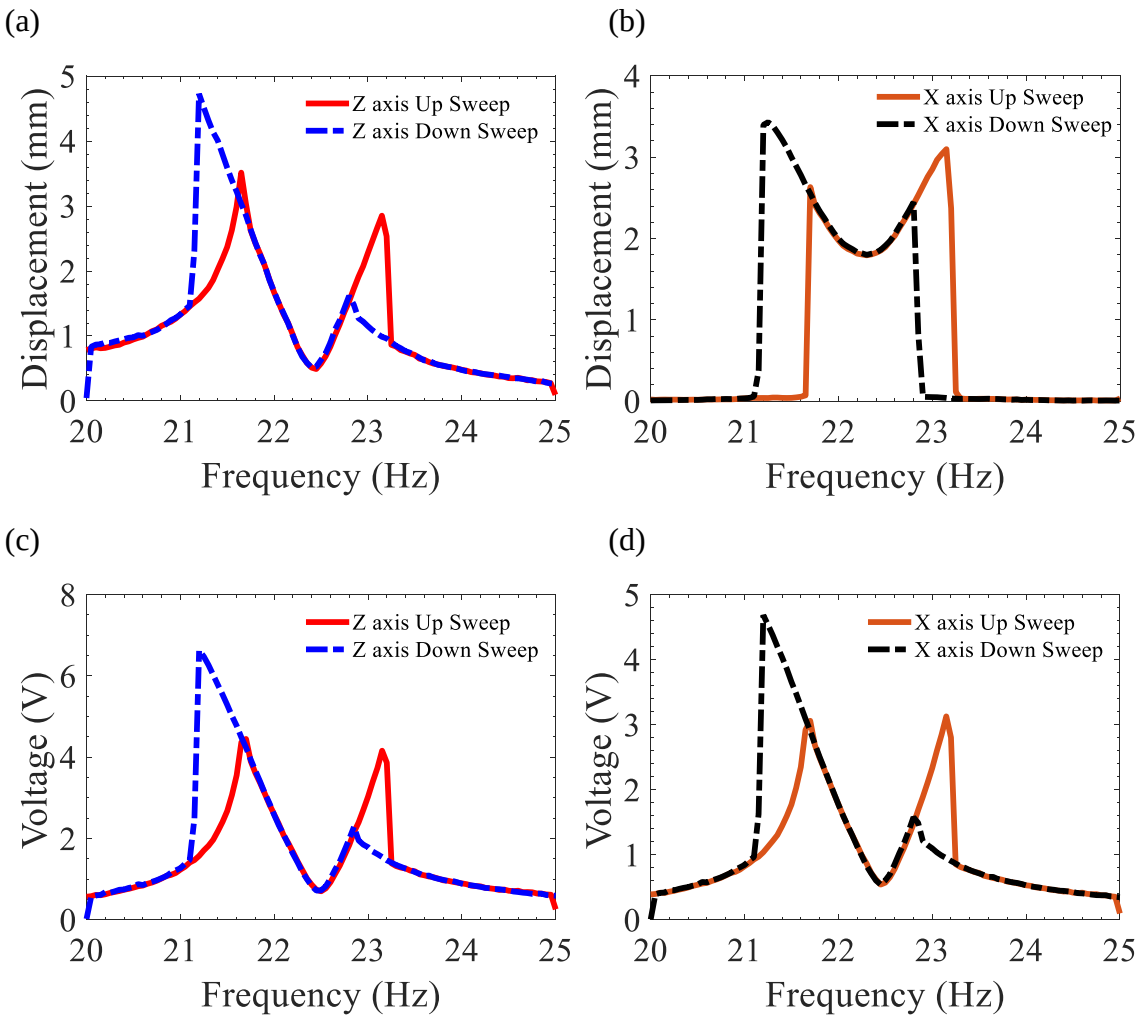

Figure. 3. The proposed device excited at its second bending mode under a 0.4 g base acceleration. Frequency responses from laser sensors of (a) bending motion and (b) torsional motion; output voltages from (c) bending PZT and (d) torsional PZT.

To understand the difference between the dynamic behaviours across the bending and torsional motions and to examine the internal-resonance phenomenon further, the time trace and frequency spectra diagrams of the two coupled modes are displayed in Fig. 4. The peaks of the right branches in both modes are selected for comparison. As shown in Figs. 4 (a) – (d), the frequency spectrum shows coexisting responses at 11.5 Hz and 23 Hz for bending and torsional motions, and there are no contributions for the first bending mode ω_1 (6.7 Hz). The time trace plots from torsional PZTs in Figs. 4 (b) and (d) show the coexistent responses clearly. Thus, we can conclude that the two-to-one internal resonance from the experimental results fall between the first torsional and second bending modes. It is predicable that the frequency spectrum of the torsional PZTs will have lower responses to the first torsional mode, because the selected transducer is a d_{31}

type contractor that will still generate charges in the fibre perpendicular directions. For future industrial applications, piezoelectric transducers work for detecting shear stress/strain can further enhance the power performance for torsional mode.

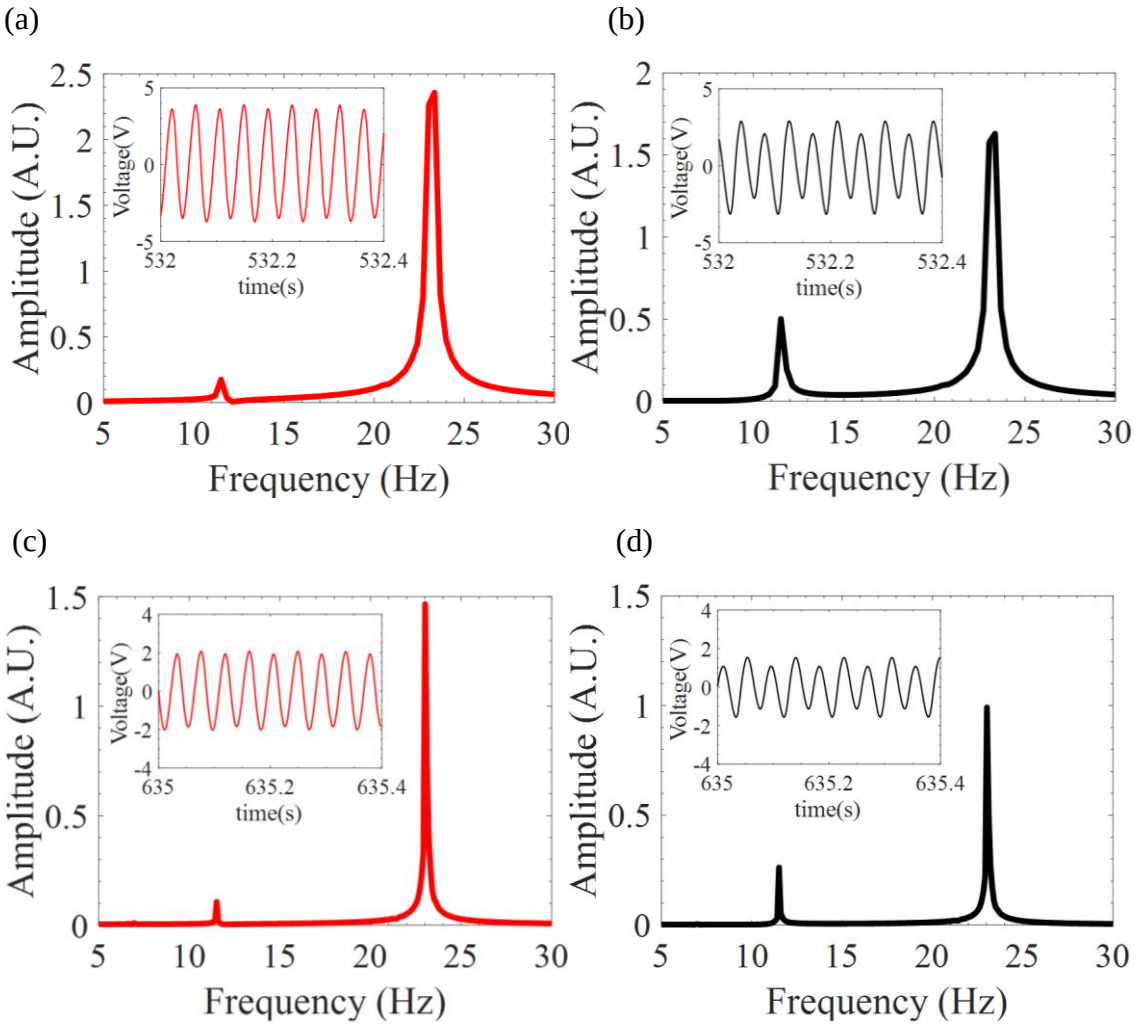

Figure 4. Time trace and frequency spectra diagrams under 0.4 g base excitations from bending (left) and torsional (right) PZTs: (a) and (b) excited at 11.65 Hz, (c) and (d) excited at 21 Hz.

The experimental results presented in Fig. 5 are the voltage phase plane diagrams measured at the steady-state responses at left peak, near centre frequency and right peak positions for both first torsional and second bending modes. The coexistent responses for bending and torsional motions are agreed with the frequency spectrums shown in Fig. 4. Although the time series and frequency spectra of the bending PZTs may not obviously illustrate if the torsional mode is induced, the phase plane diagrams identify the two coexistent responses. Given that there may exist initial geometric nonlinearities in the system, the phase plane diagrams depict asymmetric motions. Likewise, the left and right

branches in frequency responses (Figs. 2 and 3) are not perfectly symmetric. At the centre frequency position of an internal resonance phenomenon, the system generally displays the lowest amplitude. Nevertheless, as shown in Fig. 5 (b), the device exhibit large-amplitude oscillations at 11.15 Hz, which is much higher than the oscillations shown in Fig. 5 (e). As the amplitude of the centre frequency position remain as an effective level of energy harvesting, the device displays a continually effective bandwidth when the excitation is within the first torsional mode.

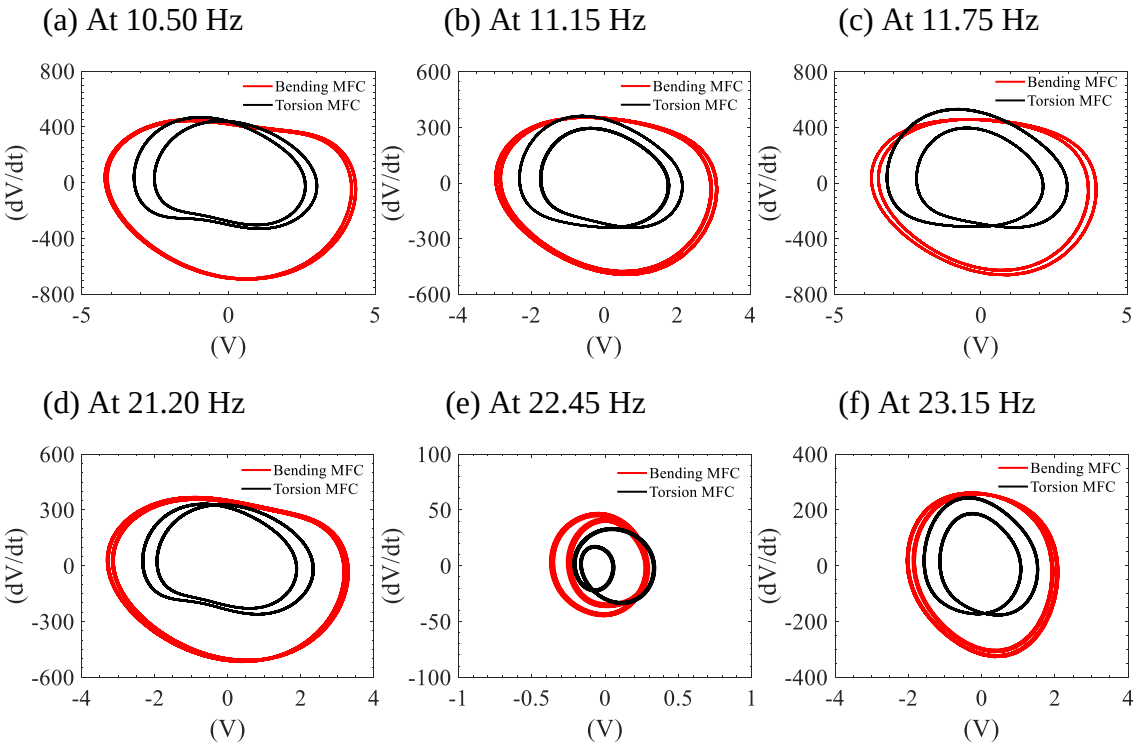

Figure 5. Phase plane diagrams of the steady-state voltage responses at left peak, centre frequency and right peak positions when excited within the first torsional mode region (a) – (c) and the second bending mode region (e) – (f).

As mentioned above, the quasi-periodic response shown in Fig. 2 implies there are unstable dynamic behaviours in the system, and the output voltage from the bonded PZTs are even higher than the peak positions of the two branches. To study the instability in the system, the time series of the overall region and motion of each frequency interval are shown in Figs. 6 (a) and (b), respectively. Eight different quasi-periodic motions are revealed in Fig. 6 (b). It should be noted that, with a settling time of 10 seconds for each interval, and a small 0.05 Hz frequency increment, the quasi-periodic motions are no longer in the transient state. In addition, the amplitudes in the time series (Fig. 6 (a)) for

both bending and torsional motions undergo periodic and uniform variations. The results suggest that, there is a certain region of quasi-periodic motions existing in the presence of this two-to-one internal resonance phenomenon when the base excitation frequency is within its first torsional mode, the bandwidth and location of this region remain as the same in either up sweep or down sweep.

(a)

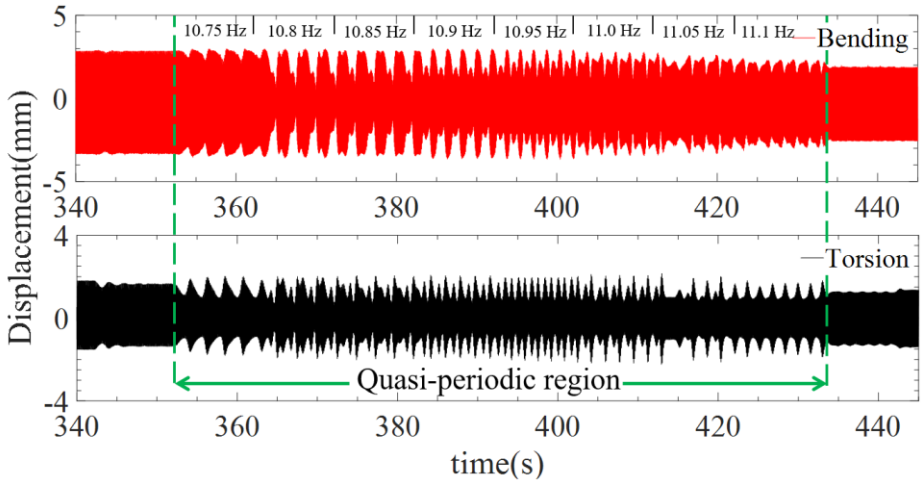

(b)

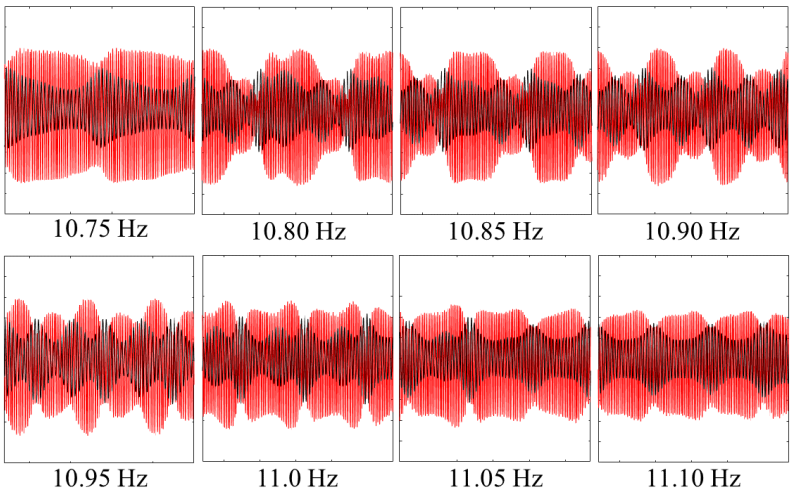

Figure 6. The time series of quasi-periodic region in bending and torsional motions when harmonically excited (up sweep) at the first torsional mode: (a) overall quasi-periodic region, (b) the quasi-periodic motions under different excitation frequency from 10.75 Hz to 11.1 Hz.

It is intriguing to investigate the effects of forcing excitation amplitude on the device: to demonstrate, if a certain threshold amplitude exists for the internal-resonance

phenomenon, bandwidth performance of the proposed device under small excitations, as well as the dynamic behaviours of the quasi-periodic motions. Fig. 7 shows the frequency responses of the device under different excitation levels. As can be seen, the internal resonance phenomenon exists even under a 0.2 g acceleration level. For excitations within the first torsional mode (Figs. 7 (a) and (b)), the left branch always has a 0.1 Hz bifurcation between the upward and downward harmonic sweep under all three excitation levels. The effective bandwidths in the bending motion from the 0.2 g to 0.4 g cases with 0.5 mm reference level are 1.35 Hz, 1.75 Hz and 2.05 Hz, respectively. With increasing levels of base excitation, the bandwidth increments become slightly smaller for the cases that excite within the first torsional mode. For the second bending mode, the double-jump phenomena were presented in Figs. 7 (c) and (d). The two branches are bent into opposite directions from the centre frequency at 22.3 Hz, the left branch in bending motion exhibits much higher and broader jumps in the downward sweep, while the torsional motion has more symmetrical bifurcations. Unlike the first torsional mode, the bandwidths for the 0.3 g case are closely similar to the 0.4 g case (2.15 Hz vs 2 Hz). However, under 0.2 g base excitations, the bandwidth has a substantial drop to 1.5 Hz. The comparison illustrates that, modes coupling occurs in all three cases, the amplitude of vibration still depends on the base excitation level, although with a further increased excitation level, its impacts on the bandwidth increment become smaller. The quasi-periodic region can still be captured at a 0.2 g base excitation, although the bandwidth becomes narrow and closer to the centre frequency at 11.15 Hz, the left branch in bending motion (Fig. 7 (a)), still has a lower peak amplitude than the quasi-periodic region. In terms of the voltage level shown in Fig. 8, the power dissipated in the loading resistor can be obtained by $P = V^2/R_L$. The peak power levels measure from bending and torsional PZTs are up to 0.56 mW and 0.28 mW, respectively, for excitations within the first torsional mode; the peak power levels reduce to 0.29 mW and 0.17 mW for bending and torsional PZTs, respectively in second bending mode with relatively lower-amplitude oscillations.

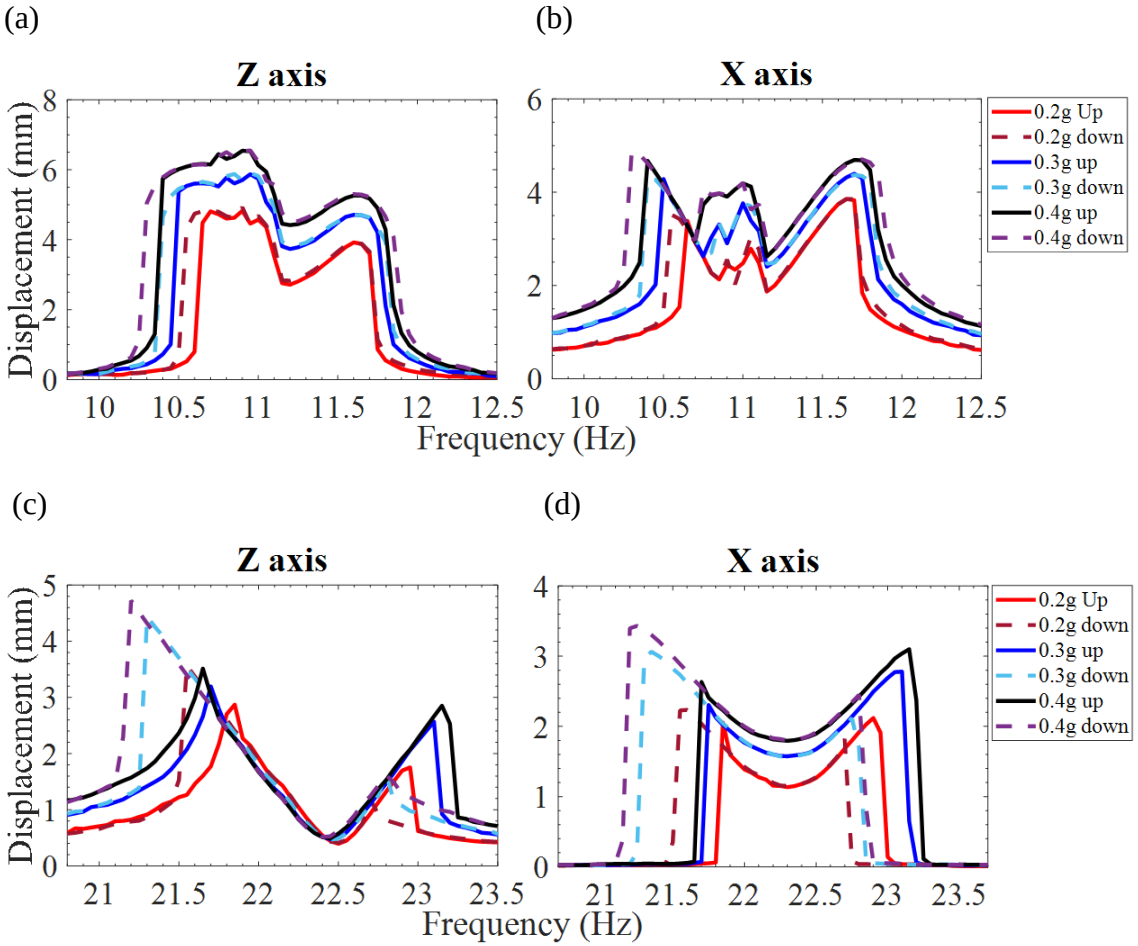

Figure 7. Displacement-frequency responses of the proposed device under 0.2 g, 0.3 g and 0.4 g base excitations. Bending (a) and torsional (b) motions when excited at the first torsional mode, Bending (c) and torsional (d) motions when excited at the second transverse mode.

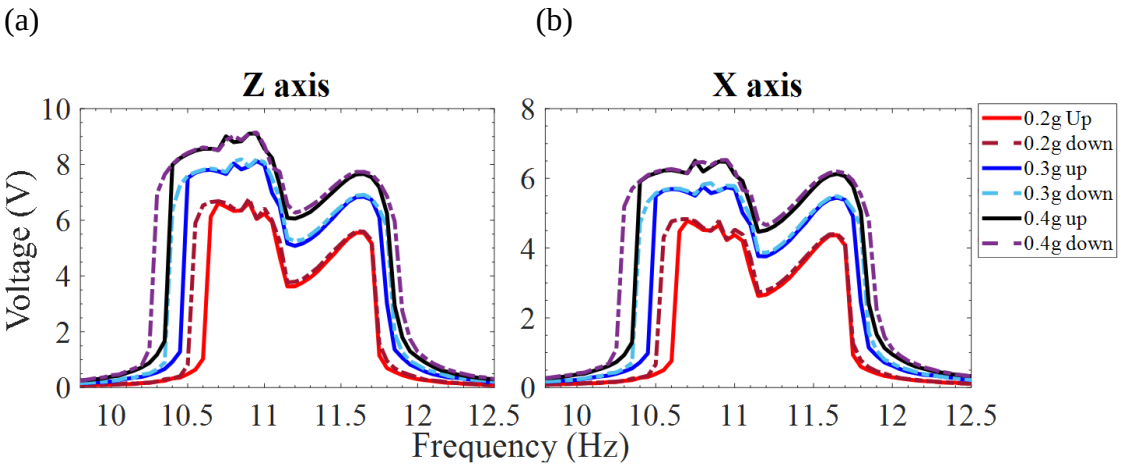

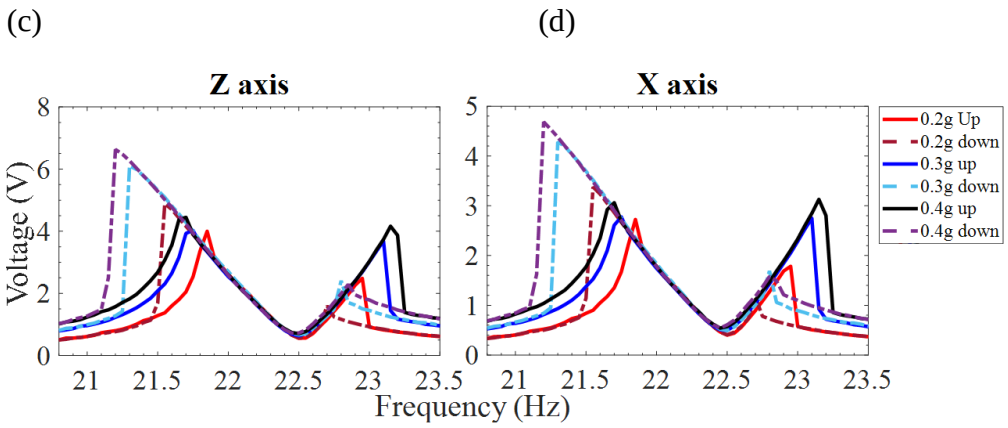

Figure 8. Voltage-frequency responses from PZTs of the proposed device under 0.2 g, 0.3 g and 0.4 g base excitations. Bending (a) and torsional (b) motions when excited at the first torsional mode, Bending (c) and torsional (d) motions when excited at the second transverse mode.

4. Conclusions

The work attempts to enhance the power and bandwidth performance of a vibration-based energy harvester by introducing bending-torsion couplings and an internal resonance phenomenon on a simple L-shaped beam-mass structure, for the first time. An enhanced power density is achieved as both bending and torsional strain changes are utilised for strain-voltage conversion; a broader overall bandwidth is obtained in the presence of an internal resonance phenomenon.

In summary, the paper presents a two-to-one internal-resonance based piezoelectric energy harvester with combined three-dimensional bending and torsional modes in an L-shaped structure. With fine-tuned system parameters, a two-to-one internal resonance phenomenon was revealed between the first torsion and second bending modes under ambient frequency range. The system with mode coupling exhibited both in-plane and out-of-plane motions simultaneously under a single excitation frequency and featured rich nonlinear dynamic behaviours such as double-jump and quasi-periodic motions. In the presence of the internal-resonance phenomenon, the frequency responses of the coupled two modes were bent into opposite directions from centre positions, which yielded broader operational bandwidths for both modes. With energy exchanges between the two coupled modes, the excitation frequency sources within the lower mode resonance region enabled large-amplitude oscillations at the higher coupled mode and vice versa, which resulted higher power density than conventional multi-mode/MDOFs devices. In order to

optimise the harvested power level to a greater extent and utilise the piezoelectric transducers more efficiently, with bending-torsion modes coupling, the torsional strain changes due to the out-of-plane motions were also captured by PZTs and converted into electrical form. The effects of excitation levels are investigated as a parametric study to justify the robustness of the device under small excitation levels. To further enhance the power output, fully covered piezoelectric materials (i.e., unimorph or bimorph) that can efficiently convert shear strain changes are suggested in practical applications.

Acknowledgement

This work has been supported by the Australian Government Research Training Program. The support is greatly appreciated.

References

1. Shaikh, F.K. and S. Zeadally, *Energy harvesting in wireless sensor networks: A comprehensive review.* Renewable and Sustainable Energy Reviews, 2016. **55**: p. 1041-1054.
2. Bedi, G., G.K. Venayagamoorthy, R. Singh, R.R. Brooks, and K. Wang, *Review of internet of things (iot) in electric power and energy systems.* IEEE Internet of Things Journal, 2018. **5**(2): p. 847-870.
3. Jiang, D., B. Shi, H. Ouyang, Y. Fan, Z.L. Wang, and Z. Li, *Emerging implantable energy harvesters and self-powered implantable medical electronics.* ACS Nano, 2020. **14**(6): p. 6436-6448.
4. Yan, Z., W. Sun, M.R. Hajj, W. Zhang, and T. Tan, *Ultra-broadband piezoelectric energy harvesting via bistable multi-hardening and multi-softening.* Nonlinear Dynamics, 2020. **100**(2): p. 1057-1077.
5. Qian, F., S. Zhou, and L. Zuo, *Approximate solutions and their stability of a broadband piezoelectric energy harvester with a tunable potential function.* Communications in Nonlinear Science and Numerical Simulation, 2020. **80**: p. 104984.
6. Derakhshani, M., N. Momenzadeh, and T.A. Berfield, *Analytical and experimental study of a clamped-clamped, bistable buckled beam low-frequency pvdf vibration energy harvester.* Journal of Sound and Vibration, 2021. **497**: p. 115937.
7. Huang, X. and B. Yang, *Improving energy harvesting from impulsive excitations by a nonlinear tunable bistable energy harvester.* Mechanical Systems and Signal Processing, 2021. **158**: p. 107797.
8. Wang, Z., T. Li, Y. Du, Z. Yan, and T. Tan, *Nonlinear broadband piezoelectric vibration energy harvesting enhanced by inter-well modulation.* Energy Conversion and Management, 2021. **246**: p. 114661.
9. Zhang, C., R.L. Harne, B. Li, and K.W. Wang, *Harmonic analysis and experimental validation of bistable vibration energy harvesters interfaced with rectifying electrical circuits.* Communications in Nonlinear Science and Numerical Simulation, 2020. **82**: p. 105069.

10. Emam, S.A., J. Hobeck, and D.J. Inman, *Experimental investigation into the nonlinear dynamics of a bistable laminate.* Nonlinear Dynamics, 2019. **95**(4): p. 3019-3039.
11. Wu, M.Q., W. Zhang, and Y. Niu, *Experimental and numerical studies on nonlinear vibrations and dynamic snap-through phenomena of bistable asymmetric composite laminated shallow shell under center foundation excitation.* European Journal of Mechanics - A/Solids, 2021. **89**: p. 104303.
12. Sengha, G.G., W.F. Kenfack, M.S. Siewe, C.B. Tabi, and T.C. Kofane, *Dynamics of a non-smooth type hybrid energy harvester with nonlinear magnetic coupling.* Communications in Nonlinear Science and Numerical Simulation, 2020. **90**: p. 105364.
13. Xie, Z., S. Zhou, J. Xiong, and W. Huang, *The benefits of a magnetically coupled asymmetric monostable dual-cantilever energy harvester under random excitation.* Journal of Intelligent Material Systems and Structures, 2019. **30**(20): p. 3136-3145.
14. Nguyen, H.T., D. Genov, and H. Bardaweel, *Mono-stable and bi-stable magnetic spring based vibration energy harvesting systems subject to harmonic excitation: Dynamic modeling and experimental verification.* Mechanical Systems and Signal Processing, 2019. **134**: p. 106361.
15. Huang, Y., W. Liu, Y. Yuan, and Z. Zhang, *High-energy orbit attainment of a nonlinear beam generator by adjusting the buckling level.* Sensors and Actuators A: Physical, 2020. **312**: p. 112164.
16. Djomo Mbong, T.L.M., M. Siewe Siewe, and C. Tchawoua, *Controllable parametric excitation effect on linear and nonlinear vibrational resonances in the dynamics of a buckled beam.* Communications in Nonlinear Science and Numerical Simulation, 2018. **54**: p. 377-388.
17. Fan, Y., M.H. Ghayesh, and T.-F. Lu, *A broadband magnetically coupled bistable energy harvester via parametric excitation.* Energy Conversion and Management, 2021. **244**: p. 114505.
18. Fan, Y., M.H. Ghayesh, and T.-F. Lu, *Enhanced nonlinear energy harvesting using combined primary and parametric resonances: Experiments with theoretical verifications.* Energy Conversion and Management, 2020. **221**: p. 113061.
19. Tan, T., Z. Wang, L. Zhang, W.-H. Liao, and Z. Yan, *Piezoelectric autoparametric vibration energy harvesting with chaos control feature.* Mechanical Systems and Signal Processing, 2021. **161**: p. 107989.
20. Wang, J., S. Cai, L. Qin, D. Liu, P. Wei, and L. Tang, *Modeling and electromechanical performance analysis of frequency-variable piezoelectric stack transducers.* Journal of Intelligent Material Systems and Structures, 2020. **31**(6): p. 897-910.
21. Baroudi, S., H. Samaali, and F. Najar, *Energy harvesting using a clamped–clamped piezoelectric–flexoelectric beam.* Journal of Physics D: Applied Physics, 2021. **54**(41): p. 415501.
22. Yuan, T.-C., J. Yang, and L.-Q. Chen, *Nonlinear dynamics of a circular piezoelectric plate for vibratory energy harvesting.* Communications in Nonlinear Science and Numerical Simulation, 2018. **59**: p. 651-656.
23. Dhote, S., Z. Yang, K. Behdinan, and J. Zu, *Enhanced broadband multi-mode compliant orthoplanar spring piezoelectric vibration energy harvester using magnetic force.* International Journal of Mechanical Sciences, 2018. **135**: p. 63-71.
24. Hu, G., J. Liang, C. Lan, and L. Tang, *A twist piezoelectric beam for multi-directional energy harvesting.* Smart Materials and Structures, 2020. **29**(11): p. 11LT01.
25. Wang, X., H. Wu, and B. Yang, *Nonlinear multi-modal energy harvester and vibration absorber using magnetic softening spring.* Journal of Sound and Vibration, 2020. **476**: p. 115332.
26. Tan, Q., K. Fan, K. Tao, L. Zhao, and M. Cai, *A two-degree-of-freedom string-driven rotor for efficient energy harvesting from ultra-low frequency excitations.* Energy, 2020. **196**: p. 117107.
27. Chen, L.-Q. and W.-A. Jiang, *Internal resonance energy harvesting.* Journal of Applied Mechanics, 2015. **82**(3).

28. Nayfeh, A.H., B. Balachandran, M.A. Colbert, and M.A. Nayfeh, *An experimental investigation of complicated responses of a two-degree-of-freedom structure*. Journal of Applied Mechanics, 1989. **56**(4): p. 960-967.
29. Chen, L.-Q., W.-A. Jiang, M. Panyam, and M.F. Daqaq, *A broadband internally resonant vibratory energy harvester*. Journal of Vibration and Acoustics, 2016. **138**(6).
30. Xiong, L., L. Tang, and B.R. Mace, *Internal resonance with commensurability induced by an auxiliary oscillator for broadband energy harvesting.* Applied Physics Letters, 2016. **108**(20): p. 203901.
31. Yang, W. and S. Towfighian, *A hybrid nonlinear vibration energy harvester*. Mechanical Systems and Signal Processing, 2017. **90**: p. 317-333.
32. Wu, Y., H. Ji, J. Qiu, W. Liu, and J. Zhao, *An internal resonance based frequency up-converting energy harvester*. Journal of Intelligent Material Systems and Structures, 2018. **29**(13): p. 2766-2781.
33. Xie, Z., B. Huang, K. Fan, S. Zhou, and W. Huang, *A magnetically coupled nonlinear t-shaped piezoelectric energy harvester with internal resonance.* Smart Materials and Structures, 2019. **28**(11): p. 11LT01.
34. Dai, H., X. Wang, M. Schnoor, and S.N. Atluri, *Analysis of internal resonance in a two-degree-of-freedom nonlinear dynamical system.* Communications in Nonlinear Science and Numerical Simulation, 2017. **49**: p. 176-191.
35. Cao, D.X., S. Leadenham, and A. Erturk, *Internal resonance for nonlinear vibration energy harvesting.* The European Physical Journal Special Topics, 2015. **224**(14): p. 2867-2880.
36. Harne, R.L., A. Sun, and K.W. Wang, *Leveraging nonlinear saturation-based phenomena in an l-shaped vibration energy harvesting system.* Journal of Sound and Vibration, 2016. **363**: p. 517-531.
37. Nie, X., T. Tan, Z. Yan, Z. Yan, and M.R. Hajj, *Broadband and high-efficient l-shaped piezoelectric energy harvester based on internal resonance.* International Journal of Mechanical Sciences, 2019. **159**: p. 287-305.
38. Li, H., D. Liu, J. Wang, X. Shang, and M.R. Hajj, *Broadband bimorph piezoelectric energy harvesting by exploiting bending-torsion of l-shaped structure.* Energy Conversion and Management, 2020. **206**: p. 112503.

Chapter 8

Conclusions and Recommendations

8.1 Conclusions

In this thesis, theoretical and experimental investigations on enhancing the bandwidth performance of vibration-based energy harvesters by employing structural and externally induced nonlinearities have been carried out, so as to optimise the overall power level for high-efficient energy harvesting. The research efforts in the literature review have demonstrated the limitations in linear VEHs; the narrow bandwidth of the resonance can only adapt to stationary excitation sources. Therefore, the nature of environmental vibration sources brings out the underlying motivation of utilising nonlinearities in VEHs – devices should be effectively operational under environmental vibration sources. Yet, for existing nonlinear VEHs, in some instances, the functionality of the devices requires harsh excitation conditions such as high excitation level and uni-direction. Thus, it is essential to justify if such designs are truly promising in broadband energy harvesting, and develop effective techniques to further enhance the bandwidth and power performance of VEHs when subjected to more realistic excitation sources. The works presented in this thesis attempt to address several critical issues in nonlinear VEHs, and the key outcomes are as follows.

Besides directly excited VEHs, parametrically excited VEHs with the principal parametric resonance can serve as an alternative method for energy harvesting. With an ultra-low natural frequency (i.e., 1-5 Hz), the primary resonance and parametric resonance can be potentially merged together by subjecting externally induced nonlinearities to the system. A continuously operational frequency bandwidth can be

formed in the presence of hardening frequency responses. The first paper (Chapter 3) presents a prototype VEH utilising both resonances that can adapt to multi-directional vibration sources. The motion limiter introduced hardening dynamic behaviours to the system, which eliminates the off-resonance regime between the two resonances. The experimental results are verified by an averaging perturbation method and a finite element method and demonstrate 178% improvement compared with linear counterparts.

The second paper (Chapter 4) further studied the parametric resonance and the effects of motion limiters. Considering the resonant amplitude growth in parametrically excited VEHs and the linear piece-wise restoring force from motion limiter, the bandwidth/power performance of such nonlinear interactions can possibly outperform directly excited counterpart. Therefore, we proposed a piezoelectric array system with three configurations of motion limiter to operate under both direct and parametric excitations. With a due-type motion limiter configuration, the results of the parametrically excited case indicate a continually operational bandwidth that consists of four parametric resonance regions, and the peak power level remains at almost the same position.

Another critical issue in parametrically excited VEHs is the initial threshold amplitude; the parametric resonance can only be activated under a certain excitation level. From the literature review, overcoming the potential barrier between potential wells is essential to trigger the large-amplitude intrawell motion in multi-stable VEHs. As the two restrictions are primarily dependent on the external excitation level, in the third paper (Chapter 5), an external oscillating element and external magnetic coupling effects were utilised to address both issues. The fabricated parametrically excited piezoelectric bistable VEH exhibits periodic interwell motions from 10-17.3 Hz. With repulsive restoring force and an external oscillating source, the device exhibits a broad steady-state bandwidth. In addition, bistability and the parametric resonance of the device can be revealed in small excitations.

Linear multi-mode/MDOF VEHs are capable of multi-directional vibration sources and have multiple resonance regimes which can adapt excitations at different ranges, though the most considerable reservation is the sacrifice of power density. To remedy this issue, in the fourth paper (Chapter 6), an internal-resonance-based VEH aims to achieve high-efficient energy harvesting. A two-to-one internal resonance between the first two bending modes of a fabricated U-shaped piezoelectric VEH is adopted. The results of this

work demonstrate that, the double-jump phenomena broaden the resonance regimes in bi-direction for the two coupled modes; enhanced power density is achieved in the presence of modal interactions; the proposed device is functional under orthogonal excitation directions.

Strain-voltage conversion in proper piezoelectric transducers can be further improved if more strain changes are able to be effectively captured, such as shear deformation. In the fifth paper (Chapter 7), we investigated bending and torsional modes of an L-shaped piezoelectric VEH with properly arranged piezoelectric layers. Moreover, a two-to-one internal resonance is achieved between the first torsional and second bending modes. The modal interactions induce mixed bending-torsional motions at one single excitation frequency. Consequently, the power level is greatly enhanced with the captured strain changes in both bending and shear directions by piezoelectric transducers. As an internal-resonance-based VEHs, the proposed device also features multi-directional, high-efficient, and broadband characteristics.

Based on presented theoretical models as well as designed prototypes, the broadband characteristics for different approaches (without combining additional nonlinearities) require certain conditions to be activated. Here, a comparison in Table 1 between selected approaches is given to indicate the design criteria under critical excitation conditions (level and direction), and also the effective bandwidth. The comparison indicates the merits of these approaches have different restrictions/limitations. In order to enhance the broadband/overall power performance, hybrid techniques (e.g., combining different nonlinearities) are recommended to overcome the existing bottlenecks, such as works presented in Chapters 3-7.

Table 1. Comparison between selected approaches

Approaches	Excitation level	Excitation directions	Effective bandwidth/overall power level
Parametrically excited VEH	Exists threshold amplitude, requires certain acceleration level	Can obtain multi-directional excitations if the primary (fundamental) resonance is also considered	Has multiple solutions under harmonic excitations; relatively narrow bandwidth without other external nonlinearities

Bistable VEH	The motion types depends on the excitation level (or the offset distance between tip and stationary magnets in typical designs)	Single direction	Multiple solutions; broadband can be achieved in periodic interwell oscillation
Motion limiter	Can suit different acceleration level by altering the offset gap distance; not suitable for random excitations	Single direction	Multiple solutions; mostly wide frequency bandwidth appeals in FW sweep case; trade-off between bandwidth and peak power level
Internal resonance-based VEH	The double-jump phenomenon can exist under small excitations	Depends on the main structure, e.g., multi-directional performance can be obtained in U-shaped or L-shaped structures.	Multiple solutions; double-jump phenomena can lead broadband performance; still limited compared to multi-stable approaches.

8.2 Recommendations

The works presented in this thesis aim to investigate the influence of internal/externally induced nonlinearities on VEHs and perform advanced approaches from mechanical and structural perspectives to enhance the effective bandwidth and power output performance by utilising theoretical, numerical and experimental verifications. For further investigations on nonlinear VEHs, because excitation source is the most critical system parameter to evaluate the performance/functionality of VEHs, The amplitude, type (if it is stationary, harmonic, or random and distributed in a wide frequency spectrum) and direction preliminarily determine what approaches should be applied to the devices. Thus, the recommended research directions are as follows.

- For excitation sources distributed in a range of frequency spectrum, it is difficult for multi-stable VEHs to stay at high-energy orbit for periodic interwell movement due to the coexisting solutions. A shallower potential barrier can indeed lower the requiring excitation level but decrease the maximum reachable

amplitude, which results in a reduced peak power level. Therefore, the effectiveness of multi-stable VEHs under stochastic/random excitation sources deserves further investigation. For example, can the depth of the potential barrier be adjustable or auto-tuned under different excitation levels?

- The motion limiters (piece-wise linear restoring force) can provide a broader frequency bandwidth; however, this approach can cause amplitude deductions due to energy loss by rapid contact. The materials, locations, and gap distances (the distances between contact position and the tip) need further investigation to enhance the power level. In addition, a motion limiter itself is capable of harvesting energy by equipping with, for example, flexure hinge and multi-layer piezoelectric structures.
- The resonant amplitude of parametrically excited VEHs under external excitations rises gradually due to periodic modulation existing in system parameters. Compared with the directly excited counterpart, the time series at a single frequency illustrates that the parametrically excited case exhibits a much longer transient state (or the amplitude of parametric resonance needs a sufficient time period to reach the same position as the amplitude of primary resonance). Can perturbations (design techniques) perform to shorten the time required and increase the flexibility of parametrically excited VEHs in dealing with non-harmonic excitations?
- Internal resonance as an inherent nonlinear phenomenon has gained great attention in vibration absorbing techniques. However, the investigations of borrowing this concept into VEHs, compared with other nonlinear approaches, are relatively limited. Further investigations on internal-resonance-based VEHs coupling with externally induced nonlinearities should be performed (i.e., softening/hardening restoring forces).
- For internal resonance-base and parametrically excited VEHs, damping effects (mechanical/electrical) are crucial, affecting required acceleration levels that trigger the phenomena, especially when PZT/MFC layers are fully covered on the core elements to maximise the power output. There may be a trade-off between power output and the threshold excitation level, which needs more in-depth investigation.
- A proof-of-concept study on an internal-resonance-based VEH is given to explore the feasibility of using combined bending-torsion motions. More in-depth

investigations are recommended to fulfil the field of nonlinear multi-directional and high-efficient VEHs under naturally multi-directional vibration sources.